

**NASA TECHNICAL
MEMORANDUM**

NASA TM X-73454

NASA TM X-73454

(NASA-TM-X-73454) ELASTOHYDRODYNAMIC
LUBRICATION OF POINT CONTACTS Ph.D. Thesis
- Leeds Univ. (NASA) 275 p HC \$9.00

N76-27571

CSCI 11H

Unclas

G3/37

44608

**ELASTOHYDRODYNAMIC LUBRICATION
OF POINT CONTACTS**

by B. J. Hamrock
Lewis Research Center
Cleveland, Ohio
June 1976

1. Report No. TM X-73454	2. Government Accession No.	3. Recipient's Catalog No.	
4. Title and Subtitle ELASTOHYDRODYNAMIC LUBRICATION OF POINT CONTACTS		5. Report Date	
		6. Performing Organization Code	
7. Author(s) B. J. Hamrock		8. Performing Organization Report No. E-7964	
		10. Work Unit No.	
9. Performing Organization Name and Address Lewis Research Center National Aeronautics and Space Administration Cleveland, Ohio 44135		11. Contract or Grant No.	
		13. Type of Report and Period Covered	
12. Sponsoring Agency Name and Address National Aeronautics and Space Administration Washington, D. C. 20546		14. Sponsoring Agency Code	
		15. Supplementary Notes Thesis submitted to the University of Leeds for the degree of Doctor of Philosophy	
16. Abstract <p>A procedure for the numerical solution of the complete, isothermal, elastohydrodynamic lubrication problem for point contacts is given. This procedure calls for the simultaneous solution of the elasticity and Reynolds equations. By using this theory the influence of the ellipticity parameter and the dimensionless speed, load, and material parameters on the minimum and central film thicknesses was investigated. Thirty-four different cases were used in obtaining the fully flooded minimum- and central-film-thickness formulas. Lubricant starvation was also studied. From the results it was possible to express the minimum film thickness for a starved condition in terms of the minimum film thickness for a fully flooded condition, the speed parameter, and the inlet distance. Fifteen additional cases plus three fully flooded cases were used in obtaining this formula. Contour plots of pressure and film thickness in and around the contact have been presented for both fully flooded and starved lubrication conditions.</p>			
17. Key Words (Suggested by Author(s)) Lubrication Elastohydrodynamics Film thickness		18. Distribution Statement	
19. Security Classif. (of this report) Unclassified	20. Security Classif. (of this page) Unclassified	21. No. of Pages	22. Price*

* For sale by the National Technical Information Service, Springfield, Virginia 22161

ELASTOHYDRODYNAMIC LUBRICATION OF POINT CONTACTS

by

B. J. HAMROCK

Thesis submitted to the University of Leeds for the
degree of Doctor of Philosophy

INSTITUTE OF TRIBOLOGY
DEPARTMENT OF MECHANICAL ENGINEERING
THE UNIVERSITY OF LEEDS

JULY 1976

ABSTRACT

A procedure for the numerical solution of the complete, isothermal elastohydrodynamic lubrication problem for point contacts is given. This procedure calls for the simultaneous solution of the elasticity and Reynolds equations. By using this theory the influence of the ellipticity parameter and the dimensionless speed, load, and material parameters on the minimum and central film thicknesses was investigated. Thirty-four different cases were used in obtaining fully flooded minimum- and central-film-thickness formulas. Lubricant starvation was also studied. From the results it was possible to express the minimum film thickness for a starved condition in terms of the minimum film thickness for a fully flooded condition, the speed parameter, and the inlet distance. Fifteen additional cases plus three fully flooded cases were used in obtaining this formula. Contour plots of pressure and film thickness in and around the contact have been presented for both fully flooded and starved lubrication conditions.

ACKNOWLEDGMENTS

I would like to express my appreciation to my thesis advisor, Professor Duncan Dowson, for his invaluable guidance and counseling. I would also like to thank Bill Anderson of NASA Lewis Research Center, whose support and encouragement made my studies at Leeds University possible.

I would like to express deep appreciation to my wife, Rosemary, who in addition to typing the first draft of the thesis, provided continual support and encouragement in the completion of this task. I would also like to thank my children, Maureen, Brian, and Jennifer, for their willingness to leave their home in Ohio so that all this could come about.

Finally, I would like to thank those at NASA Lewis Research Center who helped put the thesis in its final form.

CONTENTS

	Page
ABSTRACT	i
ACKNOWLEDGMENTS	ii
LIST OF TABLES	v
LIST OF FIGURES	vii
NOMENCLATURE	xiii
CHAPTER	
1 INTRODUCTION	1
1.1 Statement of Problem	1
1.2 Historical Developments	2
1.2.1 Line Contact	2
1.2.2 Point Contact	4
1.3 Approach to the Problem	5
2 GEOMETRY OF CONTACTING SOLIDS	8
2.1 Curvature Sum and Difference	8
2.2 Geometric Separation of Ellipsoidal Solids	8
2.3 Ellipticity Parameter	10
3 NUMERICAL EVALUATION OF THE ELASTIC DEFORMATION OF SOLIDS SUBJECTED TO A HERTZIAN CONTACT STRESS	13
3.1 Elastic Deformation Analysis	14
3.2 Hertzian Pressure Distribution	17
3.3 Film Thickness	18
3.4 Conditions Investigated	19
3.5 Discussion of Results	20
3.6 Concluding Remarks	23
4 THEORETICAL FORMULATION OF THE ELASTOHYDRODYNAMIC LUBRICATION PROBLEM	25
4.1 Reynolds Equation	25
4.2 Density	28
4.3 Viscosity	29
4.4 Film Thickness	31
4.5 Phi (ϕ) Solution	33
4.6 Finite Difference Representation	34
4.7 Nodal Structure	38
4.8 Boundary Conditions	39
4.9 Initial Conditions	39
4.10 Relaxation Method	40
4.11 Pressure Loop	40
4.12 Normal Applied Load	41
4.13 Flow Charts	42
4.14 Concluding Remarks	43

	Page
5 FULLY FLOODED RESULTS	44
5.1 Dimensionless Grouping	45
5.2 Effect of Ellipticity Parameter	47
5.3 Influence of Speed	52
5.4 Influence of Load	55
5.5 Effect of Material Properties	57
5.6 Minimum-Film-Thickness Formula	58
5.7 Central-Film-Thickness Formula	60
5.8 Concluding Remarks	65
6 STARVATION RESULTS	67
6.1 Boundary between Fully Flooded and Starved Conditions	68
6.2 Minimum-Film-Thickness Formula	71
6.3 Contour Plot of Results	72
6.4 Concluding Remarks	76
7 SUMMARY OF CONCLUSIONS	78
REFERENCES	82
APPENDIX - LISTING OF COMPUTER PROGRAMS	84

LIST OF TABLES

Table	Page
3.1. - Input conditions used for computer evaluations.	92
3.2. - Characteristics of the components of film thickness along the semimajor and semiminor axes when these axes are divided into three equal divisions and condition 1 of table 3.1 prevails . .	92
3.3. - Characteristics of the components of film thickness along the semimajor and semiminor axes when these axes are divided into four equal divisions and condition 1 of table 3.1 prevails . .	93
3.4. - Characteristics of the components of film thickness along the semimajor and semiminor axes when these axes are divided into five equal divisions and condition 1 of table 3.1 prevails. . .	94
3.5. - Characteristics of the components of film thickness along the semimajor and semiminor axes when these axes are divided into three equal divisions and condition 2 of table 3.1 prevails . .	95
3.6. - Characteristics of the components of film thickness along the semimajor and semiminor axes when these axes are divided into four equal divisions and condition 2 of table 3.1 prevails. . .	95
3.7. - Characteristics of the components of film thickness along the semimajor and semiminor axes when these axes are divided into five equal divisions and condition 2 of table 3.1 prevails. . .	96
3.8. - Characteristics of the components of film thickness along the semimajor and semiminor axes when these axes are divided into three equal divisions and condition 3 of table 3.1 prevails . .	97
3.9. - Characteristics of the components of film thickness along the semimajor and semiminor axes when these axes are divided into four equal divisions and condition 3 of table 3.1 prevails. . .	97
3.10. - Characteristics of the components of film thickness along the semimajor and semiminor axes when these axes are divided into five equal divisions and condition 3 of table 3.1 prevails. . .	98
3.11. - Characteristics of the components of film thickness along the semimajor and semiminor axes when these axes are divided into three equal divisions and condition 4 of table 3.1 prevails . .	99
3.12. - Characteristics of the components of film thickness along the semimajor and semiminor axes when these axes are divided into four equal divisions and condition 4 of table 3.1 prevails. . .	99
3.13. - Characteristics of the components of film thickness along the semimajor and semiminor axes when these axes are divided into five equal divisions and condition 4 of table 3.1 prevails. . .	100
5.1. - Effect of ellipticity parameter on minimum film thickness . . .	101
5.2. - Effect of dimensionless speed parameter on minimum film thickness	101
5.3. - Effect of dimensionless load parameter on minimum film thickness	101
5.4. - Effect of solid material and lubricant as represented in dimensionless material parameter on minimum film thickness. . .	102
5.5. - Data showing effect of ellipticity, load, speed, and material on minimum film thickness	102
5.6. - Effect of ellipticity parameter on central film thickness . . .	103

	Page
5.7. - Effect of dimensionless speed parameter on central film thickness	103
5.8. - Effect of dimensionless load parameter on central film thickness	103
5.9. - Effect of solid material and lubricant as represented in dimensionless material parameter on minimum film thickness. . .	104
5.10. - Data showing effect of ellipticity, load, speed, and material on central film thickness	104
6.1. - Effect of starvation on minimum film thickness for three groups of the dimensionless speed and load parameters.	105
6.2. - Effect of dimensionless speed and load parameters on dimensionless inlet distance at fully flooded - starved boundary	105
6.3. - Effect of dimensionless inlet distance on dimensionless central film thickness ratios	105

LIST OF FIGURES

Figure	Page
1.1. - Lubrication and contact conditions and minimum-film-thickness formulas	106
2.1. - Geometry of contacting elastic solids.	107
2.2. - Equivalent ellipsoidal solids.	107
3.1. - Types of elastic deformation	108
3.2. - Elastic deformation of a semi-infinite body subjected to a uniform pressure over a rectangular area	108
3.3. - Example division of area in and around contact zone into equal rectangular areas.	109
3.4. - Effect of location along semimajor and semiminor axes on percentage difference in elastic deformation when $d = 3$ and 9 . . .	110
3.5. - Effect of location along semimajor and semiminor axes on percentage difference in elastic deformation when $d = 3, 4,$ and 5 and on the more exact elastic deformation when $d = 9, 12,$ and $15,$ respectively	111
3.6. - Effect of location along semimajor and semiminor axes on ratio of elastic deformation to geometric separation.	112
3.7. - Effect of location along semimajor and semiminor axes on separation due to geometry of contacting solids plus elastic deformation.	113
3.8. - Effect of number of divisions across ellipse axis on computer run time	114
4.1. - Division of area in and around contact zone into equal rectangular areas.	115
4.2. - Components of film thickness for ellipsoidal solid near a plane.	115
4.3. - Mesh used in numerical analysis.	116
4.4. - Parabola and corresponding points representing ψ as a function of X	116
4.5. - Nodal structure used for numerical calculations.	116
4.6. - Flow chart of main program	117
4.7. - Flow chart of subroutine SUB6.	117
5.1. - Film thickness contours ($H_{min,L} = h_{min,L}/R_x$) for dimensionless material parameter G of 5000	118
5.2. - Contour plots of dimensionless pressure and film thickness and three-dimensional representation of pressure for ellipticity parameter (k) of 8. The dimensionless parameters $U, W,$ and G are held constant as defined in equation (5.10).	119
5.3. - Contour plots of dimensionless pressure and film thickness and three-dimensional representation of pressure for ellipticity parameter (k) of 6. The dimensionless parameters $U, W,$ and G are held constant as defined in equation (5.10).	122
5.4. - Contour plots of dimensionless pressure and film thickness and three-dimensional representation of pressure for ellipticity parameter (k) of 4. The dimensionless parameters $U, W,$ and G are held constant as defined in equation (5.10).	125

Figure	Page
5.5. - Contour plots of dimensionless pressure and film thickness and three-dimensional representation of pressure for ellipticity parameter (k) of 3. The dimensionless parameters U , W , and G are held constant as defined in equation (5.10)	128
5.6. - Contour plots of dimensionless pressure and film thickness and three-dimensional representation of pressure for ellipticity parameter (k) of 2.5. The dimensionless parameters U , W , and G are held constant as defined in equation (5.10).	131
5.7. - Contour plots of dimensionless pressure and film thickness and three-dimensional representation of pressure for ellipticity parameter (k) of 2. The dimensionless parameters U , W , and G are held constant as defined in equation (5.10)	134
5.8. - Contour plots of dimensionless pressure and film thickness and three-dimensional representation of pressure for ellipticity parameter (k) of 1.75. The dimensionless parameters U , W , and G are held constant as defined in equation (5.10).	137
5.9. - Contour plots of dimensionless pressure and film thickness and three-dimensional representation of pressure for ellipticity parameter (k) of 1.5. The dimensionless parameters U , W , and G are held constant as defined in equation (5.10).	140
5.10. - Contour plots of dimensionless pressure and film thickness and three-dimensional representation of pressure for ellipticity parameter (k) of 1.25. The dimensionless parameters U , W , and G are held constant as defined in equation (5.10).	143
5.11. - Variation of dimensionless pressure and film thickness on \bar{X} -axis for three values of ellipticity parameter. The value of \bar{Y} is held fixed near axial center of contact	146
5.12. - Contour plots of dimensionless pressure and film thickness and three-dimensional representation of pressure for dimensionless speed parameter (U) of 5.050×10^{-11} . The dimensionless parameters k , W , and G are held constant as defined in equation (5.18).	147
5.13. - Contour plots of dimensionless pressure and film thickness and three-dimensional representation of pressure for dimensionless speed parameter (U) of 4.208×10^{-11} . The dimensionless parameters k , W , and G are held constant as defined in equation (5.18).	150
5.14. - Contour plots of dimensionless pressure and film thickness and three-dimensional representation of pressure for dimensionless speed parameter (U) of 3.367×10^{-11} . The dimensionless parameters k , W , and G are held constant as defined in equation (5.18).	153
5.15. - Contour plots of dimensionless pressure and film thickness and three-dimensional representation of pressure for dimensionless speed parameter (U) of 2.946×10^{-11} . The dimensionless parameters k , W , and G are held constant as defined in equation (5.18).	156
5.16. - Contour plots of dimensionless pressure and film thickness and three-dimensional representation of pressure for dimensionless speed parameter (U) of 2.525×10^{-11} . The dimensionless parameters k , W , and G are held constant as defined in equation (5.18).	159

Figure	Page
5.17. - Contour plots of dimensionless pressure and film thickness and three-dimensional representation of pressure for dimensionless speed parameter (U) of 2.104×10^{-11} . The dimensionless parameters k, W, and G are held constant as defined in equation (5.18).	162
5.18. - Contour plots of dimensionless pressure and film thickness and three-dimensional representation of pressure for dimensionless speed parameter (U) of 1.683×10^{-11} . The dimensionless parameters k, W, and G are held constant as defined in equation (5.18).	165
5.19. - Contour plots of dimensionless pressure and film thickness and three-dimensional representation of pressure for dimensionless speed parameter (U) of 1.263×10^{-11} . The dimensionless parameters k, W, and G are held constant as defined in equation (5.18).	168
5.20. - Contour plots of dimensionless pressure and film thickness and three-dimensional representation of pressure for dimensionless speed parameter (U) of 8.416×10^{-12} . The dimensionless parameters k, W, and G are held constant as defined in equation (5.18).	171
5.21. - Contour plots of dimensionless pressure and film thickness and three-dimensional representation of pressure for dimensionless speed parameter (U) of 5.892×10^{-12} . The dimensionless parameters k, W, and G are held constant as defined in equation (5.18).	174
5.22. - Contour plots of dimensionless pressure and film thickness and three-dimensional representation of pressure for dimensionless speed parameter (U) of 4.208×10^{-12} . The dimensionless parameters k, W, and G are held constant as defined in equation (5.18).	177
5.23. - Contour plots of dimensionless pressure and film thickness and three-dimensional representation of pressure for dimensionless speed parameter (U) of 3.367×10^{-12} . The dimensionless parameters k, W, and G are held constant as defined in equation (5.18).	180
5.24. - Contour plots of dimensionless pressure and film thickness and three-dimensional representation of pressure for dimensionless speed parameter (U) of 2.525×10^{-12} . The dimensionless parameters k, W, and G are held constant as defined in equation (5.18).	183
5.25. - Contour plots of dimensionless pressure and film thickness and three-dimensional representation of pressure for dimensionless speed parameter (U) of 1.683×10^{-12} . The dimensionless parameters k, W, and G are held constant as defined in equation (5.18).	186
5.26. - Contour plots of dimensionless pressure and film thickness and three-dimensional representation of pressure for dimensionless speed parameter (U) of 8.416×10^{-13} . The dimensionless parameters k, W, and G are held constant as defined in equation (5.18).	189

Figure	Page
5.27. - Variation of dimensionless pressure and film thickness on \bar{X} -axis for three values of dimensionless speed parameter. The value of \bar{Y} is held fixed near axial center of contact.	192
5.28. - Contour plots of dimensionless pressure and film thickness and three-dimensional representation of pressure for dimensionless load parameter (W) of 0.1106×10^{-6} . The dimensionless parameters k , U , and G are held constant as defined in equation (5.23)	193
5.29. - Contour plots of dimensionless pressure and film thickness and three-dimensional representation of pressure for dimensionless load parameter (W) of 0.2211×10^{-6} . The dimensionless parameters k , U , and G are held constant as defined in equation (5.23)	196
5.30. - Contour plots of dimensionless pressure and film thickness and three-dimensional representation of pressure for dimensionless load parameter (W) of 0.3686×10^{-6} . The dimensionless parameters k , U , and G are held constant as defined in equation (5.23)	199
5.31. - Contour plots of dimensionless pressure and film thickness and three-dimensional representation of pressure for dimensionless load parameter (W) of 0.5528×10^{-6} . The dimensionless parameters k , U , and G are held constant as defined in equation (5.23)	202
5.32. - Contour plots of dimensionless pressure and film thickness and three-dimensional representation of pressure for dimensionless load parameter (W) of 0.7371×10^{-6} . The dimensionless parameter k , U , and G are held constant as defined in equation (5.23)	205
5.33. - Contour plots of dimensionless pressure and film thickness and three-dimensional representation of pressure for dimensionless load parameter (W) of 0.9214×10^{-6} . The dimensionless parameters k , U , and G are held constant as defined in equation (5.23)	208
5.34. - Contour plots of dimensionless pressure and film thickness and three-dimensional representation of pressure for dimensionless load parameter (W) of 1.105×10^{-6} . The dimensionless parameters k , U , and G are held constant as defined in equation (5.23)	211
5.35. - Contour plots of dimensionless pressure and film thickness and three-dimensional representation of pressure for dimensionless load parameter (W) of 1.290×10^{-6} . The dimensionless parameters k , U , and G are held constant as defined in equation (5.23)	214
5.36. - Variation of dimensionless pressure and film thickness on \bar{X} -axis for three values of dimensionless load parameter. The value of \bar{Y} is held fixed near axial center of contact.	217
6.1 - Computing area in and around the Hertzian contact circle	218
6.2. - Influence of inlet boundary parameter upon central film thickness ratio	219

Figure	Page
6.3. - Contour plots of dimensionless pressure and dimensionless film thickness for dimensionless inlet distance m of 4 and group 1 of table 6.2.	219
6.4. - Contour plots of dimensionless pressure and dimensionless film thickness for dimensionless inlet distance m of 3 and group 1 of table 6.2.	221
6.5. - Contour plots of dimensionless pressure and dimensionless film thickness for dimensionless inlet distance m of 2 and group 1 of table 6.2.	223
6.6. - Contour plots of dimensionless pressure and dimensionless film thickness for dimensionless inlet distance m of 1.5 and group 1 of table 6.2.	225
6.7. - Contour plots of dimensionless pressure and dimensionless film thickness for dimensionless inlet distance m of 1.25 and group 1 of table 6.2.	227
6.8. - Contour plots of dimensionless pressure and dimensionless film thickness for dimensionless inlet distance m of 6 and group 2 of table 6.2.	229
6.9. - Contour plots of dimensionless pressure and dimensionless film thickness for dimensionless inlet distance m of 4 and group 2 of table 6.2.	231
6.10. - Contour plots of dimensionless pressure and dimensionless film thickness for dimensionless inlet distance m of 3 and group 2 of table 6.2.	233
6.11. - Contour plots of dimensionless pressure and dimensionless film thickness for dimensionless inlet distance m of 2.5 and group 2 of table 6.2.	235
6.12. - Contour plots of dimensionless pressure and dimensionless film thickness for dimensionless inlet distance m of 2 and group 2 of table 6.2.	237
6.13. - Contour plots of dimensionless pressure and dimensionless film thickness for dimensionless inlet distance m of 6 and group 3 of table 6.2.	239
6.14. - Contour plots of dimensionless pressure and dimensionless film thickness for dimensionless inlet distance m of 4 and group 3 of table 6.2.	241
6.15. - Contour plots of dimensionless pressure and dimensionless film thickness for dimensionless inlet distance m of 3 and group 3 of table 6.2.	243
6.16. - Contour plots of dimensionless pressure and dimensionless film thickness for dimensionless inlet distance m of 2.5 and group 3 of table 6.2.	245
6.17. - Contour plots of dimensionless pressure and dimensionless film thickness for dimensionless inlet distance m of 2 and group 3 of table 6.2.	247
6.18. - Contour plots of dimensionless pressure and dimensionless film thickness for dimensionless inlet distance m of 1.75 and group 3 of table 6.2.	248

Figure	Page
6.19. - Contour plots of dimensionless pressure and dimensionless film thickness for dimensionless inlet distance m of 1.5 and group 3 of table 6.2.	251
6.20. - Effect of dimensionless inlet distance on dimensionless pressure along \bar{X} -axis. The value of \bar{Y} is held fixed near the axis of symmetry of the contact	253
6.21. - Effect of dimensionless inlet distance on dimensionless film thickness along \bar{X} -axis. The value of \bar{Y} is held fixed near the axis of symmetry of the contact	255

NOMENCLATURE

A, B, C	constants defined in eq. (4.26)
$\left. \begin{array}{l} \bar{A}, \bar{B}, \bar{C}, \\ \bar{D}, \bar{L}, \bar{M} \end{array} \right\}$	relaxation coefficients
a	semimajor axis of contact ellipse
\bar{a}	$a/2c$
b	semiminor axis of contact ellipse
\bar{b}	$b/2d$
c	number of equal divisions of semimajor axis
D	influence coefficient defined in eq. (4.22)
D_1	$\left(\frac{\tilde{H}_{\min} - H_{\min}}{H_{\min}} \right) 100$
D_2	$\left(\frac{\tilde{H}_c - H_c}{H_c} \right) 100$
d	number of equal divisions of semiminor axis
E	modulus of elasticity
E'	$\frac{2}{\left(\frac{1 - \nu_A^2}{E_A} + \frac{1 - \nu_B^2}{E_B} \right)}$
\mathcal{E}	elliptical integral of second kind
F	normal applied load
\bar{F}	integrated normal applied load
\mathcal{F}	elliptical integral of first kind
G	dimensionless material parameter

H	dimensionless film thickness, h/R_x
H_c	dimensionless central film thickness for a fully flooded condition as obtained from the EHL point-contact theory, h_c/R_x
\tilde{H}_c	dimensionless central film thickness for a fully flooded condition as obtained from the least-square fit of the data
H_{\min}	dimensionless minimum film thickness, h_{\min}/R_x
$H_{\min,F}$	dimensionless minimum film thickness for a fully flooded condition as obtained from the EHL point-contact theory, $h_{\min,F}/R_x$
$\tilde{H}_{\min,F}$	dimensionless minimum film thickness for a fully flooded condition as obtained from the least-square fit of the data
$H_{\min,S}$	dimensionless minimum film thickness for a starved lubrication condition as obtained from the EHL point-contact theory, $h_{\min,S}/R_x$
$\tilde{H}_{\min,S}$	dimensionless minimum film thickness for a starved lubrication condition as obtained from the least-square fit of the data
H_o	constant, initially estimated
h	film thickness
h_c	central film thickness
h_{\min}	minimum film thickness
J	function of k (eq. (2.23))
k	ellipticity parameter, a/b
m	dimensionless inlet distance (see fig. 6.1)
m^*	dimensionless inlet distance at boundary between fully flooded and starved conditions

m_w	dimensionless inlet distance boundary as obtained from Wedeven, et al. (1971)
P	dimensionless pressure, p/E'
P	pressure
$P_{iv,as}$	asymptotic isoviscous pressure
R	effective radius
R_1	S/\bar{S}
R_2	w/S
R_3	$\left(\frac{w_m - w_{3m}}{w_{3m}}\right)100$
r	radius of curvature
\bar{r}	defined in fig. 3.2
S	approximate film thickness due to geometry of contacting solids, defined in eq. (3.11)
S	exact film thickness due to geometry of contacting solids, defined in eq. (3.10)
U	dimensionless speed parameter, $u\eta_0/R_x E'$
u	surface velocity in X-direction
W	dimensionless load parameter, $F/E'R_x^2$
w	total elastic deformation
\bar{w}	elastic deformation
$x, X, \bar{X}, \tilde{X}, X^*$ $y, Y, \bar{Y}, \tilde{Y}, Y^*$ z, Z, \bar{Z}, Z^*	coordinate systems defined in thesis
Z	viscosity-pressure index, a dimensionless constant
α	pressure-viscosity constant
β, γ	fluid constants used in eq. (4.13)
Γ	curvature difference
η	lubricant viscosity

$\bar{\eta}$	dimensionless viscosity, η/η_0
η_0	atmospheric viscosity
μ	$\bar{\rho}/\bar{\eta}$
ν	Poisson's ratio
ρ	lubricant density
$\bar{\rho}$	dimensionless density, ρ/ρ_0
ρ_0	atmospheric density
ϕ	$PH^{3/2}$

Subscripts:

A	solid A
B	solid B
x,y	coordinate system

CHAPTER I

INTRODUCTION

1.1 Statement of Problem

In many contacts between machine elements, forces are transmitted through thin, but continuous, fluid films. One of the basic problems is to accurately describe the fluid film thickness between these machine elements. The provision of an adequate fluid film thickness will reduce wear and increase fatigue life and therefore avoid early damage of the machine elements. These fluid films as related to hydrodynamic lubrication in journal and thrust bearings have been well understood for some time, and experimental work confirms the theory. In the early 1900's it was recognized by Martin (1916) that many loaded contacts of low geometrical conformity, commonly referred to as nonconforming contacts, such as gears and rolling-contact bearings, behaved as though they were hydrodynamically lubricated. As opposed to the journal and thrust bearing counterpart, the original hydrodynamic lubrication theory of gears and rolling-contact bearings differed substantially from experimental findings. Only in recent years has the consideration of elastic deformation of contacts been coupled to hydrodynamics to yield a closer agreement of theory with experiments.

Elastohydrodynamic lubrication (EHL) then deals with the lubrication of elastic contacts. The analysis requires the simultaneous solution of the elasticity and Reynolds equations. The EHL theory differs from conventional hydrodynamic theory in the following way:

- (1) In defining the film thickness in EHL theory, elastic de-

formation of the contact is considered.

(2) The viscosity is no longer independent of pressure, as is assumed in conventional hydrodynamic theory.

(3) Hydrodynamic lubrication is characterized by surfaces that are conforming, but elastohydrodynamic lubrication is usually characterized by nonconforming surfaces.

Because of this last point the load in hydrodynamic lubrication is usually carried over a relatively large area. Also, typical maximum pressures for elastohydrodynamic lubrication are of the order of $1.4 \times 10^9 \text{ N/m}^2$ ($200\,000 \text{ lb/in.}^2$), and the usual hydrodynamic pressures generated in journal bearings are of the order of only $7 \times 10^6 \text{ N/m}^2$ (1000 lb/in.^2).

1.2 Historical Developments

When two solids are in contact under zero load condition, one of two types of contact is experienced:

- (1) Point contact, in which two solids touch at a single point, as in ball bearings
- (2) Line contact, in which two solids touch along a straight or curved line, as in roller bearings

After a load is applied, the point expands to an ellipse and the line to a rectangle. Although we are concerned with loaded contacts, it is convenient to distinguish between these situations by referring to them as being either point or line contact. Lubricant removal to the side of the contact is ignored in the line-contact problem and the problem becomes two dimensional. This is a considerable simplification from the point-contact, three-dimensional problem.

1.2.1 Line Contact

One of the earliest solutions of the lubrication of a line contact was presented in 1916 by Martin. By assuming rigid solids and an incompressible constant-viscosity lubricant he was able to deter-

mine a lubricating film thickness. Figure 1.1(a) shows typical pressure and film thickness curves from Martin's solution as well as his formula for minimum film thickness. Martin's formula greatly underestimates the film thickness; however, it was a useful beginning to the theoretical study of elastohydrodynamic lubrication of line contacts.

Some 30 years transpired before any significant accomplishments were made in solving the EHL line-contact problem. Grubin (1949) obtained the first satisfactory solution to this problem by taking account of elastic distortion and viscosity-pressure effects. In Grubin's analysis it was assumed that the shape of the elastically deformed solids in a highly loaded lubricated contact is the same as the shape produced in a dry Hertzian contact. A pressure distribution in a Hertzian contact is shown in figure 1.1(b). This stipulation (assuming the shape of the elastically deformed solids is the same as is produced in a Hertzian contact) facilitated the solution of the Reynolds equation in the inlet region of the contact and enabled the separation of the solids in the central region of the contact to be determined with commendable accuracy. Grubin's approach produced an excellent account of the physical mechanism of the lubrication process in highly loaded EHL line contacts, and it marked a very important development in the history of elastohydrodynamic lubrication.

Dowson and Higginson (1961) produced an empirical formula for isothermal EHL line contacts. This formula shows the effect of speed, load, and material properties on minimum film thickness and is based on their earlier theoretical solutions (1959). Figure 1.1(c) gives the pressure and film thickness for an elastohydrodynamic lubricated line contact. Also shown in figure 1.1(c) is the EHL line-contact minimum film thickness obtained from the results of

Dowson and Higginson (1961). In the Dowson-Higginson theory (1959) for EHL line contacts, a new approach of introducing a solution of the inverse hydrodynamic lubrication problem was presented. Normally a solution of the Reynolds equation calls for the determination of a pressure distribution corresponding to a given film thickness. In the inverse problem the film shape responsible for the generation of a given pressure distribution is determined. In the procedure adopted by Dowson and Higginson (1959) the computed film shape was compared with the shape of the elastically deformed solids, and the pressure curve was then modified to improve the agreement between the two shapes. By using this approach they were able to obtain satisfactory solutions of the elastic and hydrodynamic equations after a small number of numerical iterations.

The Dowson-Higginson minimum-film-thickness formula for EHL line contacts agrees quite well with experimental observations. In particular, Sibley and Orcutt's (1961) X-ray method, Christensen's (1964) slide displacement method, and Dyson, Naylor, and Wilson's (1966) capacity method all give good agreement with the Dowson-Higginson formula.

1.2.2 Point Contact

Most of the work on elastohydrodynamic lubrication has dealt with line contacts. Furthermore, the majority of the work done on the EHL point-contact problem has been experimental. Two good examples of this experimental work are Cameron and Gohar's (1966) observation of film thickness between a steel sphere and a glass plate using interference rings and Archard and Kirk's (1961) observation of film thickness between two crossed cylinders with the same diameter making an angle of 90° in a simulated point contact.

The first step toward a theoretical solution of the EHL point-contact problem was presented by Archard and Cowking (1966). They

adopted an approach similar to that used by Grubin (1949) for line-contact conditions. The Hertzian contact zone was assumed to form a parallel film region, and the generation of high pressure in the approaches to the Hertzian zone was considered.

Cheng (1970) also used a Grubin type of approach in determining a film thickness formula for the EHL of point contacts. He evaluated the deformation by using the Hertz equation and then applying the Reynolds equation to this geometry.

Recently an interesting numerical solution of the EHL point-contact problem for a sphere near a plane was put forth by Ranger, et al. (1975). This solution is presented in dimensional terms, which thereby limits its general usage. A puzzling feature of the Ranger, et al. work is the fact that his resulting equation for the minimum film thickness has a positive load exponent, which contradicts experiments (e.g., Cameron and Gohar's (1966) and Archard and Kirk (1961)).

1.3 Approach to the Problem

In the literature the EHL line-contact problem is completely solved, with theory and experiment agreeing well with each other. For the EHL point-contact problem quite a bit of experimental work has been done, but the theoretical solution to the complete isothermal elastohydrodynamic lubrication problem for point contacts has not emerged. The reason for this is the extreme difficulty of the numerical coupling of the elasticity and Reynolds equations and the vast increase in computing involved in a transfer from line- to point-contact conditions. The work presented in this dissertation is an attempt to solve this problem. A brief description of the approach to the problem follows.

The radii of curvature of the contacting solids are used to define the ratio of the semimajor and semiminor axes of the contact ellipse. From this ratio and the normal applied load, the semimajor

and semiminor axes of the contact ellipse are determined. In the elasticity analysis the computing zone is divided into equal rectangular areas, and a uniform pressure is applied over each area. Elasticity studies are performed to determine how finely the semi-major and semiminor axes need to be divided to achieve a given accuracy and how far from the center of the contact deformation becomes insignificant compared with the separation of the solids. These equations were investigated for light and heavy loads and for geometries ranging from a ball on a plate to a line-contact configuration. The answers to these questions determined what the computing zone should be in and around the contact ellipse.

In the numerical analysis of the Reynolds equation a " ϕ " (ϕ) substitution is used to aid the relaxation process, where ϕ is equal to the pressure times the film thickness to the 3/2 power. The pressure-viscosity analysis of Roelands (1966) is used. The numerical coupling of the elasticity and Reynolds equations results in a converged solution for the pressure profile. This pressure profile is then integrated over the computing zone to give the value of the corresponding normal applied load. This load is then compared with the input load, and corrections are made to the film thickness until these two loads are in agreement.

The most important practical aspect of the EHL point-contact theory is the determination of the minimum film thickness within the contact. By using the variables resulting from the theory, the dimensionless minimum film thickness can be written as a function of the dimensionless load, speed, material, and ellipticity parameters.

The influence of these parameters on minimum film thickness was investigated. The ellipticity parameter was varied from 1 (a ball on a plate) to 8 (a configuration approaching a line contact). The dimensionless speed parameter was varied over a range of nearly two

orders of magnitude. The dimensionless load parameter was varied over a range of one order of magnitude. Solid materials of bronze, steel, and silicon nitride and lubricants of paraffinic and naphthenic mineral oils were varied in obtaining the exponent in the dimensionless material parameter. Thirty-four different cases were used in obtaining the fully flooded minimum-film-thickness formula. In addition to the minimum-film-thickness formula a central-film-thickness formula was developed. Contour plots are also shown that indicate in detail the pressure spike and the two side lobes in which the minimum film thickness occurs. These theoretical solutions for film thickness have all the essential features of the previously reported experimental observations based upon optical interferometry.

The effect of lubricant starvation was also investigated. This study of lubricant starvation was achieved simply by reducing the inlet distance, which is the distance from the center of the contact to the edge of the computing area. A fully flooded condition exists when the dimensionless inlet distance ceases to influence in any significant way the minimum film thickness. Starting from a fully flooded condition and decreasing the inlet distance, the value at which the minimum film thickness first starts to change is called the fully flooded - starved boundary. Simple expressions for the fully flooded - starved boundary were obtained as a function of the fully flooded central or minimum film thickness. Simple expressions defining the central and minimum film thicknesses for a lubricant starvation condition were also obtained. Fifteen different cases from those presented in the fully flooded results were used in obtaining these formulas. Furthermore, the effects of lubricant starvation are clearly shown in contour plots of pressure and film thickness.

REPRODUCIBILITY OF THE ORIGINAL PAGE IS POOR

CHAPTER 2

GEOMETRY OF CONTACTING SOLIDS

2.1 Curvature Sum and Difference

Two solids having different radii of curvature in a pair of principal planes (x and y) passing through the contact between the solids make contact at a single point under the condition of no applied load. Such a condition is called "point contact" and is shown in figure 2.1, where the radii of curvature are denoted by r's. In the analysis that follows it was assumed that for convex surfaces as shown in figure 2.1 the curvature is positive but that for concave surfaces the curvature is negative.

The curvature sum and difference are defined as

$$\frac{1}{R} = \frac{1}{R_x} + \frac{1}{R_y} \quad (2.1)$$

$$\Gamma = R \left(\frac{1}{R_x} - \frac{1}{R_y} \right) \quad (2.2)$$

where

$$\frac{1}{R_x} = \frac{1}{r_{Ax}} + \frac{1}{r_{Bx}} \quad (2.3)$$

$$\frac{1}{R_y} = \frac{1}{r_{Ay}} + \frac{1}{r_{By}} \quad (2.4)$$

2.2 Geometric Separation of Ellipsoidal Solids

Figure 2.2 shows how the geometric separation between two ellipsoidal solids can be made equivalent to that between a single ellipsoidal solid near a plane. The geometric requirement is that for any values of x and y in figure 2.2(a) the geometric separation must be equivalent to the separation at the same x and y shown in fig-

ure 2.2(b). From figure 2.2(a) the mathematical expression for the separation of the two ellipsoidal solids can be written as

$$S = S_{Ax} + S_{Bx} + S_{Ay} + S_{By} \quad (2.5)$$

From figure 2.2(b) the mathematical expression for the separation of a single ellipsoidal solid near a plane can be written as

$$S = S_x + S_y \quad (2.6)$$

Therefore, for the two expressions to be equivalent, the following must be true:

$$S_x = S_{Ax} + S_{Bx} \quad (2.7)$$

$$S_y = S_{Ay} + S_{By} \quad (2.8)$$

From figure 2.2(a-1) the following can be written:

$$r_{Ax}^2 = x^2 + (r_{Ax} - S_{Ax})^2 \quad (2.9)$$

or

$$x^2 = S_{Ax}(2r_{Ax} - S_{Ax}) \quad (2.10)$$

But for the problem being considered, $2r_{Ax} \gg S_{Ax}$; so that equation (2.10) can be rewritten as

$$S_{Ax} \approx \frac{x^2}{2r_{Ax}} \quad (2.11)$$

This is the well-known parabolic approximation to the circular section of the solid. Similarly, by making use of figure 2.2 the following can be written:

$$S_{Bx} \approx \frac{x^2}{2r_{Bx}} \quad \text{where } 2r_{Bx} \gg S_{Bx} \quad (2.12)$$

$$S_{Ay} \approx \frac{y^2}{2r_{Ay}} \quad \text{where } 2r_{Ay} \gg S_{Ay} \quad (2.13)$$

$$S_{By} \approx \frac{y^2}{2r_{By}} \quad \text{where } 2r_{By} \gg S_{By} \quad (2.14)$$

$$S_x \approx \frac{x^2}{2R_x} \quad \text{where } 2R_x \gg S_x \quad (2.15)$$

$$S_y \approx \frac{y^2}{2R_y} \quad \text{where } 2R_y \gg S_y \quad (2.16)$$

Substituting equations (2.11) to (2.16) into equations (2.7) and (2.8) gives

$$\frac{1}{R_x} = \frac{1}{r_{Ax}} + \frac{1}{r_{Bx}} \quad (2.17)$$

$$\frac{1}{R_y} = \frac{1}{r_{Ay}} + \frac{1}{r_{By}} \quad (2.18)$$

But equations (2.17) and (2.18) are exactly equations (2.3) and (2.4), respectively. Therefore the equivalency shown in figure 2.2 is satisfied. Henceforth the geometry of an ellipsoidal solid near a plane as shown in figure 2.2(b) will be used.

2.3 Ellipticity Parameter

When the ellipsoidal solid just touches the plane shown in figure 2.2(b), contact is made at a single point when no load is applied. When a normal load is applied to the ellipsoidal solid, the point expands to an ellipse with a as the semimajor axis and b as the semiminor axis. It is assumed that the plane remains rigid while the equivalent elastic ellipsoid is pressed against it. The normal applied load lies along the axis that passes through the center of the solid and through the point of contact and is perpendicular to the plane shown in figure 2.2(b). For the special case where $R_x = R_y$, the resulting contact is a circle rather than an ellipse.

The ellipticity parameter (k) is defined as

$$k = \frac{a}{b} \quad (2.19)$$

where

- a semimajor axis of contact ellipse
- b semiminor axis of contact ellipse

Harris (1966) has shown that the ellipticity parameter can be written to relate the curvature difference and the elliptic integrals of the first and second kind as

$$J(k) = \sqrt{\frac{2\mathcal{F} - \mathcal{E}(1 + \Gamma)}{\mathcal{E}(1 - \Gamma)}} \quad (2.20)$$

where

$$\mathcal{F} = \int_0^{\pi/2} \left[1 - \left(1 - \frac{1}{k^2} \right) \sin^2 \varphi \right]^{-1/2} d\varphi \quad (2.21)$$

$$\mathcal{E} = \int_0^{\pi/2} \left[1 - \left(1 - \frac{1}{k^2} \right) \sin^2 \varphi \right]^{1/2} d\varphi \quad (2.22)$$

A one-point iteration method that has been used successfully in the past by Hamrock and Anderson (1973) was used, where

$$k_{n+1} = J(k_n) \quad (2.23)$$

The iteration process is continued until k_{n+1} differs from k_n by less than 1×10^{-7} . Note that the ellipticity parameter is a function of the radii of curvature of the contacting solids only

$$k = f(r_{Ax}, r_{Bx}, r_{Ay}, r_{By})$$

When the ellipticity parameter (k), the normal applied load (F), Poisson's ratio (ν), and modulus of elasticity (E) of the contacting solids are known, the semimajor axis of the contact ellipse can be written as

$$a = \left(\frac{6k^2 \Gamma \mathcal{E} R}{\pi E'} \right)^{1/3} \quad (2.24)$$

where

$$E' = \frac{2}{\frac{1 - \nu_A^2}{E_A} + \frac{1 - \nu_B^2}{E_B}} \quad (2.25)$$

By making use of equation (2.19) the semiminor axis of the contact

ellipse can be written as

$$b = \frac{a}{k} \quad (2.26)$$

Therefore, from the geometry of the contacting solids the ellipticity parameter, as well as the semimajor and semiminor axes, has been defined. These parameters form the foundation of the EHL point-contact analysis.

CHAPTER 3
NUMERICAL EVALUATION OF THE ELASTIC DEFORMATION OF
SOLIDS SUBJECTED TO A HERTZIAN CONTACT STRESS

Elastohydrodynamic lubrication is defined as the study of situations in which elastic deformation of the surrounding solids plays a significant role in the hydrodynamic lubrication process. This chapter is not concerned with the hydrodynamic lubrication process, but only with deformation due to the pressure of one elastic solid upon another.

Dowson (1965) distinguishes between two modes of deformation that may exist in machine elements. In one mode, the contact geometry may be affected by overall distortion of the elastic machine element resulting from applied loads, as shown in figure 3.1(a). In the other, the normal stress distribution in the vicinity of the contact zone may produce local elastic deformations that are significant when compared with the lubricant film thickness, as shown in figure 3.1(b). This is the mode of deformation with which this present investigation is concerned. The important distinction is that the first form of deformation is relatively insensitive to the distribution and magnitude of the stresses in the contact zone, whereas the second mode of deformation is intimately linked to the local stress conditions.

The correct evaluation of elastic deformation on the surface of a solid depends upon an adequate representation of the applied normal pressures. The simplest procedure is to divide the actual pressure distribution into rectangular blocks of uniform pressure and to

permit each rectangle to be of such small dimensions that adequate predictions of elastic displacements ensue. More complex representations of two-dimensional pressure distributions within each rectangle would generally permit larger rectangles to be used, but the additional complexity of the expressions and added computation time make it desirable to exploit the simpler representation to the fullest. This chapter is devoted to a study of the adequacy of representing the applied normal pressures by rectangular blocks of uniform pressure.

The deformation analysis is developed in general form since it will be used in later chapters to calculate elastic deformation in the elastohydrodynamic lubrication of point contacts. To evaluate the influence of mesh or block size upon accuracy, the numerical investigation of this chapter considers only Hertzian contact stress distributions.

The deformation analysis itself assumed that the contact zone can be divided into rectangular areas and that the pressure is uniform within each rectangular area. Once the elastic deformation had been formulated, investigations were performed to answer the following questions:

(1) How fine do the semimajor and semiminor axes need to be divided to achieve a given accuracy in deformation prediction?

(2) How far from the center of the contact does deformation become insignificant compared with the separation of solids?

These questions were investigated for both light and heavy applied loads and for both equal spheres in contact and a contact that is common to the outer race of a ball bearing.

3.1 Elastic Deformation Analysis

In chapter 2 the general geometry of two ellipsoidal solids in elastic contact was described. In the subsequent analysis it will

be convenient to consider the deformation of an equivalent elastic half-space subjected to a Hertzian pressure distribution over the ellipse of semimajor and semiminor axes, a and b , as previously defined. The resulting elastic deformation can be considered to be equivalent to the total deformation of two elastic ellipsoids having elastic constants E_A, ν_A and E_B, ν_B , respectively, if the half-space is allocated the equivalent elastic parameter (E') defined by equation (2.25).

Once the semimajor and semiminor axes of the contact ellipse have been defined, the elastic deformation that occurs inside and outside the contact zone can be evaluated. Figure 3.2 shows a rectangular area of uniform pressure with the coordinate system to be used. From Timoshenko and Goodier (1951) the elastic deformation at a point (X, Y) of a semi-infinite solid subjected to a pressure (p) at the point (X_1, Y_1) can be written as

$$d\bar{w} = \frac{2p \, dX_1 \, dY_1}{\pi E' r}$$

The elastic deformation at a point (X, Y) due to the uniform pressure over the rectangular area $2\bar{a} \times 2\bar{b}$ is thus

$$\bar{w} = \frac{2P}{\pi} \int_{-\bar{a}}^{\bar{a}} \int_{-\bar{b}}^{\bar{b}} \frac{dX_1 \, dY_1}{\sqrt{(Y - Y_1)^2 + (X - X_1)^2}}$$

where

$$P = \frac{P}{E'}$$

Integrating the preceding equation gives

$$\bar{w} = \frac{2}{\pi} P'D \tag{3.1}$$

where

$$\begin{aligned}
D = (X + \bar{b}) \ln & \left[\frac{(Y + \bar{a}) + \sqrt{(Y + \bar{a})^2 + (X + \bar{b})^2}}{(Y - \bar{a}) + \sqrt{(Y - \bar{a})^2 + (X + \bar{b})^2}} \right] \\
& + (Y + \bar{a}) \ln \left[\frac{(X + \bar{b}) + \sqrt{(Y + \bar{a})^2 + (X + \bar{b})^2}}{(X - \bar{b}) + \sqrt{(Y + \bar{a})^2 + (X - \bar{b})^2}} \right] \\
& + (X - \bar{b}) \ln \left[\frac{(Y - \bar{a}) + \sqrt{(Y - \bar{a})^2 + (X - \bar{b})^2}}{(Y + \bar{a}) + \sqrt{(Y + \bar{a})^2 + (X - \bar{b})^2}} \right] \\
& + (Y - \bar{a}) \ln \left[\frac{(X - \bar{b}) + \sqrt{(Y - \bar{a})^2 + (X - \bar{b})^2}}{(X + \bar{b}) + \sqrt{(Y - \bar{a})^2 + (X + \bar{b})^2}} \right] \quad (3.2)
\end{aligned}$$

As a check on the validity of equation (3.1) the following two cases were evaluated:

Case 1: For $\bar{b} = \bar{a}$ and $X = Y = 0$, equation (3.1) reduces to

$$\bar{w} = \frac{16}{\pi} P\bar{a} \ln(1 + \sqrt{2}) \quad (3.3)$$

Equation (3.3) represents the elastic deformation at the center of a square of uniform pressure. This equation is in agreement with that shown by Timoshenko and Goodier (1951).

Case 2: For $\bar{b} = \bar{a}$ and $X = Y = \bar{a}$, equation (3.1) reduces to

$$\bar{w} = \frac{8}{\pi} P\bar{a} \ln(1 + \sqrt{2}) \quad (3.4)$$

Equation (3.4) represents the elastic deformation at the corner of a square of uniform pressure. This equation is also in agreement with that of Timoshenko and Goodier (1951). From equations (3.3) and (3.4) we find the corner deformation to be one-half the deformation at the center of a square block of pressure.

Now the elastic deformation (\bar{w}) in equation (3.1) represents the elastic deformation at a point (X,Y) due to a rectangular area $2\bar{a} \times 2\bar{b}$ of uniform pressure (p). If the contact ellipse is divided into a number of equal rectangular areas, the total deformation at a point (X,Y) due to the contributions of the various rectangular areas

the pressure distribution developed during contact of an ellipsoidal and a plane solid (as those described in fig. 2.2(b)) that are unlubricated. Hertz found this pressure distribution to be semiellipsoidal, and for any arbitrary point within the contact ellipse it can be described by the following equation:

$$P(\bar{X}, \bar{Y}) = \frac{3F}{2\pi E' ab} \sqrt{1 - \left(\frac{\bar{Y} - a}{a}\right)^2 - \left(\frac{\bar{X} - b}{b}\right)^2} \quad (3.9)$$

Note that the coordinate system common to figure 3.3 is used in equation (3.9). Inside the contact area the pressure was assumed to be described by equation (3.9); outside the contact area it was assumed to be zero. Therefore, for example, from figure 3.3, $P_{3,4}$ would be equivalent to the dimensionless pressure (P) from equation (3.9) evaluated at $\bar{X} = 5\bar{b}$ and $\bar{Y} = 7\bar{a}$.

3.3 Film Thickness

By making use of equations (2.5) and (2.9) developed in chapter 2 the exact geometric separation between the ellipsoidal solid and the plane shown in figure 2.2(b) for the coordinate system developed in figure 3.3 can be written as

$$\bar{S} = R_x - \sqrt{R_x^2 - (\bar{X} - b)^2} + R_y - \sqrt{R_y^2 - (\bar{Y} - a)^2} \quad (3.10)$$

As discovered in chapter 2, if $2R_x \gg S_x$ and $2R_y \gg S_y$, an approximate expression for the separation between the solid and plane shown in figure 2.2(b) can be written as

$$S = \frac{(\bar{X} - b)^2}{2R_x} + \frac{(\bar{Y} - a)^2}{2R_y} \quad (3.11)$$

The degree to which the approximate equation (3.11) represents the exact separation of the ellipsoidal solid and plane is determined by the following ratio:

$$R_1 = \frac{S}{S} \quad (3.12)$$

The film thickness in an elastohydrodynamic lubricated point

contact can be written as

$$h(\bar{X}, \bar{Y}) = h_o + S(\bar{X}, \bar{Y}) + w(\bar{X}, \bar{Y}) \quad (3.13)$$

where

h_o constant

$S(\bar{X}, \bar{Y})$ the approximate geometric separation of the ellipsoidal solid and plane

$w(\bar{X}, \bar{Y})$ elastic deformation

The significance of the elastic deformation relative to the geometric separation of the ellipsoidal solid and plane can be expressed as

$$R_2 = \frac{w}{S} \quad (3.14)$$

3.4 Conditions Investigated

Figure 3.3 shows that we need to be concerned with the following questions:

(1) How fine must the divisions of a and b be? In this chapter we assume that the number of divisions of a and b will be the same. Therefore, we can define the number of divisions as

$$d = \frac{a}{2a} = \frac{b}{2b} \quad (3.15)$$

In this thesis we let d equal 3, 4, and 5.

(2) How far from the semimajor and semiminor axes does R_2 (eq. (3.14)) become insignificant? In this study R_2 was evaluated at distances from the center of the contact of four times the semimajor and semiminor axes.

To check the accuracy of the elastic deformation results for d of 3, 4, and 5, the number of equal divisions along the semimajor and semiminor axes was increased by three times (d of 9, 12, and 15), and then corresponding points were compared. The following equation describes the percentage accuracy of the results compared with the finest-mesh-size predictions:

$$R_3 = \left(\frac{w_d - w_{3d}}{w_{3d}} \right) \times 100 \quad (3.16)$$

The limiting conditions that were evaluated on a computer are shown in table 3.1. It was speculated that conclusions that could be made for these limiting conditions could also be made for any intermediate conditions. The four limiting conditions shown in table 3.1 are two extremes of applied normal load; a light load of 8.964 newtons (2 lbf), and a heavy load of 896.4 newtons (200 lbf). The two extremes of curvature of the solids shown in table 3.1 are equal spheres in contact and a ball and outer race of a ball bearing. The elliptical eccentricity parameter ($k = a/b$) is 1 for the equal spheres in contact and 5 for the ball and outer race.

The equations thus far developed were programmed on the Leeds University International Computers Limited (ICL) model 1906A digital computer.

3.5 Discussion of Results

Tables 3.2 to 3.13 give the characteristics of the deformed shape of the contacting solids along the semimajor and semiminor axes when the axes are divided into three, four, and five equal divisions and the conditions of table 3.1 prevail. Some observations can be made about these tables:

(1) Because of the coarse grid and the elliptical pressure profile, there is not much decrease in pressure in going from the innermost to the outermost point within the contact area.

(2) The agreement of \bar{S} with S is seen to be good and is borne out by the ratio of the two expressed in terms of R_1 . The biggest disagreement is in table 3.7 where $R_1 = 0.9870$, which means that \bar{S} is in agreement with S within 1.3 percent. Because of this good agreement, S will be used to define the geometric separation of the ellipsoidal solid near a plane.

(3) The ratio R_2 of the elastic deformation to the geometric separation of the contacting solids is seen to decrease substantially with increasing distance from the center of the contact zone. Furthermore, the predictions of the distance at which the elastic deformation becomes insignificant compared with the geometric separation of the solids do not change whether we have two equal spheres or a sphere and an outer race in contact.

(4) The separation due to the geometry of the contacting solids plus the elastic deformation ($S + w$) is almost constant in the contact zone. The value of ($S + w$) at the farthest point from the center of the contact zone and yet still within it differs the most from the other values of ($S + w$) in the contact zone.

(5) The percentage difference in elastic deformation calculations for two mesh sizes differing by a factor of 3 was shown to be small. For the worst case in table 3.11, R_3 was equal to 7.494 percent. That is, the elastic deformation for $d = 3$ differs from the elastic deformation at corresponding points when $d = 9$ by 7.5 percent, which is extremely good.

(6) Comparing table 3.2 with 3.5, 3.3 with 3.6, and so forth, which amounts to changing the normal applied load from 8.964 newtons (2 lbf) to 896.4 newtons (200 lbf), leads to the following conclusions:

(a) R_2 does not change in the corresponding tables. That is, regardless of the normal applied load, the ratio of the elastic deformation to the geometric separation of the solids is unchanged.

(b) R_3 does not change in the corresponding tables. This condition is undoubtedly because of the condition mentioned in (a).

To better illustrate the results shown in the tables, figures 3.4 to 3.9 are presented. In figures 3.4 to 3.6 the solid curves represent the case of equal spheres in contact, which is represented

by $R_x = R_y = 0.5558$ cm (0.2188 in.); and the dashed curves represent the ball and outer race in contact, which is represented by $R_x = 1.286$ cm (0.5055 in.), $R_y = 15.00$ cm (5.906 in.). Also as a result of the observation made in discussing the tables that R_2 and R_3 are not functions of the normal applied load, the results shown in figures 3.4 to 3.6 apply for any normal applied load.

Figures 3.4(a) and (b) show the effects of the location along the semimajor and semiminor axes, respectively, on the percentage difference in elastic deformation for d of 3 and 9. Here an "edge effect" can be seen, which is a rapid rise in percentage difference in the film thickness when $d = 3$ and for corresponding points when $d = 9$. This rapid rise is due to the pressure being either zero if the center of the rectangular area shown in figure 3.3 is outside the contact zone or of the order of 10^5 if the center of the rectangular area is within the contact zone. However, it is speculated that in lubricated contacts, where the pressure gradients are, in general, more gradual than those encountered near the edge of a dry Hertzian contact, this edge effect is likely to be less significant. Also note that outside the contact zone the value of R_3 decreases.

Figures 3.5(a) and (b) show the effect of the location along the semimajor and semiminor axes, respectively, on the percentage difference in elastic deformation for d of 3, 4, and 5 and the more exact elastic deformation for d of 9, 12, and 15. These figures show a large drop in R_3 from $d = 4$ to $d = 5$, which also brings down the edge effect considerably. There is, therefore, a good case for letting $d = 5$ in any further computer evaluations.

Figures 3.6(a) and (b) show the effect of the location along the semimajor and semiminor axes, respectively, on the ratio of the elastic deformation to the geometric separation of the ellipsoidal solid near a plane. These figures show the distance from the semimajor and

semiminor axes at which the elastic deformation becomes insignificant. To be more specific, from the curves we see that for equal spheres in contact (represented by solid lines in the figures) $R_2 < 0.05$ corresponds to $x > 2.6 b$ and $y > 2.6 a$. Thus, the elastic deformation is less than 5 percent of the geometric separation at a distance from the center of the contact zone that is no less than 2.6 times the semimajor or semiminor axis. For the ball and outer race in contact, $R_2 < 0.05$ corresponds to $y > 1.9 a$ and $x > 4.0 b$. In other words, the elastic deformation is less than 5 percent of the geometric separation at a distance of only 1.9 times the semimajor axis and 4.0 times the semiminor axis from the center of the contact zone.

Figures 3.7(a) and (b) show the effect of the location along the semimajor and semiminor axes, respectively, on the geometric separation of the ellipsoidal solid near a plane plus the elastic deformation when the load is 8.964 and 896.4 newtons (2 and 200 lbf) and the ellipticity parameter (k) is 1 and 5. The conditions mentioned in this figure correspond to those of table 3.1. These figures show the sum of the film thickness components to be essentially constant within the contact zone.

Figure 3.8 shows the effect of the number of divisions across the ellipse axes on the computer time for running all four conditions shown in table 3.1. Here we see that the computer run time quickly becomes exorbitant as d is increased. This is why only selected data for R_3 were obtained.

3.6 Concluding Remarks

A numerical analysis of the elastic deformation of a contacting ellipsoidal solid and plane has been performed. The analysis assumed that the pressure in the contact zone was Hertzian. It also assumed that the contact zone could be divided into rectangular areas

with uniform pressure within each rectangular area. The resulting equations were programmed on a digital computer. Four limiting conditions were evaluated on the computer. They consist of two extremes of applied normal load: a light load of 8.964 newtons (2 lbf), and a heavy load of 896.4 newtons (200 lbf). The two other extremes are of the curvature of the contacting solids: two equal spheres in contact, and a ball and outer race of a ball bearing. It was speculated that conclusions that could be made for the limiting conditions could also be made for any intermediate condition.

The results indicate that division of the semimajor and semiminor axes into five equal subdivisions is adequate to obtain accurate elastic deformation results. Also the elastic deformation becomes insignificant compared with the geometric separation of a sphere near a plane at a distance from the center of 2.6 times the semimajor axis. For a ball and outer race in contact, a similar observation applied at a distance from the center of 1.9 times the semimajor axis and 4.0 times the semiminor axis. Finally, the geometric separation plus the elastic deformation ($S + w$) was almost constant in the contact region. However, numerical values of ($S + w$) at points near the edge of the Hertzian contact show that a slight edge effect or error may be encountered in such regions. In lubricated contacts, where the pressure gradients are, in general, more gradual than those encountered near the edge of a dry Hertzian contact, this effect is likely to be less significant.

CHAPTER 4
THEORETICAL FORMULATION OF THE ELASTOHYDRODYNAMIC
LUBRICATION PROBLEM

The elastic deformation model was developed, along with an appropriate nodal structure, in chapter 3. The theoretical formulation of the elastohydrodynamic lubrication problem is given in this chapter. The procedure here is to give the Navier-Stokes equations of motion as well as the continuity equation. Then with the assumptions that are imposed on the problem, these equations are reduced to the Reynolds equation. The pressure-viscosity formula of Roelands (1966) is used. In the numerical analysis of the Reynolds equation, a ϕ analysis (where ϕ is equal to the pressure times the film thickness to the 3/2 power) is used to help the relaxation process. A standard finite difference representation is applied to the various terms in the Reynolds equation. By applying a Gauss-Seidel relaxation method to the finite difference form of the Reynolds equation, a converged solution of ϕ for the complete nodal structure is obtained. When ϕ is known, the pressure at the various nodes can be obtained. When the pressure is known, the integrated load is calculated, and adjustments are made for the initially guessed film constant (H_0) until the integrated load and the input load are in agreement. A flow chart of the computer program is given, as well as the complete computer FORTRAN listing.

4.1 Reynolds Equation

The derivation of the Reynolds equation governing the pressure distribution in an elastohydrodynamic lubricated (EHL) conjunction

is based on the Navier-Stokes equations of motion and the continuity equation. The most general form of the Navier-Stokes equations of motion for a Newtonian fluid in Cartesian coordinates as obtained from Pai (1956) is

$$\rho \frac{Du}{Dt} = \tilde{X} - \frac{\partial p}{\partial X} + \frac{2}{3} \frac{\partial}{\partial X} \left[\eta \left(2 \frac{\partial u}{\partial X} - \frac{\partial v}{\partial Y} - \frac{\partial \tilde{w}}{\partial Z} \right) \right] + \frac{\partial}{\partial Y} \left[\eta \left(\frac{\partial v}{\partial X} + \frac{\partial u}{\partial Y} \right) \right] + \frac{\partial}{\partial Z} \left[\eta \left(\frac{\partial \tilde{w}}{\partial X} + \frac{\partial u}{\partial Z} \right) \right] \quad (4.1)$$

$$\rho \frac{Dv}{Dt} = \tilde{Y} - \frac{\partial p}{\partial Y} + \frac{2}{3} \frac{\partial}{\partial Y} \left[\eta \left(2 \frac{\partial v}{\partial Y} - \frac{\partial u}{\partial X} - \frac{\partial \tilde{w}}{\partial Z} \right) \right] + \frac{\partial}{\partial X} \left[\eta \left(\frac{\partial v}{\partial X} + \frac{\partial u}{\partial Y} \right) \right] + \frac{\partial}{\partial Z} \left[\eta \left(\frac{\partial \tilde{w}}{\partial Y} + \frac{\partial v}{\partial Z} \right) \right] \quad (4.2)$$

$$\rho \frac{D\tilde{w}}{Dt} = \tilde{Z} - \frac{\partial p}{\partial Z} + \frac{2}{3} \frac{\partial}{\partial Z} \left[\eta \left(2 \frac{\partial \tilde{w}}{\partial Z} - \frac{\partial u}{\partial X} - \frac{\partial v}{\partial Y} \right) \right] + \frac{\partial}{\partial X} \left[\eta \left(\frac{\partial \tilde{w}}{\partial X} + \frac{\partial u}{\partial Z} \right) \right] + \frac{\partial}{\partial Y} \left[\eta \left(\frac{\partial v}{\partial Z} + \frac{\partial \tilde{w}}{\partial Y} \right) \right] \quad (4.3)$$

where

$$\frac{D}{Dt} = \frac{\partial}{\partial t} + u \frac{\partial}{\partial X} + v \frac{\partial}{\partial Y} + \tilde{w} \frac{\partial}{\partial Z} \quad (4.4)$$

In equations (4.1), (4.2), and (4.3) the left side corresponds to the inertia terms and the right side contains the body force, pressure, and viscous terms, in that order. The following assumptions are made in solving the EHL point-contact problem:

- (1) No external forces act on the film. Thus,

$$\tilde{X} = \tilde{Y} = \tilde{Z} = 0$$

- (2) Fluid inertia is small when compared with viscous shear.

These inertia forces are associated with acceleration of the fluid.

Thus,

$$\frac{Du}{Dt} = \frac{Dv}{Dt} = \frac{D\tilde{w}}{Dt} = 0$$

- (3) There is no variation of pressure across the fluid film.

Thus,

$$\frac{\partial p}{\partial Z} = 0$$

(4) The viscosity (η) and density (ρ) are constant in the \bar{z} direction.

(5) The radius of curvature of the solids bounding the oil film is large when compared with the thickness of the lubricant films. This assumption allows any effects due to curvature of the oil film to be neglected.

(6) There is no slip between the fluid and bounding solids at common boundaries. Thus,

$$\bar{z} = 0, \quad u = u_A, \quad v = 0$$

$$\bar{z} = h, \quad u = u_B, \quad v = 0$$

(7) Because of the geometry of the fluid film, the derivatives of u and v with respect to \bar{z} are large when compared with all other velocity gradients.

(8) Steady-state conditions are considered.

With these assumptions, the Navier-Stokes equations of motion (eqs. (4.1), (4.2), and (4.3)) reduce to the following:

$$\frac{\partial p}{\partial X} = \eta \frac{\partial^2 u}{\partial \bar{z}^2} \quad (4.5)$$

$$\frac{\partial p}{\partial Y} = \eta \frac{\partial^2 v}{\partial \bar{z}^2} \quad (4.6)$$

$$\frac{\partial p}{\partial \bar{z}} = 0 \quad (4.7)$$

The velocity distributions (u) and (v) can be found by integrating equations (4.5) and (4.6) twice while using the boundary conditions according to assumption 6.

The equation of continuity, representing mass conservation, is

$$\frac{\partial(\rho u)}{\partial X} + \frac{\partial(\rho v)}{\partial Y} = 0 \quad (4.8)$$

Coupling the velocity distributions with the equation of continuity leads to the following equation, which was developed by Reynolds (1886) and carries his name:

$$\frac{\partial}{\partial \bar{X}} \left(\frac{\rho h^3}{\eta} \frac{\partial p}{\partial \bar{X}} \right) + \frac{\partial}{\partial \bar{Y}} \left(\frac{\rho h^3}{\eta} \frac{\partial p}{\partial \bar{Y}} \right) = 12 \bar{u} \frac{\partial}{\partial \bar{X}} (\rho h) \quad (4.9)$$

where

$$\bar{u} = \frac{u_A + u_B}{2}$$

Letting

$$\left. \begin{aligned} X^* &= \frac{\bar{X}}{b}, & Y^* &= \frac{\bar{Y}}{a}, & \bar{\rho} &= \frac{\rho}{\rho_0} \\ \bar{\eta} &= \frac{\eta}{\eta_0}, & H &= \frac{h}{R_x}, & P &= \frac{p}{E'} \end{aligned} \right\} \quad (4.10)$$

equation (4.9) can be rewritten as

$$\frac{\partial}{\partial X^*} \left(\frac{\bar{\rho} H^3}{\bar{\eta}} \frac{\partial P}{\partial X^*} \right) + \frac{1}{k^2} \frac{\partial}{\partial Y^*} \left(\frac{\bar{\rho} H^3}{\bar{\eta}} \frac{\partial P}{\partial Y^*} \right) = 12U \left(\frac{b}{R_x} \right) \frac{\partial (\bar{\rho} H)}{\partial X^*} \quad (4.11)$$

where

k ellipticity parameter, a/b

U dimensionless speed parameter, $\eta_0 \bar{u} / E' R_x$

Equation (4.11) is the Reynolds equation in dimensionless form. The normal requirement is for dimensionless parameter (P) to be determined. Before proceeding, however, the dimensionless density ($\bar{\rho}$), the dimensionless viscosity ($\bar{\eta}$), and the dimensionless film thickness (H) need to be formulated.

4.2 Density

At the high pressures that exist in the elastohydrodynamic lubricating film, the liquid can no longer be considered as an incompressible medium, and the dependence of the density on the pressure must be considered. From Dowson and Higginson (1966) the dimensionless density for mineral oil can be written as

$$\bar{\rho} = 1 + \frac{0.009 p}{1 + 0.026 p} \quad (4.12)$$

where

p gage pressure, ton/in.²

Therefore, the general expression for the dimensionless density can be written as

$$\bar{\rho} = 1 + \frac{\gamma PE'}{1 + \beta PE'} \quad (4.13)$$

where β and γ are constants dependent on the fluid.

4.3 Viscosity

As long ago as 1893, Barus proposed the following formula for the isothermal viscosity-pressure dependence of liquids:

$$*\ln\left(\frac{\eta}{\eta_0}\right) = \alpha p \quad (4.14)$$

where

η dynamic viscosity at gage pressure (p)

η_0 dynamic viscosity at atmospheric pressure

α pressure-viscosity coefficient of lubricant

The pressure-viscosity coefficient (α) in equation (4.14) characterizes the liquid considered and depends only on temperature, not on pressure. Although equation (4.14) is extensively used, it is not generally applicable and is valid as a reasonable approximation only in a moderate pressure range.

Because of the shortcomings of equation (4.14), several isothermal viscosity-pressure formulae have been proposed that usually contain two or more parameters instead of Barus's (1893) single parameter. One of these approaches, which is used in this thesis, is that of Roelands (1966), who undertook a wide-ranging study of the effect of pressure upon the viscosity of the lubricant. For isothermal conditions, the Roelands (1966) formula (p. 95) can be written as

$$\log \eta + 1.200 = (\log \eta_0 + 1.200) \left(1 + \frac{p}{2000}\right)^Z \quad (4.15)$$

* \log denotes the common or Briggsian logarithm, \log_{10} ;
 \ln denotes the natural or Napierian logarithm, \log_e .

where

p gage pressure, kgf/cm^2

Z viscosity-pressure index, a dimensionless constant

Taking the antilog of both sides of equation (4.15) gives

$$\eta = 10^{(\log \eta_0 + 1.2) \left(1 + \frac{p}{2000}\right)^Z - 1.2}$$

Rearranging this equation yields

$$\eta = \eta_0 \left(1 + \frac{p}{2000}\right)^Z \times 10^{1.2 \left[\left(1 + \frac{p}{2000}\right)^Z - 1\right]}$$

For the dimensionless form of the viscosity given in equation (4.10), this equation becomes

$$\bar{\eta} = \frac{\eta}{\eta_0} = \eta_0 \left[\left(1 + \frac{p}{2000}\right)^Z - 1\right] \times 10^{1.2 \left[\left(1 + \frac{p}{2000}\right)^Z - 1\right]}$$

Rearranging terms in this equation gives

$$\bar{\eta} = \left(\frac{\eta_\infty}{\eta_0}\right) \left[1 - \left(1 + \frac{pE'}{\delta}\right)^Z\right] \quad (4.16)$$

where

$$\eta_\infty = 6.31 \times 10^{-5} \text{ N s/m}^2 (0.0631 \text{ cP})$$

and δ is a constant equal to $19\,609 \text{ N/cm}^2$ ($28\,440 \text{ lbf/in.}^2$).

In equations (4.13) and (4.16), care must be taken to ensure that the same dimensions are used in defining the constants.

In the Roelands (1966) formulation the lubricant is defined by the atmospheric viscosity (η_0), the viscosity-pressure index (Z), and the asymptotic isoviscous pressure ($p_{iv,as}$). The equation describing the asymptotic isoviscous pressure can be written as

$$p_{iv,as} = \eta_0 \int_0^{\infty} \frac{dp}{\eta} \quad (4.17)$$

Blok (1964) arrived at the very important conclusion that all EHL results achieved hitherto for an exponential viscosity-pressure de-

pendence (eq. (4.14)) can, to a fair approximation, be generalized for any given nonexponential dependence simply by substituting the reciprocal of the asymptotic isoviscous pressure ($1/p_{iv,as}$) for the viscosity-pressure coefficient (α) occurring in those results. This implies that

$$\alpha \approx \frac{1}{p_{iv,as}} \quad (4.18)$$

It might be pointed out how the values of the parameters η_0 , Z , and $p_{iv,as}$ are obtained for a given lubricant by using the Roelands (1966) formulation. From table II-1 (p. 48 of Roelands (1966)), for a paraffinic mineral oil, coded 31-G, the atmospheric viscosity (η_0) is found to be 41.1 centipoise. From table IV-2 (p. 106 of Roelands (1966)), for the same lubricant the viscosity-pressure index (Z) is found to be 0.67. When the atmospheric viscosity (η_0) is known, the following expression can be evaluated:

$$\log(\log \eta_0 + 1.2) = 0.4493$$

Making use of this equation in table XII-2 (p. 452 of Roelands (1966)) for $Z = 0.67$ leads to

$$\log p_{iv,as} = 2.695$$

$$\therefore p_{iv,as} = 4859 \text{ N/cm}^2$$

This, then, establishes the procedure used to obtain the parameters η_0 , Z , and $p_{iv,as}$ for a given lubricant.

4.4 Film Thickness

As was stated in chapter 2, the separation due to the geometry of the two ellipsoidal solids shown in figure 2.1 can be adequately described by an equivalent ellipsoidal solid near a plane. The geometric requirement is that the separation of the ellipsoidal solids in the initial and equivalent situations should be the same at equal values of \bar{X} and \bar{Y} . Therefore, from figure 4.1, the separation due to the geometry of the two ellipsoids shown in figure 2.1 can be

written for an ellipsoidal solid near a plane as

$$s(\bar{X}, \bar{Y}) = \frac{(\bar{X} - mb)^2}{2R_x} + \frac{(\bar{Y} - \ell a)^2}{2R_y} \quad (4.19)$$

where

m constant used to specify length of inlet region

ℓ constant used to specify length of side-leakage region

For purposes of illustration the mesh described in figure 4.1 will still be used, where $m = 4$ and $\ell = 2$. However, the equations developed will be written in general terms.

Figure 4.2 gives a physical description of the film thickness and its components for an ellipsoidal solid near a plane. Equation (3.13) describes how the components are related in describing the film thickness. In figure 4.2 it is assumed that \bar{Y} is held constant near the midplane of the contact.

Substituting equation (4.19) into equation (3.13) while at the same time making this equation dimensionless as in equation (4.10) gives

$$H = H_0 + \frac{b^2(X^* - m)^2}{2R_x^2} + \frac{a^2(Y^* - \ell)^2}{2R_x R_y} + \frac{w(X^*, Y^*)}{R_x} \quad (4.20)$$

where H_0 is a constant that is initially estimated.

In chapter 3 the elastic deformation (w in eq. (4.20)) of an equivalent ellipsoidal solid near a plane in contact and subjected to a Hertzian stress distribution has been evaluated numerically.

Therefore, by using figure 4.1 and the results of chapter 3, the elastic deformation can be written as

$$w_{k, \bar{z}}(X^*, Y^*) = \frac{2}{n} \sum_{j=1, 2, \dots}^{2\ell \times c} \sum_{i=1, 2, \dots}^{(m+n) \times \ell} P_{i, j} D_{m, n} \quad (4.21)$$

where

n constant used to determine length of outlet region

c number of equal divisions in semimajor axis (in fig. 4.1, $c = 5$)

d number of equal divisions in semiminor axis (in fig. 4.1, $d = 5$)

$$\bar{m} = |\bar{k} - i| + 1$$

and

$$\bar{n} = |\bar{l} - j| + 1$$

$$\begin{aligned}
 D = & b \left(X^* + \frac{1}{2d} \right) \ln \left[\frac{k \left(Y^* + \frac{1}{2c} \right) + \sqrt{k^2 \left(Y^* + \frac{1}{2c} \right)^2 + \left(X^* + \frac{1}{2d} \right)^2}}{k \left(Y^* - \frac{1}{2c} \right) + \sqrt{k^2 \left(Y^* - \frac{1}{2c} \right)^2 + \left(X^* + \frac{1}{2d} \right)^2}} \right] \\
 & + a \left(Y^* + \frac{1}{2c} \right) \ln \left[\frac{\left(X^* + \frac{1}{2d} \right) + \sqrt{k^2 \left(Y^* + \frac{1}{2c} \right)^2 + \left(X^* + \frac{1}{2d} \right)^2}}{\left(X^* - \frac{1}{2d} \right) + \sqrt{k^2 \left(Y^* + \frac{1}{2c} \right)^2 + \left(X^* - \frac{1}{2d} \right)^2}} \right] \\
 & + b \left(X^* - \frac{1}{2d} \right) \ln \left[\frac{k \left(Y^* - \frac{1}{2c} \right) + \sqrt{k^2 \left(Y^* - \frac{1}{2c} \right)^2 + \left(X^* - \frac{1}{2d} \right)^2}}{k \left(Y^* + \frac{1}{2c} \right) + \sqrt{k^2 \left(Y^* + \frac{1}{2c} \right)^2 + \left(X^* - \frac{1}{2d} \right)^2}} \right] \\
 & + a \left(Y^* - \frac{1}{2c} \right) \ln \left[\frac{\left(X^* - \frac{1}{2d} \right) + \sqrt{k^2 \left(Y^* - \frac{1}{2c} \right)^2 + \left(X^* - \frac{1}{2d} \right)^2}}{\left(X^* + \frac{1}{2d} \right) + \sqrt{k^2 \left(Y^* - \frac{1}{2c} \right)^2 + \left(X^* + \frac{1}{2d} \right)^2}} \right] \quad (4.22)
 \end{aligned}$$

Equation (4.23) points out more explicitly the meaning of equation (4.21) while making use of figure 4.1. The elastic deformation at the center of the rectangular area $w_{9,5}$ (fig. 4.1) caused by the pressure on the various rectangular areas in an around the contact ellipse can be written as

$$w_{9,5} = \frac{2}{\pi} \left[\begin{array}{l} P_{1,1} D_{9,5} + P_{2,1} D_{8,5} + \dots + P_{35,1} D_{27,5} \\ + P_{1,2} D_{9,4} + P_{2,2} D_{8,4} + \dots + P_{35,2} D_{27,4} \\ \vdots \\ + P_{1,20} D_{9,16} + P_{2,20} D_{8,16} + \dots + P_{35,20} D_{27,16} \end{array} \right] \quad (4.23)$$

4.5 Phi (ϕ) Solution

Having defined the density, viscosity, and film thickness, we can return to the problem of solving the Reynolds equation. It is

well known (e.g., Whomes (1966)) that the dimensionless pressure (P) of the Reynolds equation plotted as a function of X^* exhibits a very localized pressure field, giving high values of $\partial P / \partial X^*$ and $\partial^2 P / \partial X^{*2}$. Such a condition with high gradients is not welcomed when performing a numerical analysis by means of relaxation methods. In order to produce a much gentler curve, a parameter (ϕ) is introduced, where

$$\phi = PH^{3/2} \quad (4.24)$$

The pressure (P) is small at large values of film thickness (H) and conversely. This substitution also has the advantage of eliminating all terms containing derivatives of products of H and P or H and ϕ . Therefore, by using equation (4.24), equation (4.11) can be written as

$$\frac{\partial}{\partial X^*} \left[\frac{\rho}{\eta} \left(H^{3/2} \frac{\partial \phi}{\partial X^*} - \frac{3}{2} \phi H^{1/2} \frac{\partial H}{\partial X^*} \right) \right] + \frac{1}{k} \frac{\partial}{\partial Y^*} \left[\frac{\rho}{\eta} \left(H^{3/2} \frac{\partial \phi}{\partial Y^*} - \frac{3}{2} \phi H^{1/2} \frac{\partial H}{\partial Y^*} \right) \right] = 12U \left(\frac{b}{R_x} \right) \frac{\partial (\bar{\rho} H)}{\partial X^*}$$

Expanding this equation yields

$$H^{3/2} \left[\frac{\partial}{\partial X^*} \left(\frac{\rho}{\eta} \frac{\partial \phi}{\partial X^*} \right) + \frac{1}{k} \frac{\partial}{\partial Y^*} \left(\frac{\rho}{\eta} \frac{\partial \phi}{\partial Y^*} \right) \right] - \frac{3\phi}{2} \left[\frac{\partial}{\partial X^*} \left(\frac{\rho}{\eta} H^{1/2} \frac{\partial H}{\partial X^*} \right) + \frac{1}{k} \frac{\partial}{\partial Y^*} \left(\frac{\rho}{\eta} H^{1/2} \frac{\partial H}{\partial Y^*} \right) \right] = 12U \left(\frac{b}{R_x} \right) \frac{\partial (\bar{\rho} H)}{\partial X^*} \quad (4.25)$$

4.6 Finite Difference Representation

The finite difference method will be used to develop the various terms in equation (4.25). Figure 4.3 shows the mesh to be used as related to the dimensionless coordinates X^* and Y^* . Equation (4.25) must be written for the point (i, j) in figure 4.3 by substituting, for the derivatives, expressions that involve values of ρ , H , ϕ , and η at the surrounding points.

At the three points $X_{i-1, j}^*$, $X_{i, j}^*$, and $X_{i+1, j}^*$, a function of X^* such as ρ can be represented by a parabola, where

$$\psi = A(X^*)^2 + BX^* + C \quad (4.26)$$

The parabola and corresponding points are shown in figure 4.4. The expressions for $\psi_{i-1,j}$, $\psi_{i,j}$, and $\psi_{i+1,j}$ can be written directly from equation (4.26) as

$$\psi_{i-1,j} = A(X_{i-1,j}^*)^2 + BX_{i-1,j}^* + C \quad (4.27)$$

$$\psi_{i,j} = A(X_{i,j}^*)^2 + BX_{i,j}^* + C \quad (4.28)$$

$$\psi_{i+1,j} = A(X_{i+1,j}^*)^2 + BX_{i+1,j}^* + C \quad (4.29)$$

From figure 4.4 the following equations can be written:

$$X_{i,j}^* = X_{i-1,j}^* + \frac{1}{d}$$

$$X_{i+1,j}^* = X_{i-1,j}^* + \frac{2}{d}$$

Substituting these expressions into equations (4.28) and (4.29) gives

$$\psi_{i,j} = A\left(X_{i-1,j}^* + \frac{1}{d}\right)^2 + B\left(X_{i-1,j}^* + \frac{1}{d}\right) + C \quad (4.30)$$

$$\psi_{i+1,j} = A\left(X_{i-1,j}^* + \frac{2}{d}\right)^2 + B\left(X_{i-1,j}^* + \frac{2}{d}\right) + C \quad (4.31)$$

Therefore, given equations (4.27), (4.30), and (4.31), it is possible to solve for A, B, and C to give

$$A = \frac{d^2}{2} (\psi_{i+1,j} - 2\psi_{i,j} + \psi_{i-1,j}) \quad (4.32)$$

$$B = \frac{d}{2} (4\psi_{i,j} - 3\psi_{i-1,j} - \psi_{i+1,j}) - 2AX_{i-1,j}^* \quad (4.33)$$

$$C = \psi_{i-1,j} - BX_{i-1,j}^* - A(X_{i-1,j}^*)^2 \quad (4.34)$$

The following derivatives can be written by using equations (4.32), (4.33), and (4.34):

$$\frac{\partial \psi_{i-1,j}}{\partial X_{i-1,j}^*} = 2AX_{i-1,j}^* + B = B' = 0.5 d(4\psi_{i,j} - 3\psi_{i-1,j} - \psi_{i+1,j}) \quad (4.35)$$

$$\frac{\partial \psi_{i,j}}{\partial X_{i,j}^*} = 2AX_{i,j}^* + B = 2A\left(X_{i-1,j}^* + \frac{1}{d}\right) + B = 2AX_{i-1,j}^* + B + \frac{2A}{d} = B' + \frac{2A}{d} \quad (4.36)$$

$$\therefore \frac{\partial \psi_{i,j}}{\partial X_{i,j}^*} = 0.5 d(\psi_{i+1,j} - \psi_{i-1,j}) \quad (4.37)$$

$$\begin{aligned} \frac{\partial \psi_{i+1,j}}{\partial X_{i+1,j}^*} &= 2AX_{i+1,j}^* + B = 2A \left(X_{i-1,j}^* + \frac{2}{d} \right) + B = \\ &0.5 d(3\psi_{i+1,j} - 4\psi_{i,j} + \psi_{i-1,j}) \end{aligned} \quad (4.38)$$

$$\frac{\partial^2 \psi_{i-1,j}}{\partial X_{i-1,j}^{*2}} = \frac{\partial^2 \psi_{i,j}}{\partial X_{i,j}^{*2}} = \frac{\partial^2 \psi_{i+1,j}}{\partial X_{i+1,j}^{*2}} = 2A = d^2(\psi_{i+1,j} - 2\psi_{i,j} + \psi_{i-1,j}) \quad (4.39)$$

Having developed these basic equations with the dummy variable (ψ), we can now proceed to develop the various terms in equation (4.25) by using the finite difference format developed in this section. The following equation is written for the point i,j :

$$\begin{aligned} \frac{\partial}{\partial X^*} \left(\frac{\partial}{\partial \eta} H^{1/2} \frac{\partial H}{\partial X^*} \right) &= 0.5 d \left[\frac{\partial}{\partial \eta} \frac{i+1,j}{i+1,j} \sqrt{H_{i+1,j}} \left(\frac{\partial H}{\partial X^*} \right)_{i+1,j} \right. \\ &\quad \left. - \frac{\partial}{\partial \eta} \frac{i-1,j}{i-1,j} \sqrt{H_{i-1,j}} \left(\frac{\partial H}{\partial X^*} \right)_{i-1,j} \right] \end{aligned} \quad (4.40)$$

From equations (4.38) and (4.39) the following equations can be written:

$$\left(\frac{\partial H}{\partial X^*} \right)_{i+1,j} = 0.5 d(3H_{i+1,j} - 4H_{i,j} + H_{i-1,j}) \quad (4.41)$$

$$\left(\frac{\partial H}{\partial X^*} \right)_{i-1,j} = 0.5 d(-H_{i+1,j} + 4H_{i,j} - 3H_{i-1,j}) \quad (4.42)$$

Substituting equations (4.41) and (4.42) into (4.40) gives

$$\begin{aligned} \frac{\partial}{\partial X^*} \left(\frac{\partial}{\partial \eta} H^{1/2} \frac{\partial H}{\partial X^*} \right) &= 0.25 d^2 \left[\frac{\partial}{\partial \eta} \frac{i+1,j}{i+1,j} \sqrt{H_{i+1,j}} (3H_{i+1,j} - 4H_{i,j} + H_{i-1,j}) \right. \\ &\quad \left. + \frac{\partial}{\partial \eta} \frac{i-1,j}{i-1,j} \sqrt{H_{i-1,j}} (H_{i+1,j} - 4H_{i,j} + 3H_{i-1,j}) \right] \end{aligned} \quad (4.43)$$

Thus, the following equations can be directly written:

$$\frac{\partial}{\partial X^*} \left(\frac{\bar{\rho}}{\bar{\eta}} \frac{\partial \phi}{\partial X^*} \right) = 0.25 d^2 \left[\frac{\bar{\rho}_{i+1,j}}{\bar{\eta}_{i+1,j}} (3\phi_{i+1,j} - 4\phi_{i,j} + \phi_{i-1,j}) \right. \\ \left. + \frac{\bar{\rho}_{i-1,j}}{\bar{\eta}_{i-1,j}} (\phi_{i+1,j} - 4\phi_{i,j} + 3\phi_{i-1,j}) \right] \quad (4.44)$$

$$\frac{\partial}{\partial X^*} (\bar{\rho}H) = 0.5 d (\bar{\rho}_{i+1,j} H_{i+1,j} - \bar{\rho}_{i-1,j} H_{i-1,j}) \quad (4.45)$$

The derivatives with respect to Y^* can be obtained directly by substituting c for d , the subscript $i,j-1$ and $i-1,j$, and the subscript $i,j+1$ for $i+1,j$.

$$\frac{\partial}{\partial Y^*} \left(\frac{\bar{\rho}}{\bar{\eta}} H^{1/2} \frac{\partial H}{\partial Y^*} \right) = 0.25 c^2 \left[\frac{\bar{\rho}_{i,j+1}}{\bar{\eta}_{i,j+1}} \sqrt{H_{i,j+1}} (3H_{i,j+1} - 4H_{i,j} + H_{i,j-1}) \right. \\ \left. + \frac{\bar{\rho}_{i,j-1}}{\bar{\eta}_{i,j-1}} \sqrt{H_{i,j-1}} (H_{i,j+1} - 4H_{i,j} + 3H_{i,j-1}) \right] \quad (4.46)$$

$$\frac{\partial}{\partial Y^*} \left(\frac{\bar{\rho}}{\bar{\eta}} \frac{\partial \phi}{\partial Y^*} \right) = 0.25 c^2 \left[\frac{\bar{\rho}_{i,j+1}}{\bar{\eta}_{i,j+1}} (3\phi_{i,j+1} - 4\phi_{i,j} + \phi_{i,j-1}) \right. \\ \left. + \frac{\bar{\rho}_{i,j-1}}{\bar{\eta}_{i,j-1}} (\phi_{i,j+1} - 4\phi_{i,j} + 3\phi_{i,j-1}) \right] \quad (4.47)$$

Substituting equations (4.43) to (4.47) into equation (4.25) while collecting terms gives

$$\bar{A}_{i,j} \phi_{i+1,j} + \bar{B}_{i,j} \phi_{i,j-1} + \bar{C}_{i,j} \phi_{i-1,j} + \bar{D}_{i,j} \phi_{i,j+1} - \bar{L}_{i,j} \phi_{i,j} - \bar{M}_{i,j} = 0 \quad (4.48)$$

where

$$\mu = \frac{\bar{\rho}}{\bar{\eta}} \quad (4.49)$$

$$\bar{A}_{i,j} = 3\mu_{i+1,j} + \mu_{i-1,j} \quad (4.50)$$

$$\bar{B}_{i,j} = \left(\frac{c}{dk} \right)^2 (\mu_{i,j+1} + 3\mu_{i,j-1}) \quad (4.51)$$

$$\bar{C}_{i,j} = \mu_{i+1,j} + 3\mu_{i-1,j} \quad (4.52)$$

$$\bar{D}_{i,j} = \left(\frac{c}{dk}\right)^2 (3\mu_{i,j+1} + \mu_{i,j-1}) \quad (4.53)$$

$$\begin{aligned} \bar{L}_{i,j} = & 4(\mu_{i+1,j} + \mu_{i-1,j}) + 4\left(\frac{c}{dk}\right)^2 (\mu_{i,j+1} + \mu_{i,j-1}) \\ & + \frac{3}{2H_{i,j}^{3/2}} \left\{ \mu_{i+1,j} \sqrt{H_{i+1,j}} (3H_{i+1,j} - 4H_{i,j} + H_{i-1,j}) \right. \\ & + \mu_{i-1,j} \sqrt{H_{i-1,j}} (H_{i+1,j} - 4H_{i,j} + 3H_{i-1,j}) + \left(\frac{c}{dk}\right)^2 \\ & \times \left[\mu_{i,j+1} \sqrt{H_{i,j+1}} (3H_{i,j+1} - 4H_{i,j} + H_{i,j-1}) \right. \\ & \left. \left. + \mu_{i,j-1} \sqrt{H_{i,j-1}} (H_{i,j+1} - 4H_{i,j} + 3H_{i,j-1}) \right] \right\} \quad (4.54) \end{aligned}$$

$$\bar{M}_{i,j} = \frac{24Ub}{dR_x H_{i,j}^{3/2}} (\bar{\rho}_{i+1,j} H_{i+1,j} - \bar{\rho}_{i-1,j} H_{i-1,j}) \quad (4.55)$$

4.7 Nodal Structure

The nodal structure used in obtaining most of the results is shown in figure 4.5. This nodal structure was arrived at after much exploration in which the number of nodes in the semimajor and semiminor axes, as well as the distance from the center of the contact to the edges of the computing zone, was varied. The nodal structure shown in figure 4.5 was considered to be suitable when the minimum film thickness did not change when either additional nodes were placed in the semimajor and semiminor axes or the distance from the center of the contact to the edges of the computing zone was extended.

From figure 4.5 the following can be written:

$$\left. \begin{aligned} m &= 4 \\ n &= 1.15 \\ \ell &= 1.6 \\ c &= 5 \\ d &= 13 \end{aligned} \right\} \quad (4.56)$$

These values used to define the nodal structure were used for most of the evaluations. One exception was for high-speed cases when the constant used to determine inlet length (m) had to be extended from 4 to 6, with the other values being held constant.

4.8 Boundary Conditions

The boundary conditions are the following:

(1) At the edges of the rectangular computation zone (fig. 4.5) the pressure is zero, which therefore implies that ϕ is also zero. Specifically, this means that along the bottom of figure 4.5, $\phi_{i,1} = 0$; along the left side, $\phi_{1,j} = 0$; along the top, $\phi_{i,16} = 0$; and along the right side, $\phi_{67,j} = 0$.

(2) At the cavitation boundary,

$$P = \frac{\partial P}{\partial X^*} = \frac{\partial P}{\partial Y^*} = 0$$

This condition is commonly known as the Reynolds condition and will be satisfied by simply resetting $\phi_{i,j}$ to zero whenever it occurs as a negative value.

4.9 Initial Conditions

Outside the Hertzian contact ellipse the pressure is initially assumed to be zero, and therefore ϕ is also equal to zero. That is, $\phi = 0$ when

$$(X^* - m)^2 + (Y^* - \ell)^2 \geq 1$$

Inside the Hertzian contact ellipse the pressure is initially assumed to be Hertzian; that is,

$$P = \frac{3F}{2\pi abE'} \sqrt{1 - (X^* - m)^2 - (Y^* - \ell)^2} \quad (4.57)$$

or

$$\phi = \frac{3FH^{3/2}}{2\pi abE'} \sqrt{1 - (X^* - m)^2 - (Y^* - \ell)^2} \quad (4.58)$$

when

$$(X^* - m)^2 + (Y^* - \ell)^2 < 1$$

4.10 Relaxation Method

If the subscript n is the iterant and $\phi_{i,j}$ is the particular solution to be found, the relaxation method known as the Gauss-Seidel method can be expressed as

$$\phi_{i,j,n+1} = \phi_{i,j,n} - \lambda \left(\frac{\bar{M}_{i,j} - \bar{A}_{i,j} \phi_{i+1,j,n} - \bar{B}_{i,j} \phi_{i,j-1,n+1} - \bar{C}_{i,j} \phi_{i-1,j,n+1} - \bar{D}_{i,j} \phi_{i,j+1,n}}{L_{i,j}} + \phi_{i,j,n} \right) \quad (4.59)$$

where λ is an overrelaxation factor that is initially set to 1.6. Therefore, equation (4.59) is used, starting with node (2,2) and then continuing with (3,2), . . . , until (M,2) followed by (2,3), (3,3), . . . , (M,3), and ending with (2,N), (3,N) . . . , (M,N), where

$$\left. \begin{aligned} M &= (n + m)d - 1 \\ N &= 2lc - 1 \end{aligned} \right\} \quad (4.60)$$

The relaxation procedure described by equation (4.59) is continued until

$$\sum_{j=2,3,\dots}^N \sum_{i=2,3,\dots}^M \frac{|\phi_{i,j,n+1} - \phi_{i,j,n}|}{\phi_{i,j,n+1}} < 0.1$$

4.11 Pressure Loop

The relaxation method provides values of $\phi_{i,j}$ for every point within the mesh. Having determined $\phi_{i,j}$, we can write the dimensionless pressure as

$$P_{i,j} = \phi_{i,j} (H_{i,j})^{-3/2} \quad (4.61)$$

With these new values of the dimensionless pressure, new values of the dimensionless viscosity, density, and film thickness can be evaluated. Thus, the coefficients of equation (4.59)

$(\bar{A}_{i,j}, \bar{B}_{i,j}, \dots, \bar{L}_{i,j})$ should also change. Accordingly, it is necessary to reenter the relaxation loop. This process is continued until the following inequality is satisfied:

$$\sum_{j=2,3,\dots}^N \sum_{i=2,3,\dots}^M \frac{|P_{i,j,n+1} - P_{i,j,n}|}{P_{i,j,n+1}} < 0.1$$

4.12 Normal Applied Load

The constant H_0 in equation (4.20) was initially estimated. The next task is then to find the correct value for H_0 . In order to do this, the integrated normal applied load must be evaluated, where

$$\bar{F} = E'ab \int_0^{m+n} \int_0^{2\ell} P \, dY \, dX \quad (4.62)$$

By applying Simpson's rule, this double integral can be rewritten as

$$F = \frac{4E'ab}{9cd} \begin{bmatrix} 2(P_{2,2} + P_{2,3} + 2P_{2,4} + P_{2,5} + \dots + 2P_{2,2\ell-2} + P_{2,2\ell-1}) \\ + (2P_{3,2} + P_{3,3} + 2P_{3,4} + P_{3,5} + \dots + 2P_{3,2\ell-2} + P_{3,2\ell-1}) \\ \vdots \\ + 2(P_{m+n-2,2} + P_{m+n-2,3} + 2P_{m+n-2,4} + P_{m+n-2,5} + \dots + 2P_{m+n-2,2\ell-2} + P_{m+n-2,2\ell-1}) \\ + (2P_{m+n-1,2} + P_{m+n-1,3} + 2P_{m+n-1,4} + P_{m+n-1,5} + \dots + 2P_{m+n-1,2\ell-2} + P_{m+n-1,2\ell-1}) \end{bmatrix}$$

This equation can be written simply as

$$\bar{F} = \frac{4E'ab}{9cd} \sum_{i=2,3,\dots}^{m+n-1} 2^{q_1} \left(\sum_{j=2,3,\dots}^{2\ell-1} 2^{q_2} P_{i,j} \right) \quad (4.63)$$

where

$$\begin{aligned} q_1 &= 0 & \text{if } i \text{ is odd} \\ q_1 &= 1 & \text{if } i \text{ is even} \\ q_2 &= 0 & \text{if } j \text{ is odd} \\ q_2 &= 1 & \text{if } j \text{ is even} \end{aligned}$$

By using the trapezoidal rule, the normal applied load can also be expressed as

$$\bar{F} = \frac{E'ab}{cd} \sum_{i=2,3,\dots}^{m+n-1} \sum_{j=2,3,\dots}^{2\ell-1} P_{ij} \quad (4.64)$$

Both equations (4.63) and (4.64) were programmed to serve as a check on one another.

When the current values of H_o and \bar{F} (eq. (4.63)), as well as the initial normal applied load (F) are known, a new estimate for (H_o) can be expressed as

$$\bar{H}_o = H_o \left(\frac{F}{\bar{F}} \right)^{0.13} \quad (4.65)$$

With a new value for H_o the film thickness (eq. (4.20)) is recalculated, and reentry into the relaxation process is required. This process is continued until the following convergence is satisfied:

$$\frac{|\bar{F} - F|}{F} < 0.0005$$

Once this convergence criterion has been satisfied, the pressure and film thickness in and around a point contact are established.

4.13 Flow Charts

Figures 4.6 and 4.7 are flow charts for the numerical solution on the digital computer of the equations developed in the analysis. Figure 4.6 is the flow chart of the main program. There are essentially three loops within the main program: In the relaxation loop, $\phi_{i,j,n+1}$ is generated. In the pressure loop, the new values of $\phi_{i,j,n+1}$ of the relaxation loop result in new values of pressure $P_{i,j,n+1}$, which in turn result in new values of film thickness $H_{i,j}$, new values of viscosity $\bar{\eta}_{i,j}$, and new values of density $\bar{\rho}_{i,j}$. The final loop is the normal-load loop, which ensures that the integrated normal applied load agrees with the initially specified value.

Figure 4.7 is the flow chart of the subroutine SUB6. Here it can be seen that a number of calculations occur only once and need not be repeated on reentering this subroutine. With a new pressure

distribution the elastic deformation is recalculated and this subroutine is left with a new film thickness and, therefore, a new $\phi_{i,j,n+i}$. The FORTRAN listings of the main and SUB6 computer programs are given in the appendix. The FORTRAN listings of the EHL point-contact analysis were programmed on the NASA Lewis Research Center's Sperry Univac 1100/42 computer, which has 131 K primary memory and 262 K extended memory.

4.14 Concluding Remarks

In this chapter a procedure for the numerical solution of the complete, isothermal, elastohydrodynamic lubrication problem for point contacts is given. This procedure calls for the simultaneous solution of the elasticity and Reynolds equations. In the elasticity analysis the contact zone was divided into equal rectangular areas. It was assumed that a uniform pressure was applied over each area. In the numerical analysis of the Reynolds equation the parameter $\phi = PH^{3/2}$, where P is the dimensionless pressure and H the dimensionless film thickness, was introduced in order to help the relaxation process. The nodal structure, boundary conditions, and initial conditions were given and a Gauss-Seidel relaxation method was used. The computer program has three major loops: the relaxation loop, the pressure loop, and the normal-load loop. The last loop requires the integrated load to be in agreement with the input load within some tolerance. Upon the convergence of all three loops the pressure and film thickness in and around a point contact are established.

CHAPTER 5

FULLY FLOODED RESULTS

The most important practical aspect of the elastohydrodynamic lubrication (EHL) point-contact theory developed in chapter 4 is the determination of the minimum film thickness within the contact. That is, maintaining a fluid film of adequate magnitude is extremely important to the operation of some machine elements. In the present chapter the influence of contact geometry as expressed in the ellipticity parameter and the dimensionless speed, load, and material parameters on minimum film thickness is investigated for a conjunction fully immersed in lubricant (i.e., fully flooded). In the numerical work the ellipticity parameter is varied from 1 (a ball-on-plate configuration) to 8 (a configuration approaching a line contact). The dimensionless speed and load parameters are varied over ranges of about two and one orders of magnitude, respectively. Conditions equivalent to using solid materials of bronze, steel, and silicon nitride and lubricants of paraffinic and naphthenic mineral oils are considered in obtaining the exponent on the dimensionless material parameter. Thirty-four different cases are used in obtaining the fully flooded minimum-film-thickness formula. A central-film-thickness formula is also developed.

In this chapter, contour plots are shown that indicate in detail the pressure spike and the two side lobes in which the minimum film thickness occurs. These theoretical solutions for film thickness have all the essential features of previously reported experimental observations based on optical interferometry.

5.1 Dimensionless Grouping

The variables resulting from the isothermal EHL point-contact theory developed in chapter 4 are

R_x	effective radius in x-direction, mm
R_y	effective radius in y-direction, mm
h	film thickness, mm
E'	effective elastic modulus, N/mm^2
$P_{iv,as}$	asymptotic isoviscous pressure obtained from Roelands (1966), N/mm^2
u	surface velocity in x-direction, mm/sec
η_0	atmospheric viscosity, $N \cdot sec/mm^2$
Z	viscosity pressure index, a dimensionless constant
F	normal applied force, N
α, β	constants used to define density of fluid, mm^2/N

It has been found by Dowson and Higginson (1966) that density has little effect on minimum film thickness for line-contact situations; therefore, one may assume the same is true for point-contact situations. Even though the compressibility effect is still considered in the EHL theory developed in chapter 4, the constants used to define the fluid in the density equation will not be used in the minimum-film-thickness formulation. Therefore, the 11 variables mentioned above were reduced to nine, α and β being eliminated. From the nine variables the following five dimensionless groupings can be written:

(1) Dimensionless film thickness

$$H = \frac{h}{R_x} \quad (5.1)$$

where

$$\frac{1}{R_x} = \frac{1}{r_{Ax}} + \frac{1}{r_{Bx}} \quad (5.2)$$

The radii of curvature in equation (5.2) are shown in figure 2.1.

(2) Dimensionless load parameter

$$W = \frac{F}{E' R_x^2} \quad (5.3)$$

where

$$E' = \frac{2}{\left(\frac{1 - \nu_A^2}{E_A} + \frac{1 - \nu_B^2}{E_B} \right)} \quad (5.4)$$

(3) Dimensionless speed parameter

$$U = \frac{\eta_0 u}{E' R_x} \quad (5.5)$$

where

$$u = \frac{(u_A + u_B)}{2} \quad (5.6)$$

(4) Dimensionless material parameter

$$G = \frac{E'}{p_{iv,as}} \quad (5.7)$$

where $p_{iv,as}$ is the asymptotic isoviscous pressure obtained from Roelands (1966). The asymptotic isoviscous pressure can be approximated by the inverse of the pressure-viscosity coefficient

($p_{iv,as} \approx 1/\alpha$).

(5) Ellipticity parameter

$$k = \frac{a}{b} \quad (5.8)$$

where

a semimajor axis of contact ellipse

b semiminor axis of contact ellipse

The ellipticity parameter is determined entirely from the definition of the radii of curvature (r_{Ax} , r_{Bx} , r_{Ay} , and r_{By}), and the derivation can be found in chapter 2.

The dimensionless film thickness can be written as

$$H = f(k, U, W, G) \quad (5.9)$$

The most important practical aspect of the EHL point-contact theory developed in chapter 4 is the determination of the minimum film thickness within the conjunction. Therefore, in the fully flooded results to be presented in this chapter the dimensionless parameters (k , U , W , and G) will be varied and the effect upon minimum film thickness will be studied.

5.2 Effect of Ellipticity Parameter

The ellipticity parameter (k) is a function of the radii of curvature of the solids only (r_{Ax} , r_{Bx} , r_{Ay} , and r_{By}). The radii of curvature in the x -direction for both solids A and B are used in defining the dimensionless speed and load parameters. Therefore, only the radius of curvature of solid B in the y -direction will be changed in varying the ellipticity parameter from 1 (a ball-on-plate configuration) to 8 (a configuration approaching a line contact). In doing this the dimensionless speed (U), load (W), and material (G) parameters were held constant at the following values:

$$\left. \begin{aligned} U &= 0.168 \times 10^{-11} \\ W &= 0.1106 \times 10^{-6} \\ G &= 4522 \end{aligned} \right\} \quad (5.10)$$

Care was taken to ensure that the highest ellipticity parameter ($k = 8$) was in the elastic region. The approach used was to relate the operating conditions for this near-line-contact situation to the elastic region defined in figure 5.1, which was obtained from Dowson and Whitaker (1965). From this figure the elastic, intermediate, and rigid regions are defined for $G = 5000$ (which is very close to the value of G in eq. (5.10)) and for various values of dimensionless speed (U) and dimensionless load (W_D). The dimensionless speed (U) in Dowson and Whitaker (1965) is exactly that used in this thesis. The dimensionless load (W_D) used in figure 5.1 differs from that used in this thesis, and a tie between the two must be developed. The

dimensionless load parameter as defined by Dowson and Whitaker (1965) is

$$W_D = \frac{\bar{F}}{E'R_x} \quad (5.11)$$

where

$$\bar{F} = \frac{\text{Force}}{\text{Unit length}}$$

Therefore, in relating this to an elliptical contact in which the ellipticity parameter (k) is large compared with unity, a dimensionless load parameter can be written as

$$W_D = \frac{F}{2aE'R_x} \quad (5.12)$$

For this equation and $k = 8$ the location of U and W_D is shown by a circular symbol in figure 5.1. As can be seen, it lies within the elastic region. Thus, for the conditions given in equation (5.10) and for an ellipticity parameter (k) of 8, the conjunction is truly elastohydrodynamic. For k less than 8 the results move further into the elastic region.

Table 5.1 gives 10 values of k and the corresponding minimum film thickness (H_{\min}) as obtained from the EHL point-contact theory developed in chapter 4. Having these 10 pairs of data, the object is to determine an equation that describes how the ellipticity parameter affects the minimum film thickness. The general form of this equation can be written as

$$\left(1 - \frac{H_{\min}}{H_{\min,L}}\right) = \bar{A}e^{\bar{B}k} \quad (5.13)$$

A least-square exponential curve fit to the 10 pairs of data points

$$\left[k_i, \left(1 - \frac{H_{\min}}{H_{\min,L}}\right)_i \right], \quad i=1, \dots, 10$$

was used in obtaining values for \bar{A} and \bar{B} in equation (5.13).

Besides a least-square fit a coefficient of determination (r^2) is

obtained. The value of r^2 reflects the fit of the data to the resulting equation: 1 being a perfect fit, and zero the worst possible fit. The minimum film thickness for a line contact ($H_{\min,L}$) used in equation (5.13) was determined by finding the $H_{\min,L}$ that gives a coefficient of determination closest to 1. The line-contact minimum film thickness was thus deduced from the present set of results for the limiting case in which the ellipticity parameter (k) approached infinity. This value of $H_{\min,L}$ turned out to be 7.082×10^{-6} with a corresponding coefficient of determination of 0.9990, which is an excellent fit. Furthermore, the values of \tilde{A} and \tilde{B} in equation (5.13) as obtained from the least-square fit are

$$\tilde{A} = 0.9966 \approx 1.00 \quad (5.14)$$

$$\tilde{B} = -0.6752 \approx -0.68 \quad (5.15)$$

From equations (5.13), (5.14), and (5.15) the following proportionality can be written, which shows the effect of ellipticity parameter on minimum film thickness:

$$\tilde{H}_{\min} \propto (1 - e^{-0.68 k}) \quad (5.16)$$

where $\tilde{H}_{\min} = h_{\min}/R_x$, predicted by the relationship that gives the best least-square fit to the numerical solutions. It is most significant that \tilde{A} turns out to be 0.9966, or approximately 1.00, since as $k \rightarrow 0$, $H_{\min} \rightarrow 0$. Therefore, even though the smallest value of k used in obtaining equation (5.16) was unity, it would seem that equation (5.16) could be applied to smaller values since in the limiting case ($k \rightarrow 0$), equation (5.16) satisfies the physical situation. For the other extreme of large k , a line-contact situation is approached and the agreement with existing results is again good. From Dowson and Higginson (1966) the line-contact minimum film thickness for the dimensionless parameters given in equation (5.10) is 7.720×10^{-6} . Compare this with 7.082×10^{-6} from the present results. The difference of 9 percent could well be the result of

Dowson and Higginson (1966) using an exponential pressure-viscosity relationship instead of the Roelands (1966) formulation used in the present work.

Substituting equations (5.14) and (5.15) into equation (5.13) gives H_{\min} , the dimensionless minimum film thickness obtained from the least-square formulation. The \tilde{H}_{\min} for the 10 ellipticity parameters are given in table 5.1. The percentage difference between the minimum film thickness obtained from EHL point-contact theory (H_{\min}) and the minimum film thickness from the least-square-fit equation (\tilde{H}_{\min}) is expressed as

$$D_1 = \left(\frac{H_{\min} - \tilde{H}_{\min}}{H_{\min}} \right) 100 \quad (5.17)$$

Note that in table 5.1 the magnitude of D_1 never exceeds +3 percent.

Figures 5.2 to 5.10 give contour plots of pressure and film thickness for ellipticity parameters of 8, 6, 4, 3, 2.5, 2, 1.75, 1.5, and 1.25, respectively. In these figures the other dimensionless parameters (U , G , W) were held fixed, as described in equation (5.10). In parts (a) of these figures, contour plots of dimensionless pressure are given; in parts (b), contour plots of dimensionless film thickness are given; and in parts (c), three-dimensional representations of pressure are given. The + symbol in parts (a) and (b) indicates the center of the Hertzian contact. Note that, because of the dimensionless representation of the coordinates, the actual Hertzian contact ellipse becomes a circle regardless of the value of the ellipticity parameter. The Hertzian contact circle is shown in each of parts (a) and (b) by asterisks. At the top of each part the contour label and the corresponding value are given. The inlet region is to the left and the exit region is to the right.

For an ellipticity parameter (k) of 8, the maximum pressure is near the center of the contact (fig. 5.2(a)); and even though the conditions are in the elastic region, no pressure spike occurs. As the ellipticity parameter is decreased (going from fig. 5.2(a) to 5.5(a)) the maximum pressure moves to the right (i.e., downstream of the center of the Hertzian conjunction) and increases in value. In decreasing the ellipticity parameter even more (going from fig. 5.6(a) to 5.10(a)) the label of the pressure spike goes from A to C although the numerical values of the contours are different in each case. The pressure gradient is much larger at the exit end of the conjunction than at the inlet region. The pressure distribution is seen even more dramatically in figures 5.2(c), 5.3(c), . . . , 5.10(c), corresponding to ellipticity parameters of 8, 6, . . . , 1.25. The three-dimensional representation of pressure shows the details of the pressure spike more clearly.

Figures 5.2(b), 5.3(b), . . . , 5.10(b) show contour plots of film thickness when the ellipticity parameter (k) is 8, 6, 4, 3, 2.5, 2, 1.75, 1.5, and 1.25, respectively. For $k = 8$ the minimum film thickness is in a small area directly behind the axial center of the contact. As k is decreased the minimum film area moves away from the axial center of the contact. For $k = 1.25$, two minimum-film-thickness areas occur at the sides nearer the edge of the Hertzian circle. These results, showing the "side lobes" in which minimum-film-thickness areas occur, produce all the essential features of previously reported experimental observations based upon optical interferometry.

Figures 5.11(a) and (b) show the variation of pressure and film thickness, respectively, in the X -direction close to the midplane

of the contact for three values of the ellipticity parameter. As has been true for all the ellipticity parameter results presented, the values of the dimensionless speed, load, and material parameters were held fixed as per equation (5.10). In figure 5.11(a) we find that for $k = 6$ no spike occurs, but this well-known feature of theoretical solutions to the elastohydrodynamic problem is evident for $k = 2.5$ and $k = 1.25$.

In figure 5.11(b) for $k = 1.25$ the central region is not parallel with the \bar{X} -axis. The reason is probably that compressibility effects are considered in the theory developed in chapter 4. That is, when compressibility is considered, the film thickness in the center is reduced by the amount that the fluid volume decreases at high pressure.

5.3 Influence of Speed

By changing only the surface velocity in the x -direction (u) the dimensionless speed parameter (U) (eq. (5.5)) changes, but the other dimensionless parameters (k , W , and G) remain constant. The values at which these dimensionless parameters were held constant in the calculations are

$$\left. \begin{array}{l} k = 6 \\ W = 0.7371 \times 10^{-6} \\ G = 4522 \end{array} \right\} \quad (5.18)$$

Table 5.2 gives the dimensionless speed parameter (U) and the corresponding minimum film thickness (H_{\min}) as obtained from the EHL point-contact theory developed in chapter 4. There are 15 different values of the dimensionless speed parameter covering nearly two orders of magnitude. Having these 15 pairs of data, the objective is to determine an equation that describes how the dimensionless speed affects the minimum film thickness. The general form of this

equation can be written as

$$H_{\min} = IU^K \quad (5.19)$$

By applying a least-square power fit to the 15 pairs of data $\{(U_i, H_{\min,i}), i = 1, \dots, 15\}$, the values of I and K were found to be

$$I = 560.18 \quad (5.20)$$

$$K = 0.67542 \approx 0.68 \quad (5.21)$$

The coefficient of determination (r^2) for these results was excellent at 0.9998. Substituting equations (5.20) and (5.21) into equation (5.19) gives the values of \tilde{H}_{\min} shown in table 5.2. The percentage difference (D_1) between the minimum film thickness obtained from the EHL point-contact theory (H_{\min}) and the minimum film thickness obtained from the least-squares fit (\tilde{H}_{\min}) is expressed in equation (5.17) and given in table 5.2. Note that the variation of D_1 is less than ± 2 percent.

From equations (5.21) and (5.19) the effect of dimensionless speed on dimensionless minimum film thickness can be written as

$$\tilde{H}_{\min} \propto U^{0.68} \quad (5.22)$$

Figures 5.12 to 5.26 give contour plots of pressure and film thickness for dimensionless speed parameters ranging from 5.050×10^{-11} to 8.416×10^{-13} . The other dimensionless parameters (k , W , and G) were held fixed as described in equation (5.18). As was true for the ellipticity results, contour plots of pressure and film thickness are designated a and b , respectively, and three-dimensional representations of pressure are designated c .

In figure 5.12(a) the maximum-pressure area is near the center of the contact. As the dimensionless speed is decreased to and including $U = 5.892 \times 10^{-12}$ (fig. 5.21(a)), the maximum-pressure area moves downstream to the right. For dimensionless speeds greater than $U = 5.892 \times 10^{-12}$ the maximum-pressure area moves back toward the cen-

ter of the contact. Note that the "spike" pressure exceeds the Hertzian maximum pressure at $U = 5.892 \times 10^{-12}$, but at smaller speeds (e.g., $U = 4.208 \times 10^{-12}$) the Hertzian pressure is dominant. Also note in these figures that the pressure in the inlet region is higher at high speeds than at low speeds.

In figure 5.12(b), a high-speed situation, two minimum-film-thickness areas appear midway between the center of the contact and the Hertzian circle. As the speed decreases, the two minimum-film-thickness areas reduce to one, which is located at the axial center of the contact. With further reductions of speed the minimum-film-thickness area still remains in the axial center but moves closer to the Hertzian circle.

In figure 5.12(c) a three-dimensional representation of the pressure for the highest speed case is shown. Here no pressure spike occurs, and the pressure rises to a peak that was shown in figure 5.12(a) to be near the center of the contact. As the speed is reduced the pressure spike emerges, and the top of the pressure profile becomes flatter. Once the pressure spike occurs, it moves toward the exit of the conjunction as the speed decreases.

Figures 5.27(a) and (b) show the variation of pressure and film thickness, respectively, on the \bar{X} -axis at the midplane of the conjunction for three values of dimensionless speed parameter. In figure 5.27(a) the dashed line corresponds to the Hertzian pressure distribution. Figure 5.27(a) shows that the pressure in the inlet region is higher for the high-speed ($U = 5.050 \times 10^{-11}$) profile. For $U = 0.8416 \times 10^{-11}$ and $U = 0.08416 \times 10^{-11}$, the pressure spike originates very near to the Hertzian pressure, and as the speed increases the pressure spike moves upstream.

The typical elastohydrodynamic film shape with an essentially parallel section in the central region is shown in figure 5.27(b).

Also there is a considerable change in film thickness as the dimensionless speed is changed, as indicated by equation (5.22). This illustrates most clearly the dominant effect of the dimensionless speed parameter (U) upon the minimum film thickness in elastohydrodynamic contacts.

5.4 Influence of Load

By changing only the normal applied load (F) in equation (5.3) the dimensionless load parameter (W) changes while the remaining dimensionless parameters (k , U , and G) remain constant. The values at which these parameters were held constant are

$$\left. \begin{aligned} k &= 6 \\ U &= 0.1683 \times 10^{-11} \\ G &= 4522 \end{aligned} \right\} \quad (5.23)$$

Table 5.3 gives the dimensionless load parameter (W) and the corresponding minimum film thickness (H_{\min}) as obtained from the EHL point-contact theory developed in chapter 4. There are eight different values of the dimensionless load parameter, covering over an order of magnitude. Having these eight pairs of data, the objective is to determine an equation that describes how the dimensionless load affects the minimum film thickness. The general form of this equation can be written as

$$H_{\min} = QW^L \quad (5.24)$$

By applying a least-square power fit to the eight pairs of data $\{(W_i, H_{\min,i}), i = 1, \dots, 8\}$, the values of Q and L were found to be

$$Q = 2.1592 \times 10^{-6} \quad (5.25)$$

$$L = -0.072924 \approx -0.073 \quad (5.26)$$

The coefficient of determination (r^2) for these results was 0.9260, which was good, but was the lowest obtained in deriving the minimum-film-thickness equation (5.33). Substituting equations (5.25) and

(5.26) into equation (5.24) gives the values of \tilde{H}_{\min} shown in table 5.3. The percentage difference (D_1) between the minimum film thickness obtained from the EHL point-contact theory (H_{\min}) and the minimum film thickness from the least-square-fit equation (\tilde{H}_{\min}) is expressed in equation (5.17) and given in table 5.3. In table 5.3 the variation of D_1 is within ± 3 percent at all times.

From equations (5.24) and (5.26) the effect of load on minimum film thickness can be written as

$$\tilde{H}_{\min} \propto W^{-0.073} \quad (5.27)$$

Figures 5.28 to 5.35 give contour plots of pressure and film thickness for dimensionless loads ranging from 0.1106×10^{-6} to 1.290×10^{-6} . The other dimensionless parameters (k , U , and G) were held fixed as described in the relationship (5.23). Once again, in parts (a) of these figures, contour plots of pressure are given; in parts (b), film thickness contours are presented; and in parts (c), three-dimensional representations of pressure are given.

In figure 5.28(a) the maximum pressure occurs directly behind the center of the contact, with no pressure spike occurring. As the load is increased the pressure spike emerges. With further increases of load the pressure spike moves toward the exit of the conjunction. These results can be more clearly seen in the three-dimensional representation given in parts (c) of figures 5.28 to 5.35.

In figure 5.28(b), the low-load case, the minimum film thickness occurs directly behind the center of the contact. As the load is increased the minimum-film-thickness area still remains in the axial center of the contact but closer to the Hertzian circle. With further increases of load, two minimum-film-thickness areas appear equidistance from the axial center and closer to the Hertzian circle. In figure 5.35(b), the highest load case considered, the minimum

film thickness is off to the sides in two areas close to the Hertzian circle.

The variation of pressure and film thickness in the \bar{X} -direction along a line close to the midplane of the conjunction is shown in figure 5.36 for three values of the dimensionless load parameter. The values of the dimensionless speed, material, and ellipticity parameters were held fixed as described by equation (5.23) for all computations at various loads. In figure 5.36(a) note that as the dimensionless load is increased the inlet pressure becomes smaller. For the highest load case shown in figure 5.36(b), film thickness rises between the central region and the outlet restriction in the same manner as seen in figure 5.11(b). Again this is attributed to compressibility effects of the fluid. Also note that at a load of $W = 0.5528 \times 10^{-6}$ the film thickness is slightly smaller than at a load of $W = 1.106 \times 10^{-6}$. The reason is that at the lower load the minimum film thickness is closer to the axial center of the contact than at the higher load. As was pointed out in discussing figures 5.18(b) to 5.35(b), the location of the minimum-film-thickness region changes as the dimensionless load is changed.

5.5 Effect of Material Properties

Contrary to what was found in the previous three sections, the effect of the dimensionless material parameter on minimum film thickness is not a simple matter. As can be seen from equations (5.3), (5.5), and (5.7), when either the material of the solids (as expressed in E') or the lubricant (as expressed in η_0 and $p_{iv,as}$) is varied, not only does the material parameter (G) change, but so do the dimensionless speed (U) and load (W) parameters. Only the ellipticity parameter can be held fixed. For all the results presented in this section the ellipticity parameter is held fixed at a value of 6.

Table 5.4 gives the four material-parameter results. The general form showing how the minimum film thickness is a function of the dimensionless material parameter is given as

$$\tilde{C} = TG^V \quad (5.28)$$

where

$$\tilde{C} = \frac{H_{\min}}{(1 - e^{-0.68 k})U^{0.68}W^{-0.073}} \quad (5.29)$$

Note in equation (5.29) that the exponents are rounded off to two significant figures so that any error could be absorbed in T given in equation (5.28). By applying a least-square power fit to the four pairs of data, the values of T and V were found to be

$$T = 3.6891 \quad (5.30)$$

$$V = 0.48669 \approx 0.49 \quad (5.31)$$

The coefficient of determination for these results was 0.9980, which is excellent. Substituting equations (5.30) and (5.31) into equation (5.28) gives the values of \tilde{H}_{\min} shown in table 5.4. The percentage difference (D_1) shown in table 5.4 varies by only 2 percent at all times. Therefore, from equations (5.28) and (5.31) the effect of the dimensionless material parameter on the dimensionless film thickness can be written as

$$\tilde{H}_{\min} \propto G^{0.49} \quad (5.32)$$

5.6 Minimum-Film-Thickness Formula

The proportionality expressions (5.16), (5.22), (5.27), and (5.32) establish how the minimum film thickness varies with the ellipticity, speed, load, and material parameters, respectively. This enables a composite minimum-film-thickness formula for a fully flooded, isothermal, elastohydrodynamic point contact to be written as

$$\tilde{H}_{\min} = 3.63 U^{0.68} G^{0.49} W^{-0.073} (1 - e^{-0.68 k}) \quad (5.33)$$

In equation (5.33) the constant 3.63 is different from that in equa-

tion (5.30) to account for rounding off the material-parameter exponent.

Table 5.5 gives the 34 different cases used in obtaining equation (5.33). In this table, H_{\min} corresponds to the minimum film thickness obtained from the EHL point-contact theory developed in chapter 4, and \tilde{H}_{\min} is the minimum film thickness obtained from equation (5.33). The percentage difference between these two values is expressed by D_1 , which is defined in equation (5.17). In table 5.5 the values of D_1 are within ± 5 percent.

It is sometimes more convenient to express the side-leakage factor in equation (5.33) in terms of the radius of curvature ratio (R_y/R_x) instead of the ellipticity parameter (k) through the following relationship:

$$k = 1.03 \left(\frac{R_y}{R_x} \right)^{0.64} \quad (5.34)$$

where

$$\frac{1}{R_y} = \frac{1}{r_{Ay}} + \frac{1}{r_{By}} \quad (5.35)$$

$$\frac{1}{R_x} = \frac{1}{r_{Ax}} + \frac{1}{r_{Bx}} \quad (5.36)$$

A least-square power fit was used in obtaining equation (5.34). This equation is valid for R_y/R_x between 1 and 40. The coefficient of determination associated with this power fit was 0.9997, which is excellent.

Using equation (5.34) avoids the need to evaluate elliptic integrals of the first and second kind in the determination of k . The minimum film thickness can thus be derived directly from a knowledge of the radii of curvature of the contacting bodies (r_{Ax} , r_{Bx} , r_{Ay} , and r_{By}).

It is interesting to compare the new point-contact, minimum-

film-thickness formula (eq. (5.33)) with the corresponding equation generated by Dowson (1968) for line contacts

$$H_{\min,L} = 2.65 U^{0.70} G^{0.54} W^{-0.13} \quad (5.37)$$

The powers of U , G , and W in equations (5.33) and (5.37) are quite similar considering the different numerical procedures upon which they are based. It is also worth noting that the power (W) in equation (5.33) is extremely close to the value of -0.074 proposed by Archard and Cowking (1966) in their study of point contacts.

5.7 Central-Film-Thickness Formula

There is interest in knowing the central film thickness, in addition to the minimum film thickness, in elastohydrodynamic contacts. In this section a central film thickness will be formulated. The procedure used in obtaining the central film thickness is the same as that used in obtaining the minimum film thickness.

Table 5.6 gives 10 values of the ellipticity parameter (k) and the corresponding central film thickness (H_c) as obtained from the EHL point-contact theory developed in chapter 4. The other dimensionless parameters (U , W , and G) were held constant as defined by the relationship (5.10). Having these 10 pairs of data, the objective is to determine an equation that describes how the ellipticity parameter affects the central film thickness. The general form of this equation can be written as

$$\left(1 - \frac{H_c}{H_{c,L}}\right) = \tilde{I} e^{\tilde{J}k} \quad (5.38)$$

A least-square exponential curve fit to the 10 pairs of data points

$$\left[k_i, \left(1 - \frac{H_c}{H_{c,L}}\right)_i \right], \quad i = 1, \dots, 10$$

was used in obtaining values of \tilde{I} and \tilde{J} in equation (5.38). The value of $H_{c,L}$ in equation (5.38) was found to be 8.69×10^{-6} and was determined by finding the value of $H_{c,L}$ that gives a coefficient of

determination (r^2) closest to 1. The values of \tilde{I} and \tilde{J} in equation (5.38) and the coefficient of determination (r^2) as obtained from the least-square fit are

$$\tilde{I} = 0.61178 \approx 0.61 \quad (5.39)$$

$$\tilde{J} = -0.73377 \approx -0.73 \quad (5.40)$$

$$r^2 = 0.96356 \quad (5.41)$$

The value of the coefficient of determination (r^2) in equation (5.41) is not as good as that obtained for the ellipticity portion of the minimum-film-thickness formula, which was 0.9990. From equations (5.38), (5.39), and (5.40) the following proportionality shows the effect of the ellipticity parameter on central film thickness:

$$\tilde{H}_c \propto (1 - 0.61 e^{-0.73 k}) \quad (5.42)$$

Substituting equations (5.39) and (5.40) into equation (5.38) gives \tilde{H}_c , the dimensionless central film thickness obtained from the least-square formulation. The values of \tilde{H}_c for the 10 values of ellipticity parameter (k) are given in table 5.6. The percentage difference between the central film thickness obtained from the EHL point-contact theory (H_c) and the central film thickness obtained from the least-square fit (\tilde{H}_c) is expressed as

$$D_2 = \left(\frac{\tilde{H}_c - H_c}{H_c} \right) 100 \quad (5.43)$$

Note in table 5.6 that D_2 is within the range $-11\% < D_2 < 4\%$. This is a larger range than that found for the minimum-film-thickness formula, which was +3 percent.

Table 5.7 gives the dimensionless speed parameter (U) and the corresponding central film thickness as obtained from the EHL point-contact theory developed in chapter 4. The values of the other dimensionless parameters (k , W , and G) were held constant as defined in equation (5.18). The general form of the equation that describes how the dimensionless speed affects the central film thickness can

be written as

$$H_c = \tilde{K}U^{\tilde{L}} \quad (5.44)$$

By applying a least-square power fit to the 15 pairs of data $\{(U_i, H_{c,i}), i = 1, \dots, 15\}$, the values of \tilde{K} and \tilde{L} were found to be

$$\tilde{K} = 537.73 \quad (5.45)$$

$$\tilde{L} = 0.66722 \approx 0.67 \quad (5.46)$$

The coefficient of determination (r^2) for these results was 0.9990. Substituting equations (5.45) and (5.46) into equation (5.44) gives the values of \tilde{H}_c shown in table 5.7. The percentage difference (D_2) between the central film thickness obtained from the EHL point-contact theory (H_c) and the central film thickness obtained from the least-square fit (\tilde{H}_c) is expressed in equation (5.43) and given in table 5.7. In table 5.7, D_2 is in the range $-4\% \leq D_2 < 6\%$. This is to be compared to the range of D_1 for the minimum film thickness, which was ± 2 percent.

From equations (5.44) and (5.46) the effect of dimensionless speed on dimensionless central film thickness can be written as

$$\tilde{H}_c \propto U^{0.67} \quad (5.47)$$

Table 5.8 gives the dimensionless load parameter (W) and the corresponding central film thickness (H_c) as obtained from the EHL point-contact theory developed in chapter 4. The values of the other dimensionless parameters (k , U , and G) were held constant as defined in equation (5.23). The general form of the equation that describes how the dimensionless load affects the central film thickness can be written as

$$H_c = \tilde{M}W^{\tilde{N}} \quad (5.48)$$

By applying a least-square power fit to the eight pairs of data $\{(W_i, H_{c,i}), i = 1, \dots, 8\}$, the values of \tilde{M} and \tilde{N} were found

to be

$$\tilde{M} = 2.8508 \times 10^{-6} \quad (5.49)$$

$$\tilde{N} = -0.067248 \approx -0.067 \quad (5.50)$$

The coefficient of determination (r^2) for these results was 0.7303, which is not as good a fit as the 0.9260 obtained for the load portion of the minimum-film-thickness formula. Substituting equations (5.49) and (5.50) into equation (5.48) gives the values of \tilde{H}_c shown in table 5.8. The percentage difference (D_2) between the central film thickness obtained from the EHL point-contact theory (H_c) and the central film thickness obtained from the least-square fit (\tilde{H}_c) is expressed in equation (5.43) and given in table 5.8. In table 5.8, D_2 is ± 5 percent.

From equations (5.48) and (5.50) the effect of dimensionless load on dimensionless central film thickness can be written as

$$\tilde{H}_c \propto W^{-0.067} \quad (5.51)$$

Table 5.9 gives the four material parameters and the corresponding central film thickness (H_c) as obtained from the EHL point-contact theory developed in chapter 4. The ellipticity parameter (k) was held fixed at 6 for the results shown in table 5.9. The general form of the equation that describes how the dimensionless material parameter (G) affects the central film thickness can be written as

$$\tilde{Q} = \tilde{T} \tilde{G}^{\tilde{V}} \quad (5.52)$$

where

$$\tilde{Q} = \frac{H_c}{(1 - 0.61 e^{-0.73 k}) U^{0.67} W^{-0.067}}$$

By applying a least-square power fit to the four pairs of data, the values of \tilde{T} and \tilde{V} were found to be

$$\tilde{T} = 2.6595 \quad (5.53)$$

$$\tilde{V} = 0.52776 \approx 0.53 \quad (5.54)$$

The coefficient of determination (r^2) for these results was 0.9804.

Substituting equations (5.53) and (5.54) into equation (5.52) gives the values of \tilde{H}_c shown in table 5.8. The values of D_2 as expressed in equation (5.43) are shown in table 5.9. In table 5.9, the values of D_2 are within the range of $-4\% < D_2 < 5\%$.

From equations (5.52) and (5.54) the effect of dimensionless material parameter on the dimensionless central film thickness can be written as

$$\tilde{H}_c \propto G^{0.53} \quad (5.55)$$

The proportionality expressions (5.42), (5.47), (5.51), and (5.55) establish how the central film thickness varies with the ellipticity, speed, load, and material parameters, respectively. This enables a composite central-film-thickness formula for a fully flooded isothermal, elastohydrodynamic point contact to be written as

$$\tilde{H}_c = 2.69 U^{0.67} G^{0.53} W^{-0.067} (1 - 0.51 e^{-0.73 k}) \quad (5.56)$$

If it is desired, the side-leakage factor in equation (5.56) can be expressed in terms of the radius-of-curvature ratio (R_y/R_x) instead of the ellipticity parameter (k) by using equation (5.34).

Comparing the central-film-thickness formula (5.56) with the minimum-film-thickness formula (5.33) reveals a slight difference. In equation (5.56) the load exponent is small but negative, as it was for the minimum-film-thickness formula. This is in contrast with the recent numerical study of Ranger et al. (1975), who found a small but positive exponent on the dimensionless load (W) in their formulation of a central film thickness.

Table 5.10 gives the 36 different cases used to obtain equation (5.56). In this table, H_c corresponds to the central film thickness obtained from the EHL point-contact theory developed in chapter 4, and \tilde{H}_c corresponds to the central film thickness obtained from equation (5.56). The percentage difference between these two values is expressed by D_2 , which is defined in equation (5.43).

In table 7.10 the values of D_2 are within ± 10 percent.

5.8 Concluding Remarks

By using the procedures outlined in an earlier chapter the influence of the ellipticity parameter and the dimensionless speed, load, and material parameters on minimum film thickness have been investigated. The ellipticity parameter was varied from 1 (a ball-on-plate configuration) to 8 (a configuration approaching a line contact). The dimensionless speed parameter was varied over a range of nearly two orders of magnitude. The dimensionless load parameter was varied over a range of about one order of magnitude. Situations equivalent to using solid materials of bronze, steel, and silicon nitride and lubricants of paraffinic and naphthenic mineral oils were considered in an investigation of the role of the dimensionless material parameter. Thirty-four different cases were used to generate the following minimum-film-thickness and central-film-thickness relationships:

$$\begin{aligned}\tilde{h}_{\min} &= 3.63 U^{0.68} G^{0.49} W^{-0.073} (1 - e^{-0.68 k}) \\ \tilde{h}_c &= 2.69 U^{0.67} G^{0.53} W^{-0.067} (1 - 0.61 e^{-0.73 k})\end{aligned}$$

The ellipticity parameter (k) can be written as

$$k = 1.03 \left(\frac{R_y}{R_x} \right)^{0.64}$$

Contour plots have been presented that indicate in detail the pressure distribution and the film thickness. In some solutions, pressure spikes were in evidence. The theoretical solutions of film thickness have all the essential features of previously reported experimental observations based upon optical interferometry.

The importance of the present chapter lies in the fact that it presents for the first time a satisfactory theoretical film-thickness equation for elastohydrodynamic point contacts operating

under fully flooded conditions. The exponents on the various dimensionless parameters governing minimum film thickness in such conjunctions are quite similar to those developed by Dowson (1968) for line contacts. The most dominant exponent occurs in association with the speed parameter, while the exponent on the load parameter is very small and negative. The material parameter also carries a significant exponent, although the range of this parameter in engineering situations is limited. Ranger, et al. (1975) have developed a central-film-thickness formula for the contact geometry of a ball on a plate from which an estimate can be made of the minimum film thickness. However, the work presented in this chapter is valid for any contact geometry and proceeds directly to the evaluation of the minimum film thickness.

Perhaps the most significant feature of the proposed minimum-film-thickness formula is that it can be applied to any contacting solids that present an elliptical Hertzian contact region. Many machine elements, particularly rolling-element bearings, possess such geometry, and it is expected that the new minimum-film-thickness equation will find application in such fields.

CHAPTER 6

STARVATION RESULTS

It was not until the late 1960's and early 1970's that the influence of lubricant starvation upon elastohydrodynamic behavior received serious consideration. Prior to this time it was assumed that the inlets were fully flooded. This assumption seemed to be entirely reasonable in view of the minute quantities of lubricant required to provide an adequate film. However, in due course it was recognized that some machine elements suffered from lubricant starvation.

How partial filling of the inlet to an elastohydrodynamic conjunction influences pressure and film thickness can readily be explored theoretically by adopting different starting points for the inlet pressure boundary. Orcutt and Cheng (1966) appear to have been the first to proceed in this way for a specific case corresponding to a particular experimental situation. Their results showed that lubricant starvation lessened the film thickness. Wolveridge, et al. (1971) used a Grubin (1949) approach in an analysis of starved elastohydrodynamic lubricated line contacts. Wedeven, et al. (1971) analyzed a starved condition in a ball-on-plate geometry, and Castle and Dowson (1972) presented a range of numerical solutions for the starved line-contact elastohydrodynamic situation. In these references the analysis yielded values of the proportional reduction in centerline film thickness from the fully flooded condition in terms of a dimensionless inlet boundary parameter.

In the present chapter, 15 cases in addition to those pre-

sented in chapter 5 were used to obtain the starvation results. From the results a simple dimensionless inlet boundary distance was written. This inlet boundary distance defines whether a fully flooded or a starved condition exists in the contact. Furthermore, it was found that the film thickness for a starved condition could be written in dimensionless terms as a function of the film thickness for a fully flooded condition and the inlet distance parameter. Contour plots of pressure and film thickness in and around the contact are shown for fully flooded and starved conditions. The theoretical findings are compared directly with previously reported results.

6.1 Boundary between Fully Flooded and Starved Conditions

Figure 5.1 shows the computing area in and around the Hertzian contact. In this figure, as defined in chapter 4, the coordinate X is made dimensionless with respect to the semiminor axis (b) of the contact ellipse and the coordinate Y is made dimensionless with respect to the semimajor axis (a) of the contact ellipse. The ellipticity parameter (k) is defined as the semimajor axis divided by the semiminor axis of the contact ellipse ($k = a/b$). Because of the dimensionless form of the coordinates X and Y , the Hertzian contact ellipse becomes a Hertzian circle regardless of the ellipticity parameter. This Hertzian contact circle is shown in figure 6.1 with a radius of unity. The edges of the computing area, where the pressure is assumed to be ambient, are also denoted. In this figure the dimensionless inlet distance (m), which is equal to the dimensionless distance from the center of contact to the inlet edge of the computing area, is shown.

Lubricant starvation can be studied simply by reducing the dimensionless inlet distance (m). A fully flooded condition is said to exist when the dimensionless inlet distance ceases to influence in any significant way the minimum film thickness. When starting from

a fully flooded condition and decreasing m , the value at which the minimum film thickness first starts to change is called the fully flooded - starved boundary and is denoted by m^* . Therefore, lubricant starvation was studied by using the basic elastohydrodynamic lubrication point-contact theory developed in chapter 4 and observing the effect of reducing the dimensionless inlet distance.

Table 6.1 shows the effect of changing the dimensionless inlet distance upon the dimensionless minimum film thickness for three groups of dimensionless load and speed parameters. For all the results presented in this chapter the material parameter (G) is fixed at 4522 and the ellipticity parameter is fixed at 6. In this table it is seen that as the dimensionless inlet distance (m) decreases the dimensionless minimum film thickness (H_{\min}) decreases.

Table 6.2 shows how the three groups of dimensionless speed and load parameters affect the location of the dimensionless inlet boundary distance (m^*). Also given in this table are the corresponding values of dimensionless central and minimum film thickness for the fully flooded condition as obtained by interpolation of the numerical values. The value of the dimensionless inlet boundary (m^*) shown in table 6.2 was obtained by using the data from table 6.1 when the following equation was satisfied:

$$\frac{l_{\min,F} - \left(H_{\min} \right)_{m=m^*}}{H_{\min,F}} = 0.03 \quad (6.1)$$

The value of 0.03 is used in equation (6.1) since it was ascertained that the data in table 6.1 could only be obtained to an accuracy of ± 3 percent.

The general form of the equation that describes how the dimensionless inlet distance at the fully flooded - starved boundary (m^*) varies is given as

$$m^* - 1 = A^* \left[\left(\frac{R_x}{b} \right)^2 H_{c,F} \right]^{B^*} \quad (6.2)$$

The right side of equation (6.2) is similar to the forms of the equation given by Wolveridge, et al. (1971) and Wedeven, et al. (1971). By applying a least-square power fit to the data obtained from table 6.1, the following can be written:

$$m^* = 1 + 3.06 \left[\left(\frac{R_x}{b} \right)^2 H_{c,\Gamma} \right]^{0.58} \quad (6.3)$$

A fully flooded condition exists when $m \geq m^*$, and a starved condition exists when $m < m^*$. The coefficient of determination (r^2) for these results is 0.9902, which is excellent.

If in equation (6.2) the dimensionless minimum film thickness is used instead of the central film thickness, the following is obtained:

$$m^* = 1 + 3.34 \left[\left(\frac{R_x}{b} \right)^2 H_{\min,F} \right]^{0.56} \quad (6.4)$$

The coefficient of determination for these results is 0.9869, which again is excellent.

From Wedeven, et al. (1971), using the symbols of this thesis, the dimensionless inlet distance at the fully flooded - starved boundary can be written as:

$$m_W = 1 + 3.52 \left[\left(\frac{R_x}{b} \right)^2 H_{c,F} \right]^{2/3} \quad (6.5)$$

Comparing equation (6.3) with equation (6.5) indicates close agreement with Wedeven, et al. (1971). The latter, however, predicts a slightly higher value of the fully flooded - starved boundary than predicted from the present results.

6.2 Starvation Film Thickness Formulas

Having clearly established the limiting location of the inlet boundary for the fully flooded conditions (eqs. (6.3) and (6.4)), an equation defining the dimensionless film thickness for lubricant starvation conditions will be developed. The relationship between the dimensionless central film thickness in starved and fully flooded conditions can be expressed in general form as

$$\frac{H_{c,S}}{H_{c,F}} = C^* \left(\frac{m-1}{m^*-1} \right)^{D^*} \quad (6.6)$$

Table 6.3 shows how the ratio of the dimensionless inlet distance parameter to the fully flooded - starved boundary $[(m-1)/(m^*-1)]$ affects the ratio of central film thickness in the starved and fully flooded conditions $(H_{c,S}/H_{c,F})$. A least-square power curve fit to the 16 pairs of data points

$$\left[\left(\frac{H_{c,S}}{H_{c,F}} \right)_i, \left(\frac{m-1}{m^*-1} \right)_i \right], \quad i = 1, 2, \dots, 16$$

was used in obtaining values for C^* and D^* in equation (6.6). For these values of C^* and D^* the dimensionless central film thickness for a starved condition can be written as

$$H_{c,S} = H_{c,F} \left(\frac{m-1}{m^*-1} \right)^{0.29} \quad (6.7)$$

By using a similar approach while making use of the data in table 6.3, the dimensionless minimum film thickness for a starved condition can be written as

$$H_{\min,S} = H_{\min,F} \left(\frac{m-1}{m^*-1} \right)^{0.25} \quad (6.8)$$

Therefore, whenever $m < m^*$, where m^* is defined by either equation (6.3) or (6.4), a lubricant starvation condition exists. When

this is true, the dimensionless central film thickness is expressed by equation (6.6) and the dimensionless minimum film thickness is expressed by equation (6.8). If $m \geq m^*$, where m^* is defined by either equation (6.3) or (6.4), a fully flooded condition exists. The dimensionless central and minimum film thicknesses for a fully flooded condition ($H_{c,F}$ and $H_{min,F}$) were developed in chapter 5 and are expressed in equations (5.56) and (5.33), respectively. (That is, H_{min} in eq. (5.33) is equivalent to $H_{min,F}$ in eq. (6.8), and H_c in equation (5.56) is equivalent to $H_{c,F}$ in eq. (6.7).)

The ratio of dimensionless inlet distance to the fully flooded - starved boundary as obtained from Wedeven, et al. (1971), expressed as $(m - 1)/(m_w - 1)$, is also given in table 6.3. By comparing these results with the results obtained from the present thesis $[(m - 1)/(m^* - 1)]$, it can be seen that for group 1 the agreement is excellent. However, the agreement in groups 2 and 3 is not as good. A possible explanation for this difference can be that an approximate expression for the Hertzian deformation is used in the Wedeven, et al. (1971) analysis. They indicate their equation (eq. (6.5)) is only valid for small m^* or more specifically $m^* < 3$. In group 2, $m^* = 3.71$ and in group 3 $m^* = 5.57$. Since no such assumption is required in deriving equations (6.3) and (6.4), they would seem to be more appealing.

Figure 6.2 shows the influence of inlet boundary parameter upon central film thickness for the Wedeven, et al. (1971) results and those obtained from the present thesis. From this figure it is observed that the Wedeven, et al. (1971) results give slightly higher values of the central film thickness ratio of starved to fully flooded condition than those obtained from the present results.

6.3 Contour Plot of Results

To explain more fully what happens in going from a fully flooded

to a lubricant starvation condition, figures 6.3 to 6.19 are presented. As in chapter 5, in parts (a) of these figures, contour plots of dimensionless pressure are given; and in parts (b) of these figures, contour plots of dimensionless film thickness are given. In parts (a) and (b) the + symbol indicates the center of the Hertzian contact. The Hertzian contact circle is shown in each of parts (a) and (b) by asterisks. At the top of each of parts (a) and (b), the contour labels and the corresponding values are given.

In figures 6.3(a), 6.4(a), . . . , 6.7(a), contour plots of dimensionless pressure ($P = p/E'$) are given for group 1 of table 6.2 and for dimensionless inlet distances (m) of 4, 3, 2, 1.5, and 1.25, respectively. The contour labels and values are kept constant in going from figure 6.3(a) to 6.7(a). In figure 6.3(a) a fully flooded condition exists. Once starvation occurs the severity of the situation increases as m is decreased, thus implying that the most severe starvation case is shown in figure 6.7, where $m = 1.25$. In figures 6.3(a), 6.4(a), and 6.5(a) a pressure spike is clearly visible, whereas in figures 6.6(a) and 6.7(a) no pressure spike is present. Note in figure 6.7(a), the most severe starvation case, that the contour labeled H does not extend as far to the left as it did for the fully flooded pressure results shown in figure 6.3(a).

In figures 6.3(b), 6.4(b), . . . , 6.7(b), the contour plots of dimensionless film thickness ($H = h/R_x$) are given for group 1 of table 6.2 and m of 4, 3, 2, 1.5, and 1.25, respectively. The film thickness results shown in figure 6.3(b), . . . , 6.7(b) correspond to the pressure results shown in figures 6.3(a), . . . , 6.7(a). The central portion of the film thickness contours has become more parallel as starvation has increased (m decreasing) with the minimum film thickness decreasing. Note also that the film thickness contour values for the most severely starved condition (fig. 6.7(b)) are much

lower than the film thickness contour values for the fully flooded conditions (fig. 6.3(b)).

In figures 6.8(a), 6.9(a), . . . , and 6.12(a), contour plots of dimensionless pressure ($P = p/E'$) are given for group 2 of table 6.2 and for m of 6, 4, 3, 2.5, and 2, respectively. The contour values are the same for each of these figures. In figure 6.8(a) (the fully flooded conditions) the contour for the largest pressure (contour A) is present, but as starvation occurs in figures 6.9(a), 6.10(a), and 6.11(a) this contour is absent. Furthermore, for the severely starved condition shown in figure 6.12(a) both the A and B contours are absent. This implies that for group 2 the pressure peak present in a fully flooded condition gets flatter as starvation progresses.

Figures 6.8(b), 6.9(b), . . . , 6.12(b) give contour plots of film thickness for group 2 of table 6.2 and m of 6, 4, 3, 2.5, and 2, respectively. The minimum film thickness areas in these figures occur on the axial center of the contact and move slightly to the right as starvation becomes severe. Note from the contour values that film thickness decreases substantially in going from a fully flooded condition (fig. 6.8(b)) to a severely starved condition (fig. 6.12(b)). As was found for the low-speed results, the central portions of the film thickness contours become parallel as starvation is increased.

In figures 6.13(a), 6.14(a), . . . , 6.19(a), contour plots of dimensionless pressure ($P = p/E'$) are given for group 3 of table 6.2 and for m of 6, 4, 3, 2.5, 2, 1.75, and 1.5, respectively. The contour values are the same for each of these figures. Figure 6.13(a) gives the pressure contour for a fully flooded condition; figure 6.19(a) gives the pressure contour for a severely starved condition. As starvation occurs the pressure profile flattens, since in figure 6.17(a) contour A is absent, in figure 6.18(a) contours A and B are absent, and in figure 6.19(a) (the severely starved condition) con-

tours A, B, and C are absent. Also from these figures it is found that the distance from the center of the contact to the upstream location of the largest contour value (labeled H) decreases as the severity of lubricant starvation increases.

Figures 6.13(b), 6.14(b), . . . , 6.19(b) give contour plots of film thickness for group 3 of table 6.2 and m of 6, 4, 3, 2.5, 2, 1.75, and 1.5, respectively. In figure 6.13(b) (the fully flooded condition) the minimum film thickness occurs to the sides of the conjunction in two areas that are midway between the center of the contact and the Hertzian circle. As m is decreased or the severity of starvation increases (going from figs. 6.14(b) to 6.19(b)) the minimum film thickness area remains in the axial center of the conjunction but moves to the right, nearer the Hertzian circle. Note the similarity among the film thickness contours of figure 6.7(b) (group 1 case), figure 6.12(b) (group 2 case), and figure 6.19(b) (group 3 case).

The dimensionless pressure ($P = p/E'$) on the X-axis is shown for three values of dimensionless inlet distance and for groups 1 and 3 of table 6.2, respectively, in figures 6.20(a) and (b). The value of Y is held constant near the axis of symmetry of the conjunction. In these figures as a conjunction becomes starved (as m is decreased) the pressure spike diminishes.

Figures 6.21(a) and (b) show the dimensionless film thickness ($H = h/R_x$) on the X-axis for three values of dimensionless inlet distance and for groups 1 and 3 of table 6.2, respectively. The value of Y is held fixed close to the axis of symmetry of the contact. In these figures, particularly figure 6.21(b), the central region becomes flatter as starvation occurs. Also, in going from a fully flooded condition to a starved condition the film thickness decreases substantially.

6.4 Concluding Remarks

By using the theory and numerical procedure outlined in chapter 4, the influence of lubricant starvation upon minimum film thickness in starved elliptical elastohydrodynamic conjunctions has been investigated. This study of lubricant starvation was performed by moving the inlet boundary closer to the center of the conjunction. From the results it was found that the location of the dimensionless inlet boundary (m^*) between fully flooded and starved conditions could be expressed simply as

$$m^* = 1 + 3.06 \left[\left(\frac{R_x}{b} \right)^2 H_{c,F} \right]^{0.58}$$

or

$$m^* = 1 + 3.34 \left[\left(\frac{R_x}{b} \right)^2 H_{\min,F} \right]^{0.56}$$

That is, for a dimensionless inlet distance (m) less than m^* , starvation occurs and for $m \geq m^*$, a fully flooded condition exists.

Furthermore, it has been possible to express the central and minimum film thicknesses for a starved condition as

$$H_{c,S} = H_{c,F} \left(\frac{m-1}{m^*-1} \right)^{0.29}$$

$$H_{\min,S} = H_{\min,F} \left(\frac{m-1}{m^*-1} \right)^{0.25}$$

where

$H_{c,F}$ fully flooded dimensionless central film thickness

$H_{\min,F}$ fully flooded dimensionless minimum film thickness

m dimensionless inlet distance

m^* dimensionless inlet distance at the fully flooded - starved boundary

Contour diagrams of the pressure and film thickness in and

around the contact have been presented for both fully flooded and starved conditions. It is evident from the contour diagrams that the pressure spike becomes suppressed and the film thickness decreases substantially as the severity of starvation increases.

The results presented in this chapter, when combined with the findings of the previous chapter, enable the essential features of starved, elliptical, elastohydrodynamic conjunctions to be ascertained.

CHAPTER 7

SUMMARY OF CONCLUSIONS

A procedure for the numerical solution of the complete, isothermal, elastohydrodynamic lubrication problem for point contacts was given. This procedure calls for the simultaneous solution of the elasticity and Reynolds equations. In the elasticity analysis the contact zone was divided into equal rectangular areas. It was assumed that a uniform pressure was applied over each area. In the numerical analysis of the Reynolds equation the parameter $\phi = PH^{3/2}$, where P is dimensionless pressure and H is dimensionless film thickness, was introduced to help the relaxation process. The pressure-viscosity analysis of Roelands (1966) was used. The numerical coupling of the elasticity and Reynolds equations results in a converged solution for the pressure profile. This pressure profile is then integrated over the computing zone to give the value of the corresponding normal applied load. This load is then compared with the input load and corrections are made to the film thickness until these two loads are in agreement.

The most important practical aspect of the elastohydrodynamic lubricated point-contact theory developed is the determination of the minimum film thickness within the contact. That is, the maintenance of a fluid film of adequate magnitude is extremely important to the operation of some machine elements. The minimum film thickness for a fully flooded conjunction was found to be a function of the ellipticity parameter and the dimensionless speed, load, and material parameters. In the results the ellipticity parameter was varied from 1 (a ball-on-plate configuration) to 8 (a configuration approaching a line contact).

The dimensionless speed parameter was varied over a range of nearly two orders of magnitude. The dimensionless load parameter was varied over a range of one order of magnitude. Situations equivalent to the use of solid materials of bronze, steel, and silicon nitride and lubricants of paraffinic and naphthenic mineral oils were considered in an investigation of the role of the dimensionless material parameter.

Thirty-four different cases were used to generate the minimum film thickness and central film thickness formulas given below as

$$\tilde{H}_{\min,F} = 3.63 U^{0.68} G^{0.49} W^{-0.073} (1 - e^{-0.68 k}) \quad (7.1)$$

$$\tilde{H}_{c,F} = 2.69 U^{0.67} G^{0.53} W^{-0.067} (1 - 0.61 e^{-0.73 k}) \quad (7.2)$$

where the dimensionless speed parameter

$$U = \frac{\eta_0 u}{E' R_x} \quad (7.3)$$

the dimensionless load parameter

$$W = \frac{F}{E' R_x^2} \quad (7.4)$$

the dimensionless material parameter

$$G = \frac{E'}{P_{iv,as}} \quad (7.5)$$

and the dimensionless ellipticity parameter

$$k = \frac{a}{b} \quad (7.6)$$

Equations (7.5) and (7.6) can also be written in more convenient form as

$$G = E' \alpha \quad (7.7)$$

$$k = 1.03 \left(\frac{R_y}{R_x} \right)^{0.64} \quad (7.8)$$

In equation (7.8) the ellipticity parameter is expressed strictly in terms of the radii of curvature and thereby eliminates the common practice of evaluating the elliptical integrals of the first and second kind.

The importance of equation (7.1) lies in the fact that it presents for the first time a satisfactory theoretical film-thickness equation for elastohydrodynamic point contacts operating under fully flooded conditions. The exponents on the various dimensionless parameters governing minimum film thickness in such conjunctions are quite similar to those developed by Dowson (1968) for line contacts. The most dominant exponent occurs in association with the speed parameter, while the exponent on the load parameter is very small and negative. The material parameter also carries a significant exponent, although the range of this parameter in engineering situations is limited. Ranger, et al. (1975) have developed a central-film-thickness formula for the contact geometry of a ball on a plate from which an estimate can be made of the minimum film thickness. However, the work presented in this chapter is valid for any contact geometry and proceeds directly to the evaluation of the minimum film thickness.

Perhaps the most significant feature of the proposed minimum-film-thickness formula is that it can be applied to any contacting solids that present an elliptical Hertzian contact region. Many machine elements, particularly rolling-element bearings, possess such geometry, and it is expected that the new minimum-film-thickness equation will find application in such fields.

Contour plots of the fully flooded results have been presented that indicate in detail the pressure distribution and the film thickness. In some solutions, pressure spikes were in evidence. The theoretical solutions of film thickness have all the essential features of the previously reported experimental observations based upon optical interferometry.

In addition to the fully flooded studies, the influence of lubricant starvation upon minimum film thickness in starved elliptical

elastohydrodynamic conjunctions has been investigated. This study of lubricant starvation was performed by moving the inlet boundary closer to the center of the conjunction. From the results it was found that the location of the dimensionless inlet boundary (m^*) between fully flooded and starved conditions could be expressed simply as

$$m^* = 1 + 3.06 \left[\left(\frac{R_x}{b} \right)^2 \tilde{H}_{c,F} \right]^{0.58} \quad (7.9)$$

or

$$m^* = 1 + 3.34 \left[\left(\frac{R_x}{b} \right)^2 \tilde{H}_{\min,F} \right]^{0.56} \quad (7.10)$$

That is, for a dimensionless inlet distance (m) less than m^* , starvation occurs and for $m \geq m^*$, a fully flooded condition exists. Furthermore, it has been possible to express the dimensionless central and minimum film thicknesses for a starved condition as

$$\tilde{H}_{c,S} = \tilde{H}_{c,F} \left(\frac{m-1}{m^*-1} \right)^{0.29} \quad (7.11)$$

$$\tilde{H}_{\min,S} = \tilde{H}_{\min,F} \left(\frac{m-1}{m^*-1} \right)^{0.25} \quad (7.12)$$

Contour diagrams of the pressure and film thickness in and around the conjunction have been presented for starved conditions. It is evident from the contour diagrams that the pressure spike becomes suppressed and the film thickness decreases substantially as the severity of starvation increases.

The starvation results when combined with the fully flooded results enable the essential features of starved, elliptical, elastohydrodynamic conjunctions to be ascertained.

REFERENCES

- Archard, J. F., and Cowking, E. W. (1965-66) Elastohydrodynamic lubrication of point contacts, Proc. Inst. Mech. Engrs. London, vol. 180, pt. 3B, p. 47.
- Archard, J. F., and Kirk, M. T. (1964) Film thickness for a range of lubricants under severe stress, J. Mech. Eng. Sci., vol. 6, p. 101.
- Barus, C. (1893) Isotherma, isopiestic, and isometrics relative to viscosity, Amer. J. Sci., vol. 45, p. 87.
- Blok, H. (1965) Proceedings of the International Symposium on Lubrication and Wear, D. Muster and B. Sternlicht, eds., McCutchan, Berkeley, p. 1.
- Cameron, A., and Gohar, R. (1966) Theoretical and experimental studies of the oil film in lubricated point contact, Proc. Roy. Soc. (London), vol. 291A, p. 520.
- Castle, P., and Dowson, D. (1972) A theoretical analysis of the starved elastohydrodynamic lubrication problem for cylinders in line contact, Elastohydrodynamic Lubrication: 1972 Symposium, Inst. Mech. Engrs. (London), p. 131.
- Cheng, H. S. (1970) A numerical solution of the elastohydrodynamic film thickness in an elliptical contact, J. Lubric. Tech., vol. 92, p. 155.
- Christensen, H. (1964) The variation of film thickness in highly loaded contacts, ASLE Trans., vol. 7, p. 219.
- Dowson, D. (1965) Elastohydrodynamic lubrication - an introduction and a review of theoretical studies. Paper R1, Inst. Mech. Engrs., (London), May 1965.
- Dowson, D. (1968) Elastohydrodynamic, Proc. Inst. Mech. Engrs. (London), vol. 182, pt. 3A, p. 151.
- Dowson, D., and Higginson, G. R. (1959) Numerical solution to the elastohydrodynamic problem, J. Mech. Eng. Sci., vol. 1, p. 6.
- Dowson, D., and Higginson, G. R. (1961) New roller-bearing lubrication formula, Eng. (London), vol. 192, p. 158.
- Dowson, D., and Higginson, G. R. (1966) Elastohydrodynamic Lubrication, Pergamon Press, New York.
- Dowson, D., and Whitaker, A. V. (1965-66) A numerical procedure for the solution of the elastohydrodynamic problems of rolling and sliding contacts lubricated by a Newtonian fluid, Proc. Inst. Mech. Engrs. (London), vol. 180, pt. 3B, p. 57.
- Dyson, A., Naylor, H., and Wilson, A. R. (1965-66) The measurements of oil-film thickness in elastohydrodynamic contacts, Proc. Inst. Mech. Engrs. (London), vol. 180, pt. 3B, p. 119.
- Grubin, A. N., Vinogradaova, I. E., and Ketnva, F., eds. (1949) Investigation of the Contact Machine Components, Central Sci. Res. Inst. Tech. Mech. Eng., Book 30, (D.S.I.R. translation 337), Moscow.

- Harris, T. A. (1966) Rolling Bearing Analysis, Wiley, New York.
- Hamrock, Bernard J., and Anderson, William J. (1973) Analysis of an arched-outer-race ball-bearing considering centrifugal forces, J. Lubric. Tech., vol. 95, p. 265.
- Hertz, H. (1882) The contact of rigid elastic bodies, J. fur die Reiner und Angew andte Mathematik, vol. 92, p. 156.
- Martin, H. M. (1916) The lubrication of gear-teeth, Eng. (London), vol. 102, p. 119.
- Orcutt, F. K., and Cheng, H. S. (1966) Lubrication of rolling-contact instrument bearings, Gyro-Spin Axis Hydrodynamic Bearing Symposium, vol. 2, tab 5, Mass. Inst. Tech. Instrum. Lab., Cambridge.
- Pai, S. I. (1956) Viscous Flow Theory, vol. I, Van Nostrand, Princeton.
- Ranger, A. P., Ettles, C. M. M., and Cameron, A. (1975) The solution of the point contact elasto-hydrodynamic problem, Proc. Royal Soc. (London), vol. 346, p. 227.
- Reynolds, O. (1886) On the theory of lubrication and its application to Mr. Beauchamp Tower's experiments, including an experimental determination of the viscosity of olive oil, Phil. Trans. Roy. Soc. (London), vol. 177, p. 157.
- Roelands, C. J. A. (1966) Correlational Aspects of the Viscosity-Temperature-Pressure Relationship of Lubricating Oils, Druk. U.R.B., Groningen.
- Sibley, L. B., and Orcutt, F. K. (1961) Elastohydrodynamic lubrication of rolling-contact surfaces, ASLE Trans., vol. 4, p. 235.
- Timoshenko, S., and Goodier, J. H. (1951) Theory of Elasticity, 2nd ed., McGraw-Hill, New York.
- Wedeven, L. E., Evans, D., and Cameron A. (1971) Optical analysis of ball bearing starvation, J. Lubric. Tech., vol. 93, p. 349.
- Wholmes, T. L. (1966) The Effect of Surface Quality on Lubricating Film Performance, Ph.D. Dissertation, University of Leeds.
- Wolveridge, P. E., Baglin, K. P., and Archard, J. G., (1971) The Starved Lubrication of Cylinders in Line Contact, Proc. Inst. Mech. Engrs. (London), vol. 185, p. 1159.

APPENDIX - LISTING OF COMPUTER PROGRAMS

```

1*      IMPLICIT DOUBLE PRECISION (A-H,O-Z)
2*      DIMENSION P2(95,20,3)
3*      DIMENSION DENS(760),VIS(760),XMU(760),ZPR(760)
4*      DIMENSION A(760),R(760),C(760),DLZ(760),XL(760),XM(760)
5*      COMMON NSAVE,MBJ,NX,NY
6*      COMMON A1,R1,P1,RHO,RX,RY,XK,P1,SA,SB,T3,T2
7*      COMMON W(760),D(1520),S(760),H(1520),PHI(760),PRSV(760)
8*      COMMON EP,HMIN,ZC,ZD,XN,YM
9*
10*     C
11*     C      ELASTOHYDRODYNAMIC LUBRICATION OF POINT CONTACT PROGRAM
12*     C
13*     C      ALL INPUT DATA IS IN THE UNITS OF NEWTON,CENTIMETER,SECOND
14*     C
15*     C      INPUT
16*     C
17*     DLROSM=100.000
18*     PHIMX=100.00-10
19*     MRJ=0
20*     MRJ0=0
21*     MRJ04=1
22*     MRJ06=1
23*     MRJ08=1
24*     MAUR=0
25*     JFNN=0
26*     BRIAN=1.000
27*     Z7Z=.1300
28*     NPQ=0
29*     MH9=0
30*     MHB=1
31*     DFL=.000000100
32*     >T=3.1415926535900
33*     ORF=1.600
34*     DFL4=1.0600
35*     DFL1=.500
36*     ROSM=100.000
37*     C
38*     C      CONVEX SURFACES ARE POSITIVE
39*     C      CONCAVE SURFACES ARE NEGATIVE
40*     C
41*     RAY=1.1112500
42*     RAX=1.1112500
43*     RPX=1.012
44*     RPY=-1.18611E00
45*     XIA=.300
46*     GA=1.9994707
47*     PIVAS=4858.700
48*     VISO=.0000041100
49*     Z=.6700
50*     UA=50.000
51*     UR=UA
52*     ALPHA=5.827440-6
53*     BETA=1.683480-5
54*     VISE=.0000000063100
55*     VA=0.
56*     VR=VA
57*     P=20.000
58*     MO=-.0000364500
59*     C
60*     C      NODAL STRUCTURE INPUT
61*     C
62*     ZO=13.000
63*     XN=4.000
64*     NX=67
65*     ZC=5.000
66*     NY=8
67*     YM=1.600
68*     NXY=NX*NY
69*     NX1=NX-1
70*     NY1=2*NY
71*     NR=NX
72*     READ(5,99) ((P2(I,J,1),I=1,NX),J=1,NY1)
73*     99 FORMAT(8D10.5)
74*     DO 98 J=1,NY1
75*     DO 97 I=1,NX
76*     V=I+(J-1)*NX
77*     97 PR(N)=P2(I,J,1)
78*     98 CONTINUE
79*     975 CONTINUE
80*     XIR=XIA

```

```

R1*      GR=GA
R2*      JRHQY=0
R3*      JRHQZ=0
R4*      JRH=0
R5*      MAXS2=1
R6*      DEL2=.000500
R7*      DEL3=.100
R8*      M=1
R9*      MN1=2
90*      C
91*      C
92*      C      CURVATURE SUM AND DIFFERENCE
93*      C
94*      RX=(1./RAX)+(1./RRX)
95*      RY=(1./RAY)+(1./RBY)
96*      RHO=RX+RY
97*      GAMMA=(RX-RY)/RHO
98*      C
99*      C      ELLIPTIC INTEGRALS E AND F
100*      C
101*      C      XK=SQRT(2.000)
102*      C
103*      C      XK IS THE ELLIPTICITY PARAMETER
104*      C
105*      1 AK=SQRT(1.-(1./(XK**2)))
106*      CALL CEL (F,E,AK,IER)
107*      XJK=SQRT((2.*F-F*(1.+GAMMA))/(E*(1.-GAMMA)))
108*      A9=XK-XJK
109*      XK=XJK
110*      IF (ARS(A9).LT.DEL) GO TO 2
111*      GO TO 1
112*      C
113*      C      SEMIMAJOR AND SEMIMINOR AXES OF CONTACT ELLIPSE
114*      C
115*      2 S2=(1.-X1A**2)/GA+(1.-X1B**2)/GR
116*      T1=(3.*(XK**2)*E*P)/(PI*RHO)
117*      A1=(T1+S2)**(1./3.)
118*      R1=A1/XK
119*      Z1=.5*Z0
120*      Z2=.5*ZC/XK
121*      Z3=Z1**2
122*      Z4=Z2**2
123*      A1=S2/PI
124*      T3=.5*RX*(R1**2)
125*      T2=.5*RY*(A1**2)
126*      WRITE (6,3) RHO,GAMMA,XK,L,F
127*      3 FORMAT(4HPHO=,D16.5,5X,6HGAMMA=,D16.5,5X,2HXK=,D16.5,5X,
128*      1 2HE=,D16.5,5X,2HF=,D16.5)
129*      C
130*      C      DIMENSIONLESS PARAMETER GROUPING
131*      C
132*      EP=2./S2
133*      SMU=.5*(UA+UB)
134*      SMV=.5*(VA+VB)
135*      V=SQRT(SMU**2+SMV**2)
136*      THETA=ATAN(SMV/SMU)
137*      G=EP/PI*V
138*      U=VISO*RX*V/EP
139*      WLZ=P*RX*PX/EP
140*      WLZAR=P*RX/(2.*EP*A1)
141*      ARCHAR=1./(1.+(2.*RY)/(3.*RX))
142*      HMINA=2.04*(ARCHAR*G*U)**.74/(WLZ**0.74)
143*      DOWSON=2.85*G**.54*U**.7/WLZAR**.13
144*      HMINCL=16**.54*(U**.65)/(WLZ**0.73)
145*      WRITE (6,190) HMINCL
146*      190 FORMAT(1H ,8HHMINCL=,D16.6)
147*      WRITE (6,196) DOWSON
148*      196 FORMAT(1H ,38HDOWSON HIGGINSON LINE CONTACT FORMULA=,D16.6)
149*      WRITE (6,501) HMINA,WLZAR,ARCHAR
150*      501 FORMAT(1H ,6HHMINA=,D16.5,5X,6HWLZAR=,D16.5,5X,7HARCHAR=,D16.5)
151*      PI=3.141592653589793
152*      WRITE (6,4) A1,R1,P1,EP
153*      4 FORMAT (2HA=,D16.5,5X,2HB=,D16.5,5X,5HPMAX=,D16.5,5X,3HAA=,D16.5)
154*      WRITE (6,5) U,THETA,G,WLZ
155*      5 FORMAT (1HD,2HU=,D16.5,5X,6HTHETA=,D16.5,5X,2HFC=,D16.5,
156*      1 5X,2HW=,D16.5)
157*      C
158*      C      INITIAL PRESSURE AND FILM THICKNESS
159*      C
160*      ZB=1./(1.+(2.*RY)/(3.*RX))
161*      WP=P*(RHO**2)/EP
162*      WRITE (6,6) WP,H0
163*      6 FORMAT (4H WP=,D16.5,5X,3HH0=,D16.5)
164*      Q1=VISE/VISO
165*      Q2=EP/19608.5268

```

```

165*      Q5=ALPHA*EP
166*      Q6=BETA*EP
167*      14 CONTINUE
168*      CALL SUR6 (HO,M,MN1)
169*      IF (M.EQ.0) GO TO 333
170*      M=0
171*      MN1=1
172*      WRITE(6,5P0) PHIMX
173*      5P0 FORMAT(1H,6HPHIMX=,D16.5)
174*      333 CONTINUE
175*      C
176*      C      VISCOSITY AND DENSITY
177*      C
178*      DO 7 N=1,NX
179*      DENS(N)=1.+(Q5*PR(N))/(1.+Q6*PR(N))
180*      VIS(N)=Q1*(1.-(1.+Q2*PR(N))**2)
181*      XMU(N)=DENS(N)/VIS(N)
182*      7 CONTINUE
183*      C
184*      C      RELAXATION COEFFICIENTS A,B,C,D,L,AND M
185*      C
186*      300 CONTINUE
187*      SUM1=0.000
188*      DO 9 J=2,NY
189*      DO 10 I=2,NX1
190*      N=I+(J-1)*NX
191*      N1=N+1
192*      N2=N-1
193*      N3=N+NX
194*      IF (J.EQ.NY) N3=N
195*      N4=N-NX
196*      Y1=XMU(N1)
197*      Y2=XMU(N2)
198*      Y3=XMU(N3)
199*      Y4=XMU(N4)
200*      Y5=H(N1)
201*      Y6=H(N2)
202*      Y7=H(N3)
203*      Y8=H(N3)
204*      Y9=H(N4)
205*      Y10=Y1*SQRT(Y5)
206*      Y11=Y2*SQRT(Y6)
207*      Y12=Y3*SQRT(Y8)
208*      Y13=Y4*SQRT(Y9)
209*      A(N)=2.3*(3.*Y1+Y2)
210*
211*      R(N)=24*(Y3+3.*Y4)
212*      C(N)=2.3*(Y1+3.*Y2)
213*      DLZ(N)=24*(3.*Y3+Y4)
214*      XL1=4.*(2.3*(Y1+Y2)+24*(Y3+Y4))
215*      XL2=1.5/(Y7**1.5)
216*      XL3=2.3*(Y10*(3.*Y5-4.*Y7+Y6)+Y11*(Y5-4.*Y7+3.*Y6))
217*      XL4=24*(Y12*(3.*Y8-4.*Y9+Y9)+Y13*(Y8-4.*Y9+3.*Y9))
218*      XL(N)=XL1+XL2*(XL3+XL4)
219*      XM1=12.*Q6*RYR/(Y7**1.5)
220*      XM2=(Y5*DENS(N1)-Y6*DENS(N2))*COS(THETA)
221*      XM3=(Y8*DENS(N3)-Y9*DENS(N4))*SIN(THETA)
222*      XM(N)=XM1*(21.*XM2+22.*XM3)
223*      10 CONTINUE
224*      9 CONTINUE
225*      307 SUM1=0.000
226*      MSUM9=0
227*      C
228*      C      RELAXATION FORMULA
229*      C
230*      DO 308 J=2,NY
231*      DO 309 I=2,NX1
232*      MN=I+(J-1)*NX
233*      MNA=MN+1
234*      MNR=MN-1
235*      MNC=MN+NX
236*      IF (J.EQ.NY) MNC=MN
237*      MND=MN-NX
238*      ZPR(MN)=PHI(MN)-ORF*(PHI(MN)+(XM(MN)-A(MN)*PHI(MNA)-B(MN)*PHI(MND))-
239*      1 -C(MN)*PHI(MNR)-DLZ(MN)*PHI(MNC))/XL(MN);
240*      IF (ZPR(MN).LT.PHIMX) GO TO 550
241*      MSUM9=MSUM9+1
242*      ZPR(MN)=PHIMX
243*      550 CONTINUE
244*      IF (ZPR(MN).LE.0.) GO TO 389
245*      VIR=(ZPR(MN)-PHI(MN))/ZPR(MN)
246*      SUM1=SUM1+ARS(Y18)
247*      GO TO 389
248*      389 ZPR(MN)=0.000

```

```

249*      3P8 PHI(MN)=ZPR(MN)
250*      309 CONTINUE
251*      30A CONTINUE
252*      310 CONTINUE
253*      MAUR=MAUR+1
254*      IF (SUM1.LT.DEL3) GO TO 311
255*      GO TO 307
256*
257*      C
258*      C      VISCOSITY AND DENSITY ITERATION
259*      C
260*      311 SUM2=0.000
261*      WRITE (6,480) MAUR,MSUM9
262*      4A0 FORMAT(1H ,5HMAUR=,I8,5X,6HMSUM9=,I8)
263*      MAUR=0
264*      PSUM=0.000
265*      DO 315 J=2,NY
266*      DO 316 I=2,NX
267*      N=I+(J-1)*NX
268*      PR(N)=(PHI(N)/(H(N)**1.5)+(POS(M-1.)*PPSV(N))/POS
269*      PRSV(N)-PR(N)
270*      PSUM=PSUM+PR(N)
271*      DENSN=1.+(05*PR(N))/(1.+06*PR(N))
272*      VISN=01*(1.-(1.+02*PR(N))**2)
273*      XMUN=DENSN/VISN
274*      Y99=(XMUN-XMU(N))/XMUN
275*      SUM2=SUM2+ABS(Y99)
276*      DENSN=DENSN
277*      VIS(N)=VISN
278*      316 XMU(N)=XMUN
279*      315 CONTINUE
280*      MN1=1
281*      IF (MH9.EQ.1) GO TO 459
282*      CALL SUB6(MO,M,MN1)
283*      459 CONTINUE
284*      JFNN=JFNN+1
285*      WRITE(6,810) SUM2
286*      810 FORMAT(1H ,5HSUM2,016.5)
287*      IF (SUM2.LT.DEL1) GO TO 13
288*      IF (MAXS2.GT.300) GO TO 950
289*      MAXS2=MAXS2+1
290*      GO TO 300
291*
292*      C
293*      C      APLIED NOPMAL LOAD
294*      C
295*      13 CONTINUE
296*      MAXS2=1
297*      IF (MH9.EQ.1) GO TO 401
298*      WRITE(6,4P1) JFNN
299*      4P1 FORMAT(1H ,9HJENNIFER=,I8)
300*      JFNN=0
301*      QU4=0.000
302*      DO 16 I=2,NX1
303*      QU1=2.000
304*      QU3=0.000
305*      IM=I/2
306*      IRM=IM*IM
307*      IF (IBM.NE.1) QU1=1.000
308*      DO 17 J=2,NY
309*      N=I+(J-1)*NX
310*      17 QU3=QU3+PR(N)
311*      16 QU4=QU4+QU3*QU1
312*      PRAR=4.*EP*A1*RI*QU4/(3.*ZC*ZD)
313*      PCHECK=2.*EP*A1*RI*PSUM/(ZC*ZD)
314*      WRITE (6,500) PRAR,PCHECK
315*      500 FORMAT (1H ,5HPRAR=,016.5,5X,7HPCHECK=,016.5)
316*
317*      C
318*      C      NEW CENTRAL FILM THICKNESS
319*      C
320*      IF (JENN.LE.5) XJENN=.500
321*      IF (JENN.GT.5) XJENN=.600
322*      IF (JENN.GT.10) XJENN=.800
323*      IF (JENN.GT.15) XJENN=.900
324*      IF (ABS(HO).LT.1.D-8) HO=-HO
325*      IF (HO.LT.0.) HORAR=HO*(XJENN*(1.-XJENN)*(P/PRAR)**277)
326*      IF (HO.GT.0.) HORAR=HO*(XJENN*(1.-XJENN)*(PRAR/P)**277)
327*      ZSUM3=(P-PRAR)/P
328*      SUMT=ABS(ZSUM3)
329*      WRITE (6,1A) P,PRAR,HO,HORAR,SUM3
330*      1A FORMAT(1H ,7HP=,016.8,5X,5HPBAR=,016.8,5X,3HHC=,016.8,
331*      1 5X,6HHOBAR=,016.8,5X,5HSUM3=,016.8)
332*      IF (SUM3.LT.DEL2) GO TO 19
333*      HO=HORAR
334*      191 CONTINUE
335*      DO 440 J=1,NY

```

```

333*      DO 441 I=1,NX
334*          N3=I*(J-1)*NX
335*          H(IN3)=HC*PX*(S(IN3)*W(IN3))
336*      441 PHI(IN3)=PR(IN3)*(H(IN3)**1.5)
337*      440 CONTINUE
338*          GO TO 300
339*      19 CONTINUE
340*          IF (JRH.EQ.1) GO TO 700
341*          JRH=1
342*          DEL1=.300
343*          GO TO 755
344*      700 IF (JRHQZ.EQ.1) GO TO 750
345*          JRHQZ=1
346*          DEL1=.200
347*          GO TO 755
348*      750 IF (JRHQY.EQ.1) GO TO 756
349*          JRHQY=1
350*          DEL1=.100
351*      755 CONTINUE
352*          DO 698 J=1,NY
353*              DO 692 I=1,NX
354*                  N=I+NX*(J-1)
355*                  P2(I,J,1)=PR(IN)
356*      692 P2(I,J,2)=H(IN)
357*      690 CONTINUE
358*          DO 694 J=1,NY
359*              DO 696 I=1,NX
360*                  J1=NY+J
361*                  J2=NY+1-J
362*                  P2(I,J1,1)=P2(I,J2,1)
363*                  P2(I,J1,2)=P2(I,J2,2)
364*      694 CONTINUE
365*          PUNCH 654, ((P2(I,J,K),I=1,NX),J=1,NY),K=1,2)
366*      654 FORMAT(8D10.5)
367*          HC=HOPAR
368*          DO 701 J=1,NY
369*              DO 702 I=1,NX
370*                  N3=I*(J-1)*NX
371*                  H(IN3)=HC*PX*(S(IN3)*W(IN3))
372*          PHI(N3)=PP(IN3)*(H(IN3)**1.5)
373*      701 CONTINUE
374*          GO TO 300
375*      756 CONTINUE
376*      401 CONTINUE
377*          WRITE (6,409) (PR(IN),N=1,700)
378*      409 FORMAT(1H ,2HPR,/,70(1H ,10D13.5,/)1)
379*          WRITE (6,410) (PHI(N),N=1,700)
380*      410 FORMAT(1H ,2HPH,/,70(1H ,10D13.5,/)1)
381*          WRITE (6,403) (H(IN),N=1,700)
382*          WRITE (6,404) (W(IN),N=1,700)
383*          WRITE (6,405) (S(IN),N=1,700)
384*      403 FORMAT(1H ,1HH,/,70(1H ,10D13.5,/)1)
385*      404 FORMAT(1H ,1HW,/,70(1H ,10D13.5,/)1)
386*      405 FORMAT(1H ,1HS,/,70(1H ,10D13.5,/)1)
387*          WRITE (6,317) (DENS(N),N=1,700)
388*      317 FORMAT(1H ,7HDENSITY,/,70(1H ,10D13.5,/)1)
389*          WRITE (6,318) (VISC(N),N=1,700)
390*      318 FORMAT(1H ,9HVISCOSITY,/,70(1H ,10D13.5,/)1)
391*          WRITE (6,301) (AIN(N),N=1,700)
392*          WRITE (6,302) (R(N),N=1,700)
393*          WRITE (6,303) (C(N),N=1,700)
394*          WRITE (6,304) (OL2(N),N=1,700)
395*          WRITE (6,305) (XL(N),N=1,700)
396*          WRITE (6,306) (XMEN(N),N=1,700)
397*      301 FORMAT(1H ,1HA,/,70(1H ,10D13.5,/)1)
398*      302 FORMAT(1H ,1HP,/,70(1H ,10D13.5,/)1)
399*      303 FORMAT(1H ,1HC,/,70(1H ,10D13.5,/)1)
400*      304 FORMAT(1H ,1HO,/,70(1H ,10D13.5,/)1)
401*      305 FORMAT(1H ,1HL,/,70(1H ,10D13.5,/)1)
402*      306 FORMAT(1H ,1HM,/,70(1H ,10D13.5,/)1)
403*      C
404*          DO 650 J=1,NY
405*              DO 651 I=1,NX
406*                  N=I+NX*(J-1)
407*                  P2(I,J,1)=PR(IN)
408*      651 P2(I,J,2)=H(IN)
409*      650 CONTINUE
410*          DO 698 J=1,NY
411*              DO 696 I=1,NX
412*                  J1=NY+J
413*                  J2=NY+1-J
414*                  P2(I,J1,1)=P2(I,J2,1)
415*                  P2(I,J1,2)=P2(I,J2,2)
416*      698 CONTINUE

```

```

4170      PUNCH 652,((P2(I,J,K),I=1,NX),J=1,NY),M=1,2)
4180      652 FORMAT(1D10.5)
4190      C
4200      C   FLOW RATE ANALYSIS
4210      C
4220      DO 776 J=2,NY
4230      DO 777 I=2,NX1
4240      N=I+(J-1)*NX
4250      N1=N+1
4260      N2=N-1
4270      N3=N+NX
4280      IF (J.EQ.NY) N3=N
4290      N4=N-NX
4300      PGRX=.5*Z0*(PP(N1)-PR(N2))
4310      PGRY=.5*Z0*(PP(N3)-PR(N4))
4320      QX1=V*DENSI(N)*H(N)*COS(THETA)
4330      QY1=U*DENSI(N)*H(N)*SIN(THETA)
4340      QX5=DFNS(N)*H(N)*.31/(12.*RX+VIS(N))
4350      QX2=QX5*PGRX/P1
4360      QY2=QX5*PGRY/A1
4370      QX=QX1-QX2
4380      QY=QY1-QY2
4390      QTOT=QX+QY
4400      QTV=SQRT(QX**2+QY**2)
4410      P2(I,J,3)=QTV
4420      QANG=ATAN(QY/QX)
4430      WRITE(6,778) N,QTV,QANG
4440      778 FORMAT(1H ,2HN=,I10,5X,4HQTV=,D13.5,5X,5HQANG=,D13.5)
4450      WRITE(6,779) QX1,QX2,QY1,QY2
4460      779 FORMAT(1H ,4HQX1=,D13.5,5X,4HQX2=,D13.5,5X,4HQY1=,D13.5,5X,
4470      1 4HQY2=,D13.5)
4480      WRITE(6,780) QTOT,QY,QX,PGRX,PGRY
4490      780 FORMAT(1H ,5HQTOT=,D13.5,5X,3HQY=,D13.5,5X,3HQX=,D13.5,5X,
4500      1 5HPGRX=,D13.5,5X,5HPGRY=,D13.5)
4510      777 CONTINUE
4520      776 CONTINUE
4530      406 CONTINUE
4540      DO 659 I=1,NX
4550      DO 658 J=1,NY
4560      J1=NY+J
4570      J2=NY+1-J
4580      P2(I,J1,3)=P2(I,J2,3)
4590      659 CONTINUE
4600      PUNCH 656,((P2(I,J,3),I=1,NX),J=1,NY)
4610      656 FORMAT(1D10.5)
4620      DFL1=.500
4630      JRM=0
4640      IF (MRJ.EQ.1) GO TO 970
4650      MRJ=1
4660      Z0=26.000
4670      XN=1.500
4680      NY=67
4690      H0=-.70003800
4700      ROSM=ROSM+200.000
4710      GO TO 975
4720      970 CONTINUE
4730      IF (MRJ0.EQ.1) GO TO 979
4740      MRJ0=1
4750      Z0=28.000
4760      XN=1.2500
4770      NY=65
4780      H0=-.7000400
4790      ROSM=ROSM+200.000
4800      GO TO 975
4810      979 CONTINUE
4820      IF (MRJ04.EQ.1) GO TO 101
4830      MRJ04=1
4840      GO TO 975
4850      101 CONTINUE
4860      IF (MRJ06.EQ.1) GO TO 102
4870      MRJ06=1
4880      GO TO 975
4890      102 CONTINUE
4900      IF (MRJ08.EQ.1) GO TO 103
4910      MRJ08=1
4920      GO TO 975
4930      950 CONTINUE
4940      ROSM=ROSM+DLROSM
4950      WRITE(6,969) ROSM
4960      969 FORMAT(1H ,4HROSM=,D13.5)
4970      MAXS2=1
4980      GO TO 300
4990      103 CONTINUE
5000      STOP
5010      END

```

```

10      SUBROUTINE CEL(R1,R2,AK,ILR)
20      IMPLICIT DOUBLE PRECISION (A-H,O-Z)
30      IFR=0
40      C   TEST MODULUS
50      C
60      GFO=1.-AK*AK
70      IF (GEO11,2,6
80      1 IFR=1
90      RETURN
100     C
110     C   SET RESULT VALUE=OVERFLOW
120     C
130     2 R1=1.03P
140     R2=1.000
150     RETURN
160     C
170     C   COMPUTE INTEGRAL
180     C
190     6 W=GFO
200     AN=1.+GFO
210     ANI=2.000
220     GFO=SQRT(GFO)
230     API=1.000
240     AA=1.000
250     7 W=W+AA*GFO
260     W=W*W
270     AA=AN
280     AARI=API
290     API=GFO*API
300     ANEW=API*AN
310     ANI=2.*ANI
320     C
330     C   TEST OF ACCURACY
340     C
350     IF (AARI-GEO-1).D-4*AAPI)9,9,8
360     8 GEO=SQRT(GEO*AAPI)
370     GEO=GEO*GEO
380     GO TO 7
390     9 R1=.7P539P163/API
400     R2=R1*AN
410     R1=R1*ANI
420     RETURN
430     END

```

END OF COMPILATION NO DIAGNOSTICS.

```

10      SUBROUTINE SUBKIND1,M1,MN,1
20      IMPLICIT DOUBLE PRECISION (A-H,O-Z)
30      COMMON NSAVE,MBJ,NX,NY
40      COMMON A1,B1,P1,RHO,RY,RY,XN,P1,SA,SB,T1,T2
50      COMMON W(760),D(1520),S(760),H(1520),PR(1520),PHI(760),PRSV(760)
60      COMMON EP,HMIN,ZC,ZD,XN,YM
70      HMIN=1.0E0
80      NX=NX*NY
90      NY1=NY-1
100     NY1=2*NY
110     ND=NX
120     SA=.5/ZC
130     SB=.5/ZD
140     IF (MN2.EQ.1) GO TO 20
150     IF (MI.NE.1) GO TO 100
160     YESA
170     C
180     C   HERTZIAN PRESSURE
190     C
200     DO 1 J=1,NY
210     X=SB
220     DO 2 I=1,NX
230     N=(I+J-1)*NX
240     S2=(Y-YM)**2
250     S1=(X-XN)**2
260     S1=S2+.521
270     S=(S1+S2+.17*521)
280     IF (MBJ.EQ.0) GO TO 4
290     IF (ABS(S1).GT.1.) GO TO 3
300     PR(N)=.000
310     GO TO 4

```

```

320      3 PRINT=PI*SQRT(1.-S1)/EP
330      4 PRSV(N)=PP(N)
340      2 X=X*SP+SB
350      1 Y=Y*SA+SA
360      100 CONTINUE
370
380      C
390      C      INFLUENCE COEFFICIENT USED IN ELASTIC DEFORMATION
400      C
410      Y=0.000
420      DO 5 J=1,NY1
430      X=0.000
440      DO 6 I=1,NX
450      V=I*(J-1)*NX
460      S3=SQRT((IX**2)*((Y+SA)**2)+(X+SB)**2)
470      S4=SQRT((IX**2)*((Y-SA)**2)+(X+SB)**2)
480      S5=SQRT((IX**2)*((Y+SA)**2)+(X-SB)**2)
490      S7=(IX*(Y+SA)+S3)/(IX*(Y-SA)+S4)
500      S8=(X+SB+S3)/(X-SB+S5)
510      S2=(IX*(Y-SA)+S6)/(IX*(Y+SA)+S5)
520      S10=(X-SB+SA)/(X+SB+SA)
530      DENS=PI*(X+SB)*ALOG(S7)+A1*(Y+SA)*ALOG(S9)+
540      1 - PI*(X-SB)*ALOG(S9)+A1*(Y-SA)*ALOG(S10)
550      X=X*SP+SB
560      Y=Y*SA+SA
570      WRITE (6,400) (PR(N),N=1,700)
580      FORMAT (1H,20PR,7,70(1H,100)3.5,7)
590      WRITE (6,400) (S(N),N=1,700)
600      FORMAT (1H,1MS,7,70(1H,100)3.5,7)
610      WRITE (6,300) (D(N),N=1,700)
620      FORMAT (1H,1MD,7,70(1H,100)3.5,7)
630
640      C
650      C      FILM THICKNESS
660      C
670      20 CONTINUE
680      DO 700 J=1,NY
690      DO 701 I=1,NX
700      M3=I*(J-1)*NX+NX*Y
710      M4=I-J*NX+NX*Y
720      701 P2(M3)=P2(M4)
730      700 CONTINUE
740      DO 7 J=1,NY
750      DO 8 I=1,NX
760      N3=I*(J-1)*NX
770      SUM=0.000
780      DO 9 JJ=1,NY1
790      N40=(JJ-1)*NX
800      N=IANS(JJ-JJ)+1
810      N50=1+(N-1)*NX
820      DO 10 II=1,NX
830      N4=II*N40
840      M=IANS(1-II)
850      N5=M*N50
860      10 SUM=SUM+P2(N4)*DENS)
870      9 CONTINUE
880      WEN3=2.*SUM/PI
890      HEN3=(M3)*RY*(S(N3)+WEN3)
900      IF (HEN3).GT.(HMIN) GO TO 400
910      HMIN=HEN3
920      NSAVE=N1
930      400 CONTINUE
940      8 PRINT=(PR(N3))*(HEN3**0.5)
950      7 CONTINUE
960      WRITE (6,401) NSAVE, HMIN
970      401 FORMAT (1H,6HNSAVE=,110,10X,5HMIN=,016.5)
980      RETURN
990      END

```

END OF COMPILATION

NO DIAGNOSTICS.

TABLE 3.1. - INPUT CONDITIONS USED FOR COMPUTER EVALUATIONS

[Effective elastic modulus, E' , 21.97 MN/cm^2 ($3.187 \cdot 10^7$ psi); radius of curvature for solid A, $r_{Ax} = r_{Ay} = 1.111 \text{ cm}$ (0.4375 in.)]

Condition	Dimensionless load parameter, W	Normal applied force, F		Effective radius				Radius of curvature for solid B			
		N	lbf	R_x		R_y		r_{Bx}		r_{By}	
				cm	in.	cm	in.	cm	in.	cm	in.
1	$0.5105 \cdot 10^{-7}$	8.964	2	0.5558	0.2188	0.5558	0.2188	1.111	0.4375	1.111	0.4375
2	$.5105 \cdot 10^{-5}$	896.4	200	.5558	.2188	.5558	.2188	1.111	.4375	1.111	.4375
3	$.2102 \cdot 10^{-7}$	8.964	2	1.284	.5055	15.00	5.906	-8.260	-3.252	-1.200	-.4725
4	$.2102 \cdot 10^{-5}$	896.4	200	1.284	.5055	15.00	5.906	-8.260	-3.252	-1.200	-.4725

TABLE 3.2. - CHARACTERISTICS OF THE COMPONENTS OF FILM THICKNESS ALONG THE SEMIMAJOR AND SEMIMINOR AXES WHEN THESE AXES ARE DIVIDED INTO THREE EQUAL DIVISIONS

AND CONDITION 1 OF TABLE 3.1 PREVAILS

Coordinates		Pressure, p		Ratio	Elastic deformation, w		Ratio	Total separation, S + w		Ratio
X	Y	N cm^2	psi	$R_1 \frac{S}{S}$	cm	in.	$R_2 \frac{w}{S}$	cm	in.	R_3
7b	7a	$0.0851 \cdot 10^6$	$6.1235 \cdot 10^6$	1.000	$0.0856 \cdot 10^{-3}$	$0.0337 \cdot 10^{-3}$	35.33	$0.0881 \cdot 10^{-3}$	$0.0347 \cdot 10^{-3}$	0.7910
	9a	.0745	.1080		.0759	.0299	6.275	.0881	.0347	.9363
	11a	.0462	.0670		.0577	.0227	1.830	.0892	.0351	1.984
	13a	0	0		.0366	.0144	.6021	.0970	.0382	1.787
	15a			.9999	.0269	.0106	.2720	.1265	.0498	.8633
	17a			.9999	.0216	.0085	.1468	.1697	.0668	.4847
	19a			.9998	.0183	.0072	.0882	.2243	.0883	-----
	21a			.9998	.0157	.0062	.0572	.2896	.1140	-----
	23a			.9997	.0137	.0054	.0392	.3653	.1438	-----
	25a			.9996	.0122	.0048	.0282	.4511	.1776	-----
	27a			.9995	.0112	.0044	.0207	.5469	.2153	-----
	29a			.9994	.0102	.0040	.0158	.6525	.2569	-----
9b	7a	.0745	.1080	1.000	.0759	.0299	6.279	.0881	.0347	.9363
	11b	.0462	.0670	1.000	.0704	.0277	1.832	.0892	.0351	1.987
	13b	0	0	1.000	.0366	.0144	.6027	.0970	.0382	1.787
	15b			.9999	.0269	.0106	.2723	.1262	.0497	.8617
	17b			.9999	.0216	.0085	.1469	.1694	.0667	.4849
	19b			.9998	.0183	.0072	.0883	.2240	.0882	-----
	21b			.9998	.0157	.0062	.0572	.2893	.1139	-----
	23b			.9997	.0137	.0054	.0392	.3650	.1437	-----
	25b			.9996	.0122	.0048	.0280	.4509	.1775	-----
	27b			.9995	.0112	.0044	.0207	.5464	.2151	-----
	29b			.9994	.0102	.0040	.0153	.6520	.2567	-----

TABLE 3.3. - CHARACTERISTICS OF THE COMPONENTS OF FILM THICKNESS ALONG THE SEMIMAJOR AND SEMIMINOR AXES WHEN THESE AXES ARE DIVIDED INTO FOUR EQUAL DIVISIONS AND CONDITION 1 OF TABLE 3.1 PREVAILS

Coordinates		Pressure, p		Ratio $\frac{S}{S_0}$	Elastic deformation, w		Ratio $\frac{w}{S}$	Total separation, S + w		Ratio R_3							
X	Y	N cm ²	psi		cm	in.		cm	in.								
9b	9a	0.0863 · 10 ⁶	0.1251 · 10 ⁶	1.000	0.0864 · 10 ⁻³	0.0340 · 10 ⁻³	63.43	0.0879 · 10 ⁻³	0.0346 · 10 ⁻³	0.7284							
	11a	.0805	.1168	↓	.0810	.0319	11.89	.0879	.0346	.7808							
	13a	.0675	.0979		.0704	.0277	3.965	.0881	.0347	.9380							
	15a	.0410	.0594		.0546	.0215	1.603	.0886	.0349	1.674							
	17a	0	0		.0378	.0149	.6762	.0937	.0369	-----							
	19a	↓	↓		.0295	.0116	.3543	.1125	.0443	-----							
	21a				.9999	.0244	.0096	.2106	.1402	.0552	-----						
	23a				.9999	.0208	.0082	.1358	.1748	.0688	-----						
	25a				.9998	.0183	.0072	.0926	.2159	.0850	-----						
	27a				.9998	.0163	.0064	.0660	.2631	.1036	-----						
	29a				.9997	.0147	.0058	.0487	.3160	.1244	-----						
	31a				.9997	.0135	.0053	.0371	.3744	.1474	-----						
	33a				.9996	.0122	.0048	.0288	.4387	.1727	-----						
	35a				.9996	.0114	.0045	.0228	.5088	.2003	-----						
	37a				.9995	.0107	.0042	.0184	.5842	.2300	-----						
	39a				.9994	.0099	.0039	.0151	.6652	.2619	-----						
	11b				9a	.0805	.1168	1.000	.0810	.0319	11.90	.0879	.0346	.7808			
	13b				↓	↓	↓	.0704	.0277	3.968	.0879	.0346	.9381				
	15b							.0410	.0594	.0546	.0215	1.604	.0886	.0349	1.674		
	17b							0	0	.0378	.0149	.6768	.0937	.0369	-----		
	19b							↓	↓	↓	.0295	.0116	.3547	.1125	.0443	-----	
	21b										.9999	.0244	.0096	.2108	.1402	.0552	-----
	23b										.9999	.0208	.0082	.1358	.1748	.0688	-----
	25b										.9999	.0183	.0072	.0927	.2159	.0850	-----
	27b										.9998	.0163	.0064	.0661	.2629	.1035	-----
	29b										.9998	.0147	.0058	.0488	.3157	.1243	-----
	31b										.9997	.0135	.0053	.0371	.3744	.1474	-----
	33b										.9997	.0122	.0048	.0288	.4387	.1727	-----
	35b										.9996	.0114	.0045	.0228	.5088	.2003	-----
	37b										.9995	.0107	.0042	.0184	.5842	.2300	-----
	39b										.9994	.0099	.0039	.0151	.6652	.2619	-----

TABLE 3.4 - CHARACTERISTICS OF THE COMPONENTS OF FILM THICKNESS ALONG THE SEMIMAJOR AND SEMIMINOR AXES WHEN THESE AXES ARE DIVIDED INTO FIVE EQUAL DIVISIONS

AND CONDITION 1 OF TABLE 3.1 PREVAILS

Coordinates		Pressure p		Ratio $\frac{S}{S_0}$	Plastic deformation, w		Ratio $\frac{w}{S}$	Total separation, S - w		Ratio R_3
X	Y	N cm ²	psi		cm	in.		cm	in.	
11b	11a	0.9867 10 ⁶	0.1258 10 ⁶	1.000	0.0864 10 ⁻³	0.9340 10 ⁻³	99.95	0.6874 10 ⁻³	0.9344 10 ⁻³	0.0291
	13a	.0832	.1206	↓	.0828	.0326	19.01	.0874	.0344	.0378
	15a	.0754	.1093	↓	.0759	.0299	6.698	.0874	.0344	.0757
	17a	.0620	.0899	↓	.0655	.0258	3.008	.0874	.0344	.1921
	19a	.0372	.0539	↓	.0521	.0205	1.459	.0879	.0346	.7276
	21a	0	0	↓	.0384	.0151	.7195	.0914	.0360	-----
	23a			.9999	.0310	.0122	.4170	.1052	.0414	-----
	25a			↓	.0262	.0103	.2652	.1247	.0491	-----
	27a			↓	.0229	.0090	.1804	.1494	.0588	-----
	29a			↓	.0203	.0080	.1282	.1783	.0702	-----
	31a			.9998	.0183	.0072	.0944	.2111	.0831	-----
	33a			.9998	.0165	.0065	.0717	.2479	.0976	-----
	35a			.9998	.0152	.0060	.0556	.2883	.1135	-----
	37a			.9997	.0140	.0055	.0440	.3325	.1309	-----
	39a			.9997	.0130	.0051	.0355	.3895	.1498	-----
	41a			.9996	.0122	.0048	.0290	.4321	.1701	-----
	43a			.9996	.0114	.0045	.0240	.4869	.1917	-----
	45a			.9995	.0107	.0042	.0201	.5456	.2148	-----
	47a			.9995	.0102	.0040	.0170	.6081	.2394	-----
	49a			.9994	.0097	.0038	.0145	.6739	.2653	-----
13b	11a	.0832	.1206	1.000	.0828	.0326	19.02	.0874	.0344	.0408
15b		.0754	.1093	↓	.0759	.0299	6.702	.0874	.0344	.0757
17b		.0620	.0899	↓	.0655	.0258	3.010	.0874	.0344	.1921
19b		.0372	.0539	↓	.0521	.0205	1.460	.0879	.0346	.7243
21b		0	0	↓	.0384	.0151	.7202	.0914	.0360	-----
23b				.9999	.0310	.0122	.4174	.1052	.0414	-----
25b				↓	.0262	.0103	.2660	.1247	.0491	-----
27b				↓	.0229	.0090	.1805	.1494	.0588	-----
29b				↓	.0203	.0080	.1283	.1781	.0701	-----
31b				.9998	.0183	.0072	.0945	.2108	.0830	-----
33b				.9998	.0165	.0065	.0717	.2477	.0975	-----
35b				.9998	.0152	.0060	.0556	.2880	.1134	-----
37b				.9997	.0140	.0055	.0441	.3322	.1308	-----
39b				.9997	.0130	.0051	.0355	.3802	.1497	-----
41b				.9996	.0122	.0048	.0290	.4315	.1699	-----
43b				.9995	.0114	.0045	.0240	.4867	.1916	-----
45b				.9995	.0107	.0042	.0201	.5453	.2147	-----
47b				.9995	.0102	.0040	.0170	.6076	.2392	-----
49b				.9994	.0097	.0038	.0145	.6734	.2651	-----

TABLE 3.5. - CHARACTERISTICS OF THE COMPONENTS OF FILM THICKNESS ALONG THE SEMIMAJOR AND SEMIMINOR AXES WHEN THESE AXES ARE DIVIDED INTO THREE EQUAL DIVISIONS AND CONDITION 2 OF TABLE 3.1 PREVAILS

Coordinates		Pressure, p		Ratio $\frac{S}{S}$	Elastic deformation, w		Ratio $\frac{w}{S}$	Total separation, S + w		Ratio R_3
X	Y	N cm ²	psi		cm	in.		cm	in.	
7b	7a	0.3953 · 10 ⁶	0.5734 · 10 ⁶	1.000	1.844 · 10 ⁻³	0.7261 · 10 ⁻³	35.33	1.897 · 10 ⁻³	0.7467 · 10 ⁻³	0.8136
	9a	.3457	.5014	.9998	1.639	.6451	6.275	1.900	.7479	1.088
	11a	.2144	.3109	.9994	1.243	.4892	1.830	1.922	.7565	3.102
	13a	0	0	.9989	.7861	.3095	.6021	2.092	.8235	4.897
	15a			.9981	.5824	.2293	.2720	2.723	1.072	4.170
	17a			.9972	.4676	.1841	.1468	3.653	1.438	3.924
	19a			.9960	.3917	.1543	.0883	4.829	1.901	-----
	21a			.9947	.3317	.1329	.072	6.236	2.455	-----
	23a			.9932	.2967	.1168	.0392	7.864	3.096	-----
	25a			.9915	.2647	.1042	.0280	9.710	3.823	-----
	27a			.9896	.2390	.0942	.0207	11.77	4.635	-----
	29a			.9874	.2179	.0858	.0158	14.05	5.531	-----
9b	7a	.3457	.5014	.9998	1.639	.6451	6.279	1.900	.7479	1.086
	11b	.2144	.3109	.9994	1.243	.4893	1.832	1.922	.7564	3.104
	13b	0	0	.9989	.7861	.3096	.6027	2.092	.8232	4.896
	15b			.9981	.5824	.2294	.2723	2.723	1.072	4.164
	17b			.9972	.4676	.1841	.1469	3.653	1.438	3.922
	19b			.9960	.3917	.1543	.0883	4.829	1.901	-----
	21b			.9947	.3317	.1329	.072	6.236	2.455	-----
	23b			.9932	.2967	.1168	.0392	7.864	3.096	-----
	25b			.9915	.2649	.1043	.0280	9.710	3.823	-----
	27b			.9896	.2393	.0942	.0207	11.77	4.635	-----
	29b			.9874	.2182	.0859	.0155	14.05	5.531	-----

TABLE 3.6. - CHARACTERISTICS OF THE COMPONENTS OF FILM THICKNESS ALONG THE SEMIMAJOR AND SEMIMINOR AXES WHEN THESE AXES ARE DIVIDED INTO FOUR EQUAL DIVISIONS AND CONDITION 2 OF TABLE 3.1 PREVAILS

Coordinates		Pressure, p		Ratio $\frac{S}{S}$	Elastic deformation, w		Ratio $\frac{w}{S}$	Total separation, S + w		Ratio R_3
X	Y	N cm ²	psi		cm	in.		cm	in.	
9b	9a	0.4004 · 10 ⁶	0.5807 · 10 ⁶	1.000	1.863 · 10 ⁻³	0.7333 · 10 ⁻³	63.43	1.892 · 10 ⁻³	0.7448 · 10 ⁻³	0.7391
	11a	.3736	.5419	.9999	1.746	.6874	11.89	1.893	.7452	.8450
	13a	.3134	.4546	.9997	1.514	.5962	3.965	1.896	.7465	1.180
	15a	.1902	.2759	.9994	1.177	.4633	1.603	1.911	.7525	2.748
	17a	0	0	.9989	.8143	.3200	.6768	2.018	.7948	-----
	19a			.9984	.6350	.2500	.3547	2.426	.9550	-----
	21a			.9978	.5258	.2070	.2106	3.023	1.190	-----
	23a			.9970	.4503	.1773	.1356	3.769	1.484	-----
	25a			.9962	.3942	.1552	.0920	4.653	1.832	-----
	27a			.9952	.3510	.1382	.0660	5.669	2.232	-----
	29a			.9942	.3165	.1246	.0487	6.810	2.681	-----
	31a			.9930	.2883	.1135	.0370	8.072	3.178	-----
	33a			.9917	.2647	.1042	.0288	9.459	3.724	-----
	35a			.9903	.2446	.0963	.0228	10.97	4.318	-----
	37a			.9888	.2276	.0896	.0184	12.60	4.959	-----
	39a			.9872	.2126	.0837	.0150	14.34	5.647	-----
11b	9a	.3736	.5419	.9999	1.746	.6874	11.90	1.893	.7452	.8450
	13b	.3134	.4546	.9997	1.514	.5962	3.968	1.896	.7464	1.178
	15b	.1902	.2759	.9994	1.177	.4634	1.604	1.911	.7523	2.747
	17b			.9989	.8143	.3200	.6768	2.018	.7946	-----
	19b			.9984	.6350	.2500	.3547	2.426	.9550	-----
	21b			.9978	.5258	.2071	.2106	3.020	1.189	-----
	23b			.9970	.4503	.1773	.1358	3.767	1.483	-----
	25b			.9962	.3942	.1553	.0927	4.651	1.831	-----
	27b			.9952	.3510	.1382	.0661	5.664	2.230	-----
	29b			.9942	.3165	.1246	.0488	6.805	2.679	-----
	31b			.9930	.2883	.1135	.0371	8.067	3.176	-----
	33b			.9917	.2647	.1042	.0288	9.454	3.722	-----
	35b			.9903	.2446	.0963	.0228	10.96	4.315	-----
	37b			.9888	.2276	.0896	.0184	12.59	4.955	-----
	39b			.9872	.2126	.0837	.0151	14.33	5.643	-----

TABLE 3.7. - CHARACTERISTICS OF THE COMPONENTS OF FILM THICKNESS ALONG THE SEMIMAJOR AND SEMIMINOR AXES WHEN THESE AXES ARE DIVIDED INTO FIVE EQUAL DIVISIONS AND CONDITION 2 OF TABLE 3.1 PREVAILS

Coordinates		Pressure, p		Ratio	Elastic deformation, w		Ratio	Total separation, S - w		Ratio
X	Y	N cm ²	psi	R ₁ $\frac{S}{S}$	cm	in.	R ₂ $\frac{w}{S}$	cm	in.	R ₃
11b	11a	0.4027 · 10 ⁶	0.5840 · 10 ⁶	1.000	1.862 · 10 ⁻³	0.7329 · 10 ⁻³	99.05	1.880 · 10 ⁻³	0.7403 · 10 ⁻³	0.0287
	13a	.3859	.5597	.9999	1.787	.7034	19.01	1.881	.7404	.0398
	15a	.3499	.5075	.9998	1.637	.6445	6.698	1.881	.7407	.0854
	17a	.2876	.4172	.9996	1.414	.5566	3.008	1.884	.7417	.2558
	19a	.1726	.2503	.9993	1.124	.4427	1.459	1.895	.7461	1.228
	21a	0	0	.9990	.8252	.3249	.7195	1.972	.7764	-----
	23a			.9986	.6662	.2623	.4170	2.264	.8915	-----
	25a			.9981	.5646	.2223	.2658	2.690	1.059	-----
	27a			.9976	.4917	.1936	.1804	3.218	1.267	-----
	29a			.9970	.4361	.1717	.1282	3.840	1.512	-----
	31a			.9963	.3922	.1544	.0944	4.547	1.790	-----
	33a			.9955	.3566	.1404	.0716	5.339	2.102	-----
	35a			.9947	.3272	.1288	.0556	6.213	2.446	-----
	37a			.9938	.3020	.1189	.0440	7.165	2.821	-----
	39a			.9928	.2807	.1105	.0355	8.197	3.227	-----
	41a			.9918	.2621	.1032	.0290	9.307	3.664	-----
	43a			.9907	.2459	.0968	.0240	10.49	4.131	-----
	45a			.9895	.2316	.0912	.0201	11.76	4.629	-----
	47a			.9883	.2189	.0862	.0170	13.10	5.157	-----
49a			.9870	.2075	.0817	.0145	14.52	5.715	-----	
13b	11a	.3859	.5597	.9999	1.787	.7034	19.02	1.881	.7404	.0412
15b		.3499	.5075	.9998	1.637	.6445	6.702	1.881	.7407	.0854
17b		.2876	.4172	.9996	1.414	.5567	3.010	1.884	.7416	.2557
19b		.1726	.2503	.9993	1.124	.4427	1.460	1.895	.7460	1.228
21b	0	0		.9990	.8252	.3249	.7202	1.971	.7761	-----
23b				.9986	.6662	.2624	.4174	2.263	.8911	-----
25b				.9981	.5646	.2224	.2660	2.687	1.058	-----
27b				.9976	.4917	.1936	.1805	3.216	1.266	-----
29b				.9970	.4361	.1718	.1283	3.838	1.511	-----
31b				.9963	.3922	.1545	.0945	4.544	1.789	-----
33b				.9955	.3566	.1404	.0717	5.337	2.101	-----
35b				.9947	.3272	.1288	.0556	6.208	2.444	-----
37b				.9938	.3020	.1190	.0441	7.160	2.819	-----
39b				.9929	.2807	.1105	.0355	8.192	3.225	-----
41b				.9918	.2621	.1032	.0290	9.299	3.661	-----
43b				.9907	.2459	.0969	.0240	10.49	4.128	-----
45b				.9895	.2316	.0912	.0201	11.75	4.625	-----
47b				.9883	.2189	.0862	.0170	13.09	5.153	-----
49b				.9870	.2075	.0817	.0145	14.51	5.711	-----

TABLE 3.8. CHARACTERISTICS OF THE COMPONENTS OF FILM THICKNESS ALONG THE SEMIMAJOR AND SEMIMINOR AXES WHEN THESE AXES ARE DIVIDED INTO THREE EQUAL DIVISIONS AND CONDITION 3 OF TABLE 3.1 PREVAILS

Coordinates		Pressure, p		Elastic deformation, w		Ratio $\frac{w}{S}$	Total separation, S + w		Ratio R_3
X	Y	N cm ²	psi	cm	m.		cm	m.	
7b	7a	0.0248 10 ⁶	0.0360 10 ⁶	0.0399 10 ⁻³	0.0157 10 ⁻³	35.42	0.0409 10 ⁻³	0.0161 10 ⁻³	1.030
	9a	.0217	.0315	.0338	.0133	4.662	.0409	.0161	1.135
	11a	.0134	.0195	.0210	.0087	1.132	.0414	.0163	4.030
	13a	0	0	.0102	.0040	.2705	.0480	.0185	7.494
	15a			.0071	.0028	.1128	.0691	.0272	4.993
	17a			.0056	.0022	.0591	.0983	.0387	4.350
	19a			.0046	.0018	.0351	.1339	.0527	-----
	21a			.0038	.0015	.0225	.1700	.0693	-----
	23a			.0033	.0013	.0154	.2243	.0883	-----
	25a			.0030	.0012	.0109	.2789	.1098	-----
	27a			.0028	.0011	.0081	.3396	.1337	-----
	29a			.0025	.0010	.0061	.4067	.1601	-----
9b	7a	.0217	.0315	.0371	.0146	9.205	.0411	.0162	1.271
11b		.0134	.0195	.0315	.0124	3.210	.0414	.0163	2.243
13b		0	0	.0249	.0098	1.340	.0434	.0171	2.820
15b				.0211	.0083	.6966	.0511	.0201	2.544
17b				.0183	.0072	.4114	.0630	.0248	2.517
19b				.0163	.0064	.2638	.0782	.0308	-----
21b				.0147	.0058	.1794	.0970	.0382	-----
23b				.0135	.0053	.1276	.1189	.0468	-----
25b				.0124	.0049	.0940	.1438	.0566	-----
27b				.0114	.0045	.0712	.1720	.0677	-----
29b				.0107	.0042	.0552	.2029	.0799	-----

TABLE 3.9. CHARACTERISTICS OF THE COMPONENTS OF FILM THICKNESS ALONG THE SEMIMAJOR AND SEMIMINOR AXES WHEN THESE AXES ARE DIVIDED INTO FOUR EQUAL DIVISIONS AND CONDITION 3 OF TABLE 3.1 PREVAILS

Coordinates		Pressure, p		Elastic deformation, w		Ratio $\frac{w}{S}$	Total separation, S + w		Ratio R_3
X	Y	N cm ²	psi	cm	m.		cm	m.	
9b	9a	0.0252 10 ⁶	0.0365 10 ⁶	0.0401 10 ⁻³	0.0158 10 ⁻³	43.53	0.0409 10 ⁻³	0.0161 10 ⁻³	0.8000
	11a	.0235	.0341	.0368	.0145	6.039	.0409	.0161	.9554
	13a	.0197	.0286	.0300	.0118	2.735	.0409	.0161	1.290
	15a	.0119	.0173	.0201	.0079	.9417	.0411	.0162	3.867
	17a	0	0	.0107	.0042	.3032	.0455	.0179	-----
	19a			.0076	.0030	.1478	.0599	.0230	-----
	21a			.0061	.0024	.0854	.0790	.0311	-----
	23a			.0053	.0021	.0542	.1021	.0402	-----
	25a			.0046	.0018	.0367	.1268	.0507	-----
	27a			.0041	.0016	.0260	.1593	.0627	-----
	29a			.0036	.0014	.0191	.1930	.0760	-----
	31a			.0033	.0013	.0145	.2306	.0908	-----
	33a			.0030	.0012	.0112	.2715	.1069	-----
	35a			.0028	.0011	.0089	.3160	.1244	-----
	37a			.0025	.0010	.0071	.3640	.1433	-----
	39a			.0023	.0009	.0058	.4153	.1635	-----
11b	9a	.0235	.0341	.0386	.0152	17.06	.0409	.0161	.9431
13b		.0197	.0286	.0353	.0139	6.410	.0409	.0161	1.161
15b		.0119	.0173	.0307	.0121	2.948	.0411	.0162	1.855
17b		0	0	.0254	.0100	1.501	.0424	.0167	-----
19b				.0221	.0087	.8849	.0472	.0186	-----
21b				.0198	.0078	.5700	.0546	.0215	-----
23b				.0180	.0071	.3900	.0643	.0253	-----
25b				.0165	.0065	.2789	.0759	.0299	-----
27b				.0152	.0060	.2065	.0892	.0351	-----
29b				.0142	.0056	.1572	.1044	.0411	-----
31b				.0132	.0052	.1225	.1214	.0478	-----
33b				.0124	.0049	.0973	.1402	.0552	-----
35b				.0117	.0046	.0785	.1605	.0632	-----
37b				.0109	.0043	.0643	.1829	.0720	-----
39b				.0104	.0041	.0533	.2068	.0814	-----

TABLE 3. 10. - CHARACTERISTICS OF THE COMPONENTS OF FILM THICKNESS ALONG THE SEMI-MAJOR AND SEMI-MINOR AXES WHEN THESE AXES ARE DIVIDED INTO FIVE EQUAL DIVISIONS AND CONDITION 3 OF TABLE 3. 1 PREVAILS

Coordinates		Pressure, p		Ratio	Elastic deformation, w		Ratio	Total separation, S - w		Ratio
\bar{x}	\bar{y}	N cm ²	psi	R ₁ $\frac{S}{S}$	cm	in.	R ₂ $\frac{w}{S}$	cm	in.	R ₃
11b	11a	0. 1179 · 10 ⁶	0. 1704 · 10 ⁶	1. 000	0. 8661 · 10 ⁻³	0. 3410 · 10 ⁻³	99. 24	0. 8750 · 10 ⁻³	0. 3445 · 10 ⁻³	0. 1998
	13a	. 1126	. 1633		. 8179	. 3220	14. 58	. 8740	. 3441	. 1244
	15a	. 1021	. 1481		. 7216	. 2841	4. 786	. 8725	. 3435	. 0668
	17a	. 0839	. 1217		. 5804	. 2285	1. 981	. 8733	. 3438	. 0988
	19a	. 0503	. 0730		. 3975	. 1565	. 8242	. 8799	. 3464	1. 617
	21a	0	0		. 2316	. 0912	. 3220	. 9507	. 3743	-----
	23a				. 1755	. 0691	. 1749	1. 179	. 4640	-----
	25a				. 1448	. 0570	. 1085	1. 480	. 5825	-----
	27a			. 9999	. 1242	. 0489	. 0725	1. 838	. 7236	-----
	29a				. 1092	. 0430	. 0510	2. 249	. 8855	-----
	31a				. 0975	. 0384	. 0373	2. 710	1. 067	-----
	33a				. 0884	. 0348	. 0282	3. 223	1. 269	-----
	35a				. 0808	. 0318	. 0218	3. 785	1. 490	-----
	37a				. 0744	. 0293	. 0172	4. 392	1. 729	-----
	39a			. 9998	. 0688	. 0271	. 0138	5. 050	1. 988	-----
	41a				. 0643	. 0253	. 0113	5. 756	2. 266	-----
	43a				. 0602	. 0237	. 0093	6. 510	2. 563	-----
	45a				. 0566	. 0223	. 0078	7. 310	2. 878	-----
	47a			. 9997	. 0536	. 0211	. 0066	8. 161	3. 213	-----
	49a			. 9997	. 0508	. 0200	. 0056	9. 058	3. 566	-----
13b	11a	. 1126	. 1633	1. 000	. 8440	. 3323	27. 05	. 8753	. 3446	. 2262
	15b	. 1021	. 1481	1. 000	. 7996	. 3148	10. 50	. 8755	. 3447	. 2836
	17b	. 0839	. 1217	1. 000	. 7330	. 2886	5. 105	. 8766	. 3451	. 4141
	19b	. 0503	. 0730	. 9999	. 6459	. 2543	2. 767	. 8793	. 3462	. 8447
	21b	0	0	. 9999	. 5525	. 2175	1. 597	. 8981	. 3536	-----
	23b			. 9998	. 4925	. 1939	1. 025	. 9731	. 3831	-----
	25b			. 9998	. 4478	. 1763	. 7020	1. 086	. 4275	-----
	27b			. 9997	. 4117	. 1621	. 5036	1. 230	. 4841	-----
	29b			. 9996	. 3818	. 1503	. 3742	1. 402	. 5519	-----
	31b			. 9995	. 3559	. 1401	. 2859	1. 601	. 6302	-----
	33b			. 9994	. 3335	. 1313	. 2235	1. 825	. 7187	-----
	35b			. 9993	. 3137	. 1235	. 1781	2. 075	. 8171	-----
	37b			. 9992	. 2962	. 1. 66	. 1442	2. 350	. 9252	-----
	39b			. 9991	. 2804	. 1104	. 1184	2. 649	1. 043	-----
	41b			. 9990	. 2664	. 1049	. 0984	2. 972	1. 170	-----
	43b			. 9988	. 2535	. 0998	. 0827	3. 320	1. 307	-----
	45b			. 9987	. 2418	. 0952	. 0702	3. 688	1. 452	-----
	47b			. 9985	. 2311	. 0910	. 0600	4. 082	1. 607	-----
	49b			. 9985	. 2212	. 0871	. 0517	4. 501	1. 772	-----

REPRODUCIBILITY OF THE ORIGINAL PAGE IS POOR

TABLE 3. 11. - CHARACTERISTICS OF THE COMPONENTS OF FILM THICKNESS ALONG THE SEMIMAJOR AND SEMIMINOR AXES WHEN THESE AXES ARE DIVIDED INTO THREE EQUAL DIVISIONS AND CONDITION 4 OF TABLE 3. 1 PREVAILS

Coordinates		Pressure, p		Ratio $\frac{R_1}{S}$	Elastic deformation, w		Ratio $\frac{R_2}{S}$	Total separation, S - w		Ratio R_3
X	Y	N cm ²	psi		cm	in.		cm	in.	
7b	7a	0.1153 · 10 ⁶	0.1673 · 10 ⁶	1.000	0.8588 · 10 ⁻³	0.3381 · 10 ⁻³	35.42	0.8829 · 10 ⁻³	0.3476 · 10 ⁻³	1.028
	9a	.1009	.1463		.7262	.2659	4.662	.8821	.3473	1.135
	11a	.0625	.0907		.4745	.1698	1.132	.8933	.3517	4.033
	13a	0	0		.2202	.0867	.2705	1.034	.4069	7.494
	15a				.1511	.0595	.1128	1.491	.5869	4.994
	17a			.9999	.1181	.0465	.0591	2.116	.8329	4.353
	19a			.9999	.0978	.0385	.0351	2.885	1.136	-----
	21a			.9999	.0836	.0329	.0225	3.792	1.493	-----
	23a			.9998	.0732	.0288	.0154	4.634	1.903	-----
	25a			.9998	.0650	.0256	.0109	6.010	2.366	-----
	27a			.9998	.0587	.0231	.0061	7.318	2.881	-----
	29a			.9997	.0533	.0210	.001	8.760	3.449	-----
9b	7a	.1009	.1463	1.000	.7978	.3141	9.205	.8844	3.462	1.267
11b		.0625	.0907	.9999	.6789	.2673	3.210	.8905	3.506	2.280
13b	0	0	0	.9999	.5344	.2104	1.340	.9332	.3674	2.820
15b				.9998	.4519	.1779	.6966	1.100	.4332	2.543
17b				.9996	.3952	.1556	.4114	1.556	.5338	2.517
19b				.9995	.3523	.1387	.2638	1.687	.6643	-----
21b				.9993	.3180	.1252	.1794	2.090	.8229	-----
23b				.9991	.2898	.1141	.1376	2.560	1.008	-----
25b				.9989	.2662	.1048	.0940	3.099	1.220	-----
27b				.9987	.2461	.0969	.0712	3.708	1.458	-----
29b				.9984	.2289	.0901	.0552	4.374	1.722	-----

TABLE 3. 12. - CHARACTERISTICS OF THE COMPONENTS OF FILM THICKNESS ALONG THE SEMIMAJOR AND SEMIMINOR AXES WHEN THESE AXES ARE DIVIDED INTO FOUR EQUAL DIVISIONS AND CONDITION 4 OF TABLE 3. 1 PREVAILS

Coordinates		Pressure, p		Ratio $\frac{R_1}{S}$	Elastic deformation, w		Ratio $\frac{R_2}{S}$	Total separation, S - w		Ratio R_3
X	Y	N cm ²	psi		cm	in.		cm	in.	
9b	9a	0.1168 · 10 ⁶	0.1694 · 10 ⁶	1.000	0.8664 · 10 ⁻³	0.3411 · 10 ⁻³	63.53	0.8801 · 10 ⁻³	0.3465 · 10 ⁻³	0.8604
	11a	.1090	.1581		.7922	.3119	9.039	.8799	.3464	.9549
	13a	.0914	.1326		.6444	.2537	2.735	.8801	.3465	1.290
	15a	.0555	.0805		.4310	.1697	.9417	.8849	.3498	3.869
	17a	0	0		.2286	.0900	.3032	.9822	.3867	-----
	19a				.1661	.0654	.1478	1.290	.5077	-----
	21a			.9999	.1339	.0527	.0854	1.702	.6699	-----
	23a			.9999	.1130	.0445	.0542	2.199	.8657	-----
	25a				.0983	.0387	.0367	2.776	1.093	-----
	27a				.0869	.0342	.0260	3.432	1.351	-----
	29a				.0780	.0307	.0191	4.161	1.638	-----
	31a			.9998	.0709	.0279	.0145	4.998	1.956	-----
	33a			.9998	.0650	.0256	.0112	5.850	2.303	-----
	35a			.9998	.0599	.0236	.0089	6.807	2.680	-----
	37a			.9997	.0556	.0219	.0071	7.838	3.086	-----
	39a			.9997	.0518	.0204	.0058	8.946	3.522	-----
11b	9a	.1090	.1581	1.000	.8319	.3275	17.06	.8806	.3467	.9433
13b		.0914	.1326	1.000	.7628	.3003	6.410	.8816	.3471	1.162
15b		.0555	.0805	.9999	.6612	.2603	2.946	.8854	.3486	1.855
17b	0	0	0	.9999	.5476	.2156	1.501	.9124	.3592	-----
19b				.9998	.4780	.1882	.8849	1.019	.4010	-----
21b				.9997	.4280	.1685	.5700	1.179	.4642	-----
23b				.9996	.3886	.1530	.3899	1.368	.5455	-----
25b				.9995	.3564	.1403	.2789	1.634	.6433	-----
27b				.9994	.3292	.1296	.2065	1.923	.7576	-----
29b				.9993	.3058	.1204	.1572	2.251	.8861	-----
31b				.9991	.2855	.1124	.1225	2.646	1.030	-----
33b				.9989	.2677	.1054	.0973	3.020	1.189	-----
35b				.9988	.2520	.0992	.0785	3.492	1.363	-----
37b				.9986	.2380	.0937	.0631	3.940	1.551	-----
39b				.9984	.2253	.0887	.0533	4.453	1.753	-----

TABLE 5.1. - EFFECT OF ELLIPTICITY PARAMETER ON
MINIMUM FILM THICKNESS

Ellipticity parameter, k	Minimum film thickness		Difference between H_{min} and \tilde{H}_{min} ' D_1 , percent
	Obtained from EHL point- contact theory, H_{min}	Obtained from least-square fit, \tilde{H}_{min}	
1	3.387×10^{-6}	3.464×10^{-6}	+2.88
1.25	4.105	4.031	-1.80
1.5	4.565	4.509	-1.22
1.75	4.907	4.913	+ .11
2	5.255	5.252	- .05
2.5	5.755	5.781	+ .45
3	6.091	6.156	+1.08
4	6.636	6.613	- .34
6	6.969	6.961	- .12
8	7.048	7.050	+ .02

TABLE 5.2. - EFFECT OF DIMENSIONLESS SPEED
PARAMETER ON MINIMUM FILM THICKNESS

Dimensionless speed param- eter, U	Minimum film thickness		Difference between H_{min} and \tilde{H}_{min} ' D_1 , percent
	Obtained from EHL point- contact theory, H_{min}	Obtained from least-square fit, \tilde{H}_{min}	
0.08416×10^{-11}	3.926×10^{-6}	3.915×10^{-6}	-0.275
.1683	6.156	6.252	+1.564
.2525	8.372	8.223	-1.780
.3367	9.995	9.987	- .078
.4208	11.61	11.61	- .004
.5892	14.39	14.57	+1.280
.8416	18.34	18.54	+1.104
1.263	24.47	24.39	- .320
1.683	29.75	29.61	- .467
2.104	34.58	34.43	- .432
2.525	39.73	38.95	-1.977
2.946	43.47	43.22	- .576
3.367	47.32	47.30	- .042
4.208	54.57	54.99	+ .765
5.050	61.32	62.20	+1.430

TABLE 5.3. - EFFECT OF DIMENSIONLESS LOAD PARAMETER
ON MINIMUM FILM THICKNESS

Dimensionless load param- eter, W	Minimum film thickness		Difference between H_{min} and \tilde{H}_{min} ' D_1 , percent
	Obtained from EHL point- contact theory, H_{min}	Obtained from least-square fit, \tilde{H}_{min}	
0.1106×10^{-6}	6.969×10^{-6}	6.941×10^{-6}	-0.41
.2211	6.492	6.599	+1.65
.3686	6.317	6.358	+ .64
.5528	6.268	6.172	-1.52
.7371	6.156	6.044	-1.81
.9214	6.085	5.947	-2.27
1.106	5.811	5.868	+ .98
1.290	5.657	5.803	+2.58

TABLE 5.4. - EFFECT OF SOLID MATERIAL AND LUBRICANT AS REPRESENTED IN DIMENSIONLESS

MATERIAL PARAMETER ON MINIMUM FILM THICKNESS

Solid material	Lubricant	Dimensionless material parameter, G	Dimensionless speed parameter, U	Dimensionless load parameter, W	Minimum film thickness		Difference between \bar{H}_{min} and \bar{H}'_{min} , D_1 , percent
					Obtained from EHL point-contact theory, \bar{H}_{min}	Obtained from least-square fit, \bar{H}'_{min}	
Bronze	Paraffinic	2310	0.3296×10^{-11}	0.7216×10^{-6}	6.931×10^{-6}	6.873×10^{-6}	-0.84
Bronze	Naphthenic	3591	.9422	.7216	17.19	17.404	+1.25
Steel	Paraffinic	4522	.1683	.3686	6.317	6.336	+ .31
Silicon nitride	Paraffinic	6785	.1127	.2456	6.080	6.038	- .70

TABLE 5.5. - DATA SHOWING EFFECT OF ELLIPTICITY, LOAD, SPEED, AND MATERIAL ON MINIMUM FILM THICKNESS

Case	Ellipticity parameter, k	Dimensionless load parameter, W	Dimensionless speed parameter, U	Dimensionless material parameter, G	Minimum film thickness		Difference between \bar{H}_{min} and \bar{H}'_{min} , D_1 , percent	Results
					Obtained from EHL point-contact theory, \bar{H}_{min}	Obtained from least-square fit, \bar{H}'_{min}		
1	1	0.1106×10^{-6}	0.1683×10^{-11}	4522	3.367×10^{-6}	3.514×10^{-6}	+4.37	} Ellipticity
2	1.25	↓	↓	↓	4.105	4.078	- .66	
3	1.5	↓	↓	↓	4.565	4.554	- .24	
4	1.75	↓	↓	↓	4.907	4.955	+ .98	
5	2	↓	↓	↓	5.255	5.294	+ .74	
6	2.5	↓	↓	↓	5.755	5.821	+1.15	
7	3	↓	↓	↓	6.091	6.196	+1.72	
8	4	↓	↓	↓	6.636	6.652	+ .24	
9	6	↓	↓	↓	6.969	7.001	+ .46	
10	8	↓	↓	↓	7.048	7.091	+ .61	
11	6	.2211	↓	↓	8.492	8.656	+2.50	} Load plus case 9
12	↓	.3686	↓	↓	6.317	6.412	+1.50	
13	↓	.5528	↓	↓	6.268	6.225	- .69	
14	↓	.7371	↓	↓	6.156	6.095	- .99	
15	↓	.9214	↓	↓	6.085	5.997	-1.45	
16	↓	1.106	↓	↓	5.811	5.918	+1.84	
17	↓	1.290	↓	↓	5.657	5.851	+3.43	
18	↓	.7371	.08416	↓	3.926	3.805	-3.08	
19	↓	↓	.2525	↓	8.372	8.032	-4.06	
20	↓	↓	.3367	↓	9.995	9.769	-2.26	} Speed plus case 14
21	↓	↓	.4208	↓	11.61	11.37	-2.07	
22	↓	↓	.5092	↓	14.39	14.29	- .69	
23	↓	↓	.8416	↓	18.34	18.21	- .71	
24	↓	↓	1.263	↓	24.47	24.00	-1.92	
25	↓	↓	1.683	↓	29.75	29.18	-1.92	
26	↓	↓	2.104	↓	34.56	33.96	-1.76	
27	↓	↓	2.525	↓	39.73	38.44	-3.25	
28	↓	↓	2.946	↓	43.47	42.89	-1.79	
29	↓	↓	3.367	↓	47.32	46.76	-1.18	
30	↓	↓	4.208	↓	54.57	54.41	- .29	
31	↓	↓	5.050	↓	61.32	61.59	+ .44	} Materials plus case 9
32	↓	.7216	.3296	2310	6.931	6.938	+ .10	
33	↓	.7216	.9422	3491	17.19	17.59	+2.33	
34	↓	.2456	.1122	6785	6.080	6.116	+ .59	

TABLE 5.6. - EFFECT OF ELLIPTICITY PARAMETER
ON CENTRAL FILM THICKNESS

Ellipticity parameter, k	Central film thickness		Difference between H_c and \tilde{H}_c , D_2 , percent
	Obtained from EHL point- contact theory, H_c	Obtained from least-square fit, \tilde{H}_c	
1	6.860×10^{-6}	6.132×10^{-6}	-10.52
1.25	6.964	6.565	-5.73
1.5	7.001	6.921	-1.14
1.75	7.015	7.218	+2.89
2	7.402	7.465	+ .85
2.5	7.653	7.841	+2.46
3	7.845	8.102	+3.28
4	8.292	8.408	+1.40
6	8.657	8.625	- .37
8	8.672	8.675	+ .03

TABLE 5.7. - EFFECT OF DIMENSIONLESS SPEED
PARAMETER ON CENTRAL FILM THICKNESS

Dimensionless speed param- eter, U	Central film thickness		Difference between H_c and \tilde{H}_c , D_2 , percent
	Obtained from EHL point- contact theory, H_c	Obtained from least-square fit, \tilde{H}_c	
0.08416×10^{-11}	$4.917 \cdot 10^{-6}$	$4.720 \cdot 10^{-6}$	-4.00
.1683	7.517	7.495	- .29
.2525	9.999	9.825	-1.74
.3367	11.40	11.91	+4.47
.4208	13.07	13.81	+5.66
.5092	17.13	17.29	+ .93
.8416	21.35	21.94	+2.76
1.263	25.62	28.76	-2.90
1.683	35.50	34.83	-1.89
2.104	41.05	40.43	-1.51
2.525	46.64	45.66	-2.10
2.946	51.08	50.61	- .92
3.367	55.56	55.33	- .41
4.208	63.81	64.20	+ .61
5.050	71.25	72.51	+1.77

TABLE 5.8. - EFFECT OF DIMENSIONLESS LOAD PARAMETERS
ON CENTRAL FILM THICKNESS

Dimensionless load param- eter, W	Central film thickness		Difference between H_c and \tilde{H}_c , D_2 , percent
	Obtained from EHL point- contact theory, H_c	Obtained from least-square fit, \tilde{H}_c	
$0.1006 \cdot 10^{-6}$	$8.637 \cdot 10^{-6}$	$8.424 \cdot 10^{-6}$	2.69
.2211	7.796	7.990	+2.49
.3686	7.505	7.720	+2.86
.5528	7.309	7.512	+2.78
.7371	7.317	7.368	-1.98
.9214	7.611	7.258	-4.63
1.106	7.416	7.170	-3.32
1.290	6.762	7.096	-4.94

TABLE 5.9. - EFFECT OF SOLID MATERIAL AND LUBRICANT AS REPRESENTED IN DIMENSIONLESS

MATERIAL PARAMETER ON MINIMUM FILM THICKNESS

Solid material	Lubricant	Dimensionless material parameter, G	Dimensionless speed parameter, U	Dimensionless load parameter, W	Central film thickness		Difference between H_c and \tilde{H}_c , D_2 , percent
					Obtained from EHL point-contact theory, H_c	Obtained from least square fit, \tilde{H}_c	
Bronze	Paraffinic	2310	0.3296×10^{-11}	$0.7216 \cdot 10^{-6}$	$8.422 \cdot 10^{-6}$	$8.226 \cdot 10^{-6}$	-2.33
Bronze	Naphthenic	3591	.9422	.7216	20.70	20.99	+1.40
Steel	Paraffinic	4522	.1683	.3686	7.505	7.819	+4.18
Silicon nitride	Paraffinic	6785	.1122	.2456	7.825	7.585	-3.07

TABLE 5.10. - DATA SHOWING EFFECT OF ELLIPTICITY, LOAD, SPEED, AND MATERIAL ON CENTRAL FILM THICKNESS

Case	Ellipticity parameter, k	Dimensionless load parameter, W	Dimensionless speed parameter, U	Dimensionless material parameter, G	Central film thickness		Difference between H_c and \tilde{H}_c , D_2 , percent	Results	
					Obtained from EHL point-contact theory, H_c	Obtained from least-square fit, \tilde{H}_c			
1	1	0.1106×10^{-6}	0.1683×10^{-11}	4522	8.960×10^{-6}	$6.215 \cdot 10^{-6}$	-9.40	Ellipticity	
2	1.25				6.964	6.647	-4.55		
3	1.5				7.001	7.006	+0.07		
4	1.75				7.015	7.306	+4.15		
5	2				7.402	7.556	+2.08		
6	2.5				7.653	7.937	+3.71		
7	3				7.845	8.202	+4.55		
8	4				8.292	8.513	+2.67		
9	6				8.657	8.736	+0.91		
10	8				8.672	8.787	+1.33		
11	6	.2211			7.796	8.339	+6.67	Load plus case 9	
12		.3686			7.505	8.059	+7.38		
13		.5528			7.309	7.843	+7.31		
14		.7371			7.517	7.693	+2.34		
15		.9214			7.611	7.578	-0.43		
16		1.106			7.416	7.487	+0.96		
17		1.290			6.762	7.410	+9.58		
18		.7371	.08416		4.917	4.836	-1.65		
19			.2525		9.999	10.10	+1.01		
20			.3367		11.40	12.24	+7.37		
21			.4208		13.07	14.21	+8.72		
22			.5092		17.13	17.81	+3.97		
23			.6416		21.35	22.61	+5.90		
24			1.263		29.62	29.68	+0.20	Speed plus case 14	
25			1.683		35.50	35.98	+1.35		
26			2.104		41.05	41.79	+1.80		
27			2.525		46.64	47.22	+1.24		
28			2.946		51.08	52.36	+2.51		
29			3.367		55.56	57.26	+3.06		
30			4.208		63.81	66.49	+4.20		
31			5.050		71.25	75.13	+5.45		
32		.7216	.3296	2310	8.422	8.466	+0.52		Materials plus case 9
33		.7215	.9422	3591	20.70	21.62	+4.44		
34		.2456	.1122	6785	7.825	7.825	0		

TABLE 6.1. - EFFECT OF STARVATION ON MINIMUM FILM THICKNESS FOR THREE GROUPS OF THE DIMENSIONLESS SPEED AND LOAD PARAMETERS

Dimensionless inlet distance, m	Group		
	1	2	3
	Dimensionless load parameter, W		
	$0.3686 \cdot 10^{-6}$	$0.7371 \cdot 10^{-6}$	$0.7371 \cdot 10^{-6}$
	Dimensionless speed parameter, U		
	$0.1683 \cdot 10^{-11}$	$1.683 \cdot 10^{-11}$	$5.050 \cdot 10^{-11}$
Minimum film thickness, H_{min}			
6	-----	$29.75 \cdot 10^{-6}$	$61.32 \cdot 10^{-6}$
4	$6.317 \cdot 10^{-6}$	29.27	57.50
3	6.261	27.84	51.70
2.5	-----	26.38	46.89
2	5.997	23.46	39.91
1.75	-----	21.02	34.61
1.5	5.236	-----	27.90
1.25	3.945	-----	-----

TABLE 6.2. - EFFECT OF DIMENSIONLESS SPEED AND LOAD PARAMETERS ON DIMENSIONLESS INLET DISTANCE AT FULLY FLOODED - STARVED BOUNDARY

Group	Dimensionless speed parameter, U	Dimensionless load parameter, W	Dimensionless radius parameter, $R_x b$	Fully flooded central film thickness, $H_{c,F}$	Fully flooded minimum film thickness, $H_{min,F}$	Dimensionless inlet distance at fully flooded - starved boundary, m^*
1	$0.1683 \cdot 10^{-11}$	$0.3686 \cdot 10^{-6}$	205.9	$7.480 \cdot 10^{-6}$	$6.221 \cdot 10^{-6}$	2.62
2	1.683	.7371	163.5	33.55	29.20	3.71
3	5.050	7371	163.5	70.67	60.92	5.57

TABLE 6.3. - EFFECT OF DIMENSIONLESS INLET DISTANCE ON DIMENSIONLESS CENTRAL FILM THICKNESS RATIOS

Group	Dimensionless inlet distance, m	Ratio of central film thicknesses for starved and flooded conditions, $H_{c,S} / H_{c,F}$	Ratio of minimum film thicknesses for starved and flooded conditions, $H_{min,S} / H_{min,F}$	Inlet boundary parameter, $(m-1) / (m^*-1)$	Inlet boundary parameter, et al. Wedeven, et al. (1971), $(m-1) / (m_W-1)$
1	2.62	1	1	1	0.9895
	2	.9430	.9640	.5173	.6108
	1.5	.7697	.8417	.3086	.3054
	1.25	.3689	.6341	.1343	.1527
2	3.71	1	1	1	.8281
	3	.9574	.9534	.7380	.6111
	2.5	.8870	.9034	.5535	.4584
	2	.7705	.8034	.3690	.3056
	1.75	.7151	.7199	.2768	.2292
3	5.57	1	1	1	.8498
	4	.9348	.9439	.6565	.5579
	3	.8330	.8467	.4376	.3719
	2.5	.7440	.7697	.3282	.2789
	2	.6223	.6551	.2188	.1860
	1.75	.5309	.5681	.1641	.1395
1.5	.4155	.4580	.1094	.0930	

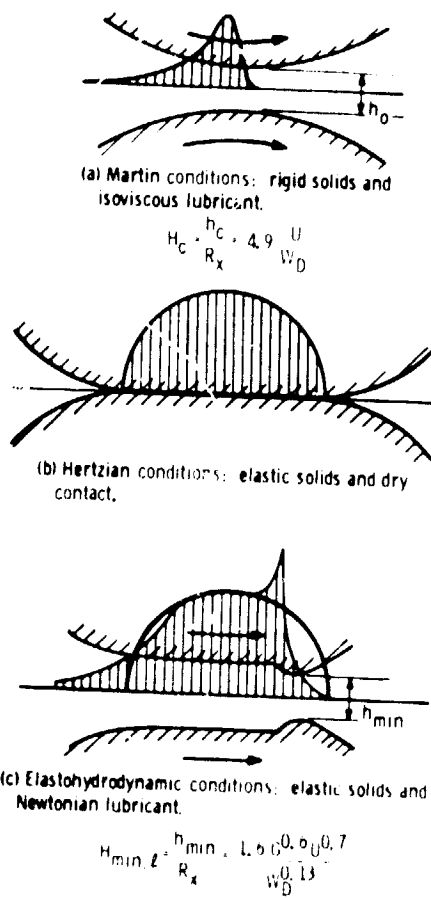


Figure 1.1. Lubrication and contact conditions and minimum film thickness formulas.

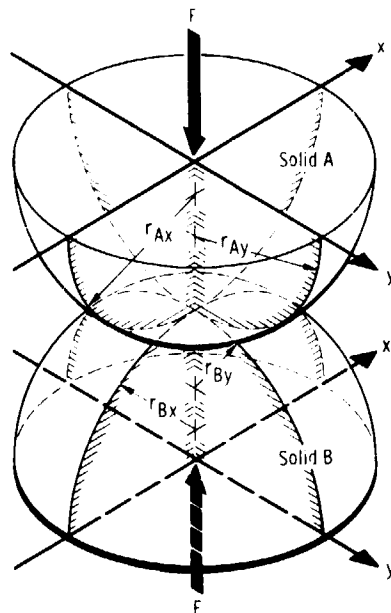


Figure 2.1. - Geometry of contacting elastic solids.

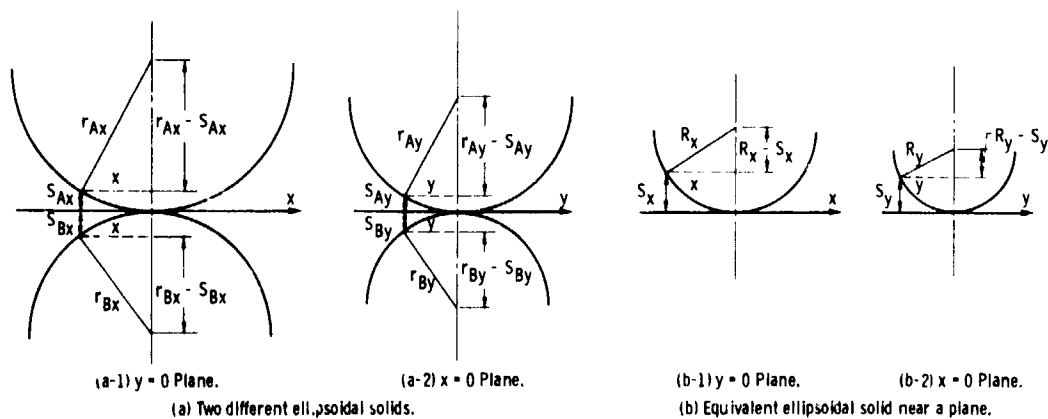


Figure 2.2. - Equivalent ellipsoidal solids.

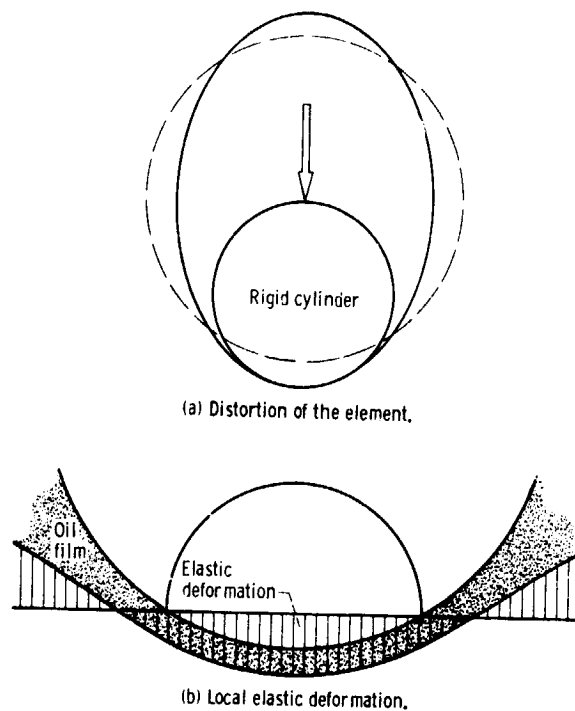


Figure 3.1. - Types of elastic deformation.

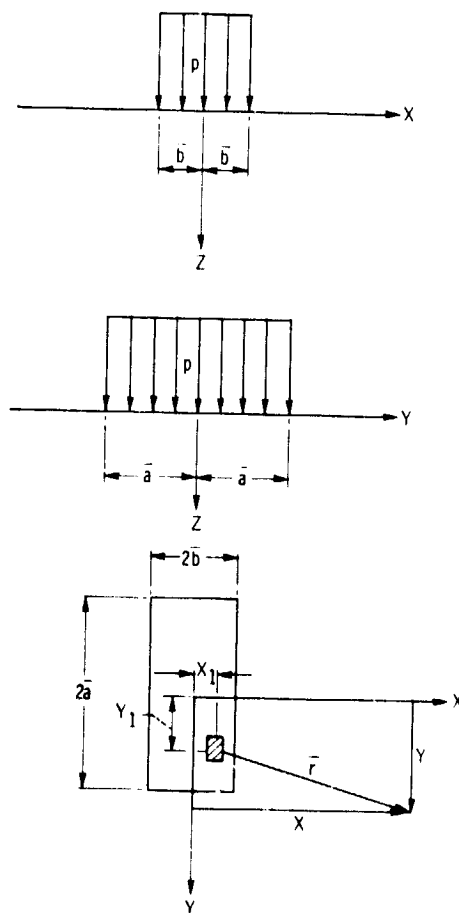


Figure 3.2. - Elastic deformation of a semi-infinite body subjected to a uniform pressure over a rectangular area.

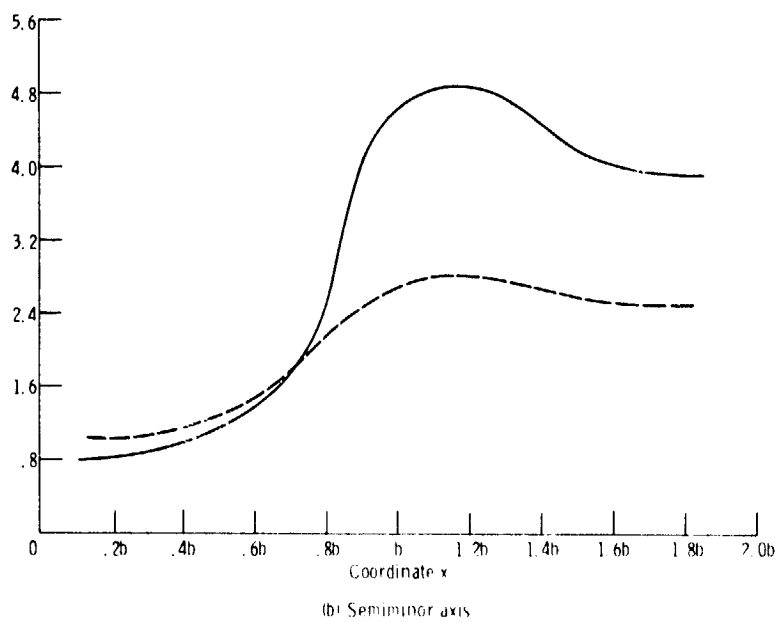
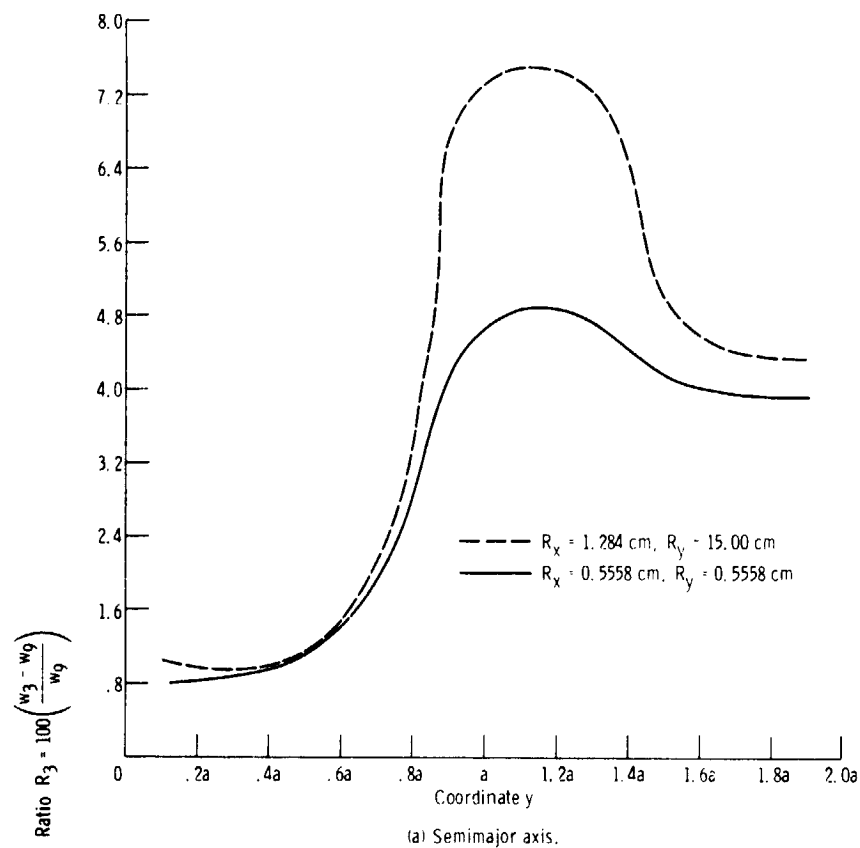


Figure 3.4. - Effect of location along semimajor and semiminor axes on percentage difference in elastic deformation when $d = 3$ and 9 .

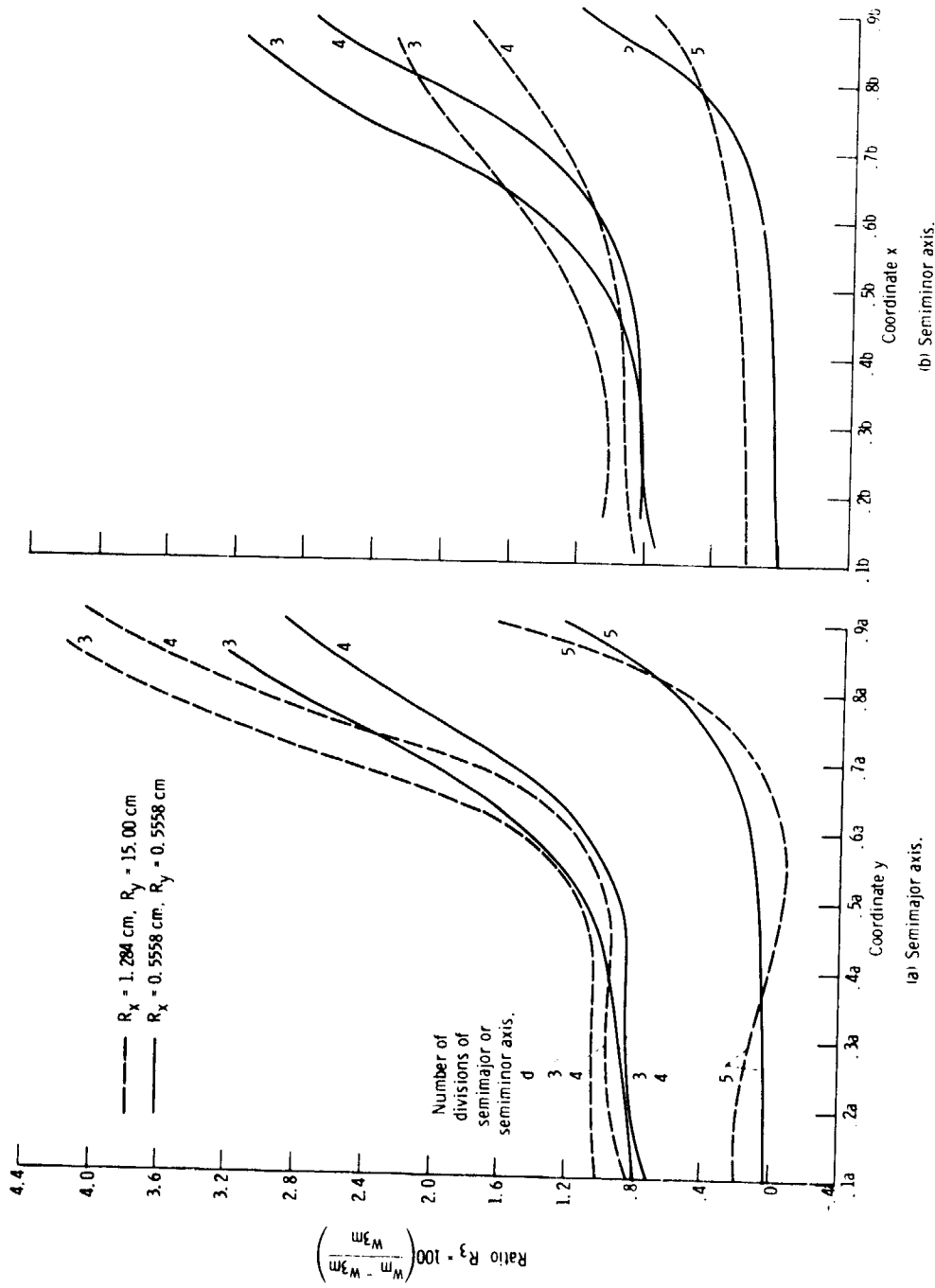


Figure 3.5. - Effect of location along semimajor and semiminor axes on percentage difference in elastic deformation when $d = 3, 4,$ and 5 and on the more exact elastic deformation when $d = 9, 12,$ and $15,$ respectively.

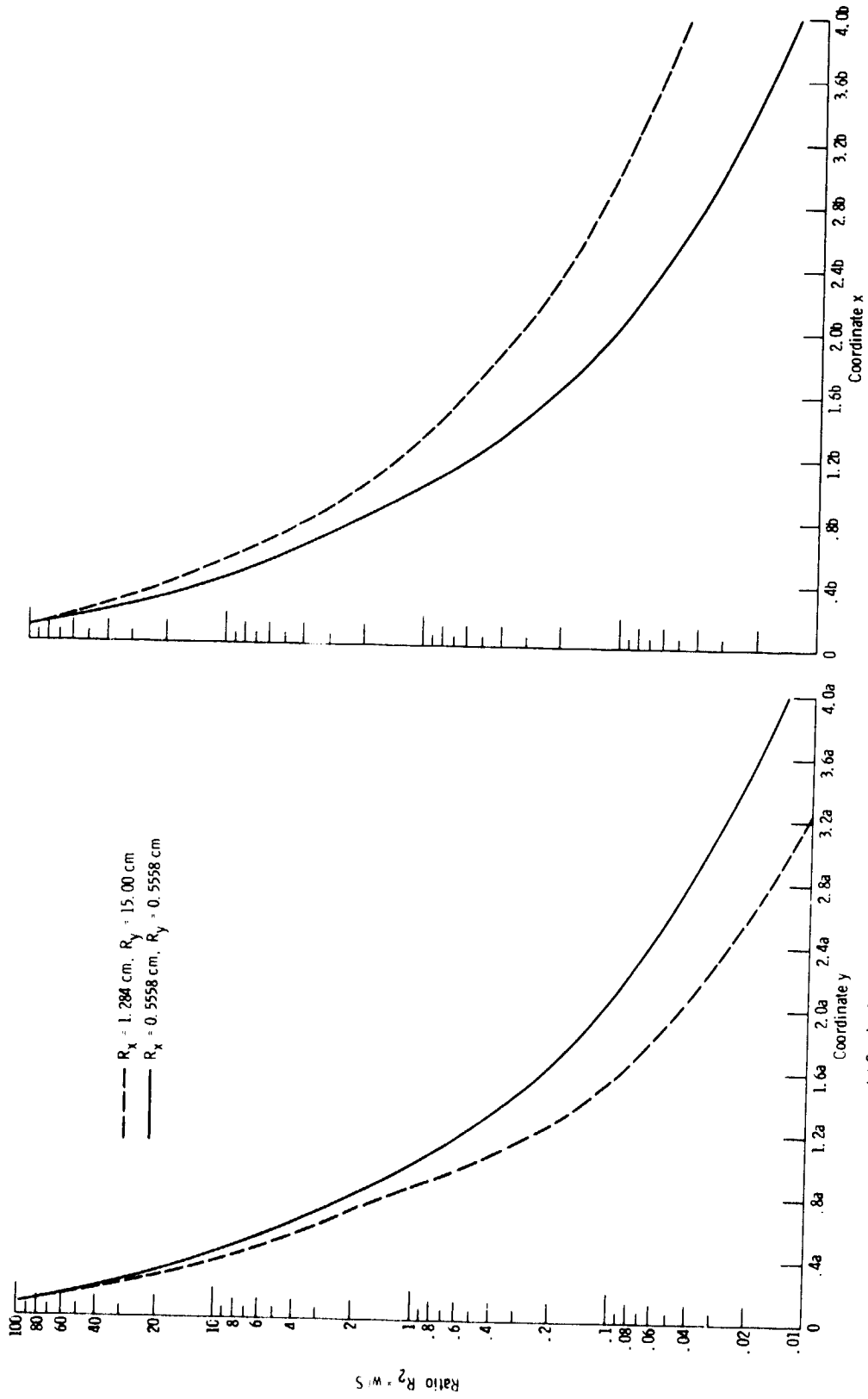


Figure 3. 6. - Effect of location along semimajor and semiminor axes on ratio of elastic deformation to geometric separation.

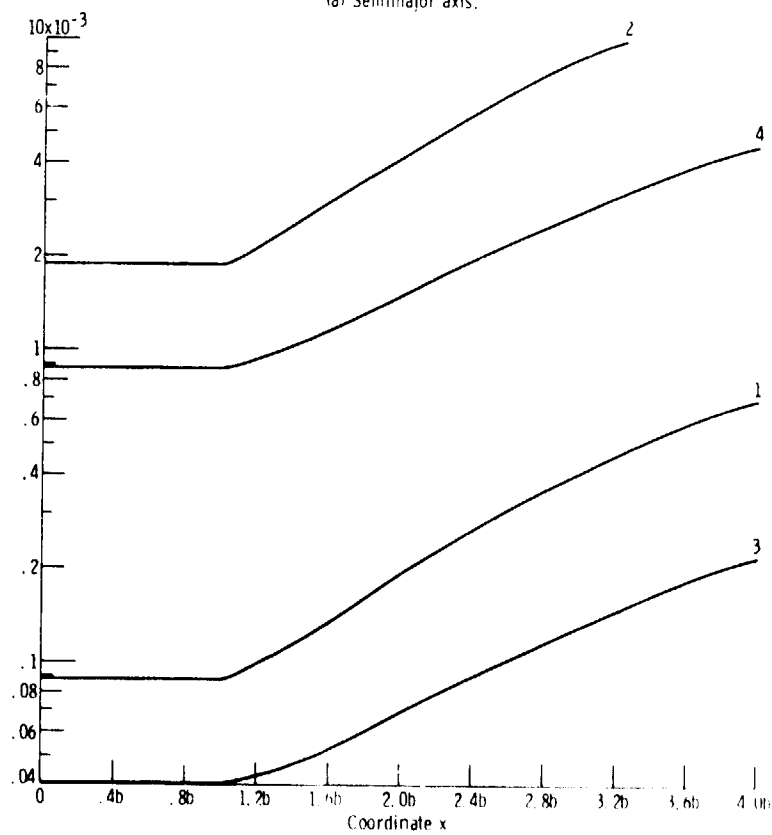
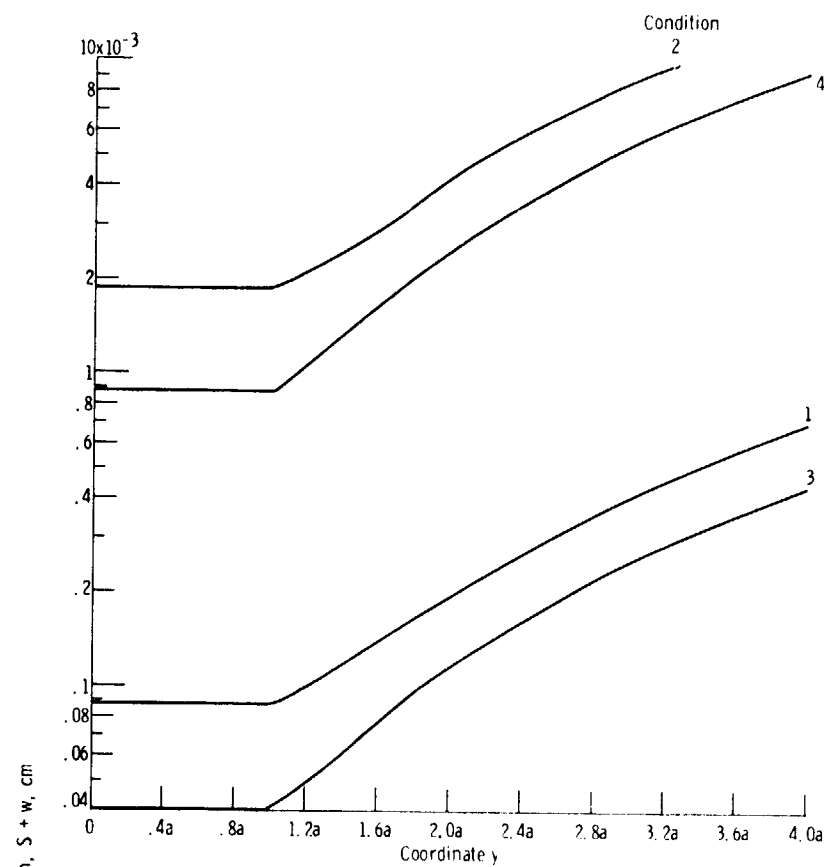


Figure 3.7. - Effect of location along semimajor and semiminor axes on separation due to geometry of contacting solids plus elastic deformation.

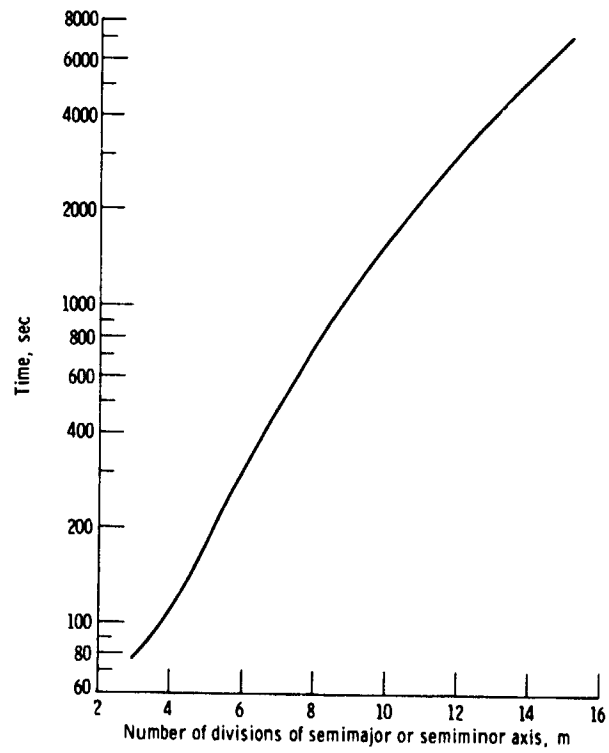


Figure 3.8. - Effect of number of divisions across ellipse axis on computer run time.

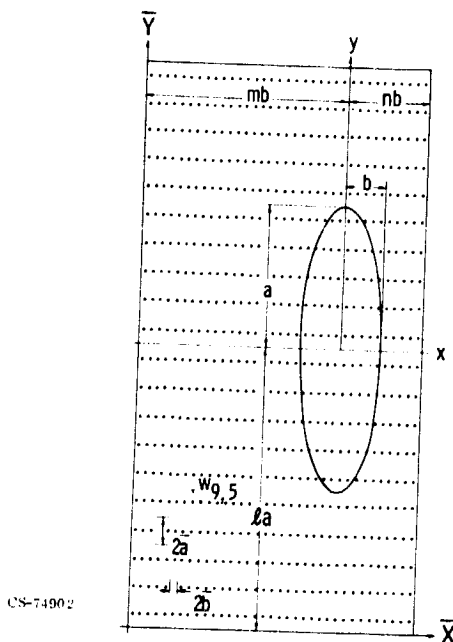


Figure 4.1. - Division of area in and around contact zone into equal rectangular areas.

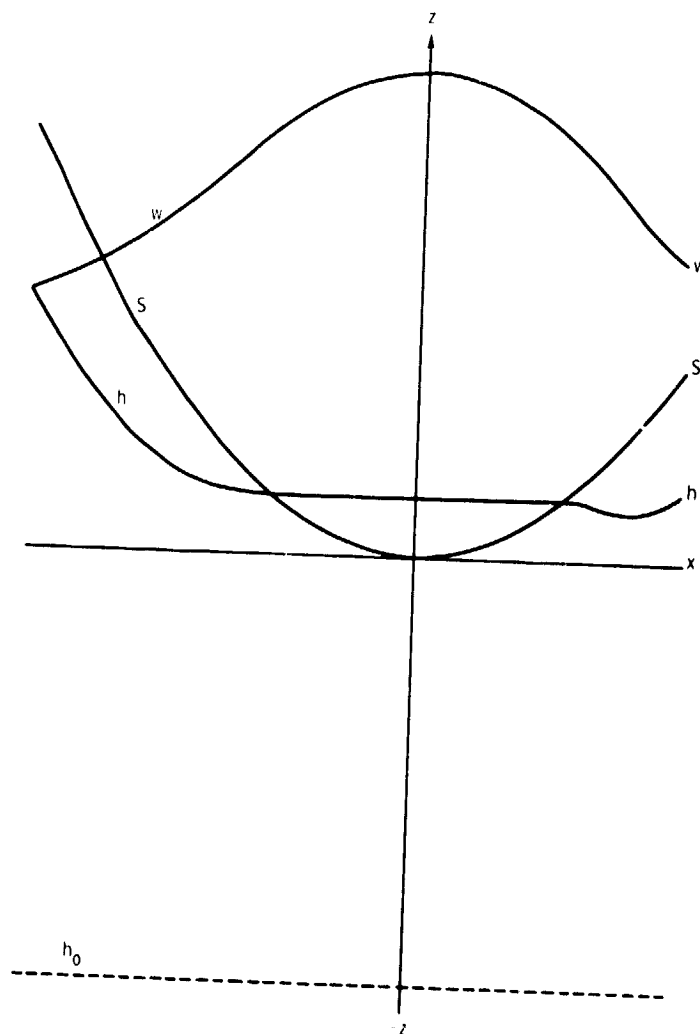


Figure 4.2. - Components of film thickness for ellipsoidal solid near a plane.

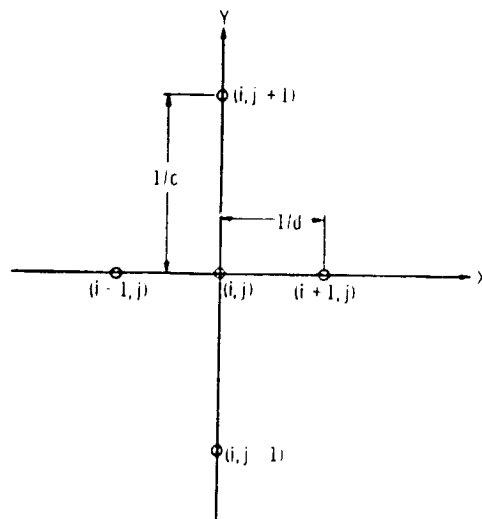


Figure 4.3. - Mesh used in numerical analysis.

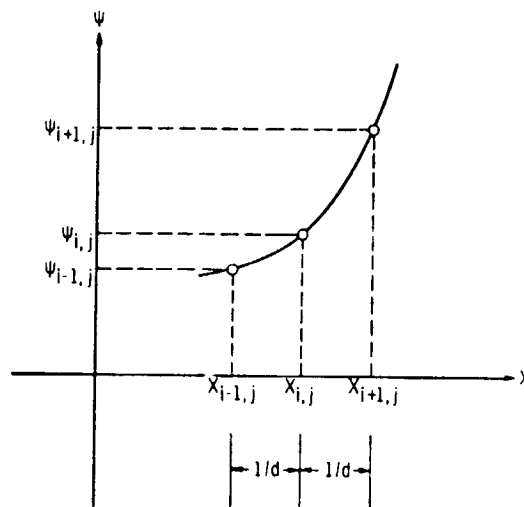
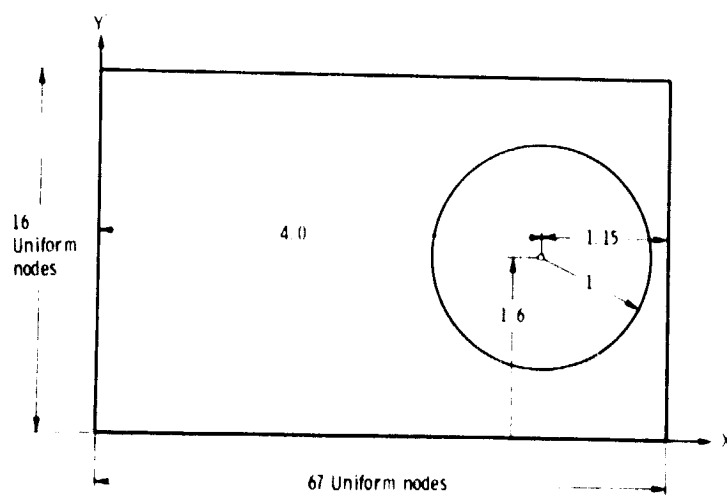
Figure 4.4. - Parabola and corresponding points representing ψ as a function of X .

Figure 4.5 Nodal structure used for numerical calculations.

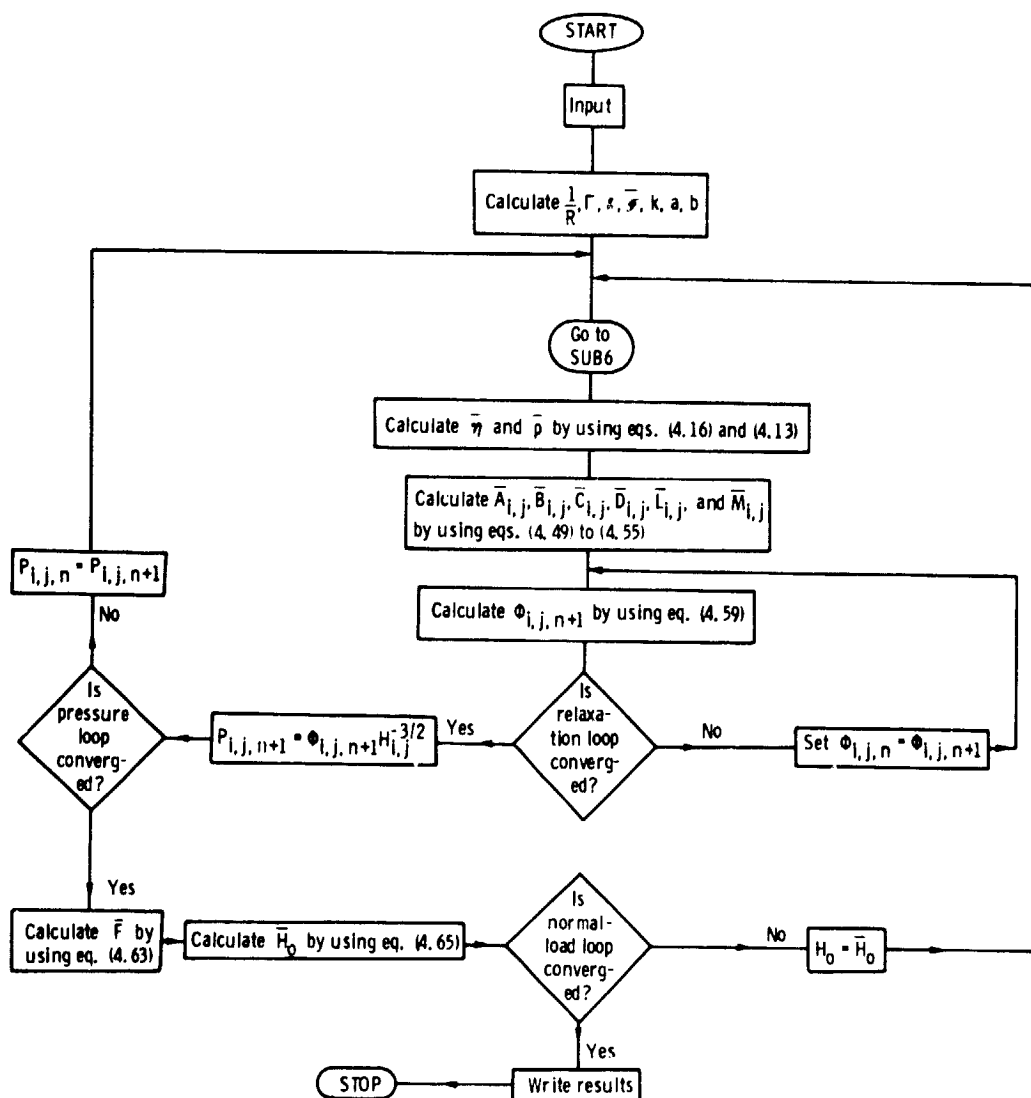


Figure 4.6. - Flow chart of main program.

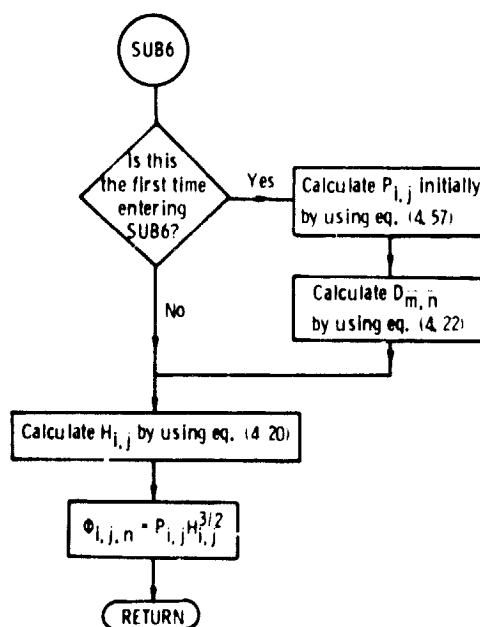


Figure 4.7. - Flow chart of subroutine SUB6.

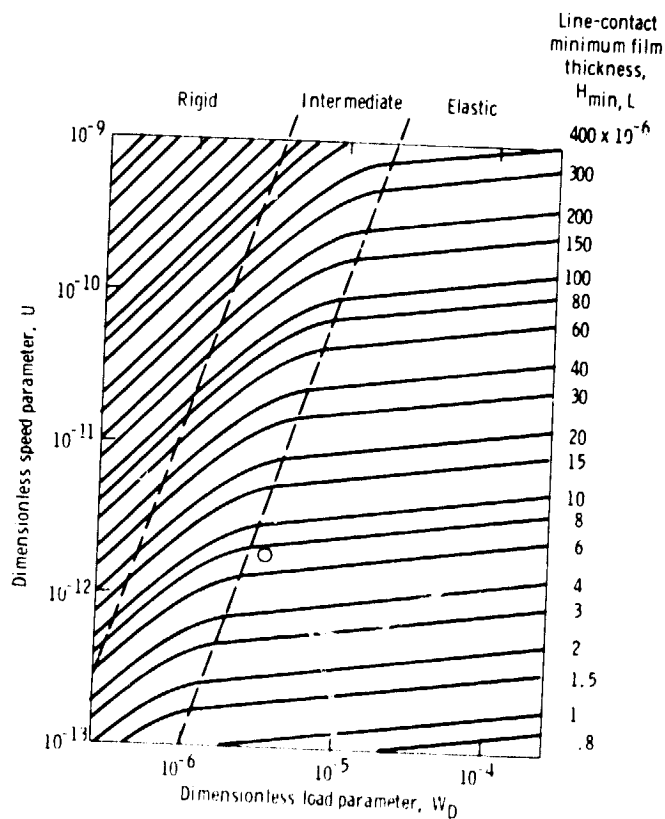


Figure 5. 1. - Film-thickness contours ($h_{min, L} = h_{min, L}^{(R_x)}$) for dimensionless material parameter G of 5000.

REPRODUCIBILITY OF THE ORIGINAL PAGE IS POOR

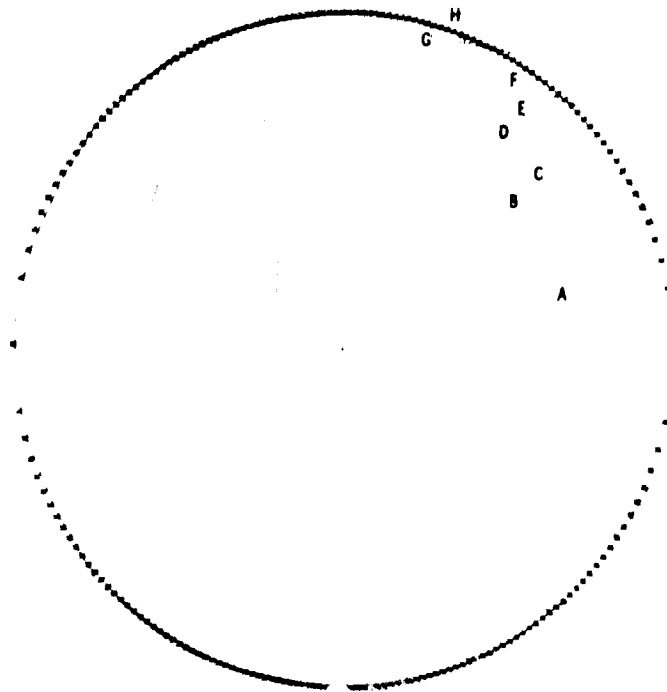


(a) Contour plot of dimensionless pressure.

Figure 5.2. - Contour plots of dimensionless pressure and film thickness and three-dimensional representation of pressure for ellipticity parameter (k) of 8. The dimensionless parameters U , W , and G are held constant as defined in equation (5.10).

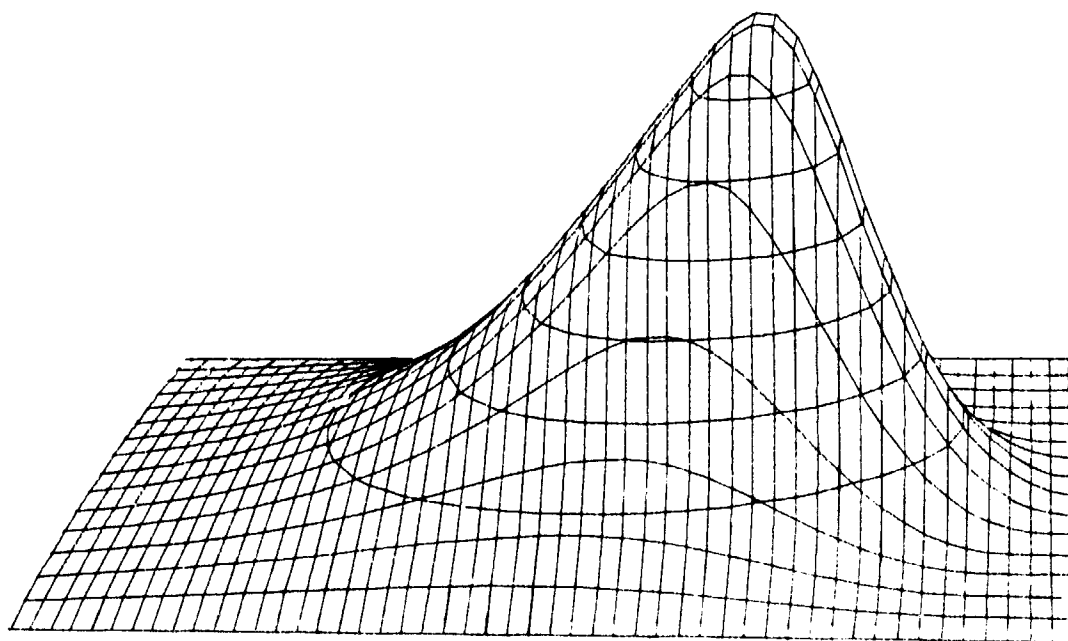
Dimensionless
film thickness,
 $H = h/R_0$

A	7.08×10^{-6}
B	7.20
C	7.40
D	7.70
E	8.20
F	8.90
G	9.80
H	11.00



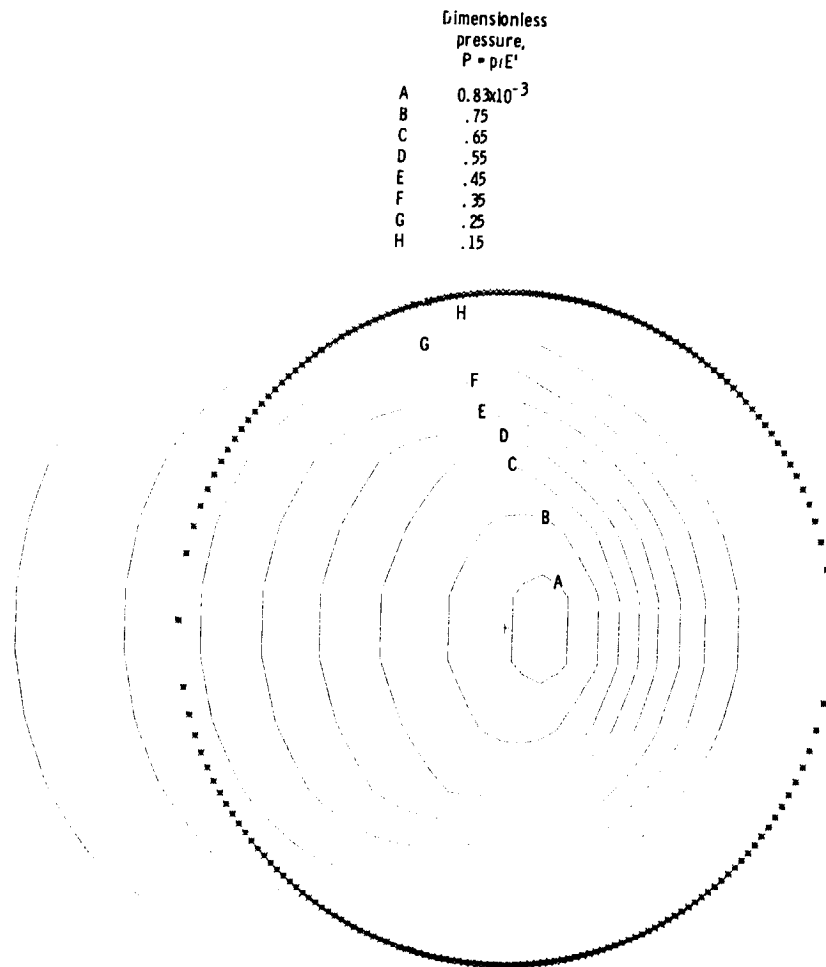
(b) Contour plot of dimensionless film thickness.

Figure 5.2. - Continued.



(c) Three-dimensional representation of pressure.

Figure 5.2 - Concluded.

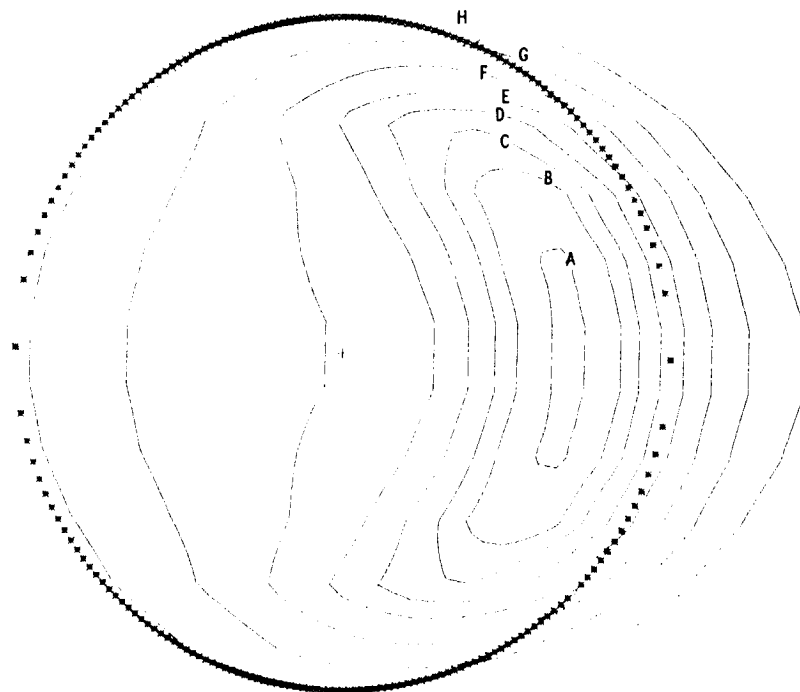


(a) Contour plot of dimensionless pressure.

Figure 5.3 - Contour plots of dimensionless pressure and film thickness and three-dimensional representation of pressure for ellipticity parameter (k) of 6. The dimensionless parameters U , W , and G are held constant as defined in equation (5.10).

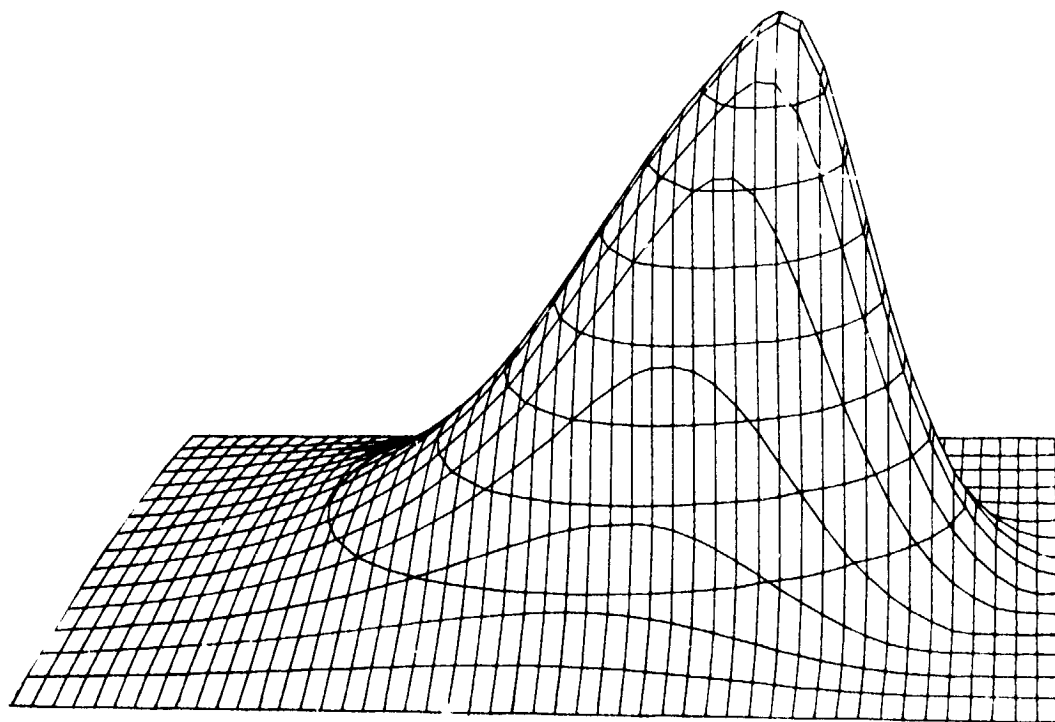
Dimensionless
film thickness,
 $H = h/R_x$

A	7.0×10^{-6}
B	7.2
C	7.4
D	7.7
E	8.1
F	8.7
G	9.5
H	10.7



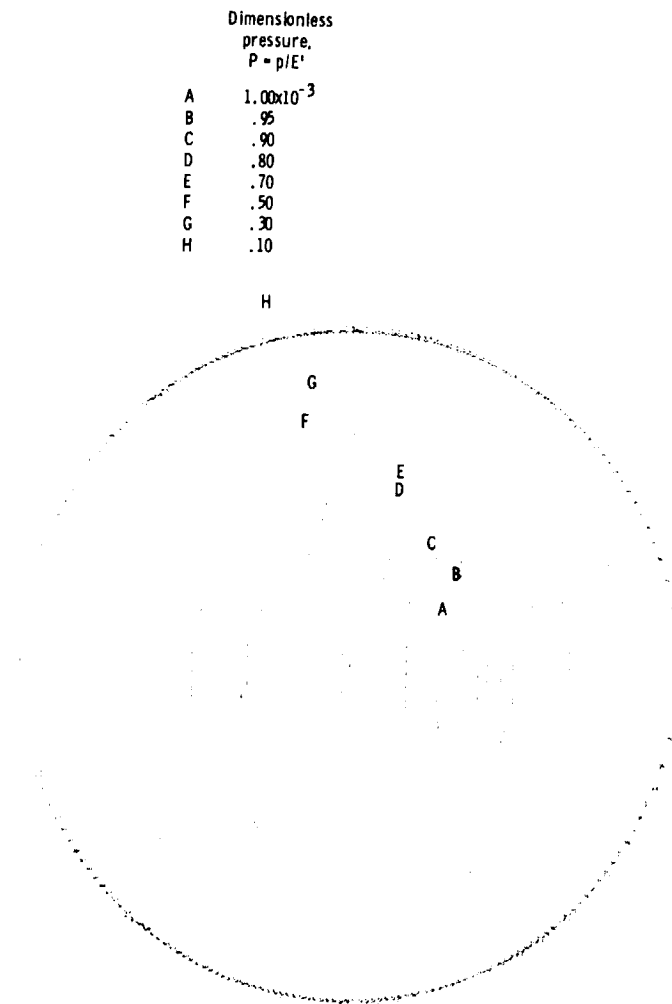
(b) Contour plot of dimensionless film thickness.

Figure 5.3. - Continued.



(c) Three-dimensional representation of pressure.

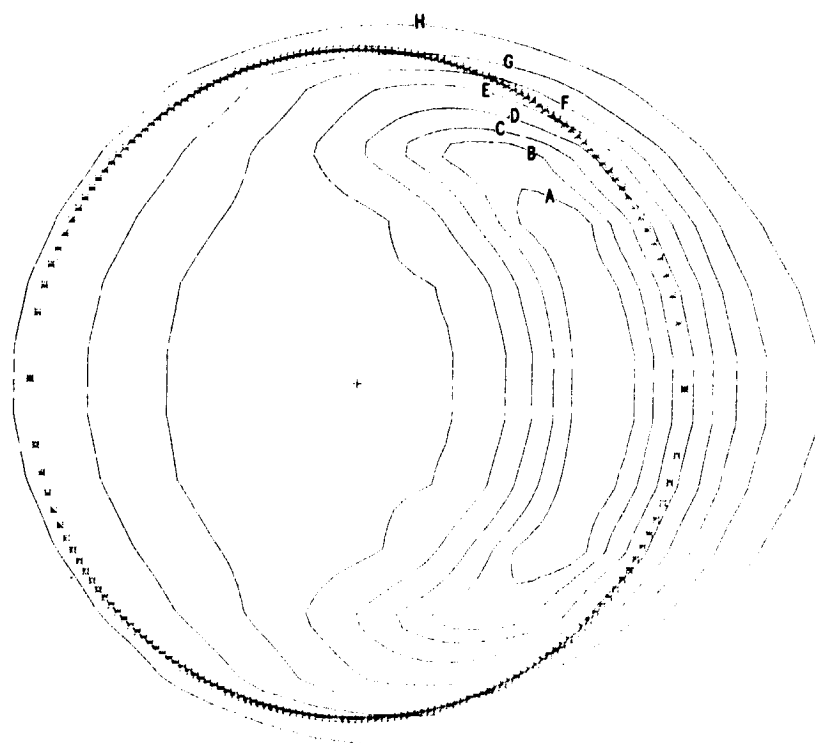
Figure 5.3. - Concluded.



(a) Contour plot of dimensionless pressure.

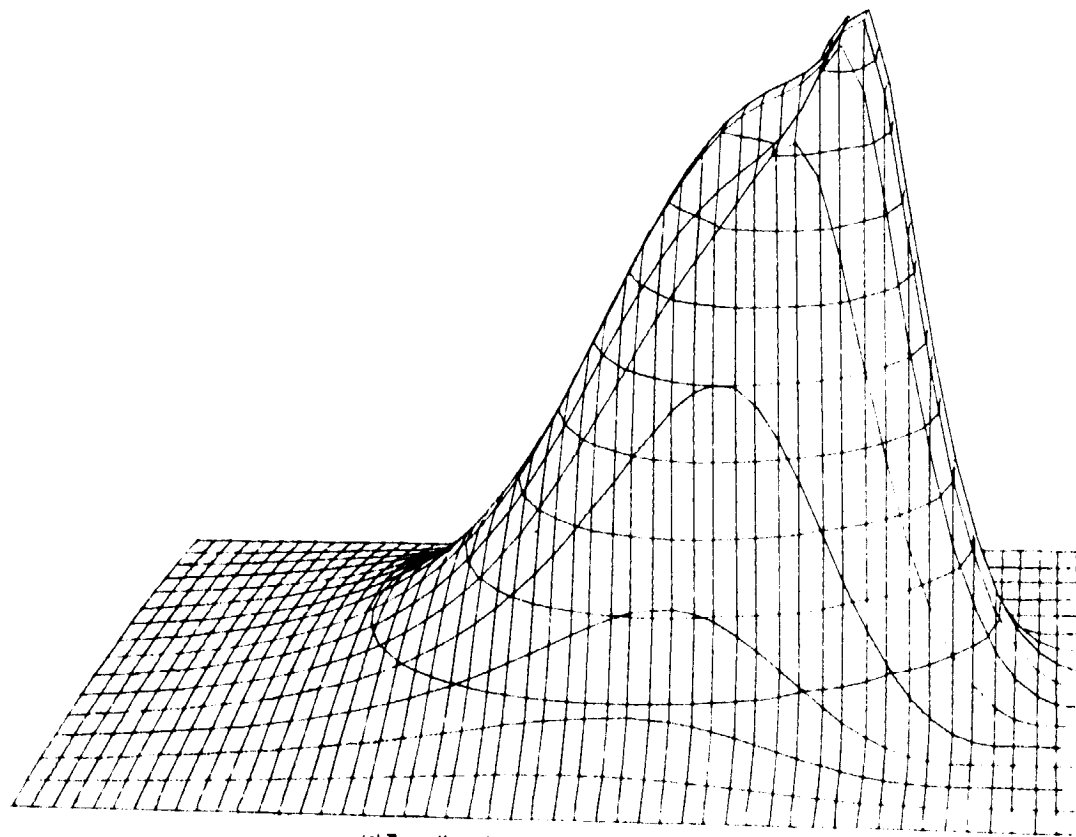
Figure 5.4. - Contour plots of dimensionless pressure and film thickness and three-dimensional representation of pressure for ellipticity parameter (k) of 4. The dimensionless parameters U , W , and G are held constant as defined in equation (5.10).

Dimensionless film thickness, $H = h/R_x$	
A	6.8×10^{-6}
B	7.0
C	7.3
D	7.7
E	8.2
F	8.8
G	9.6
H	11.0



(b) Contour plot of dimensionless film thickness.

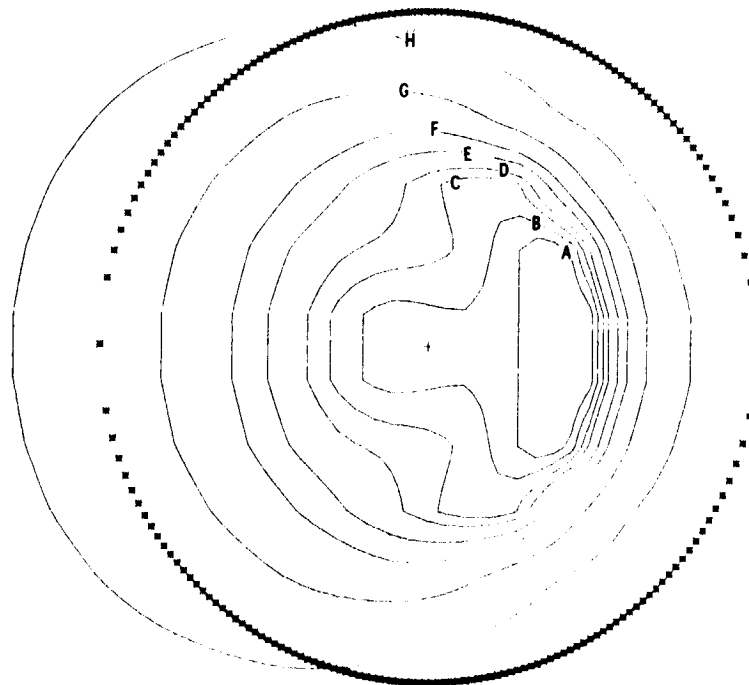
Figure 5.4. - Continued.



(c) Three-dimensional representation of pressure.

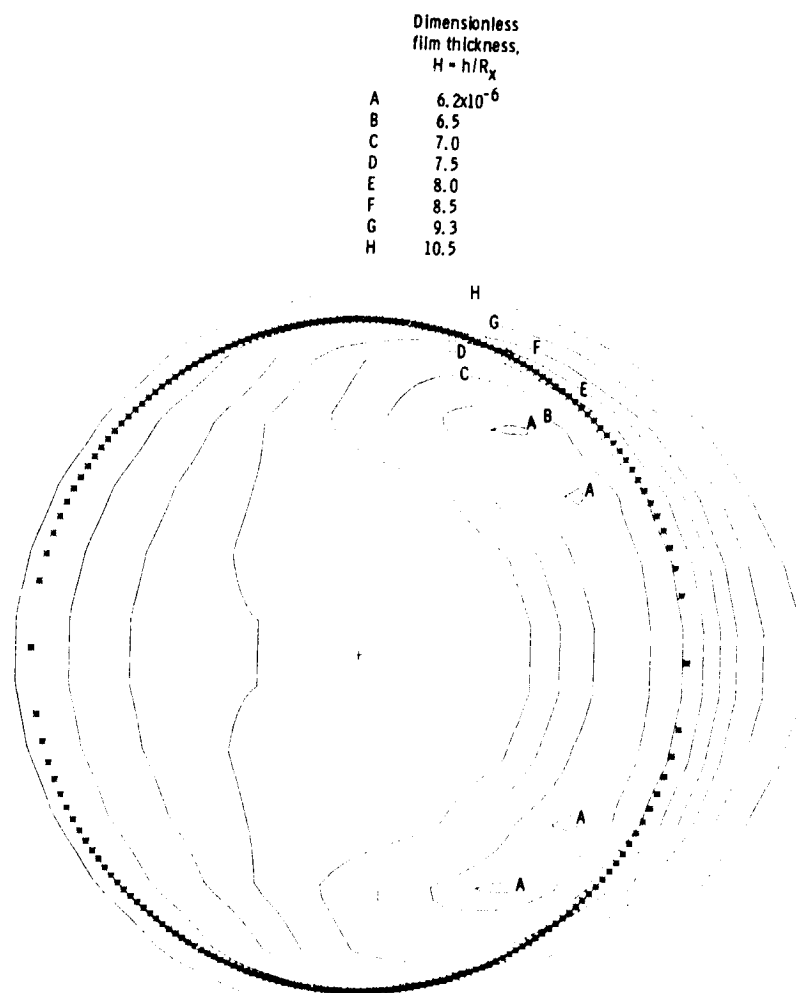
Figure 5.4. - Concluded.

Dimensionless pressure, $P = p/E'$	
A	1.05×10^{-3}
B	1.00
C	.95
D	.90
E	.80
F	.70
G	.50
H	.20



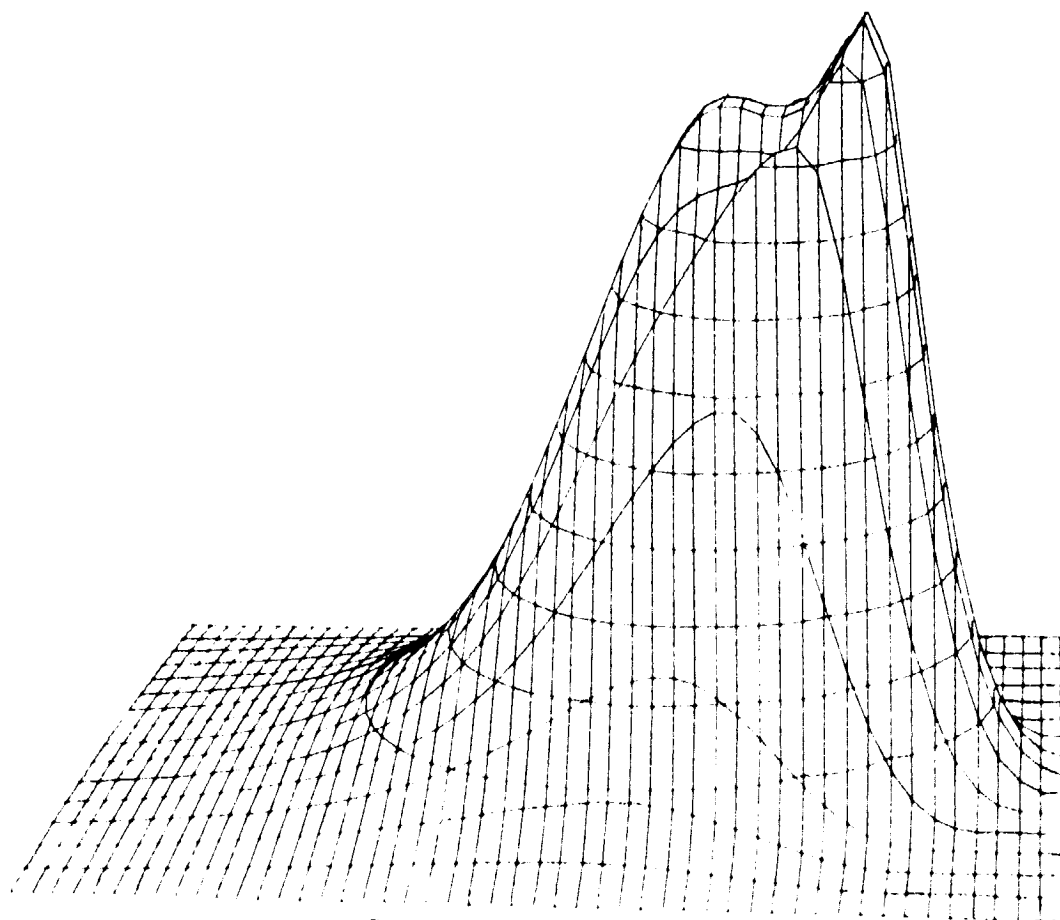
(a) Contour plot of dimensionless pressure.

Figure 5.5. - Contour plots of dimensionless pressure and film thickness and three-dimensional representation of pressure for ellipticity parameter (k) of 3. The dimensionless parameters U , W , and G are held constant as defined in equation (5.10).



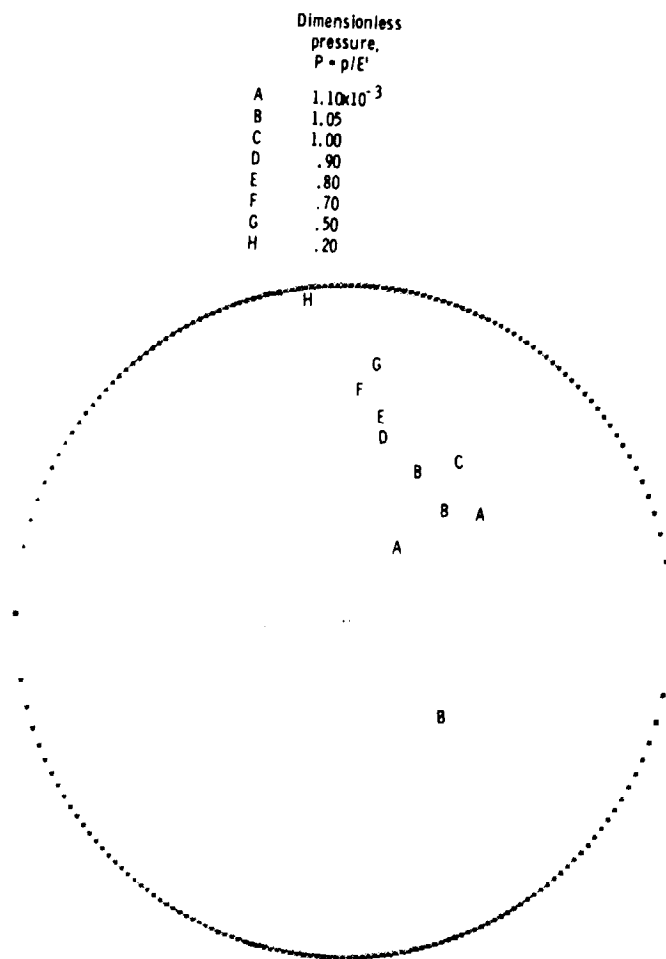
(b) Contour pic. of dimensionless film thickness.

Figure 5.5. - Continued.



(c) Three dimensional representation of pressure.

Figure 5.5. Concluded.

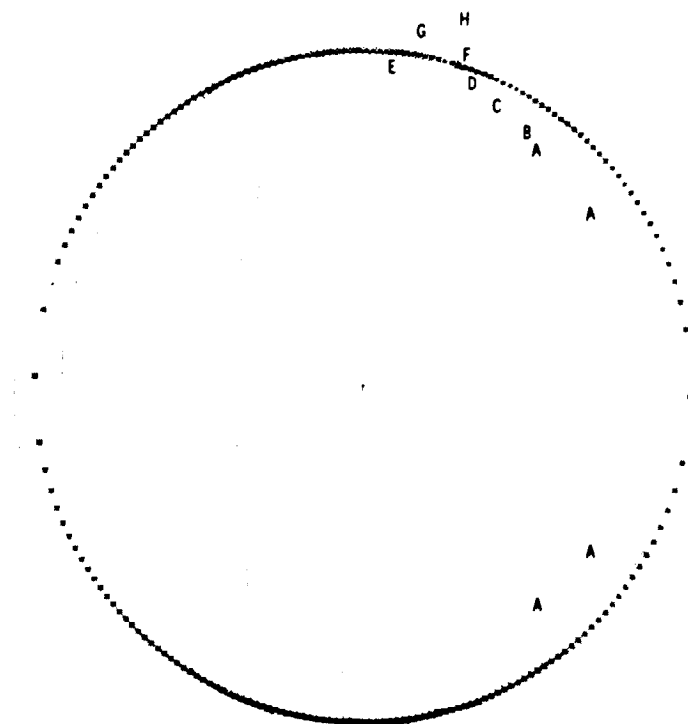


(a) Contour plot of dimensionless pressure.

Figure 5.6. - Contour plots of dimensionless pressure and film thickness and three-dimensional representation of pressure for ellipticity parameter (k) of 2.5. The dimensionless parameters l , w , and G are held constant as defined in equation (5.10).

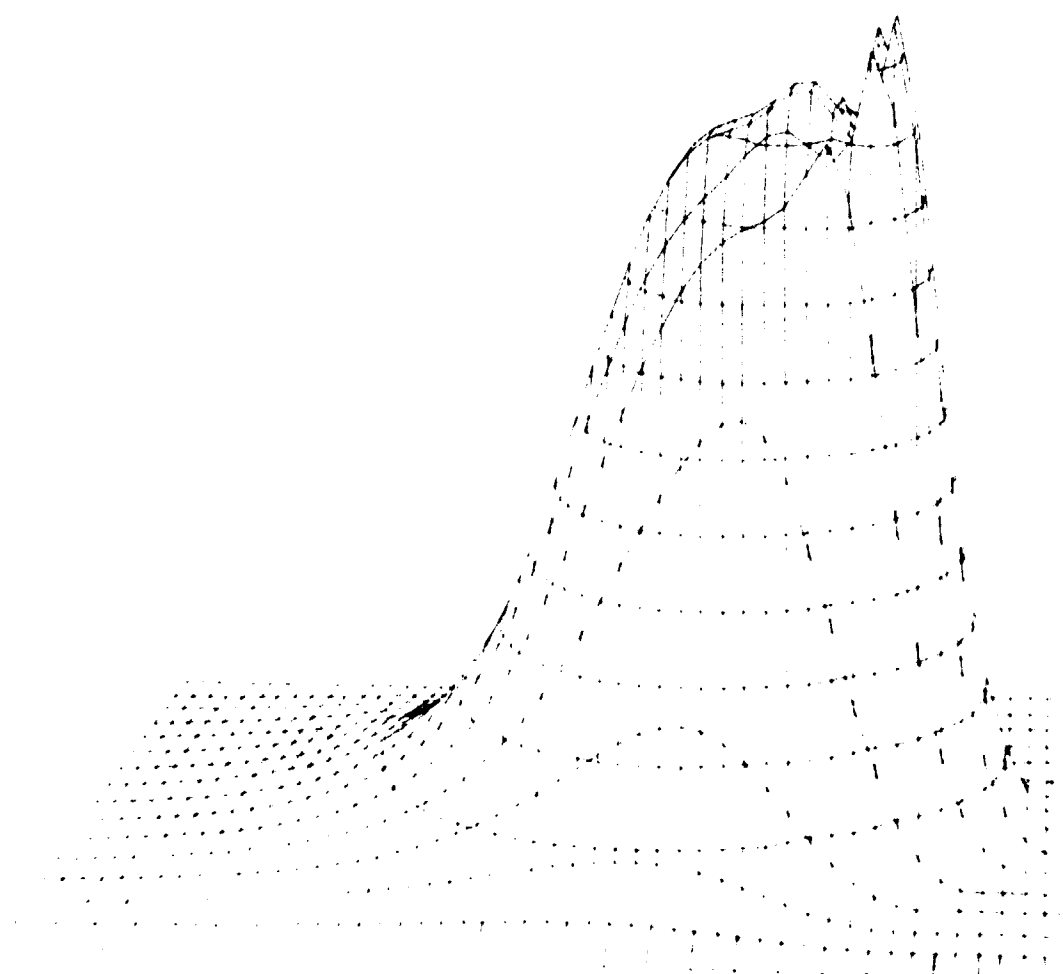
Dimensionless
film thickness,
 $H = h/R_x$

A	6.0×10^{-6}
B	6.3
C	6.7
D	7.2
E	7.8
F	8.5
G	9.3
H	10.5

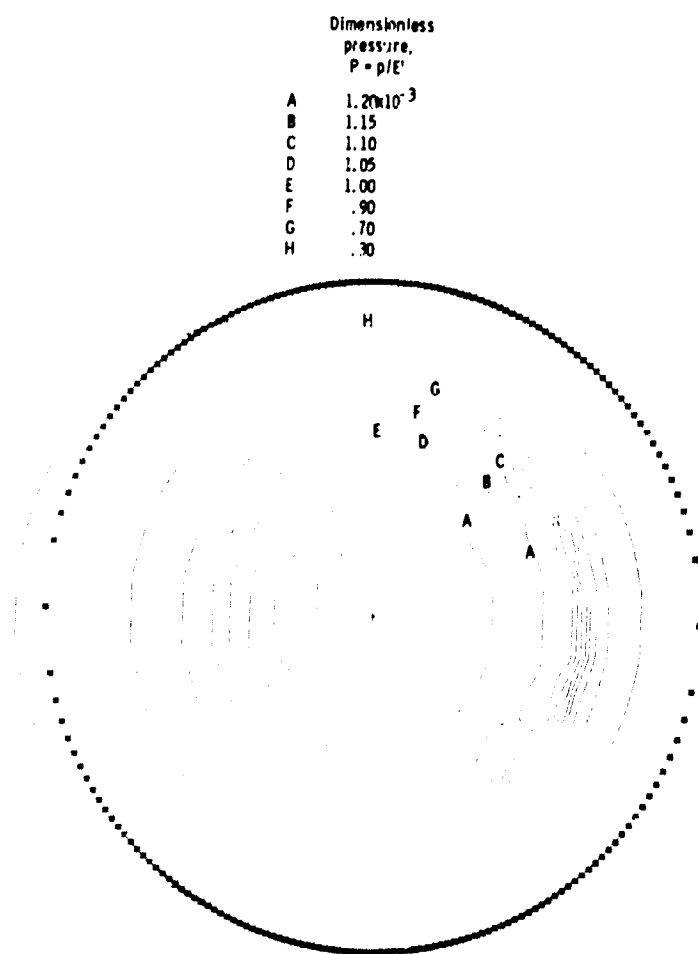


(b) Contour plot of dimensionless film thickness.

Figure 5.6. - Continued.



Three-dimensional representation of pressure
Figure 5.6 (Continued)

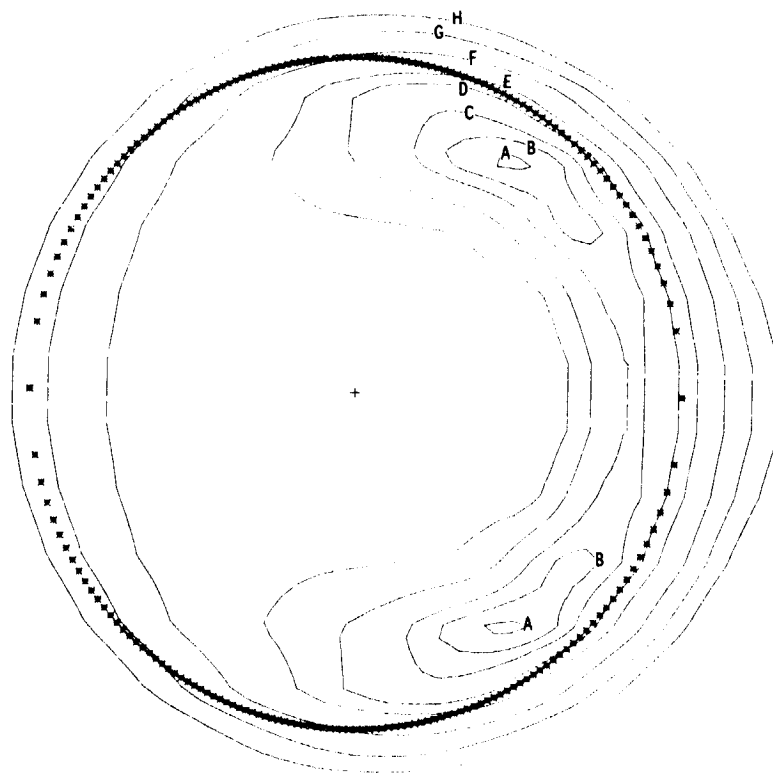


(a) Contour plot of dimensionless pressure.

Figure 5.7. - Contour plots of dimensionless pressure and film thickness and three-dimensional representation of pressure for ellipticity parameter β of 2. The dimensionless parameters U , W , and C are held constant as defined in equation (5.10).

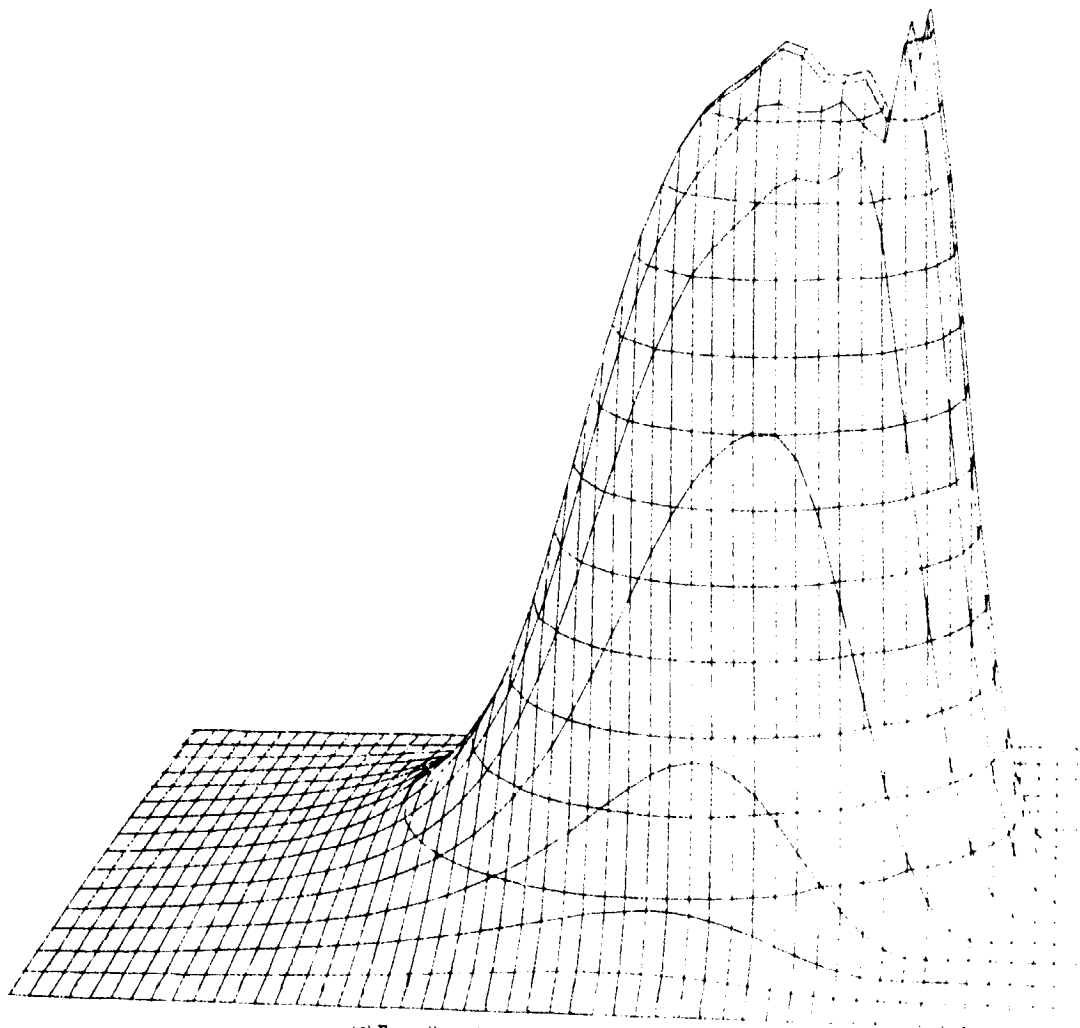
Dimensionless
film thickness,
 $H = h/R_x$

A	5.4×10^{-6}
B	5.7
C	6.0
D	6.5
E	7.0
F	8.0
G	9.0
H	10.0



(b) Contour plot of dimensionless film thickness.

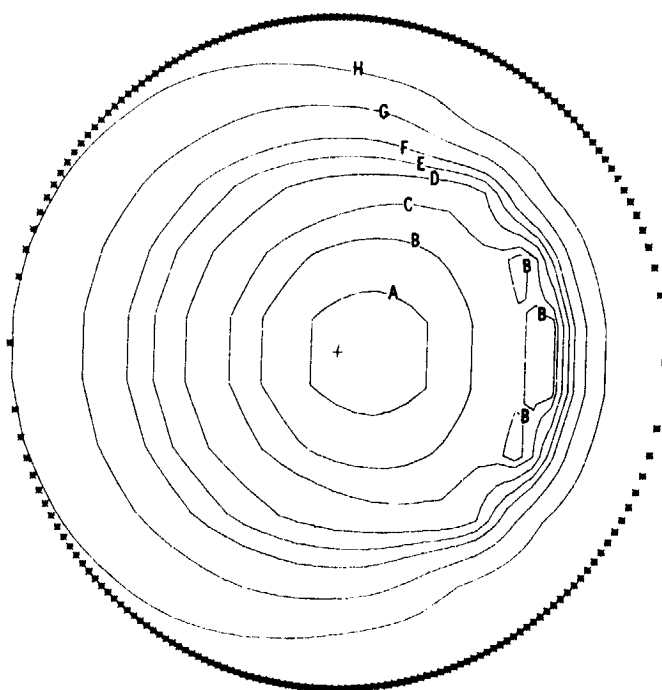
Figure 5.7. - Continued.



(c) Three-dimensional representation of pressure.

Figure 5.7. - Concluded.

	Dimensionless pressure, $P = p/E'$
A	1.30×10^{-3}
B	1.25
C	1.20
D	1.10
E	1.00
F	.90
G	.70
H	.40

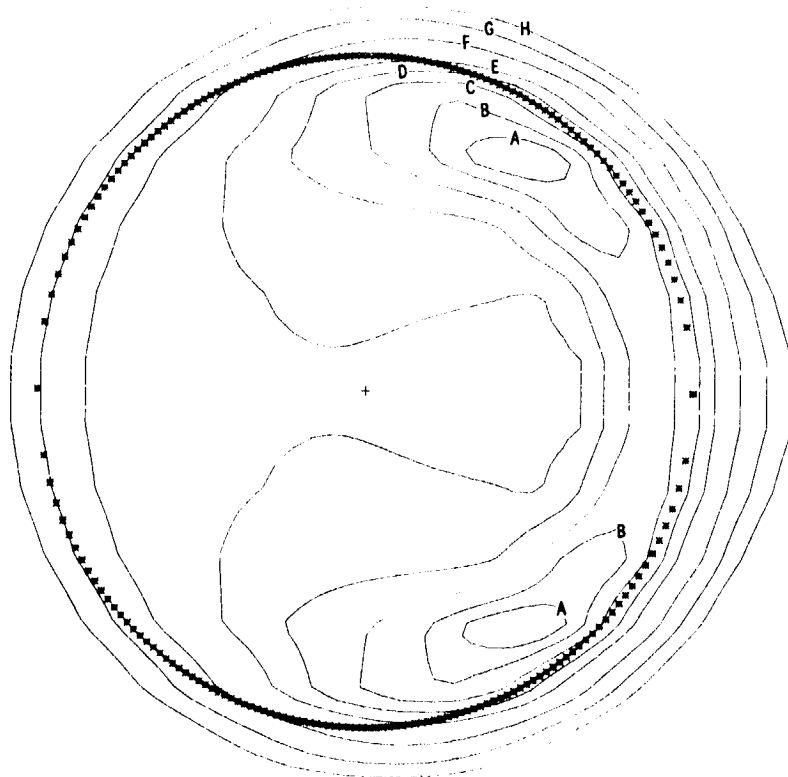


(a) Contour plot of dimensionless pressure.

Figure 5.8. - Contour plots of dimensionless pressure and film thickness and three-dimensional representation of pressure for ellipticity parameter (k) of 1.75. The dimensionless parameters U , W , and G are held constant as defined in equation (5.10).

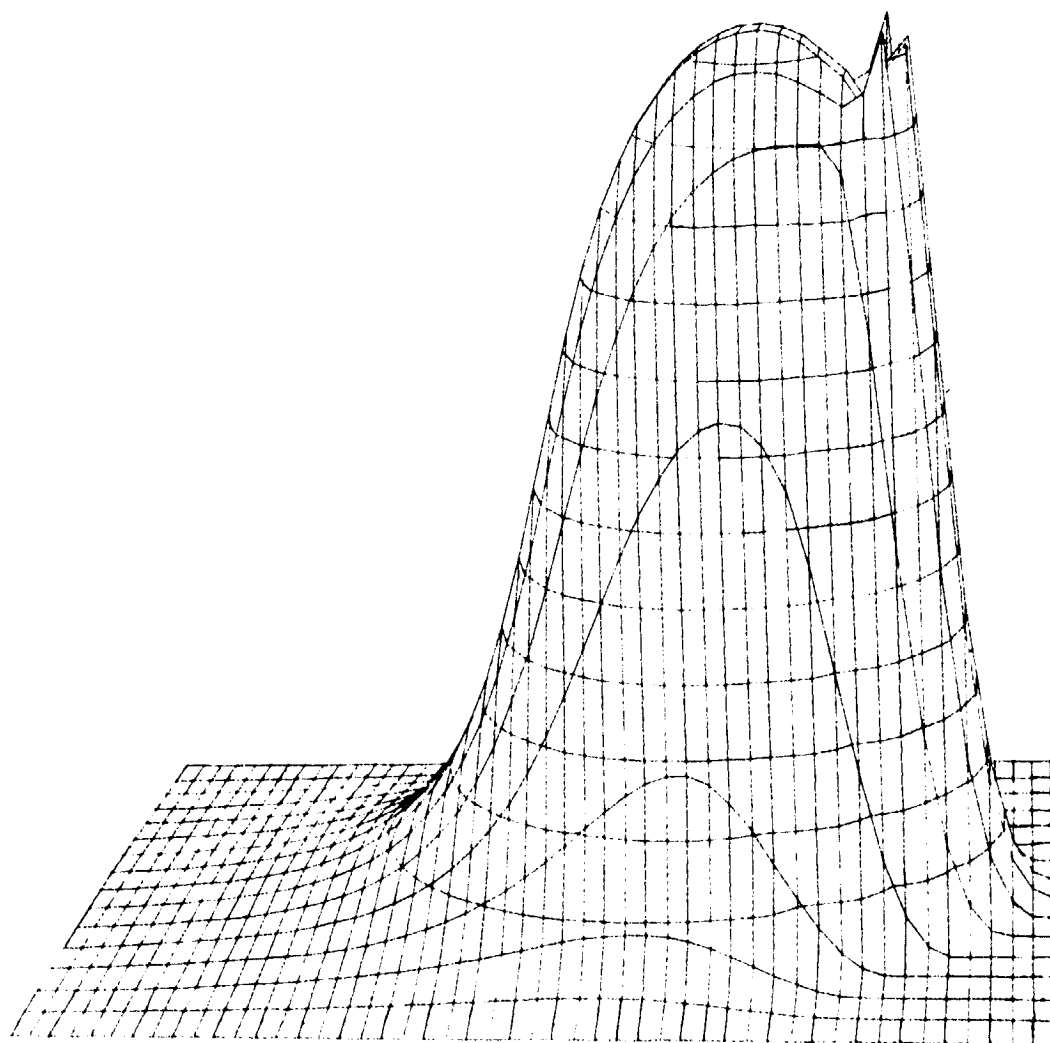
Dimensionless
film thickness,
 $H = h/R_x$

A	5.2×10^{-6}
B	5.5
C	6.0
D	6.5
E	7.0
F	8.0
G	9.0
H	10.0



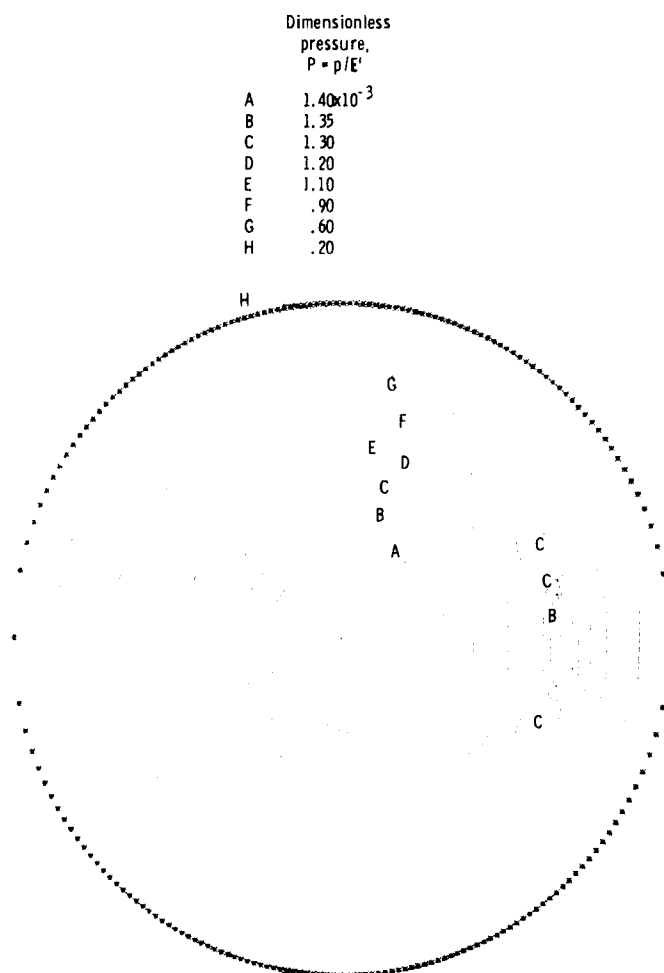
(b) Contour plot of dimensionless film thickness.

Figure 5.8. - Continued.



(c) Three-dimensional representation of pressure.

Figure 5.8. - Concluded.

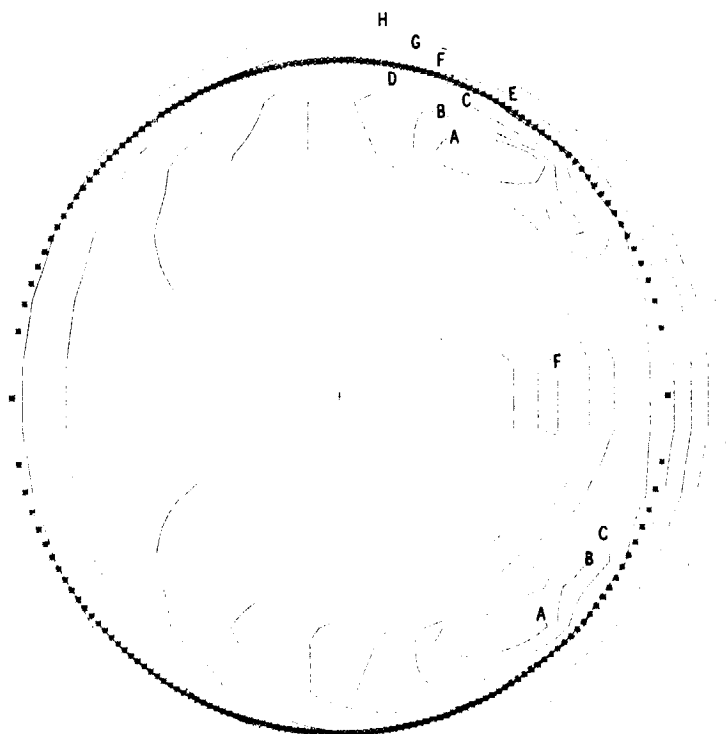


(a) Contour plot of dimensionless pressure.

Figure 5.9. - Contour plots of dimensionless pressure and film thickness and three-dimensional representation of pressure for ellipticity parameter (k) of 1.5. The dimensionless parameters U , W , and G are held constant as defined in equation (5.10).

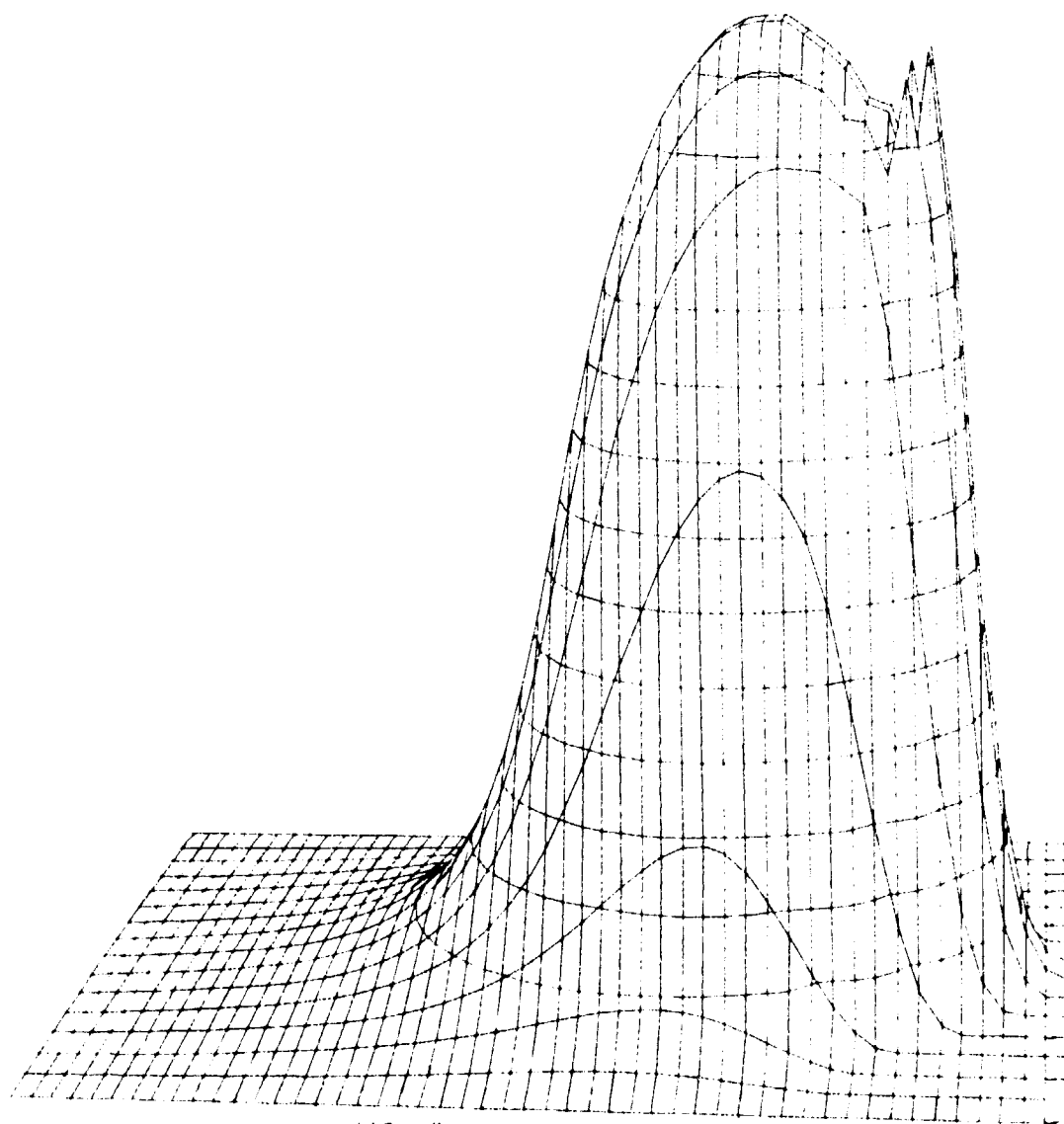
Dimensionless
film thickness,
 $H = h/R_x$

A	4.8×10^{-6}
B	5.0
C	5.3
D	5.7
E	6.2
F	6.8
G	7.5
H	8.4



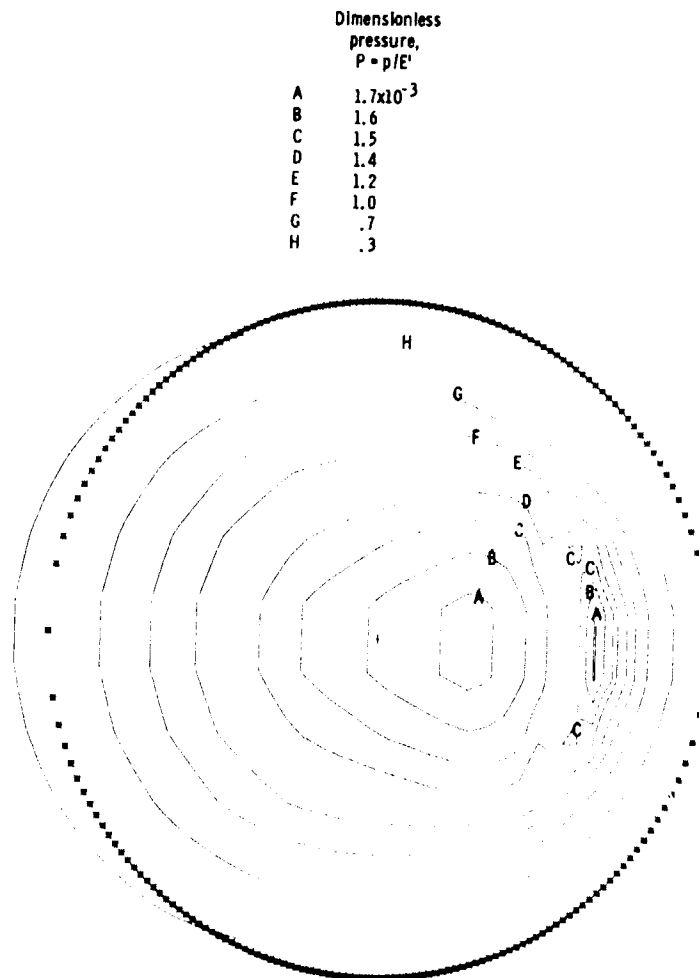
(b) Contour plot of dimensionless film thickness.

Figure 5.9. - Continued.



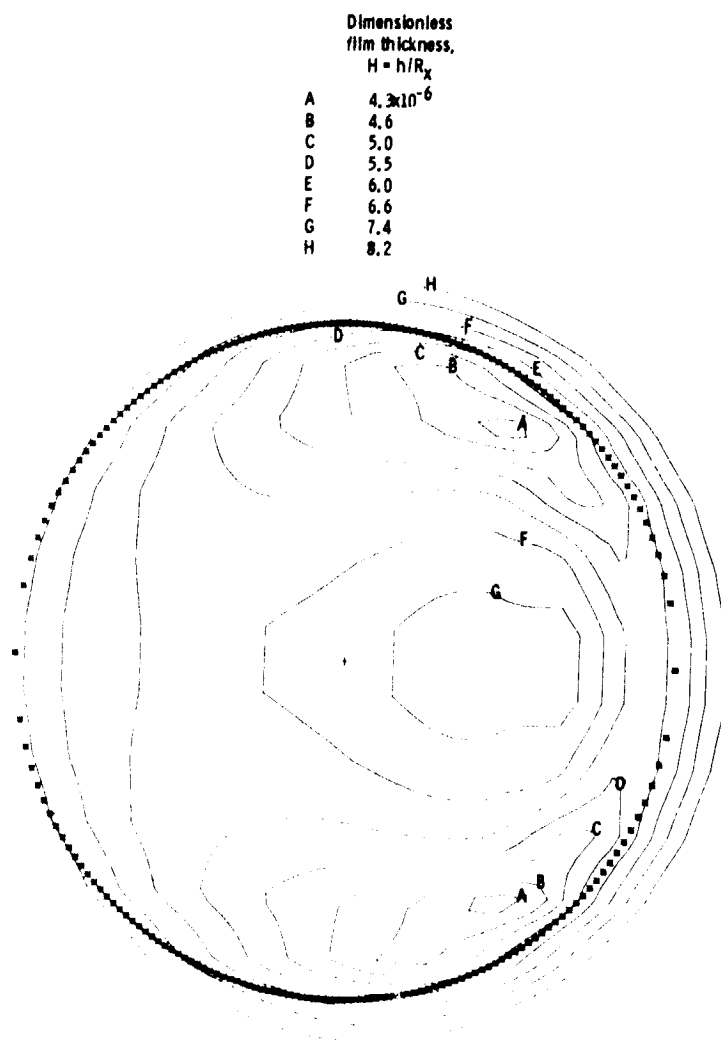
(c) Three-dimensional representation of pressure.

Figure 5.9. - Concluded.



(a) Contour plot of dimensionless pressure.

Figure 5.10. - Contour plots of dimensionless pressure and film thickness and three-dimensional representation of pressure for ellipticity parameter (k) of 1.25. The dimensionless parameters U , W , and G are held constant as defined in equation (5.10).



(b) Contour plot of dimensionless film thickness.

Figure 5.10. - Continued.

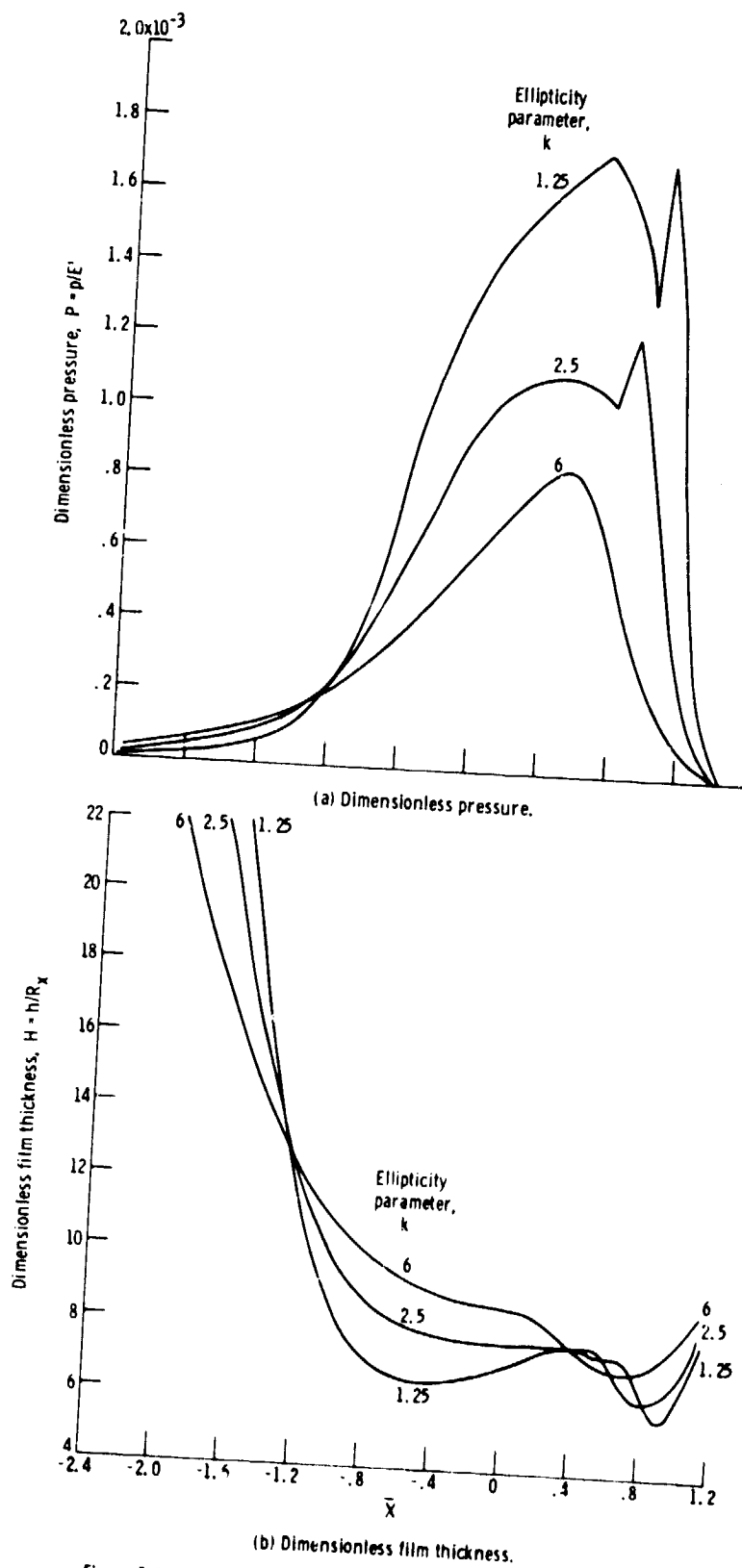
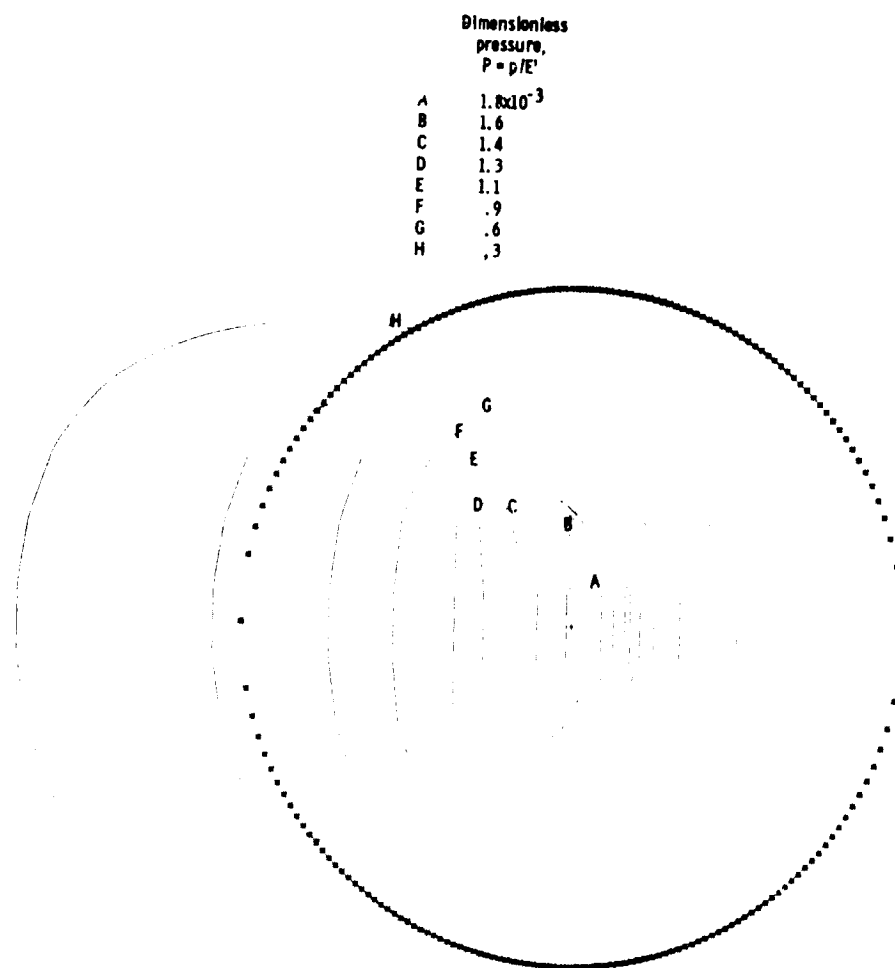


Figure 5.11. - Variation of dimensionless pressure and film thickness on \bar{X} -axis for three values of ellipticity parameter. The value of Y is held fixed near axial center of contact.



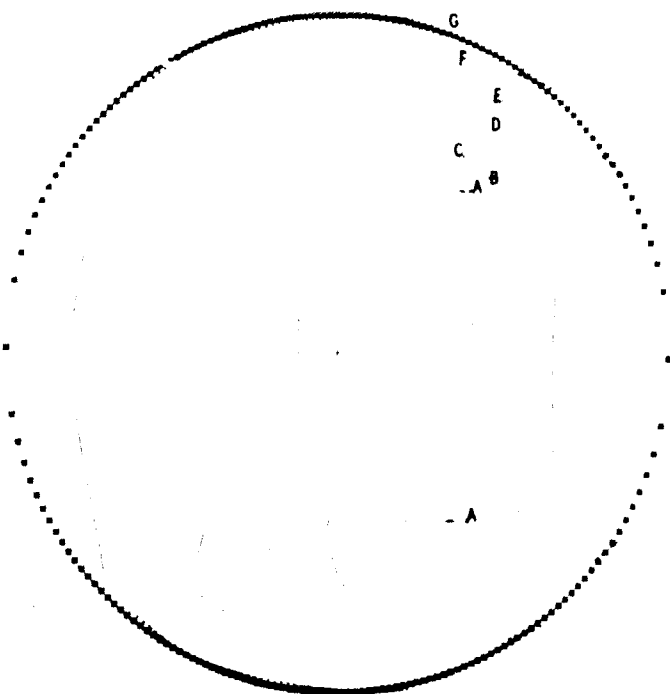
(a) Contour plot of dimensionless pressure.

Figure 5.12. - Contour plots of dimensionless pressure and film thickness and three-dimensional representation of pressure for dimensionless speed parameter (U) of 5.05×10^{-11} . The dimensionless parameters k , W , and G are held constant as defined in equation (5.18).

Dimensionless
film thickness,
 $H = h/R_x$

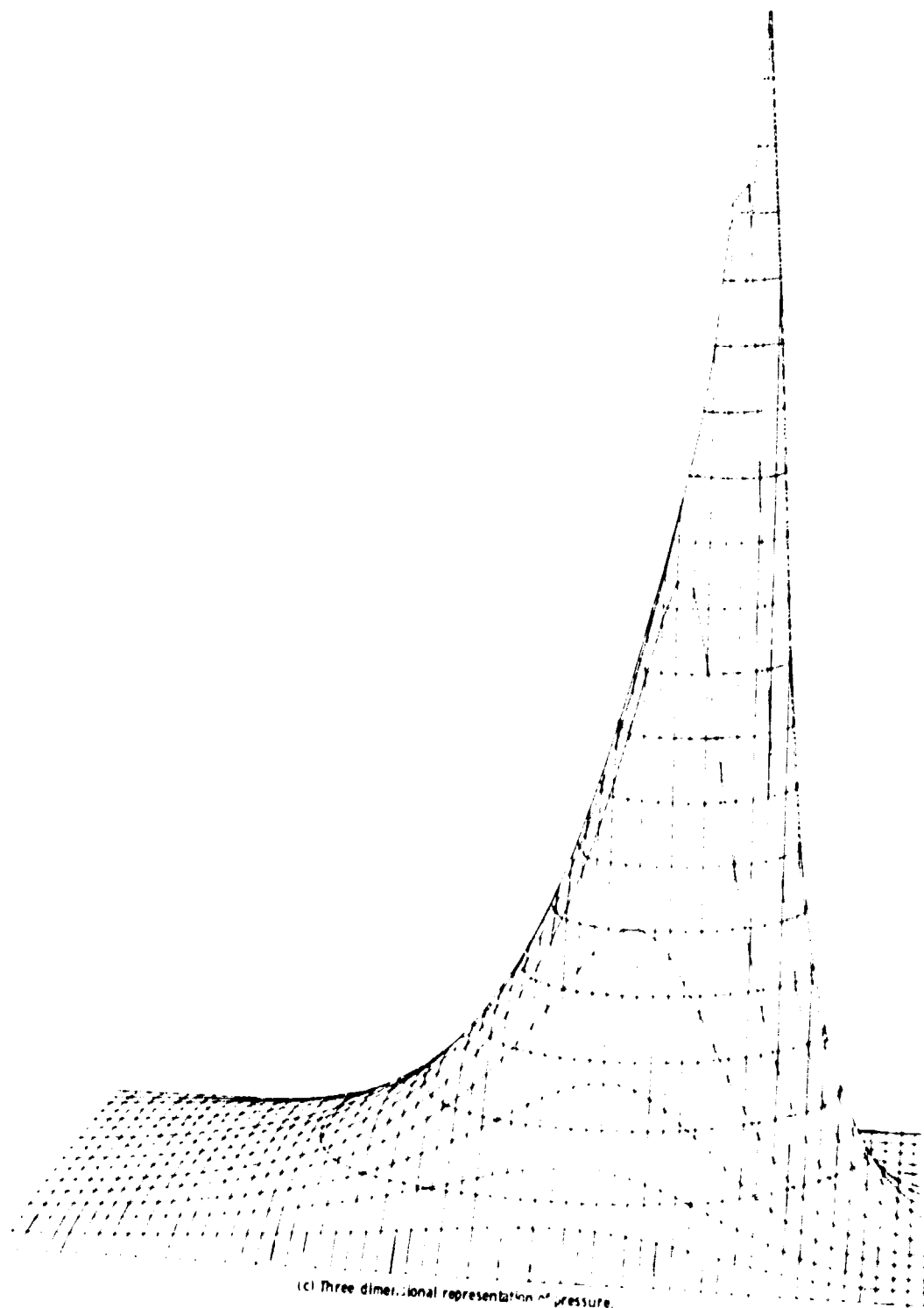
A	61.4×10^{-6}
B	62.0
C	63.0
D	65.0
E	68.0
F	72.0
G	78.0
H	86.0

H



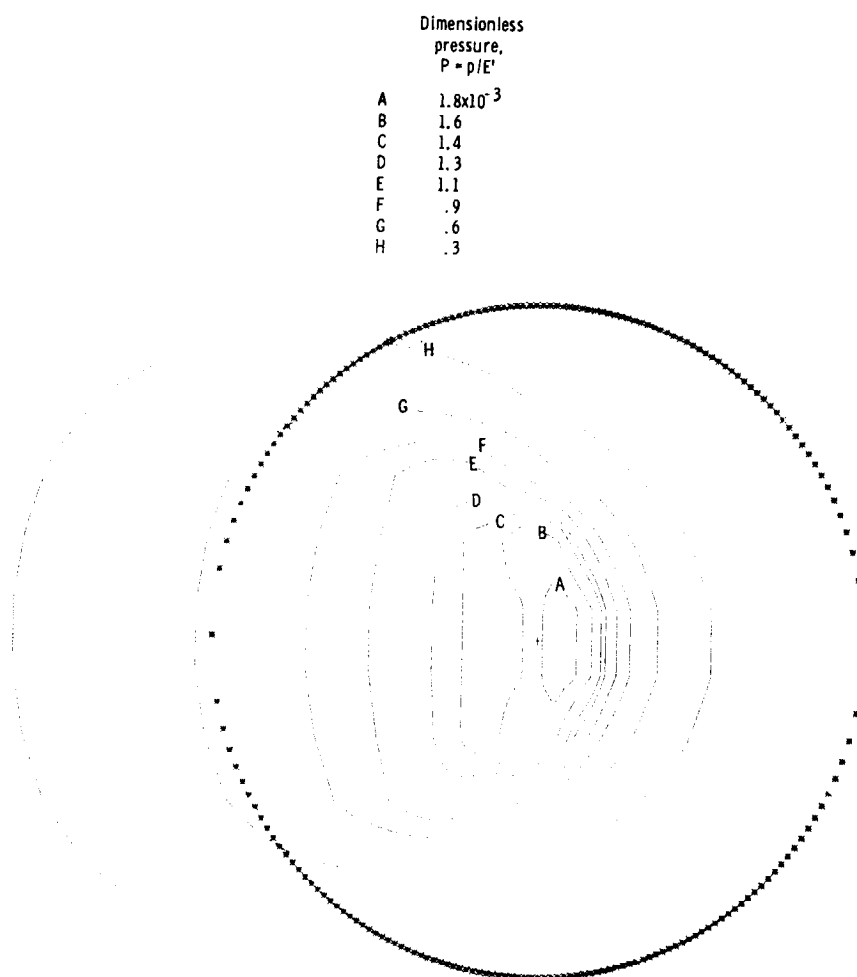
(c) Contour plot of dimensionless film thickness.

Figure 5.12. - Continued.



(c) Three dimensional representation of pressure.

Figure 5.12. Concluded.

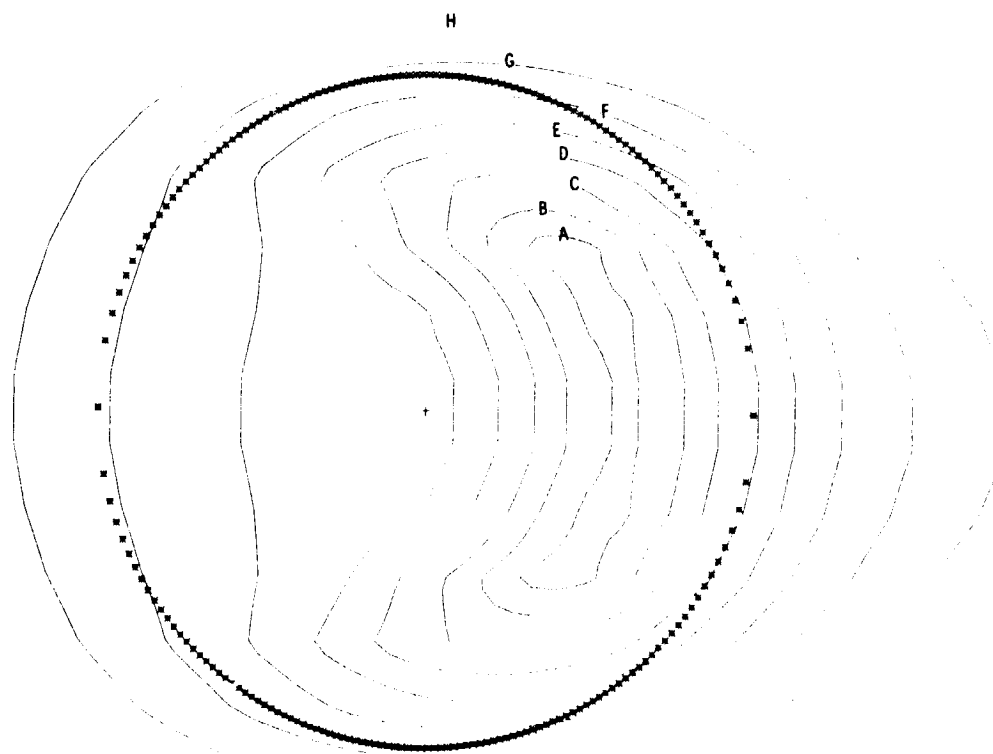


(a) Contour plot of dimensionless pressure.

Figure 5.13. - Contour plots of dimensionless pressure and film thickness and three-dimensional representation of pressure for dimensionless speed parameter (U) of 4.208×10^{-14} . The dimensionless parameters k , W , and ξ are held constant as defined in equation (5.18).

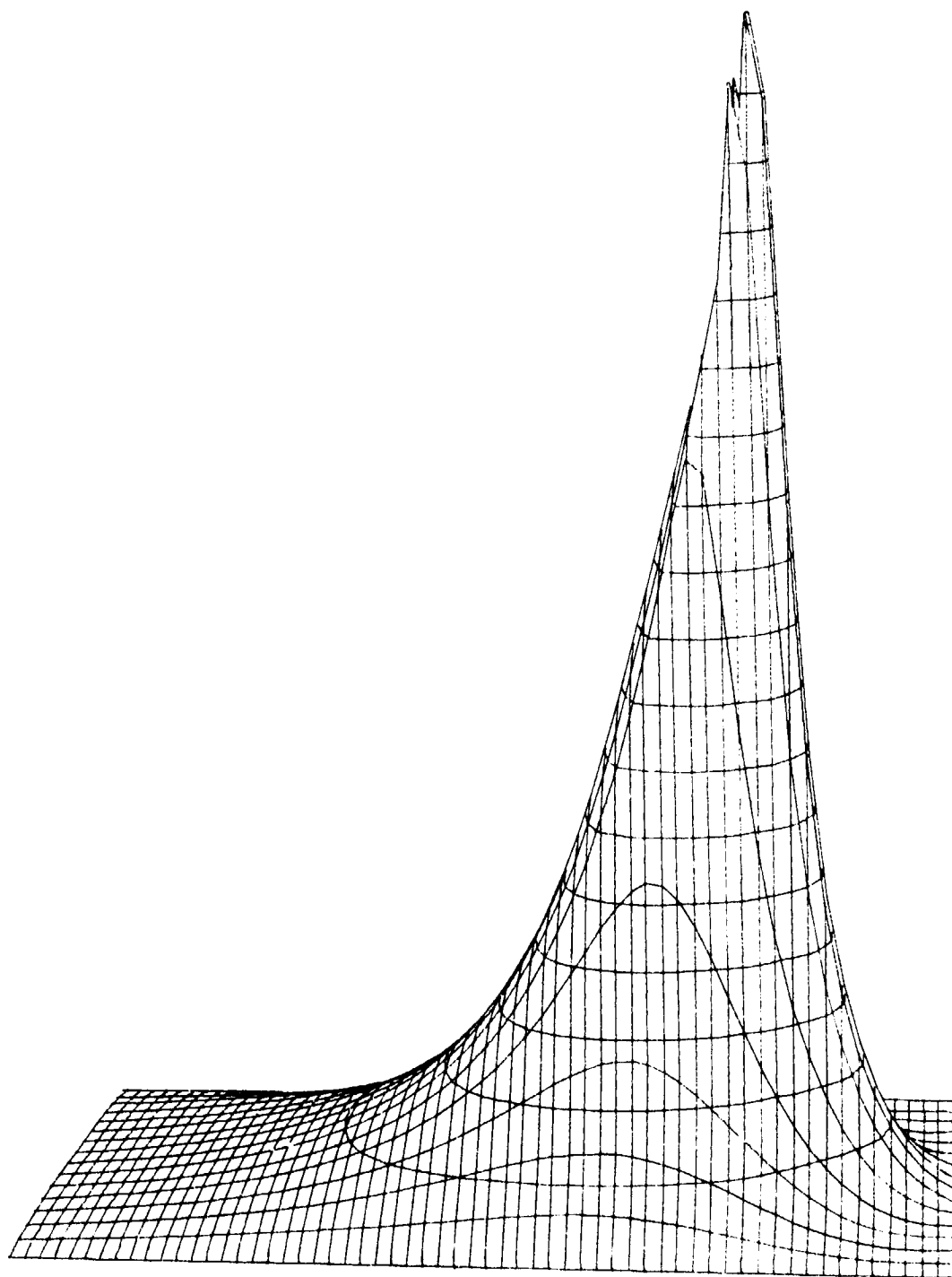
Dimensionless
film thickness,
 $H = h/R_x$

A	55.0×10^{-6}
B	56.0
C	57.5
D	60.0
E	63.0
F	67.0
G	73.0
H	81.0



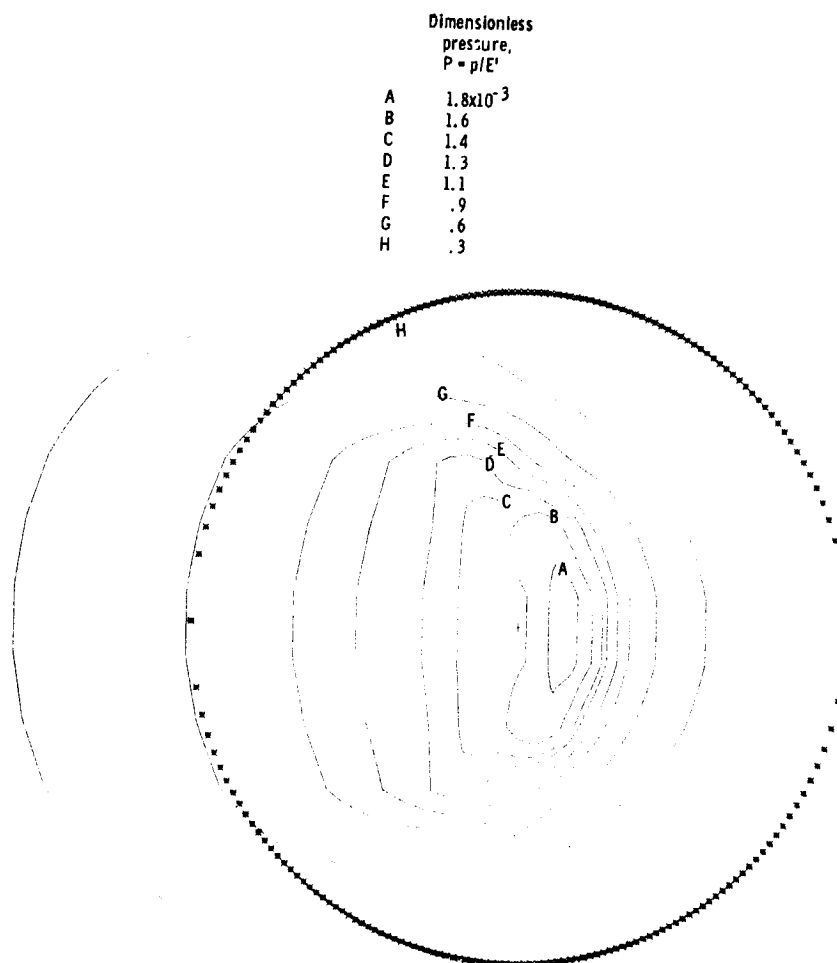
(b) Contour plot of dimensionless film thickness.

Figure 5.13. - Continued.



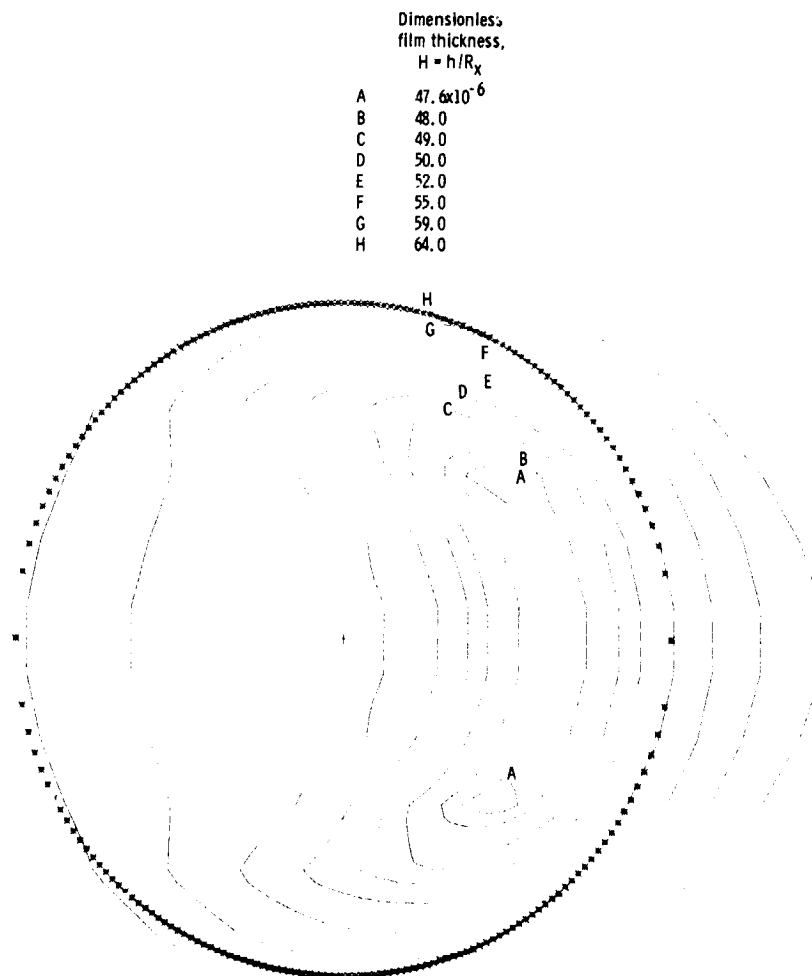
(c) Three-dimensional representation of pressure.

Figure 5.13. - Concluded.



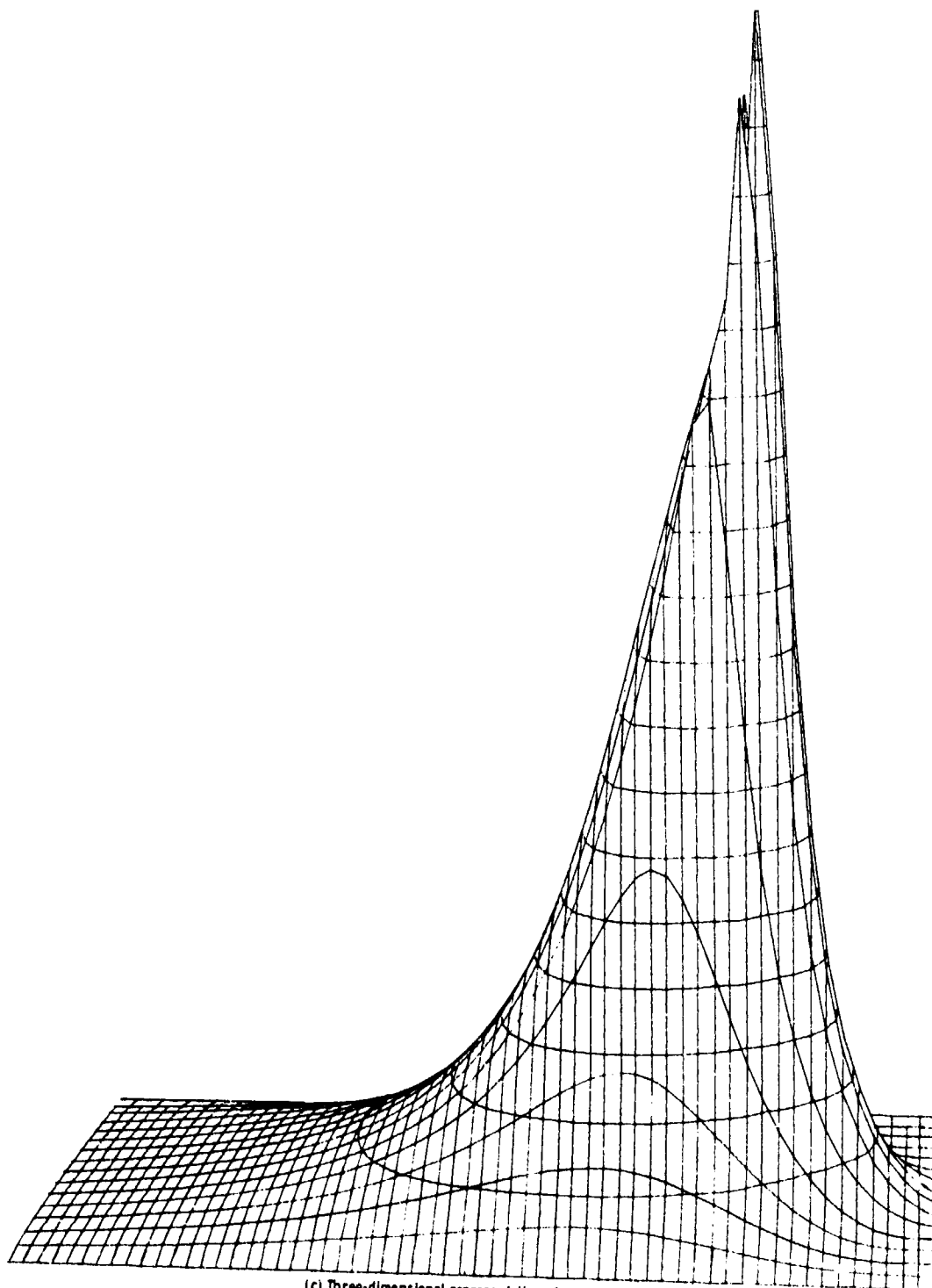
(a) Contour plot of dimensionless pressure.

Figure 5.14. - Contour plots of dimensionless pressure and film thickness and three-dimensional representation of pressure for dimensionless speed parameter (U) of 3.367×10^{-11} . The dimensionless parameters k , W , and G are held constant as defined in equation (5.18).



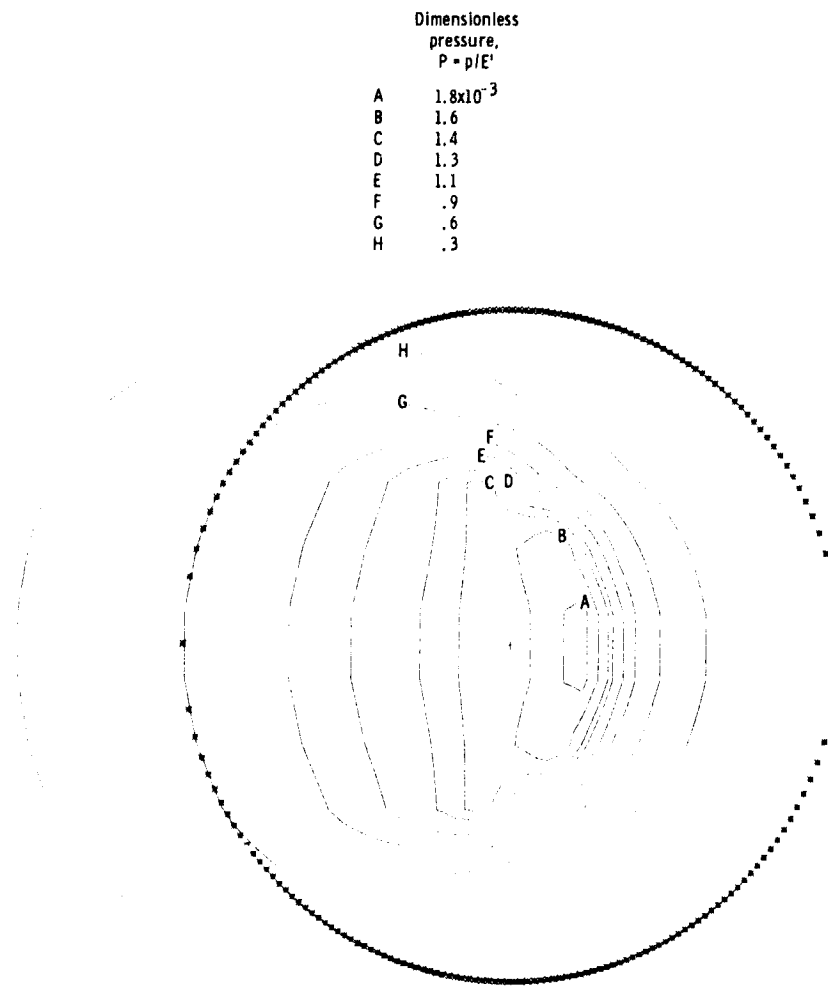
(b) Contour plot of dimensionless film thickness.

Figure 5.14. - Continued.



(c) Three-dimensional representation of pressure.

Figure 5.14. - Concluded.

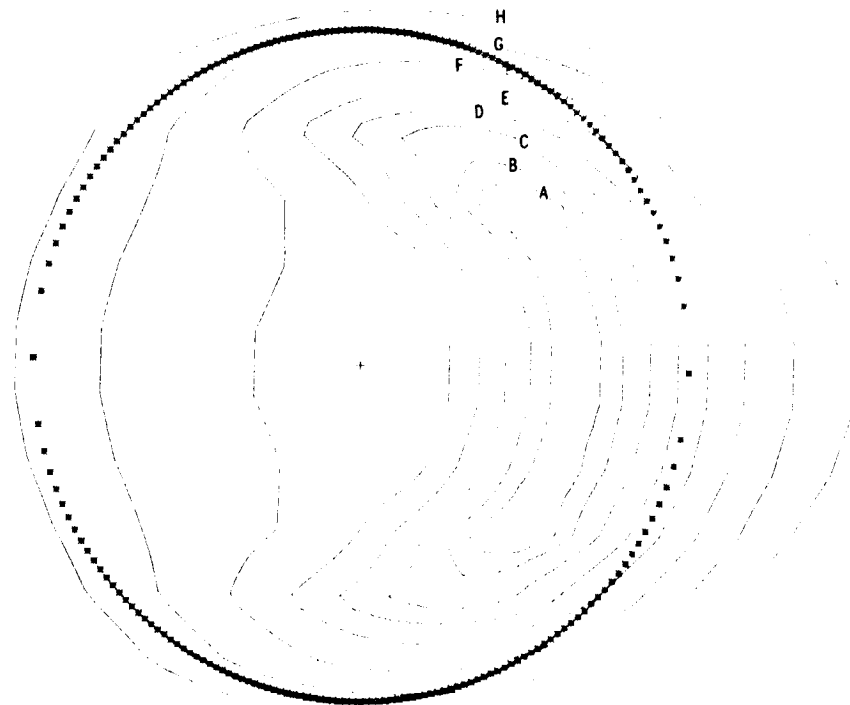


(a) Contour plot of dimensionless pressure.

Figure 5.15. - Contour plots of dimensionless pressure and film thickness and three-dimensional representation of pressure for dimensionless speed parameter (U) of 2.946×10^{-11} . The dimensionless parameters k , W , and G are held constant as defined in equation (5.18).

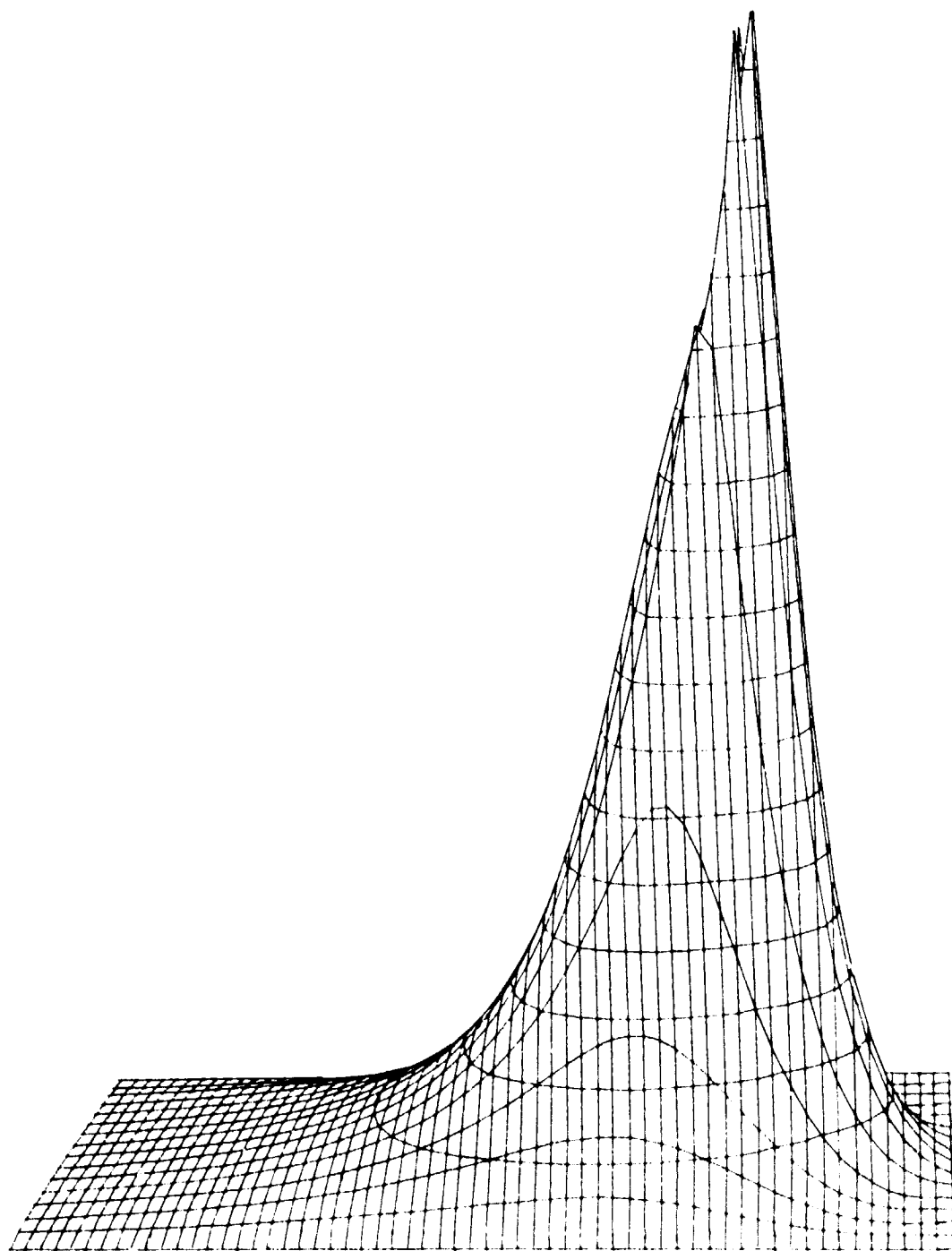
Dimensionless
film thickness,
 $H = h/R_x$

A	44.0×10^{-6}
B	44.5
C	45.5
D	47.0
E	49.0
F	52.0
G	56.0
H	61.0



(b) Contour plot of dimensionless film thickness.

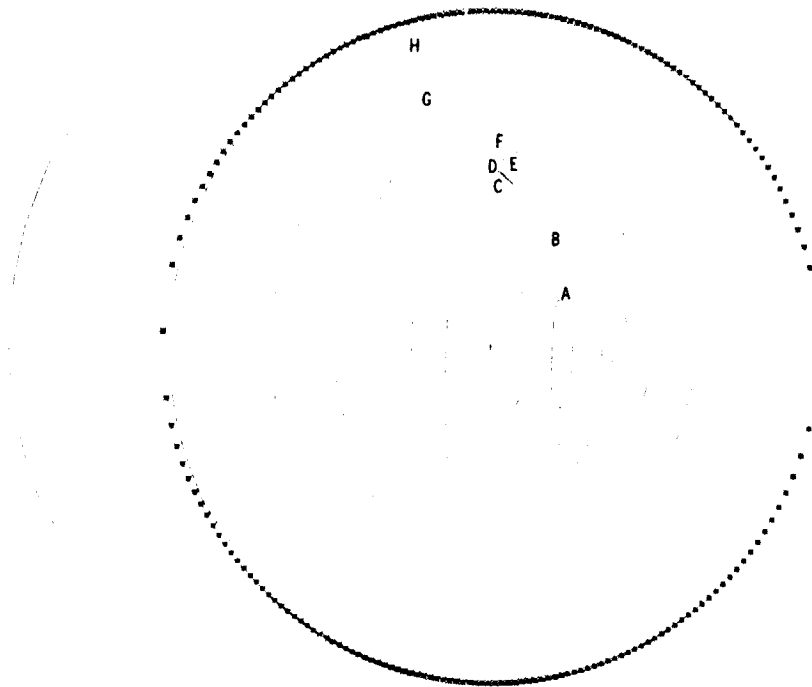
Figure 5.15. - Continued.



(c) Three-dimensional representation of pressure.

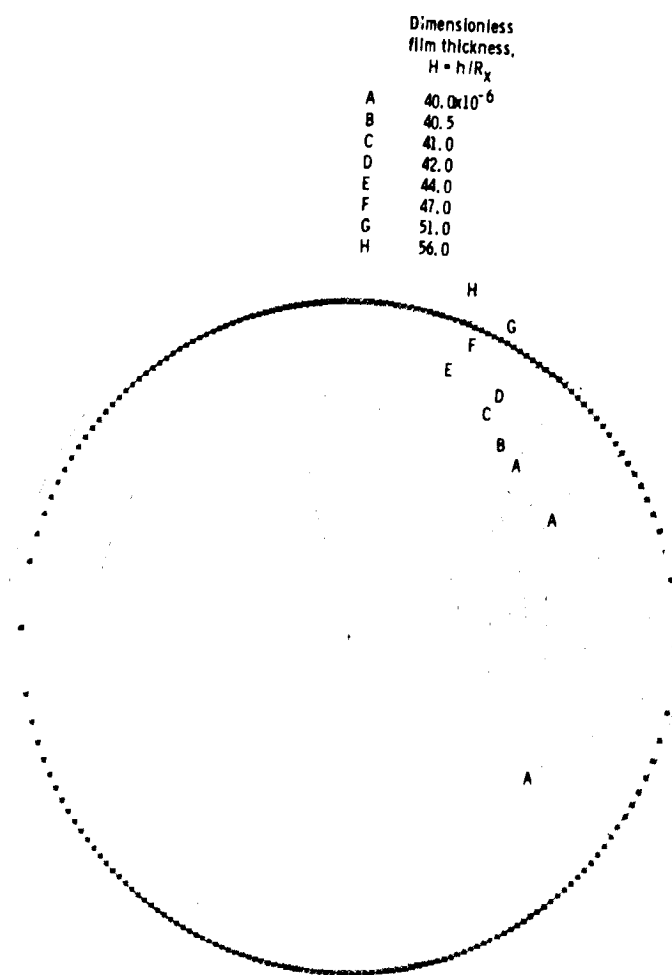
Figure 5.15. - Concluded.

	Dimensionless pressure, $P = p/E'$
A	1.8×10^{-3}
B	1.6
C	1.4
D	1.3
E	1.1
F	.9
G	.6
H	.3



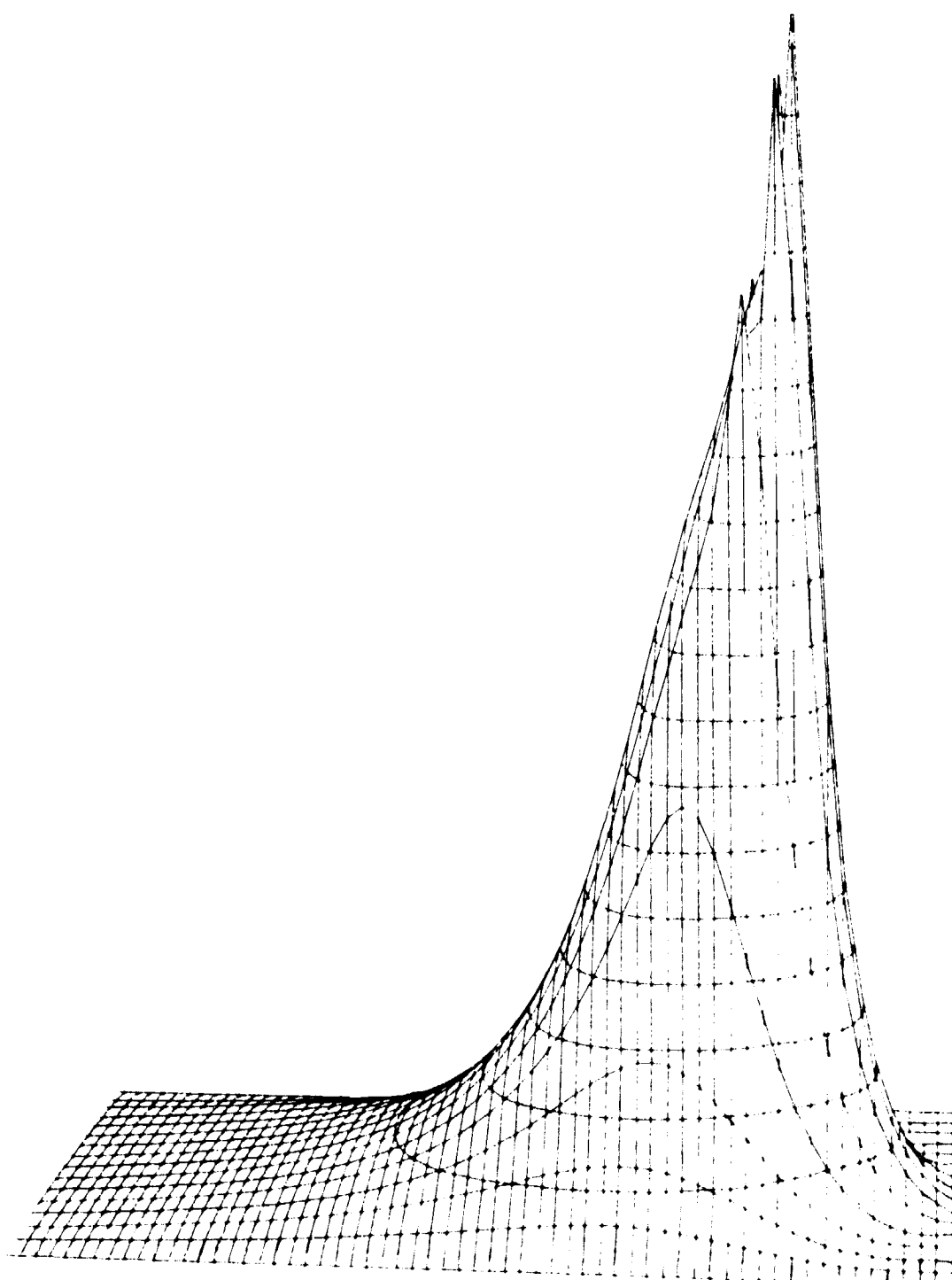
(a) Contour plot of dimensionless pressure.

Figure 5.16. - Contour plots of dimensionless pressure and film thickness and three-dimensional representation of pressure for dimensionless speed parameter (U) of 2.525×10^{-11} . The dimensionless constants k , W , and G are held constant as defined in equation (5.18).



(b) Contour plot of dimensionless film thickness.

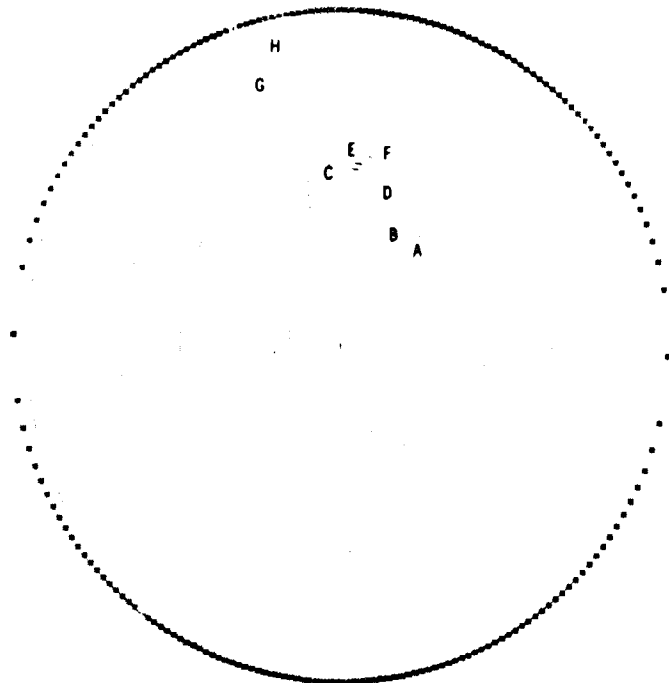
Figure 5.16. - Continued.



(c) Three-dimensional representation of pressure.

Figure 5.16 - Concluded.

	Dimensionless pressure, $P = p/E'$
A	1.8×10^{-3}
B	1.6
C	1.4
D	1.3
E	1.1
F	.9
G	.6
H	.3

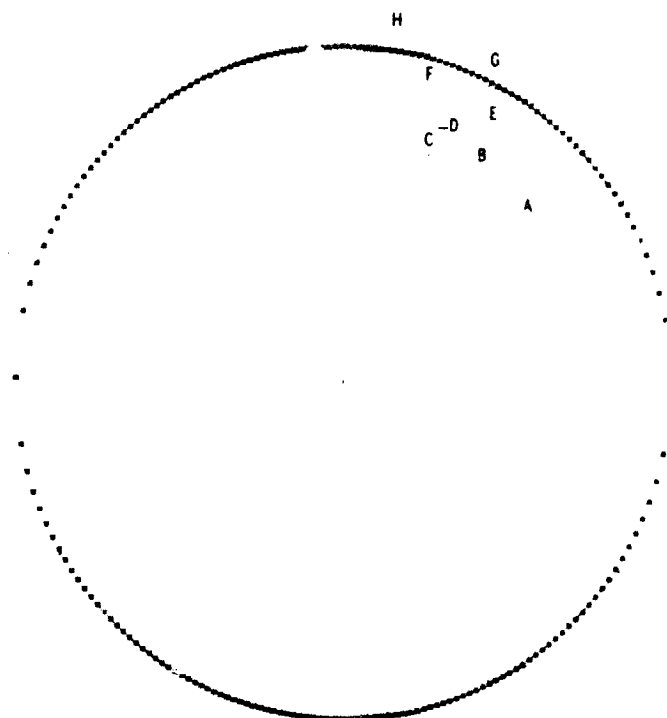


(a) Contour plot of dimensionless pressure.

Figure 5.17. - Contour plots of dimensionless pressure and film thickness and three-dimensional representation of pressure for dimensionless speed parameter (U) of 2.10×10^{-11} . The dimensionless constants k , W , and G are held constant as defined in equation (5.18).

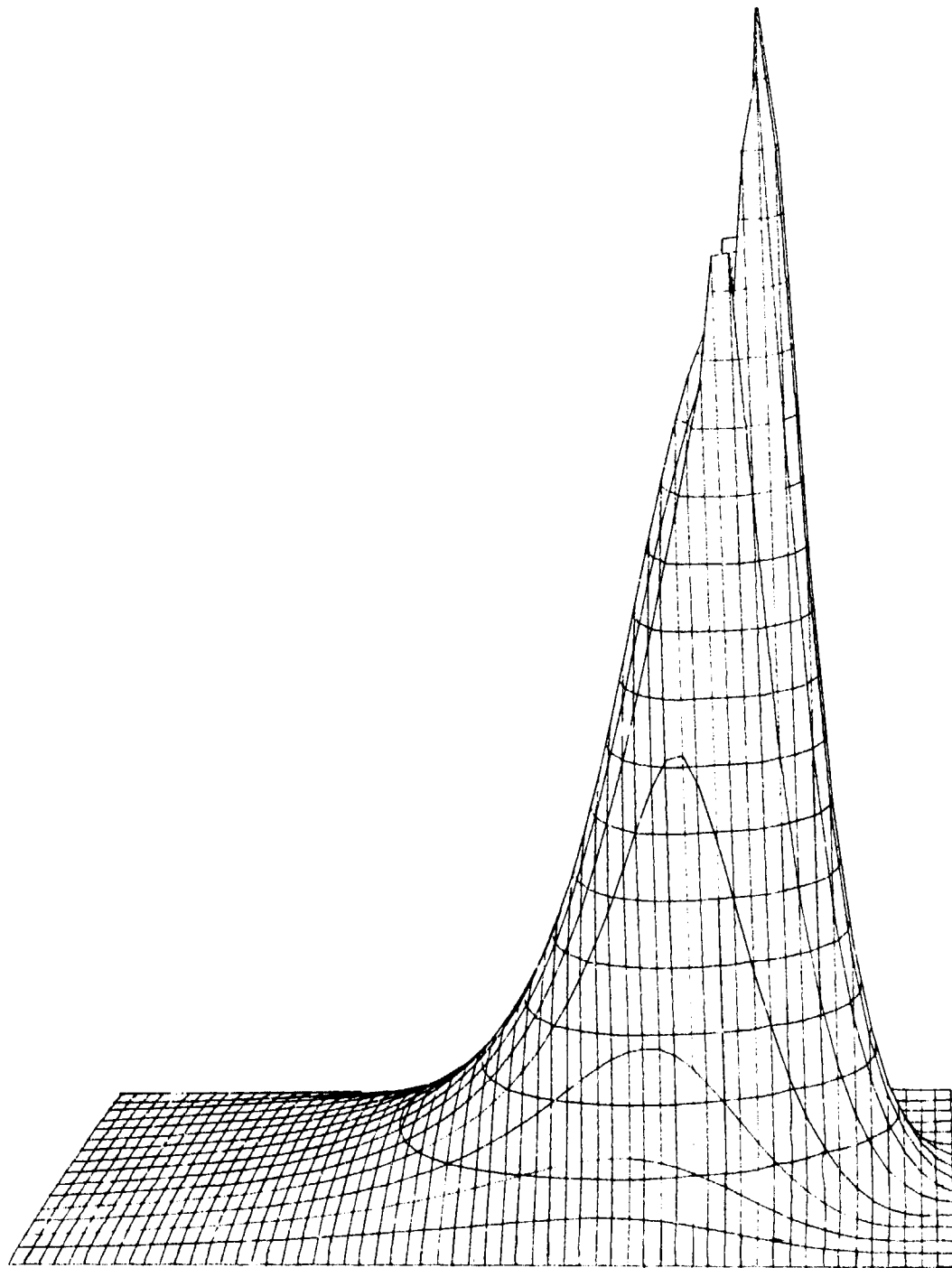
Dimensionless
film thickness,
 $H = h/R_x$

A	34.9 $\times 10^{-6}$
B	35.4
C	36.0
D	37.0
E	39.0
F	42.0
G	46.0
H	51.0



(b) Contour plot of dimensionless film thickness.

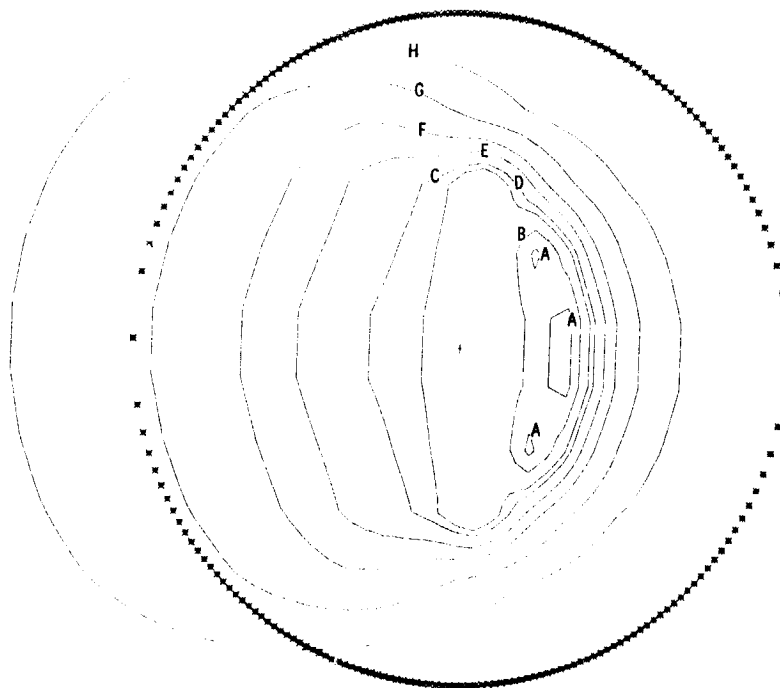
Figure 5.17. - Continued.



(c) Three-dimensional representation of pressure.

Figure 5.17. - Concluded.

	Dimensionless pressure, $P = p/E'$
A	1.8×10^{-3}
B	1.6
C	1.4
D	1.3
E	1.1
F	.9
G	.6
H	.3

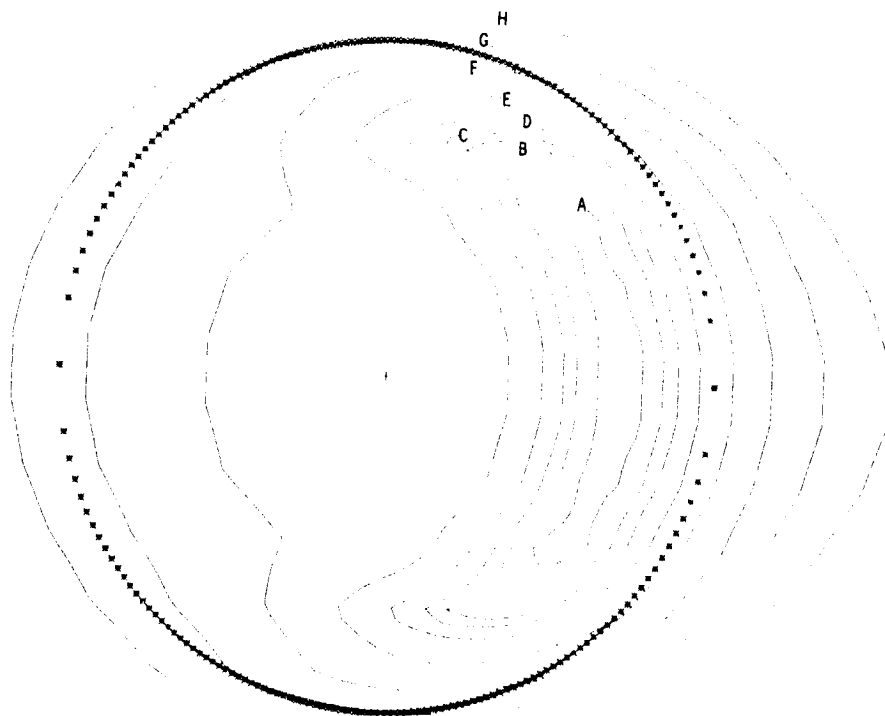


(a) Contour plot of dimensionless pressure.

Figure 5.18. - Contour plots of dimensionless pressure and film thickness and three-dimensional representation of pressure for dimensionless speed parameter (U) of 1.68×10^{-11} . The dimensionless parameters k , W , and G are held constant as defined in equation (5.18).

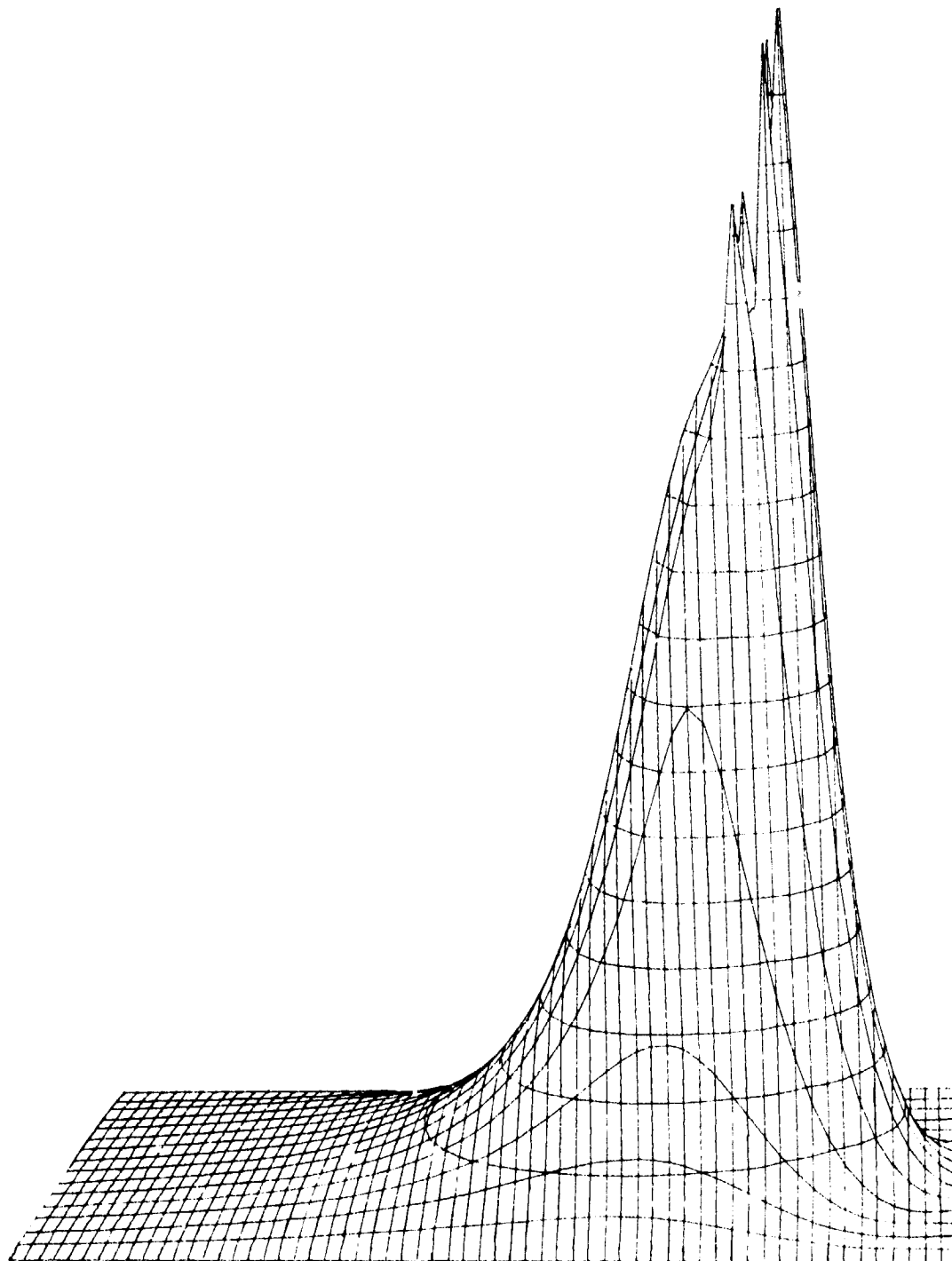
Dimensionless
film thickness,
 $H = h/R_x$

A	30.0×10^{-6}
B	30.5
C	31.0
D	32.0
E	34.0
F	37.0
G	41.0
H	46.0



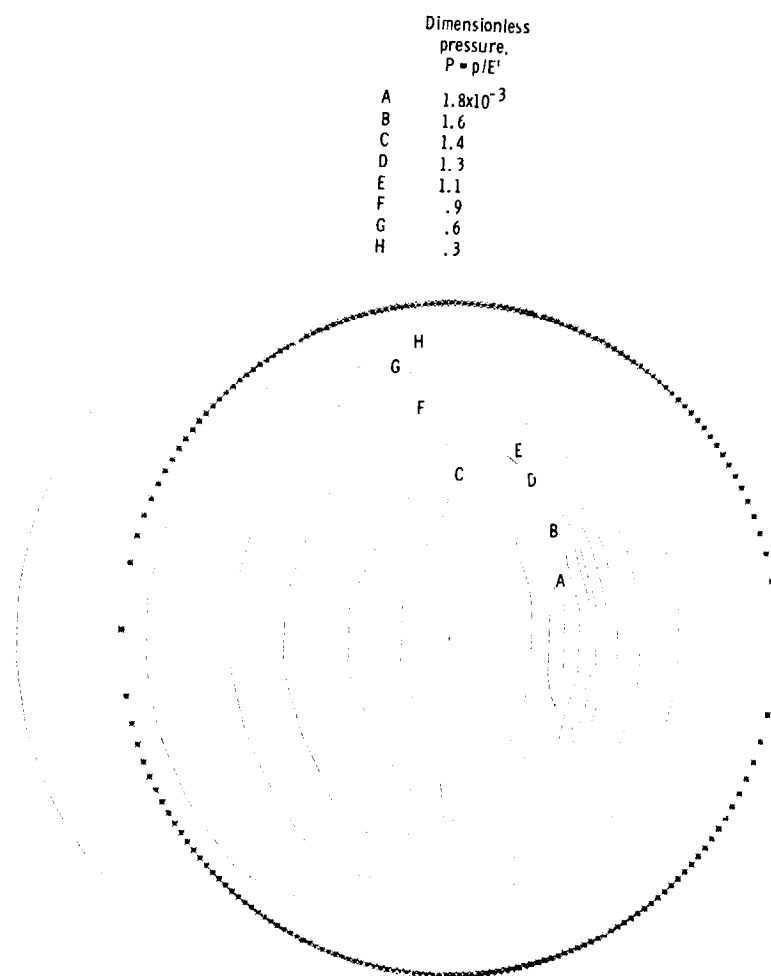
(b) Contour plot of dimensionless film thickness.

Figure 5.18. - Continued.



(c) Three-dimensional representation of pressure.

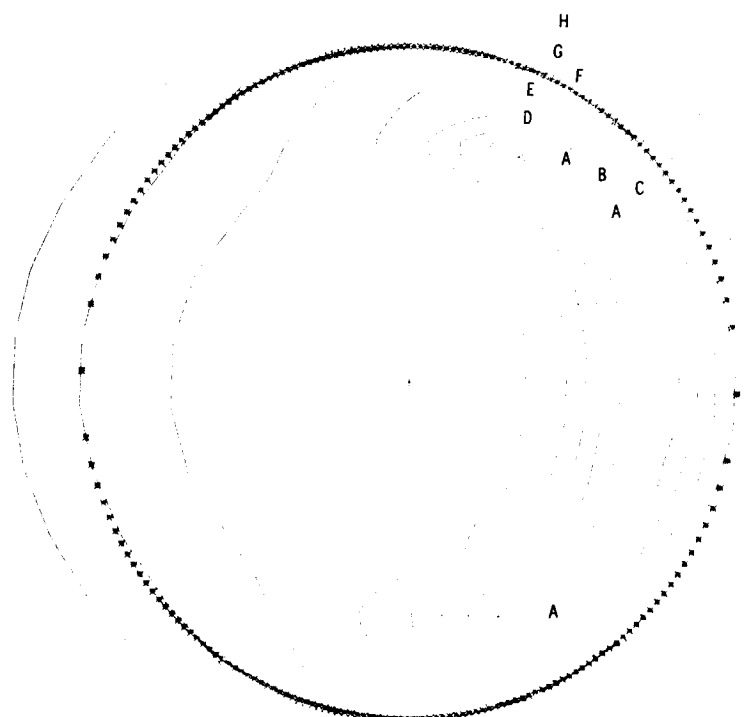
Figure 5.18. - Concluded.



(a) Contour plot of dimensionless pressure.

Figure 5.19. - Contour plots of dimensionless pressure and film thickness and three-dimensional representation of pressure for dimensionless speed parameter (U) of 1.26×10^{-11} . The dimensionless parameters k , W , and G are held constant as defined in equation (5.18).

	Dimensionless film thickness, $H = h/R_x$
A	24.8×10^{-6}
B	25.3
C	26.0
D	27.5
E	29.0
F	32.0
G	36.0
H	41.0



(b) Contour plot of dimensionless film thickness.

Figure 5.19. - Continued.

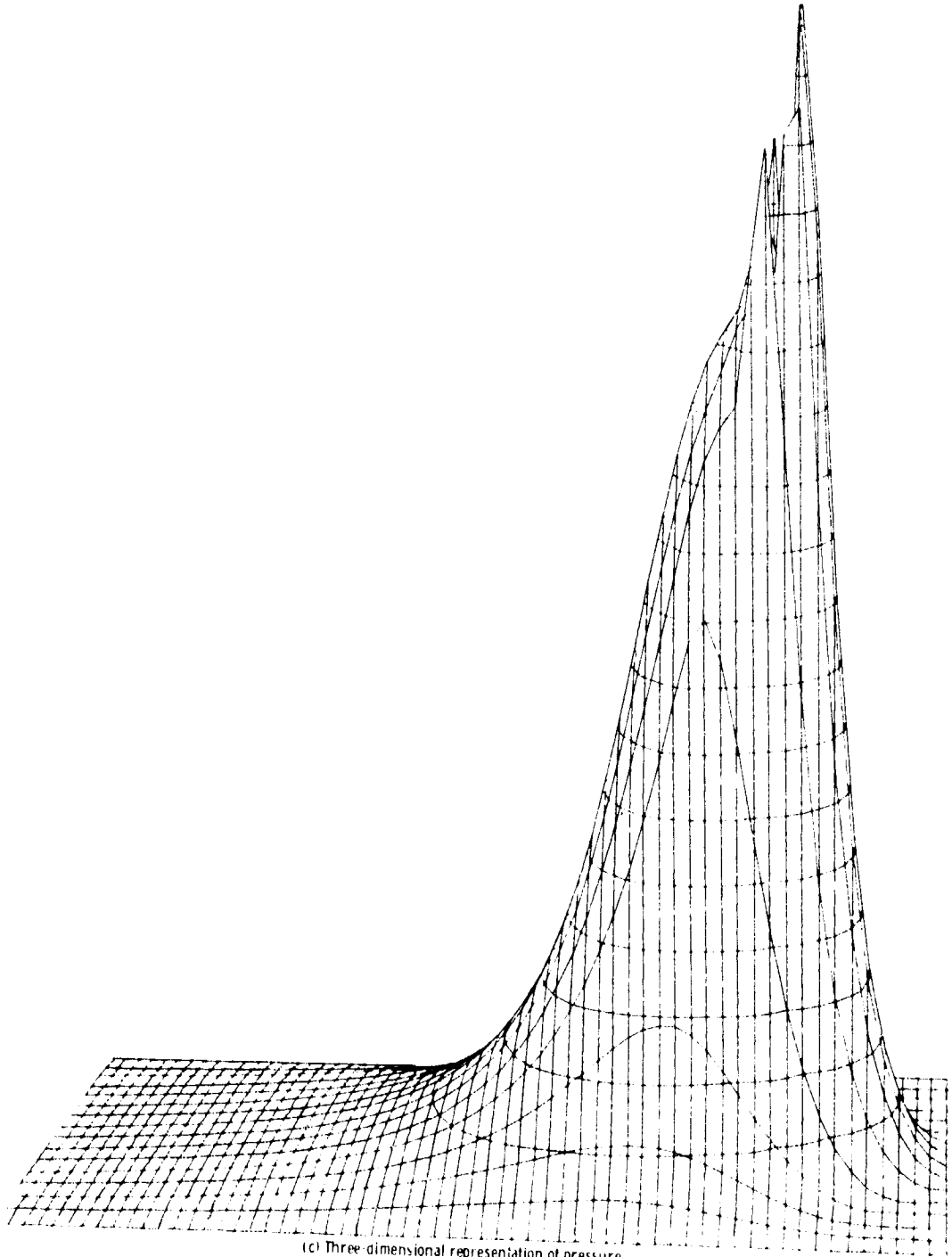
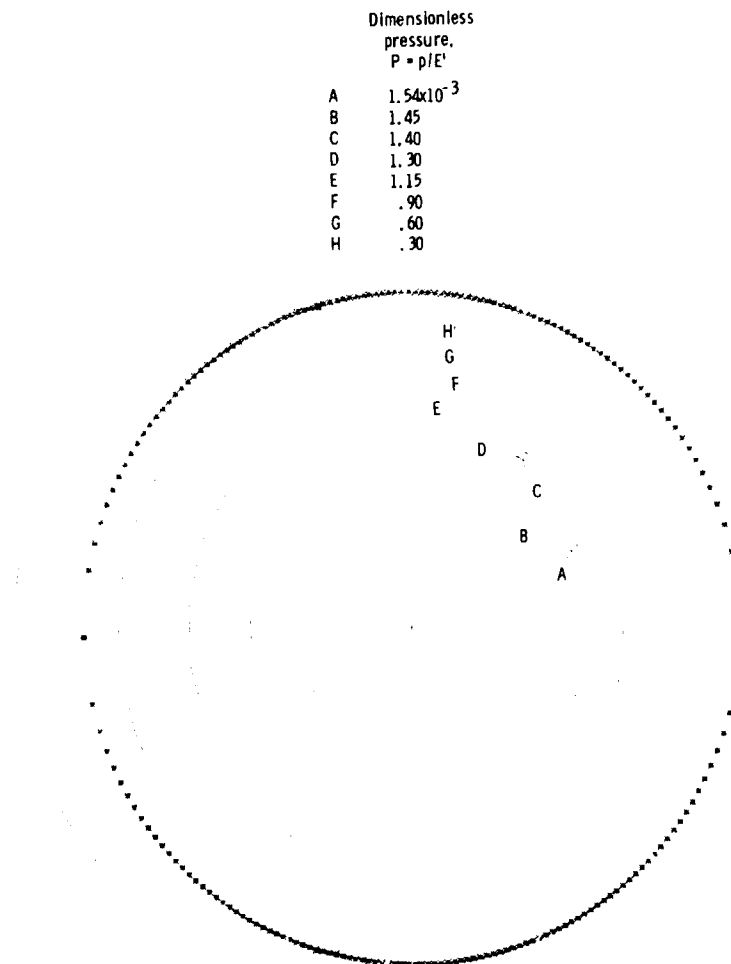


Figure 5. 19. - Concluded.

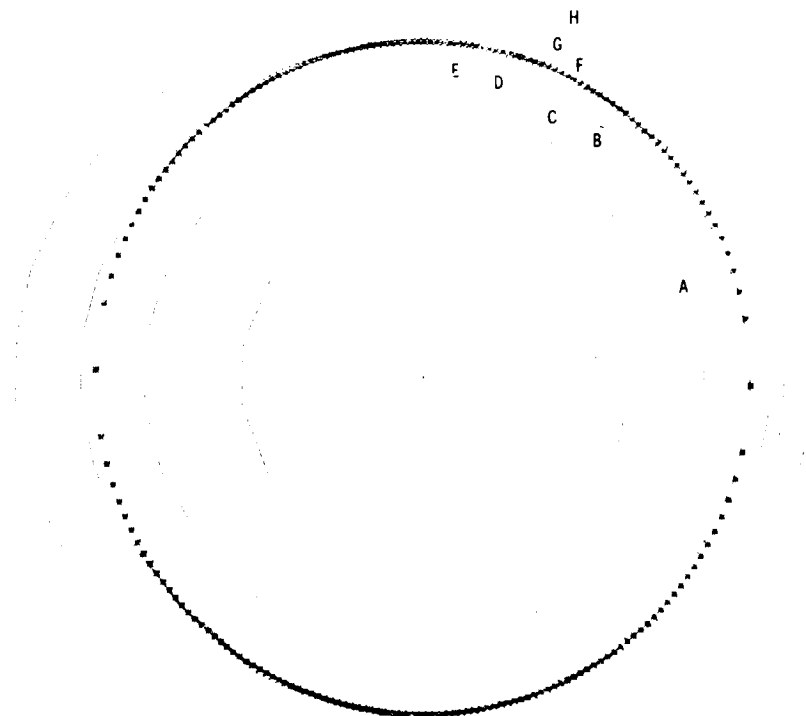


(a) Contour plot of dimensionless pressure.

Figure 5.20. - Contour plots of dimensionless pressure and film thickness and three-dimensional representation of pressure for dimensionless speed parameter (U) of 8.416×10^{-12} . The dimensionless parameters k , W , and G are held constant as defined by equation (5.18).

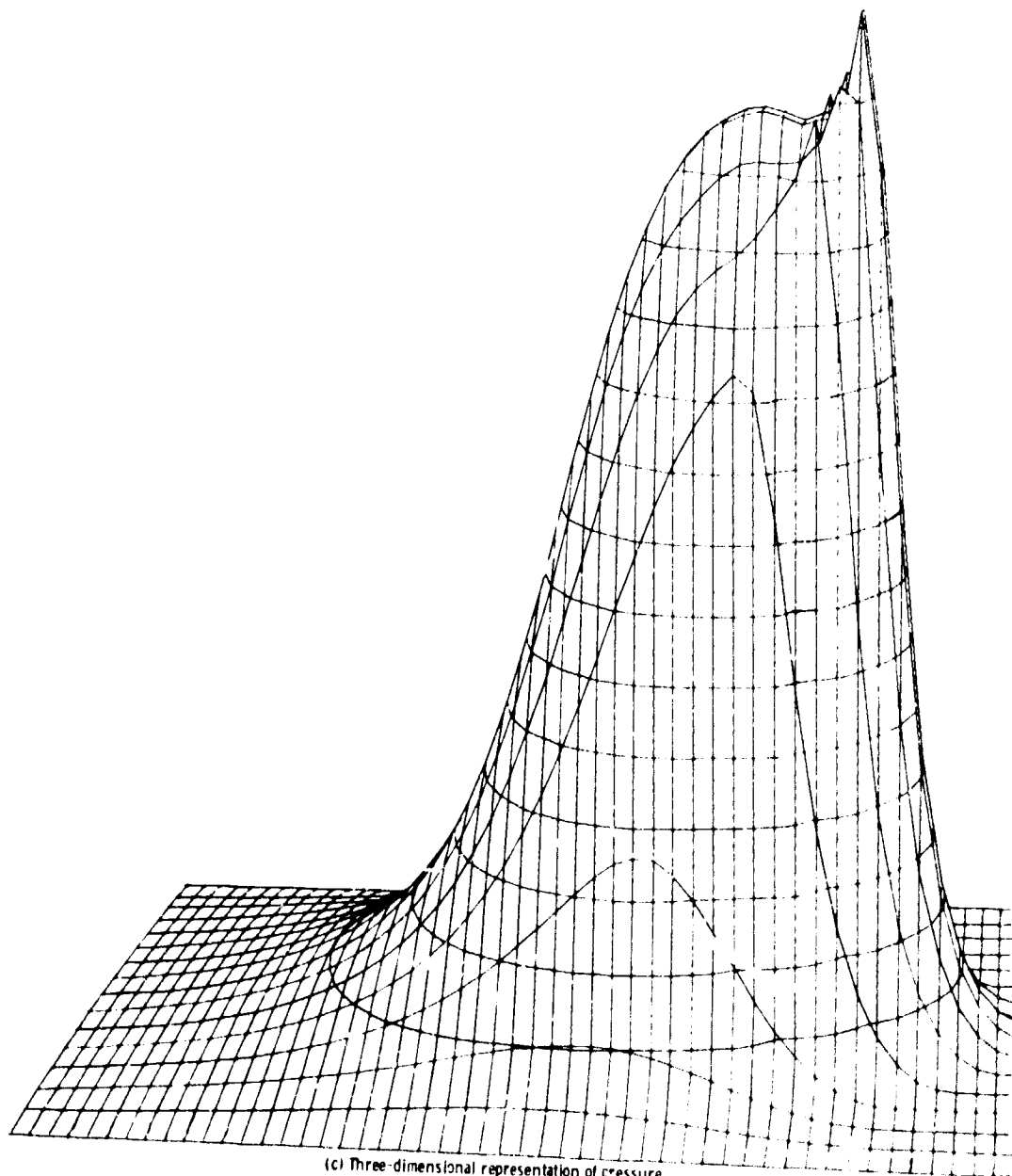
Dimensionless
film thickness,
 $H = h/R_x$

A	18.5×10^{-6}
B	19.0
C	20.0
D	21.0
E	22.0
F	24.0
G	27.0
H	32.0



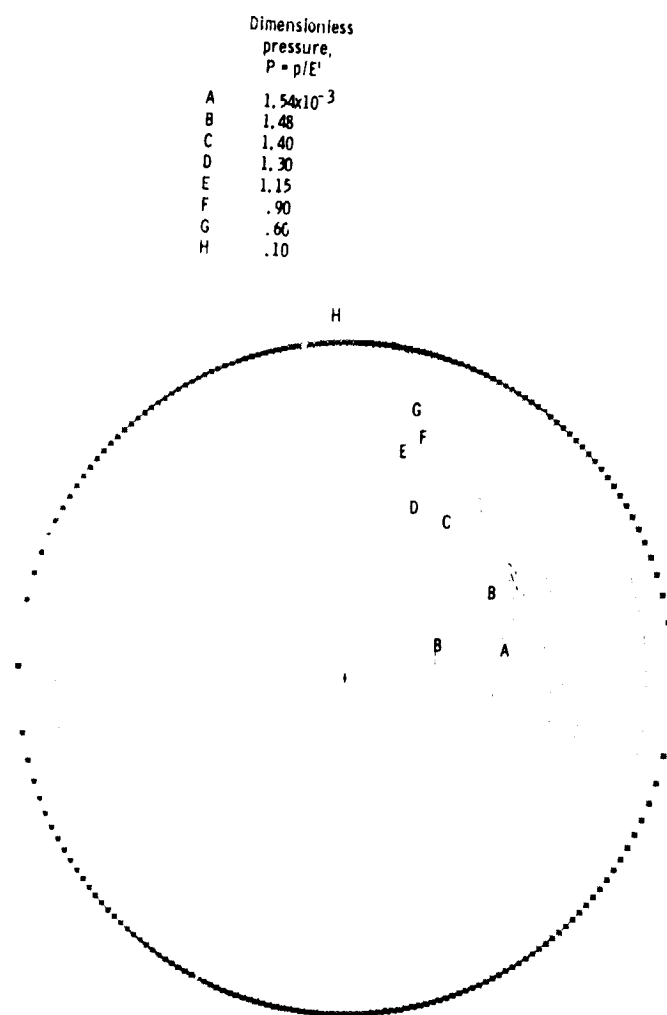
(b) Contour plot of dimensionless film thickness.

Figure 5.20. - Continued.



(c) Three-dimensional representation of pressure.

Figure 5.20. Concluded.

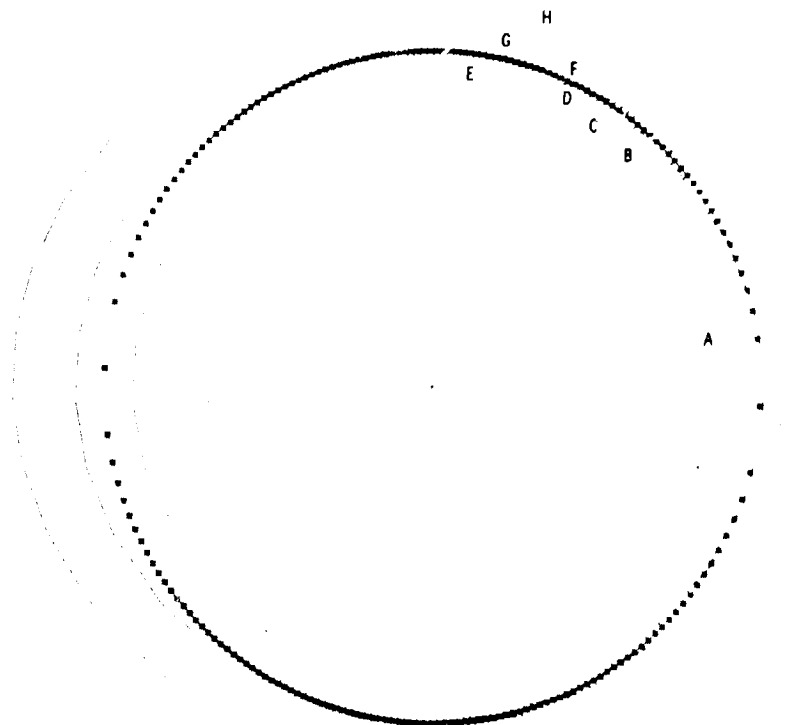


(a) Contour plot of dimensionless pressure.

Figure 5.21. - Contour plots of dimensionless pressure and film thickness and three-dimensional representation of pressure for dimensionless speed parameter (U) of 5.892×10^{-12} . The dimensionless parameters ν , W , and G are held constant as defined in equation (5.18).

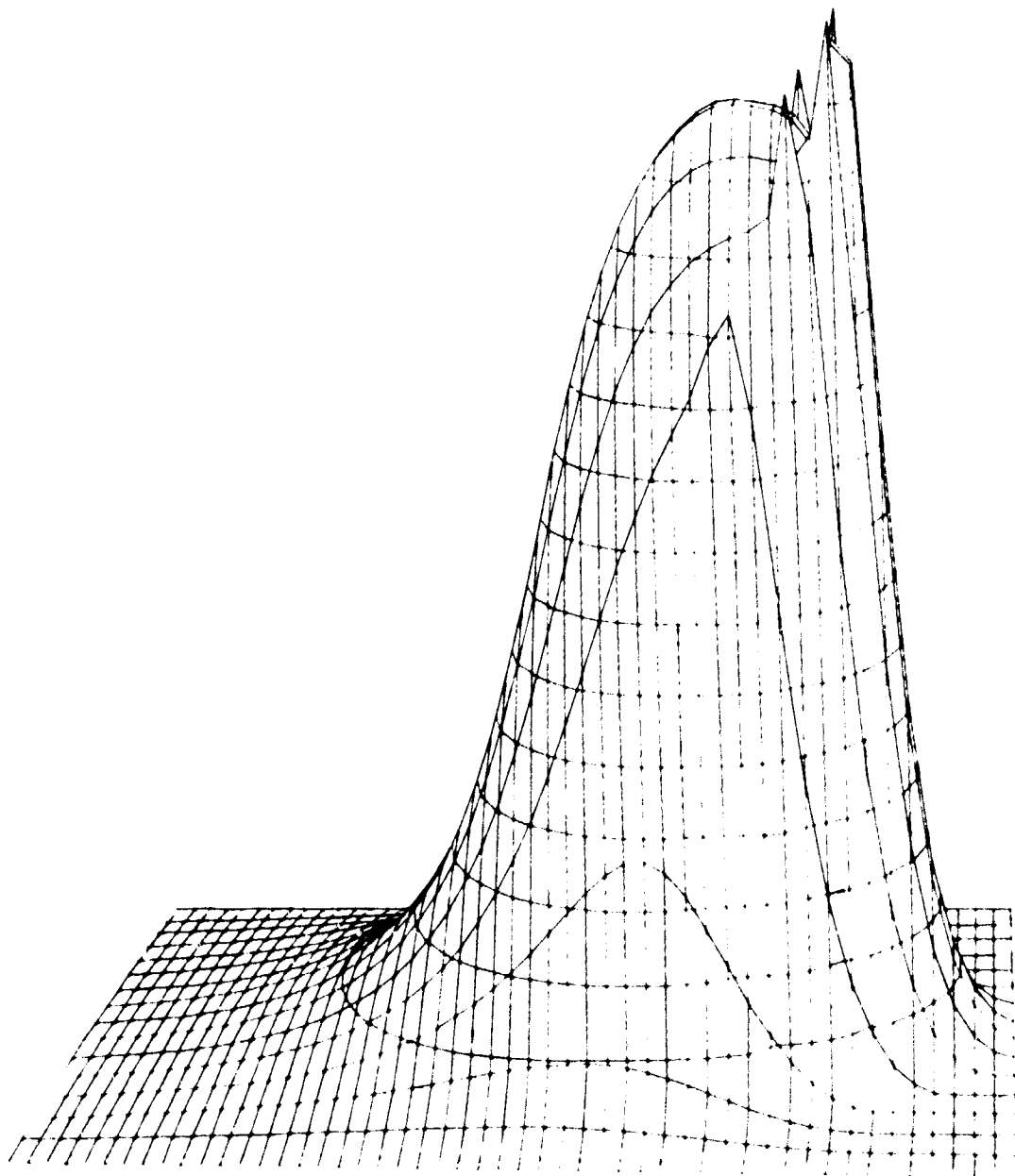
Dimensionless
film thickness,
 $H = h/R_x$

A	14.5×10^{-6}
B	15.0
C	16.0
D	17.0
E	18.0
F	20.0
G	23.0
H	28.0



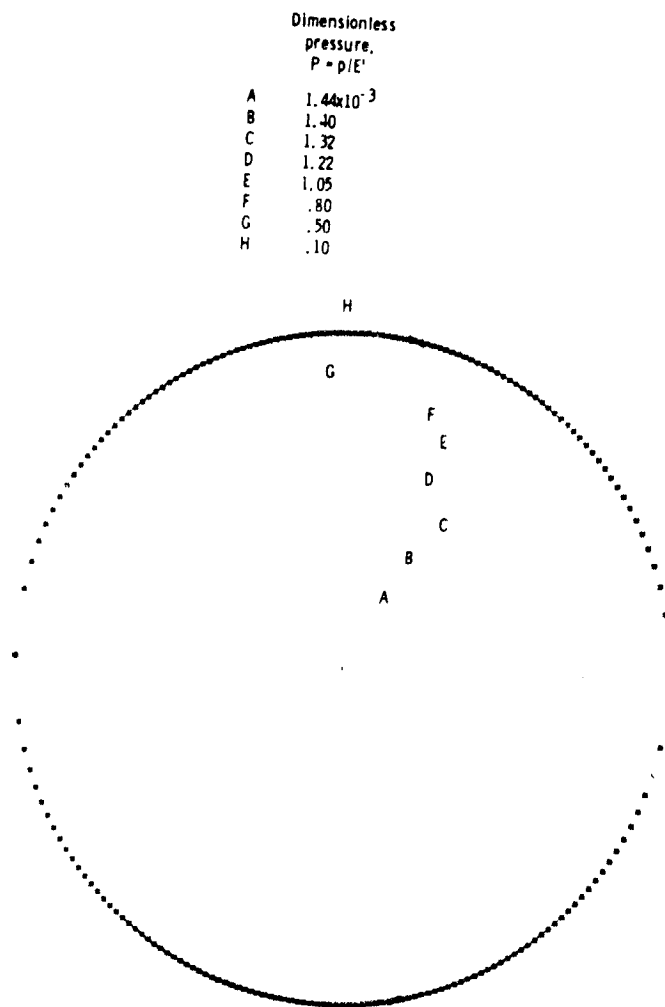
(b) Contour plot of dimensionless film thickness.

Figure 5.21. - Continued.



(c) Three-dimensional representation of pressure

Figure 5.21. Concluded.

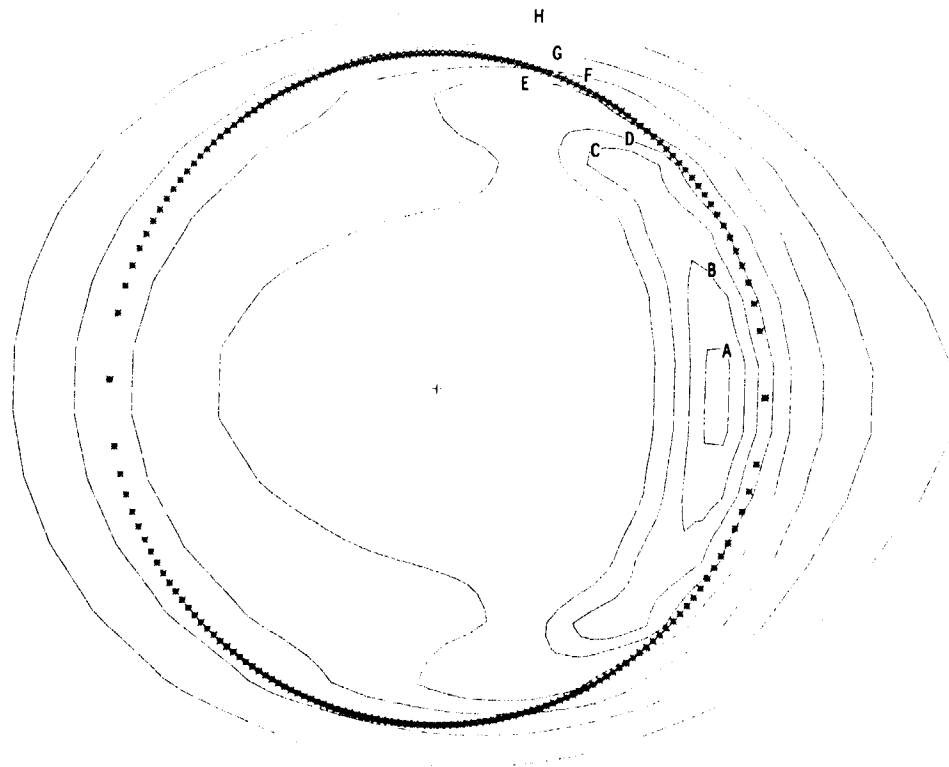


(a) Contour plot of dimensionless pressure.

Figure 5.22. Contour plots of dimensionless pressure and film thickness and three-dimensional representation of pressure for dimensionless speed parameter (U) of 4.20×10^{-12} . The dimensionless parameters k , W , and G are held constant as defined by equation (5.18).

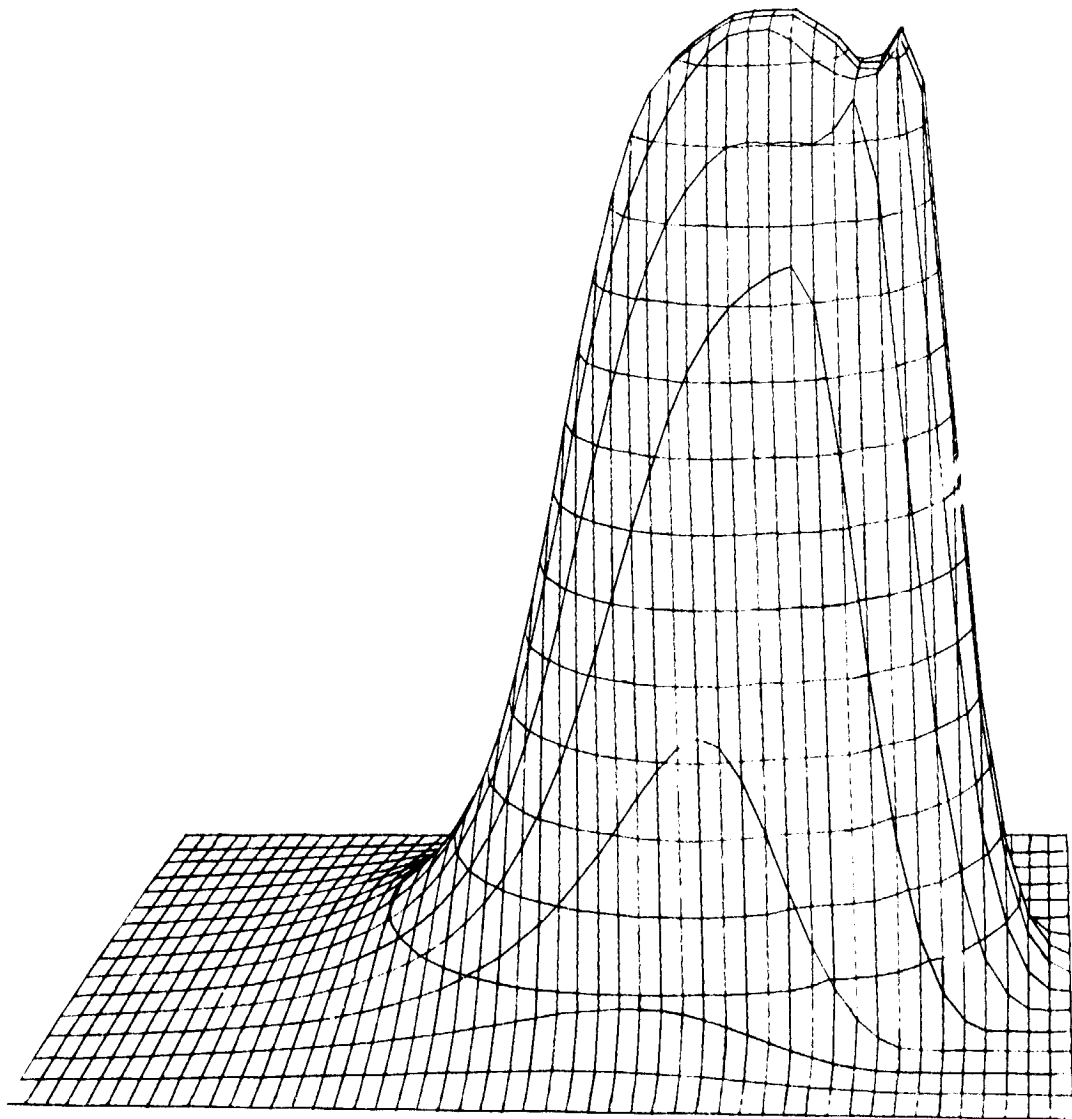
Dimensionless
film thickness,
 $H = h/R_x$

A	11.7×10^{-6}
B	12.0
C	12.4
D	13.0
E	14.0
F	16.0
G	19.0
H	24.0



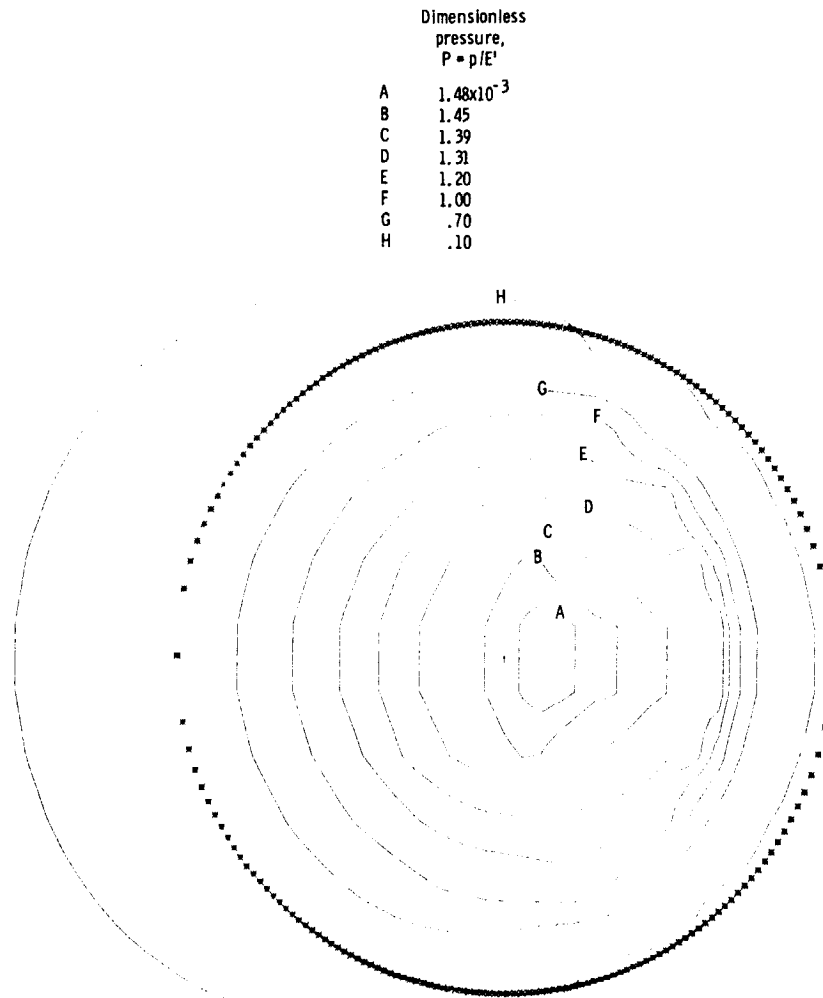
(b) Contour plot of dimensionless film thickness.

Figure 5.22. - Continued.



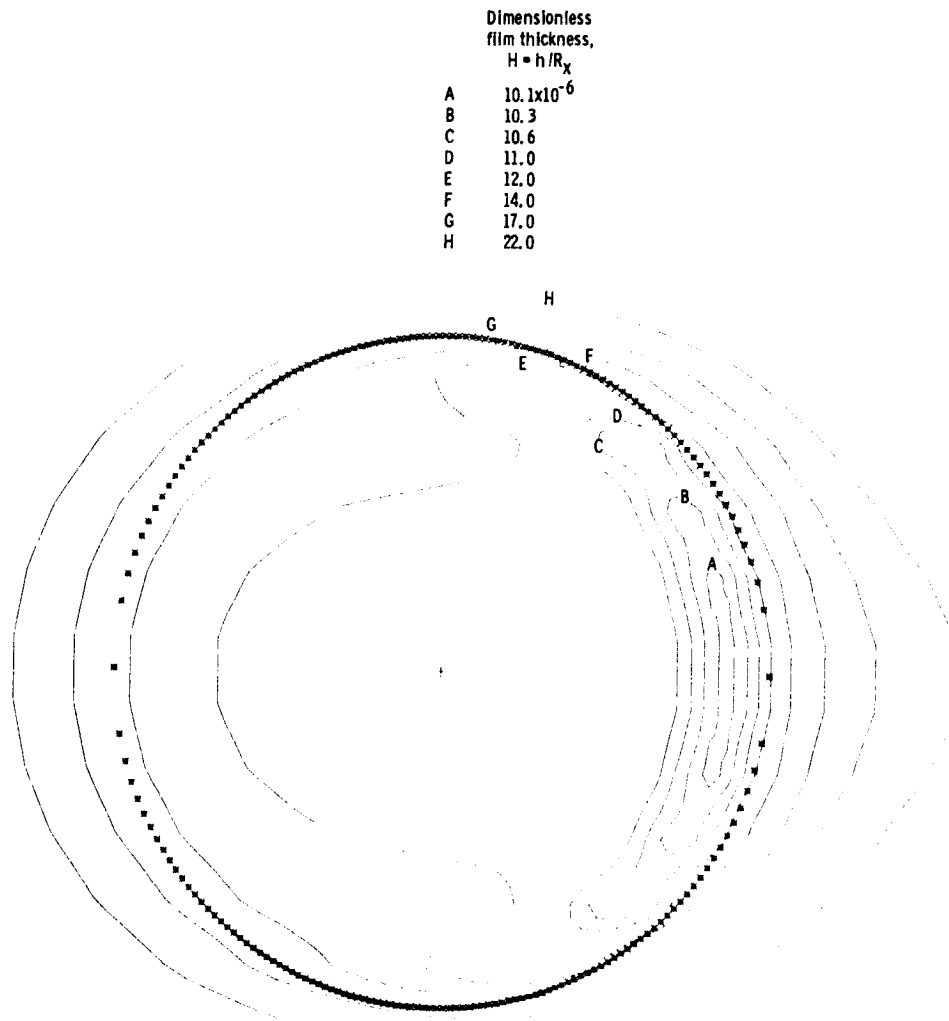
(c) Three-dimensional representation of pressure.

Figure 5 22. - Concluded.



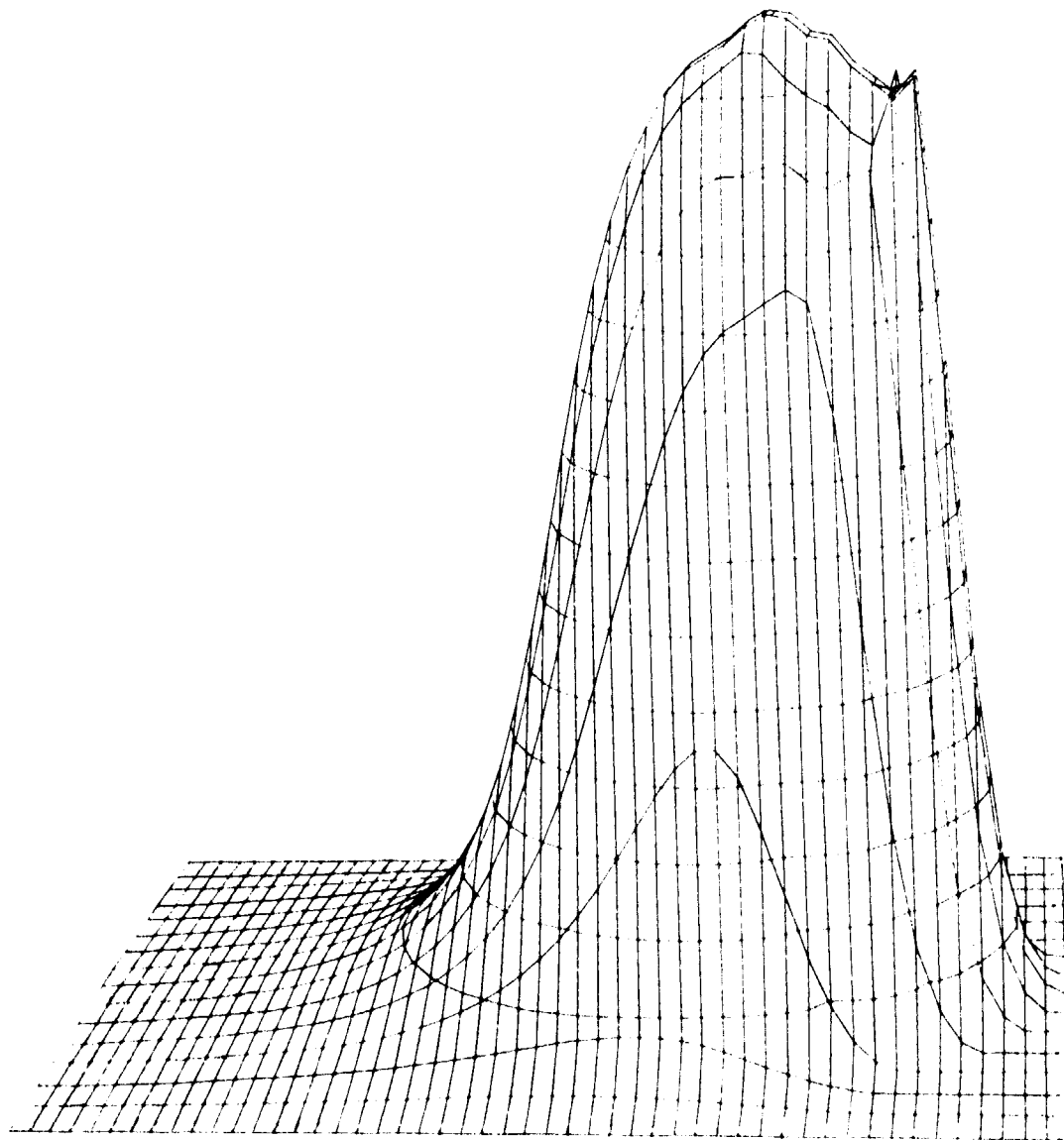
(a) Contour plot of dimensionless pressure.

Figure 5.23. - Contour plots of dimensionless pressure and film thickness and three-dimensional representation of pressure for dimensionless speed parameter (U) of 3.367×10^{-12} . The dimensionless constants k , W , and G are held constant as defined in equation (5.18).



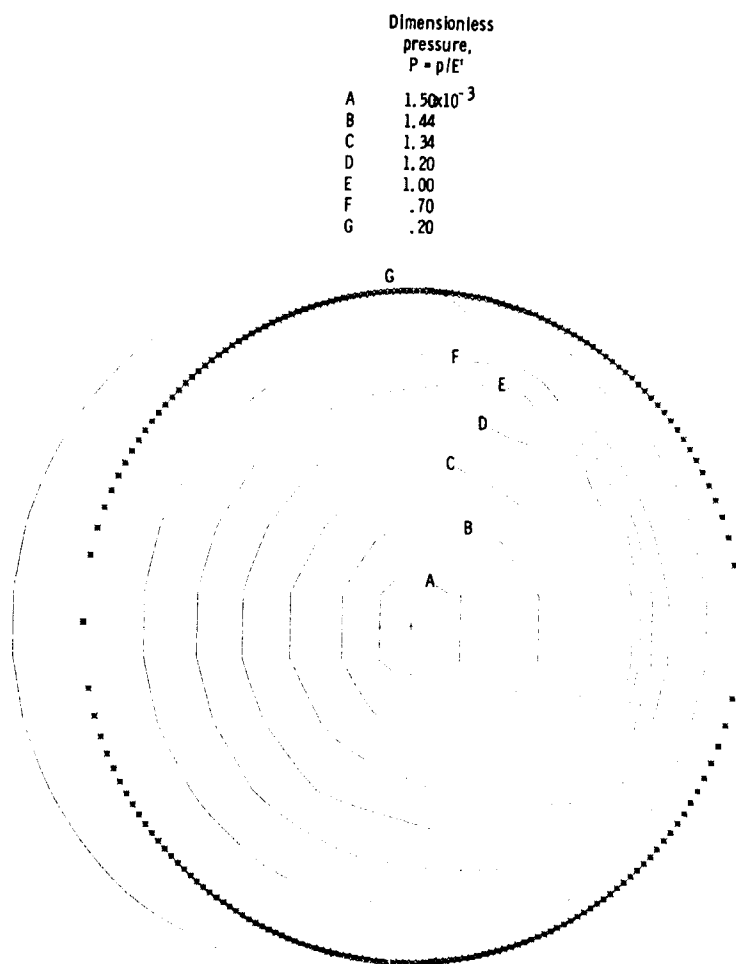
(b) Contour plot of dimensionless film thickness.

Figure 5.23. - Continued.



(c) Three-dimensional representation of pressure.

Figure 5.23. - Concluded.

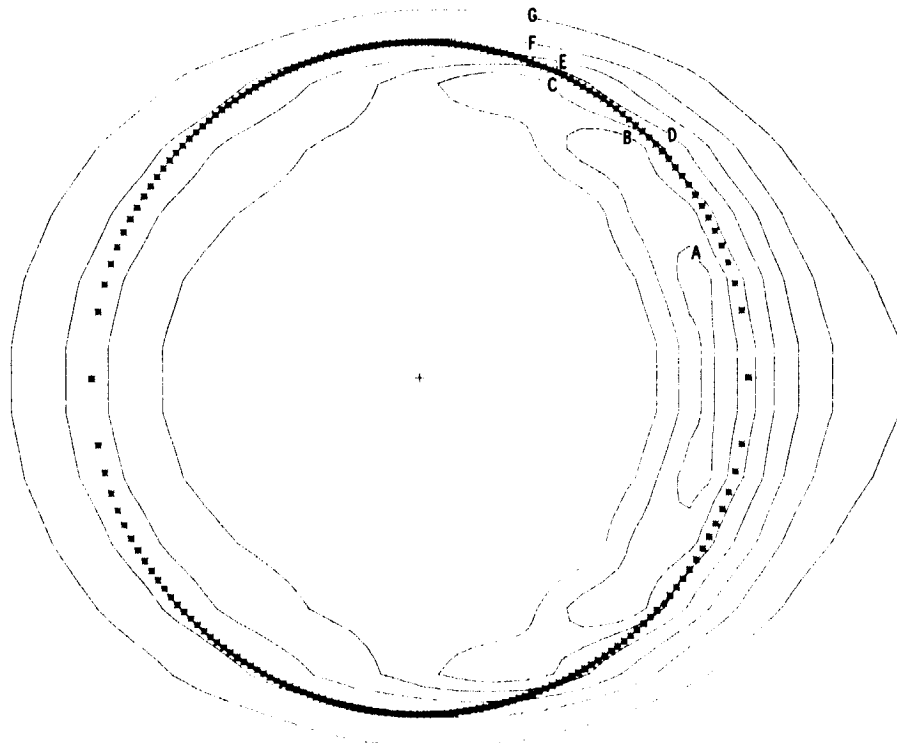


(a) Contour plot of dimensionless pressure.

Figure 5.24. - Contour plots of dimensionless pressure and film thickness and three-dimensional representation of pressure for dimensionless speed (U) of 2.525×10^{-12} . The dimensionless parameters k , W , and G are held constant as defined in equation (5.18).

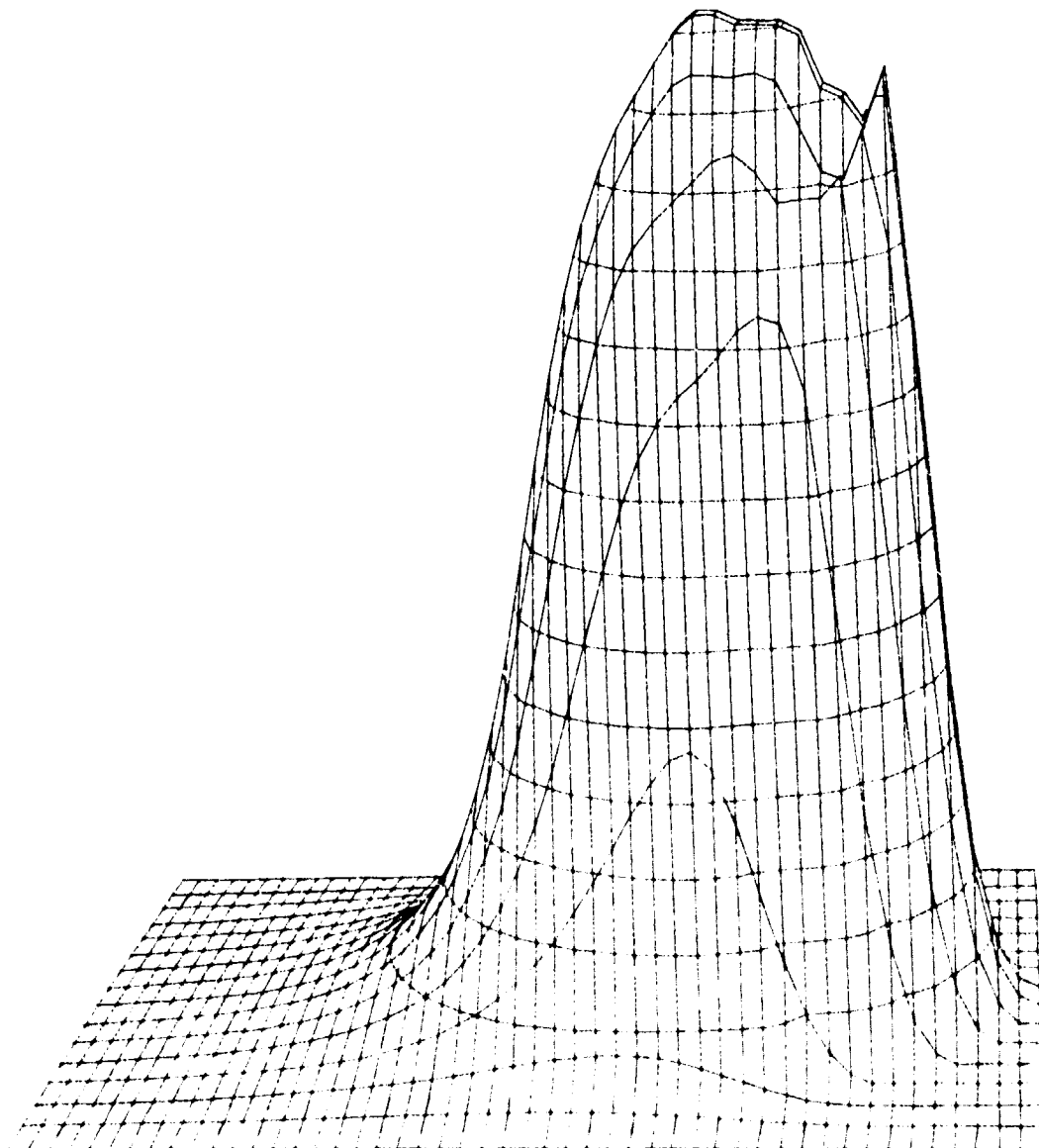
Dimensionless
film thickness,
 $H = h/R_x$

A	8.6×10^{-6}
B	9.0
C	9.6
D	10.6
E	12.0
F	14.0
G	18.0



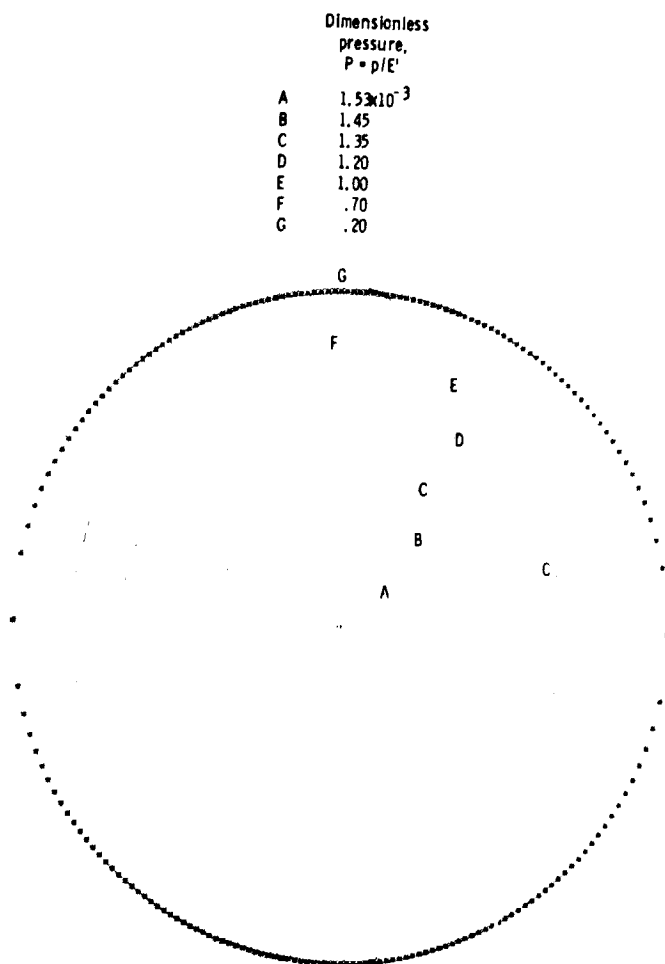
(b) Contour plot of dimensionless film thickness.

Figure 5. 24. - Continued.



(c) Three-dimensional representation of pressure.

Figure 5.24. Concluded.

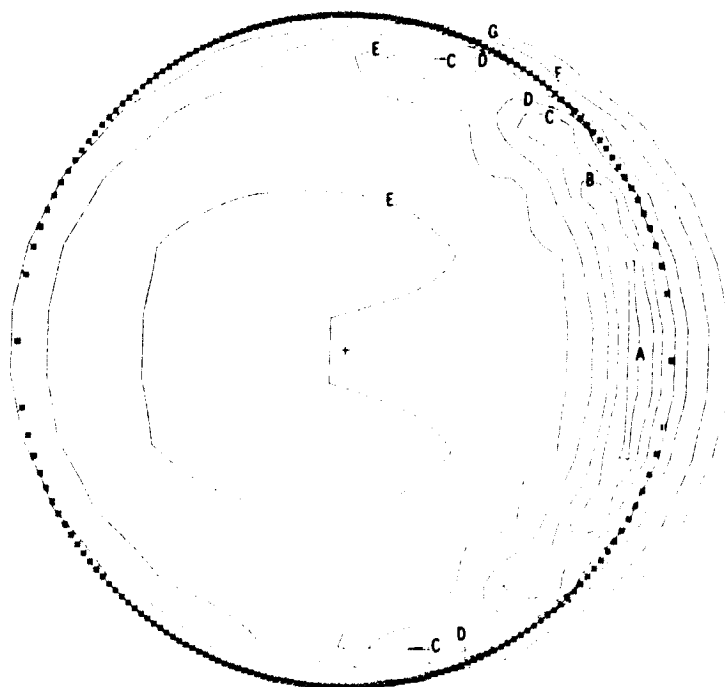


(a) Contour plot of dimensionless pressure.

Figure 5.25. - Contour plots of dimensionless pressure and film thickness and three-dimensional representation of pressure for dimensionless speed parameter (U) of 1.683×10^{-12} . The dimensionless parameters k , W , and G are held constant as defined in equation (5.18).

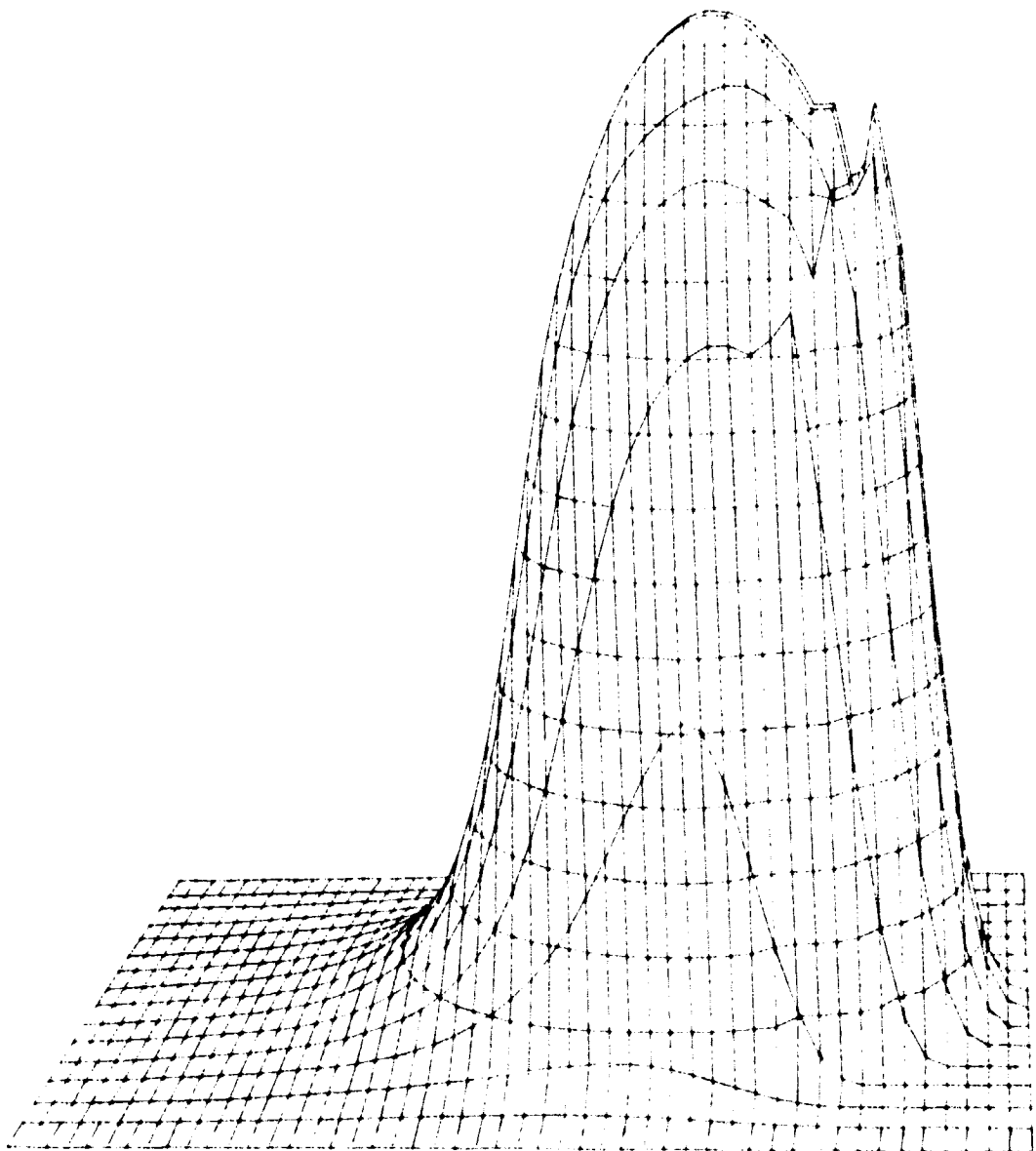
Dimensionless
film thickness,
 $H = h/R_x$

A	6.25×10^{-6}
B	6.40
C	6.60
D	7.00
E	7.50
F	8.70
G	10.00



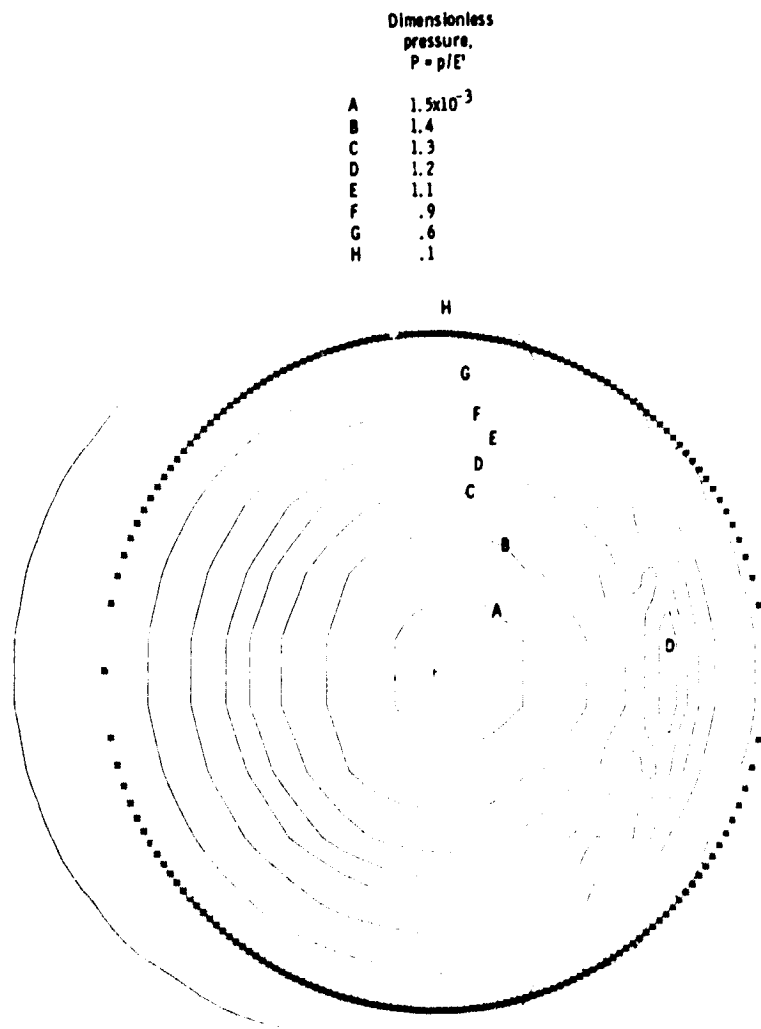
(b) Contour plot of dimensionless film thickness.

Figure 5.25. - Continued.



(c) Three dimensional representation of pressure.

Figure 5.25. - Concluded.

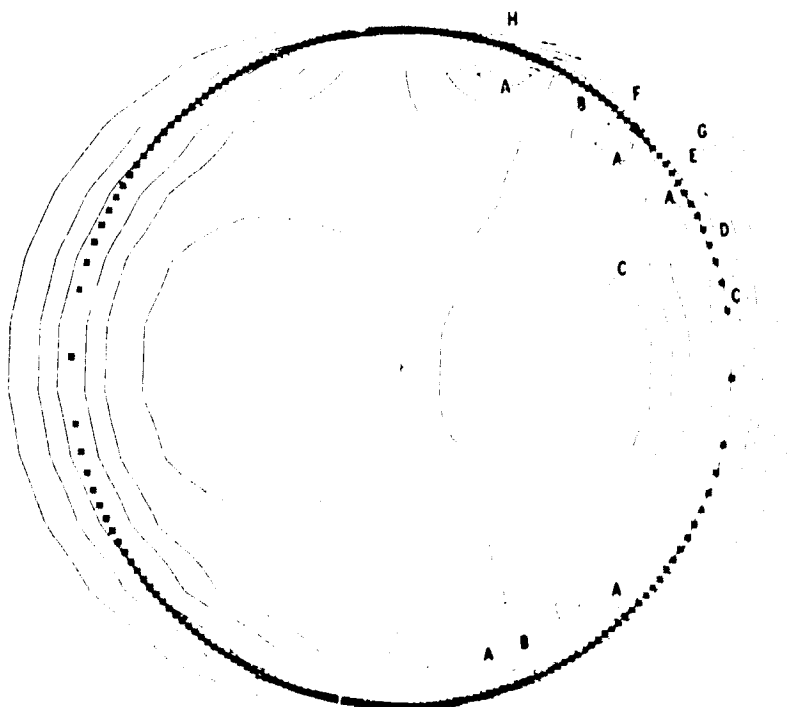


(a) Contour plot of dimensionless pressure.

Figure 5.26. - Contour plots of dimensionless pressure and film thickness and three-dimensional representation of pressure for dimensionless speed parameter (U) of 8.41×10^{-13} . The dimensionless parameters k , W , and G are held constant as defined in equation (5.18).

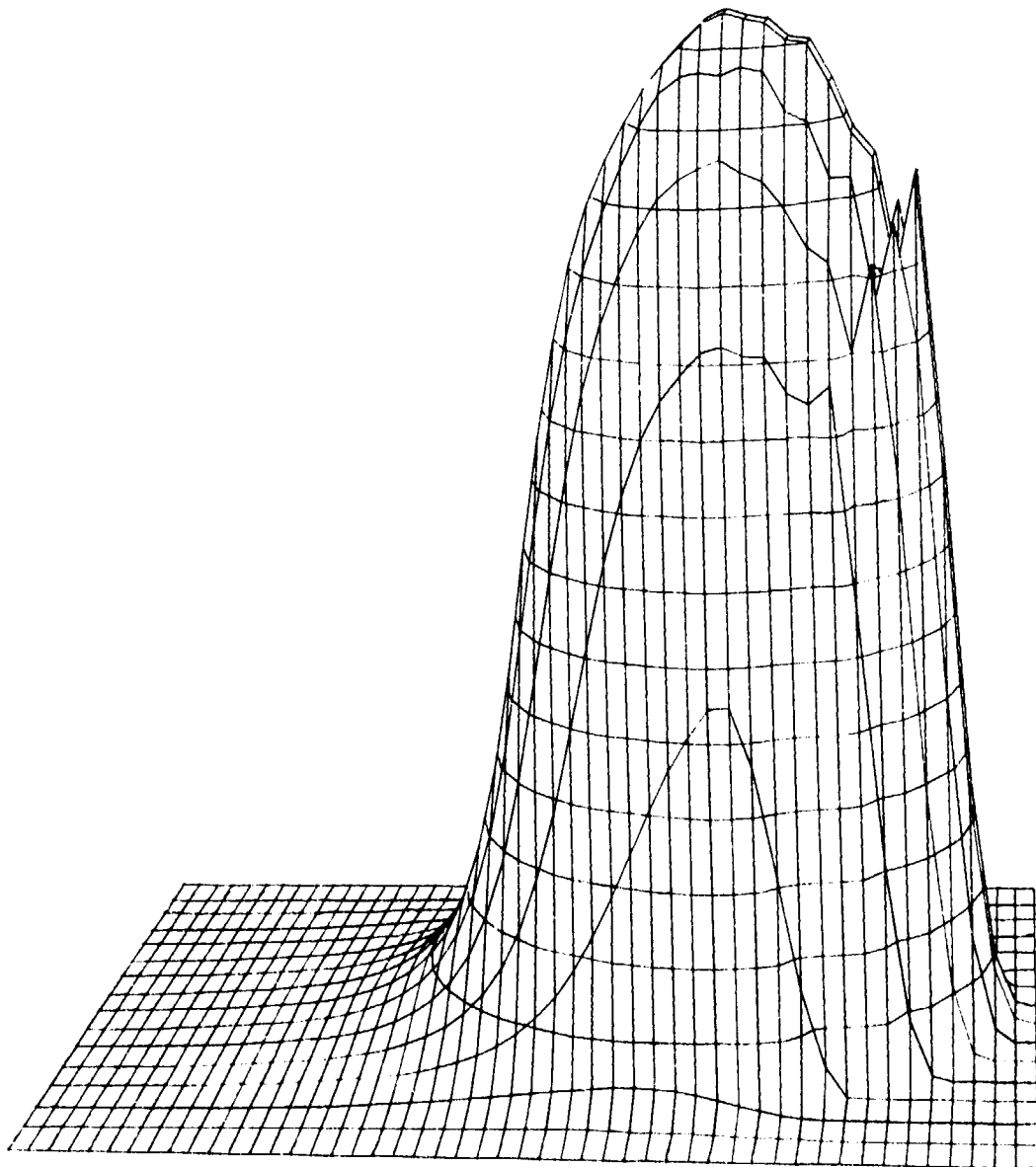
Dimensionless
film thickness,
 $H = h/R_x$

A	4.25×10^{-6}
B	4.60
C	5.00
D	5.90
E	6.00
F	7.00
G	8.00
H	10.00



(b) Contour plot of dimensionless film thickness.

Figure 5.26. - Continued.



(c) Three-dimensional representation of pressure.

Figure 5.26. - Concluded.

REPRODUCIBILITY OF THE
ORIGINAL PAGE IS POOR

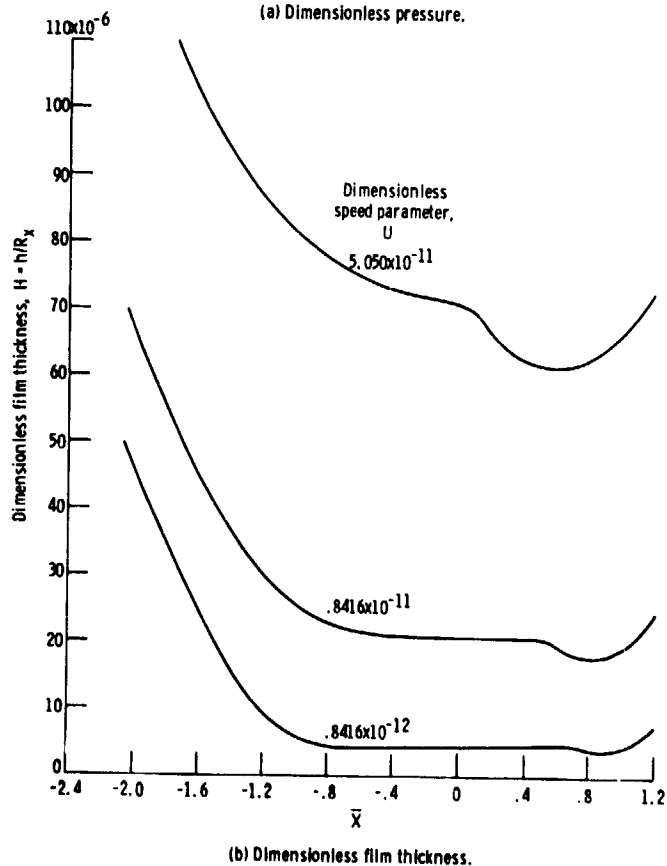
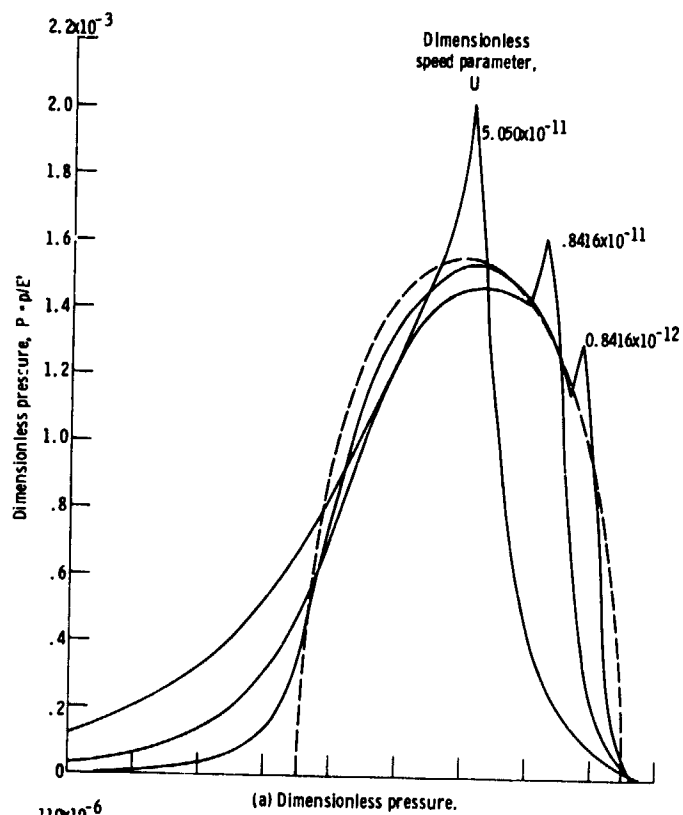
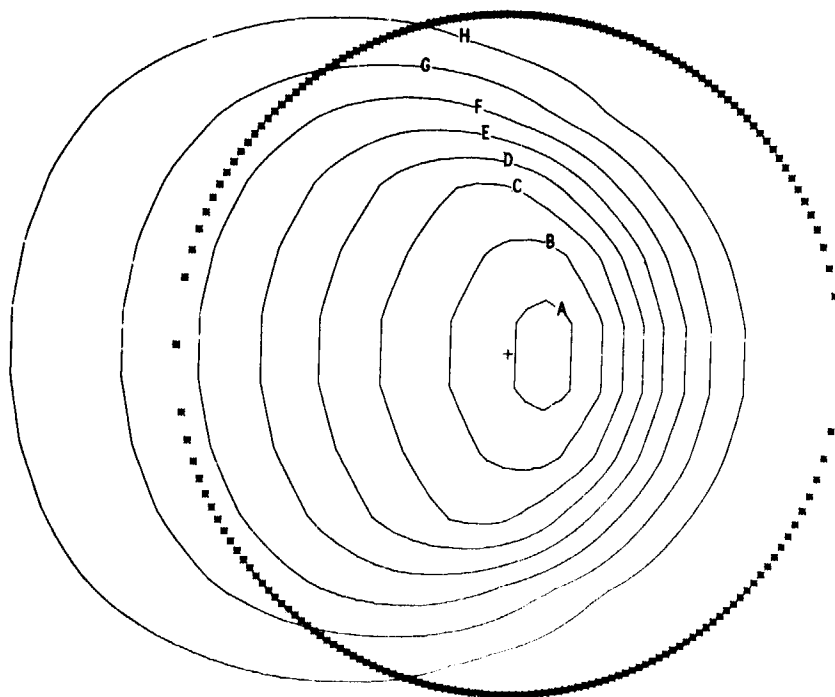


Figure 5.27. - Variation of dimensionless pressure and film thickness on \bar{X} -axis for three values of dimensionless speed parameter. The value of \bar{Y} is held fixed near axial center of contact.

	Dimensionless pressure, $P = p/E'$
A	0.83×10^{-3}
B	.75
C	.65
D	.55
E	.45
F	.35
G	.25
H	.15

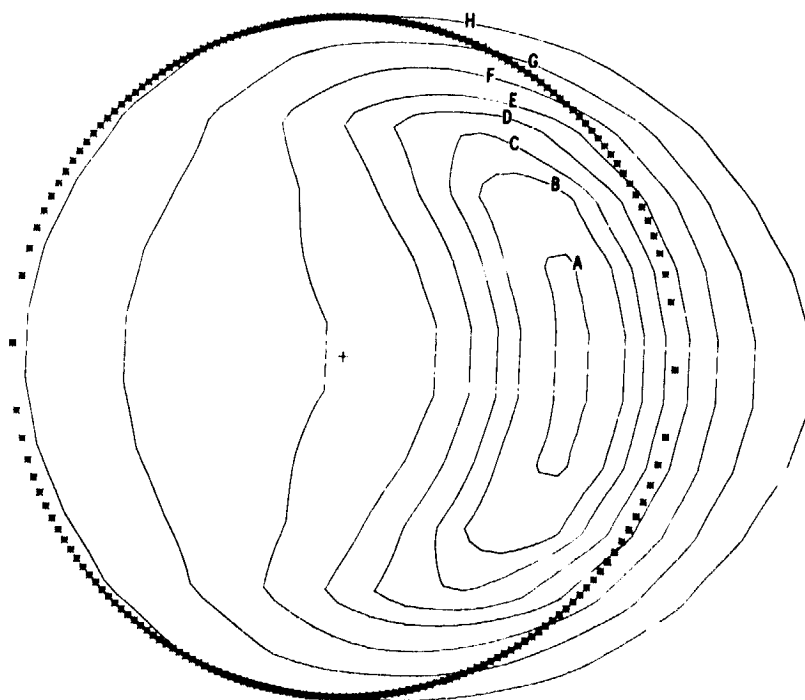


(a) Contour plot of dimensionless pressure.

Figure 5.28. - Contour plots of dimensionless pressure and film thickness and three-dimensional representation of pressure for dimensionless load parameter (W) of 0.1106×10^{-6} . The dimensionless parameters k , U , and G are held constant as defined in equation (5.23).

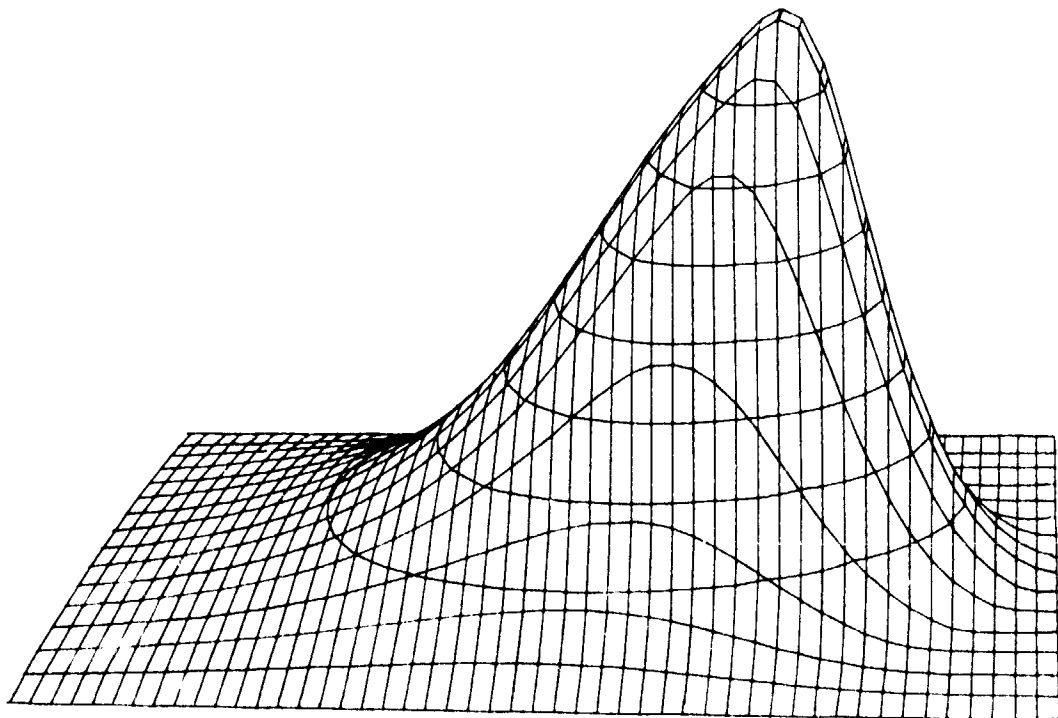
Dimensionless
film thickness,
 $H = h/R_x$

A	7.0×10^{-6}
B	7.2
C	7.4
D	7.7
E	8.1
F	8.7
G	9.5
H	10.7



(b) Contour plot of dimensionless film thickness.

Figure 5.28. - Continued.



(c) Three-dimensional representation of pressure.

Figure 5.28. - Concluded.

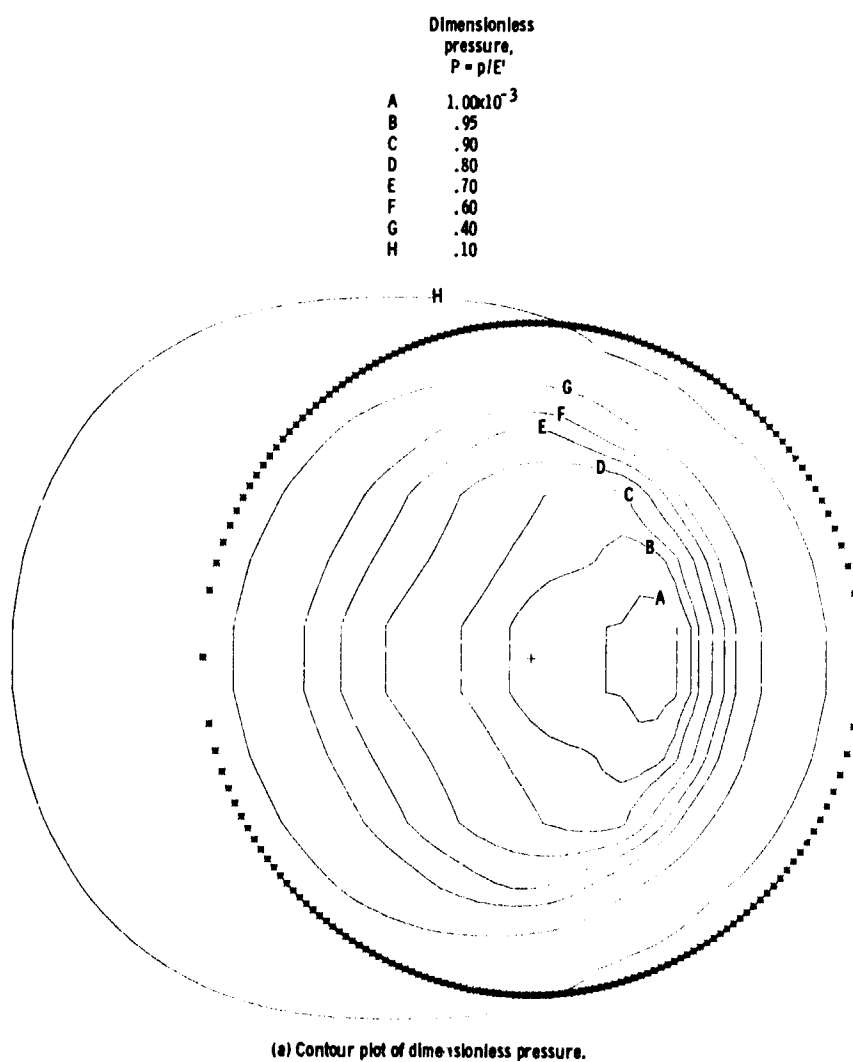
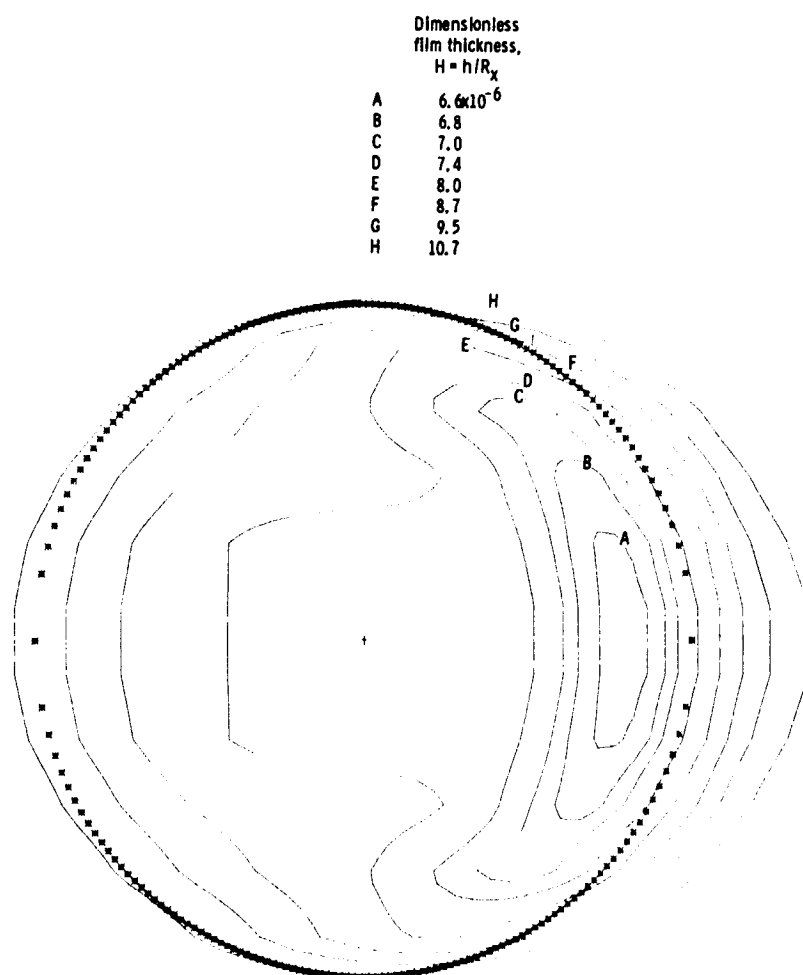
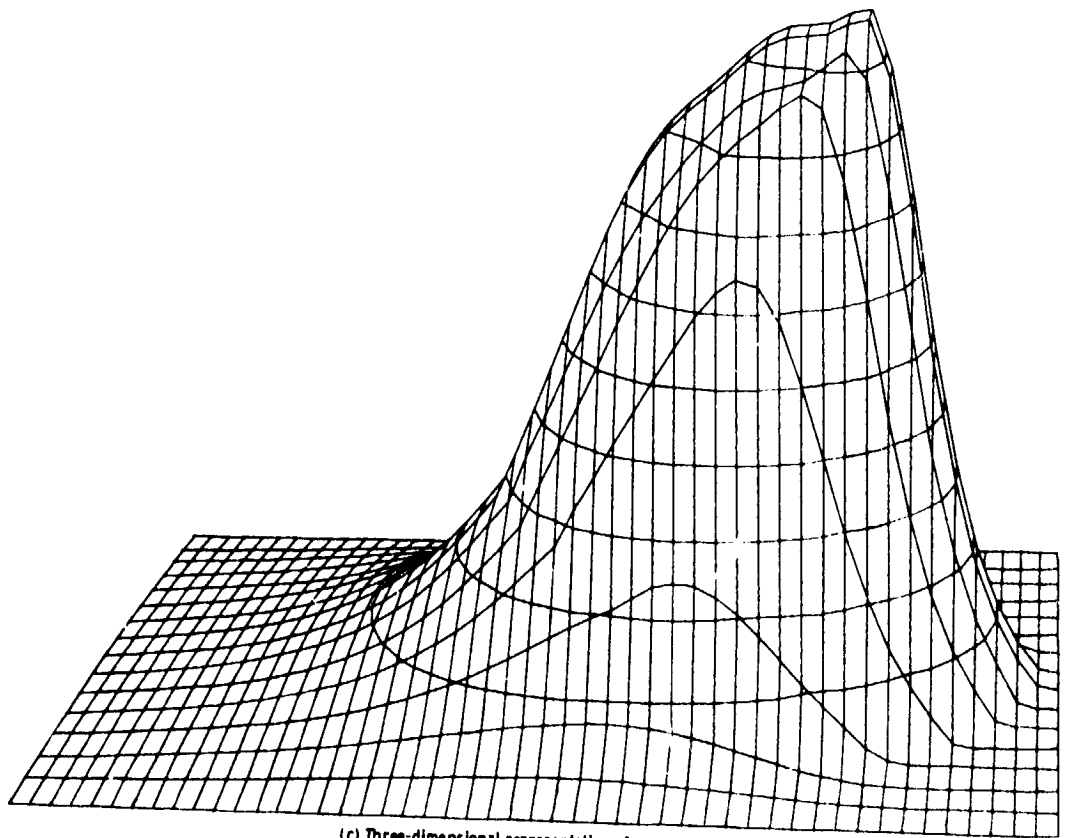


Figure 5.29. - Contour plots of dimensionless pressure and film thickness and three-dimensional representation of pressure for dimensionless load parameter (W) of 0.2211×10^{-6} . The dimensionless parameters k , U , and G are held constant as defined in equation (5.23).



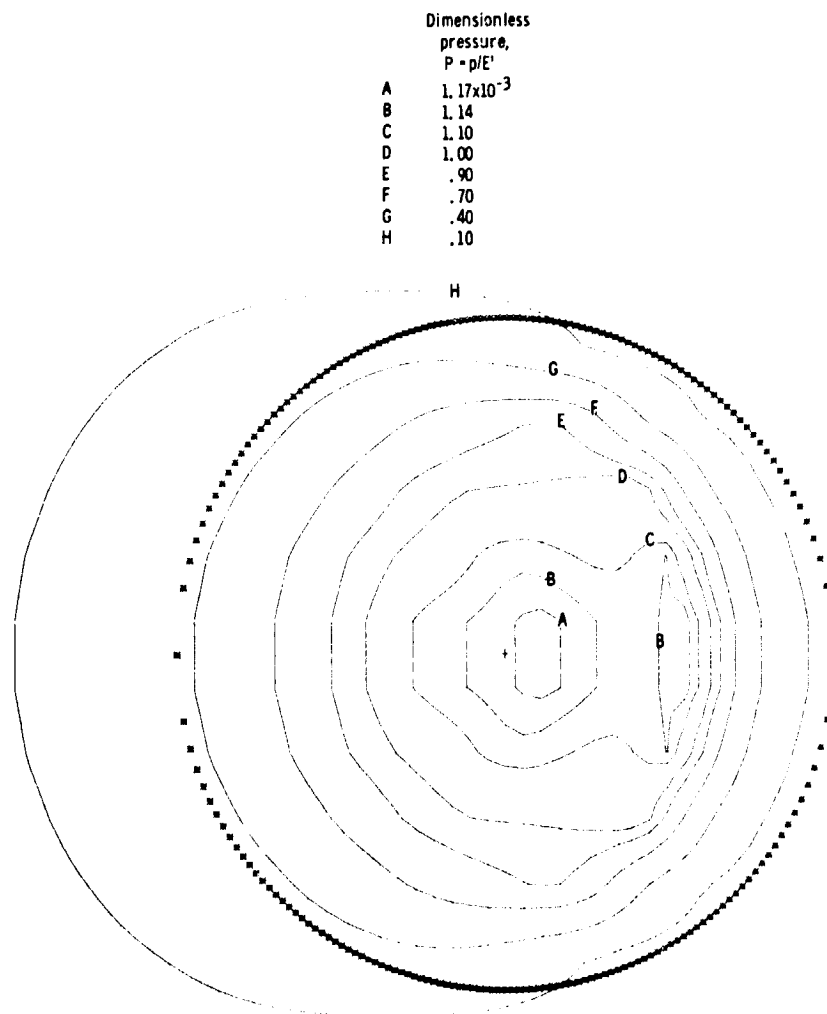
(b) Contour plot of dimensionless film thickness.

Figure 5.29. - Continued.



(c) Three-dimensional representation of pressure.

Figure 5. 29. - Concluded.

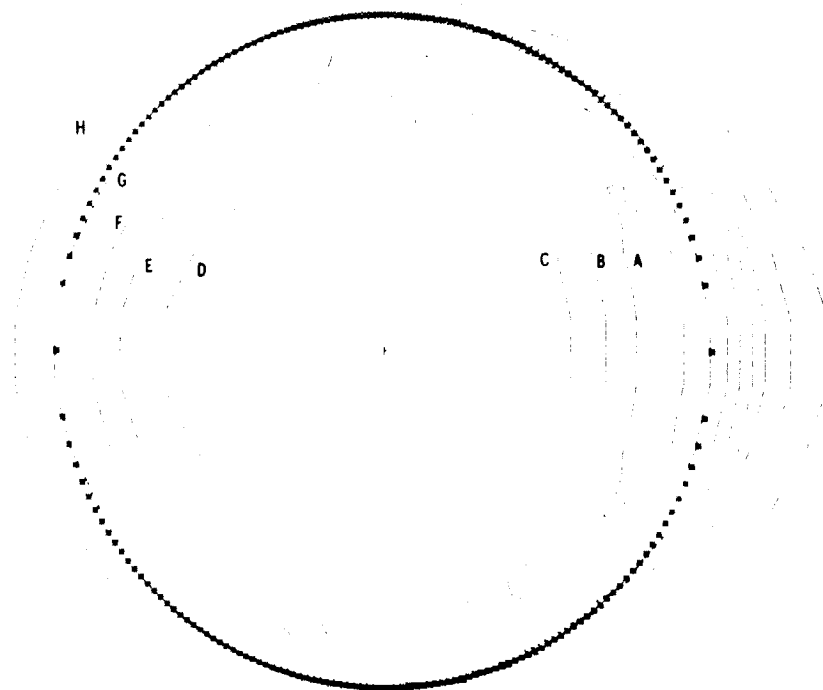


(a) Contour plot of dimensionless pressure.

Figure 5. 30. - Contour plots of dimensionless pressure and film thickness and three-dimensional representation of pressure for dimensionless load parameter (W) of 0.3684×10^{-6} . The dimensionless parameters k , U , and G are held constant as defined in equation (5. 23).

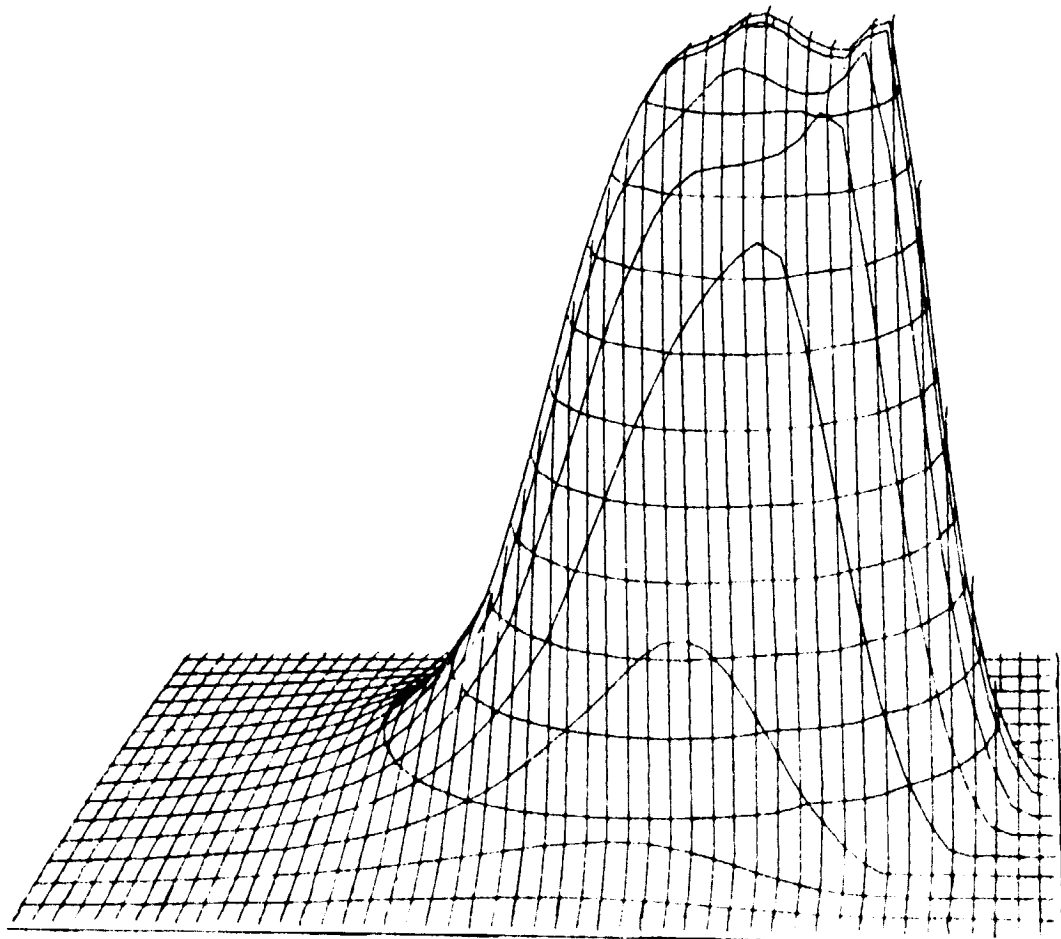
Dimensionless
film thickness,
 $H = h/R_x$

A	6.5×10^{-6}
B	7.0
C	7.5
D	8.0
E	8.5
F	9.0
G	10.0
H	11.5



(b) Contour plot of dimensionless film thickness.

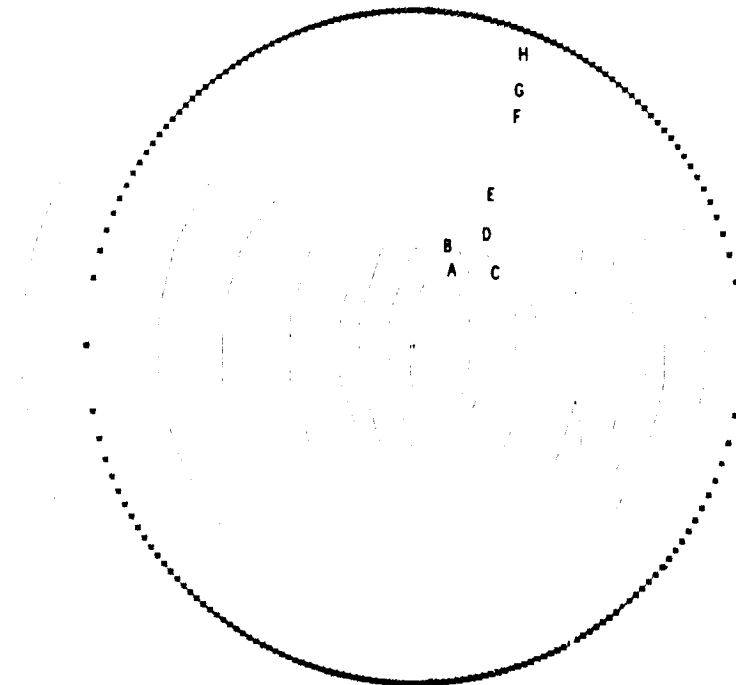
Figure 5.30. - Continued.



(c) Three-dimensional representation of pressure.

Figure 30. - Concluded.

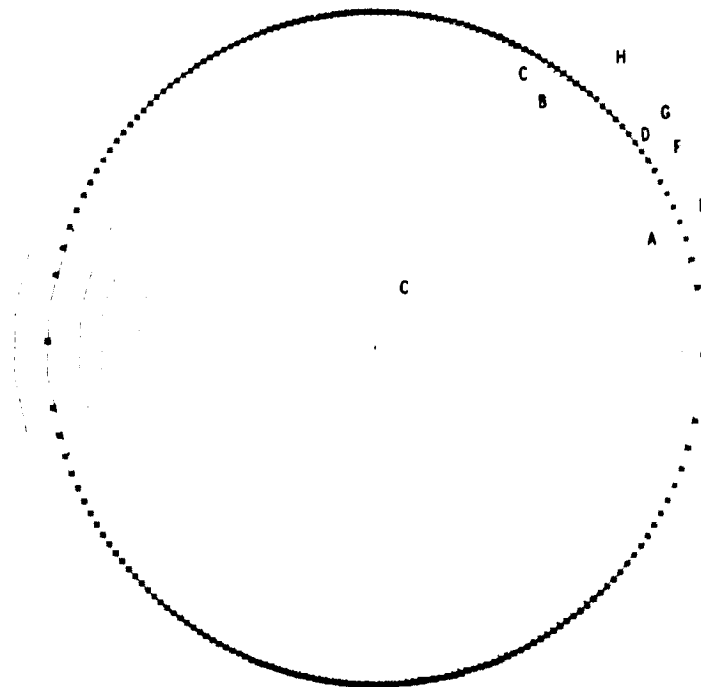
	Dimensionless pressure, $P = p/E'$
A	1.33×10^{-3}
B	1.32
C	1.30
D	1.28
E	1.20
F	1.00
G	.70
H	.20



(a) Contour plot of dimensionless pressure.

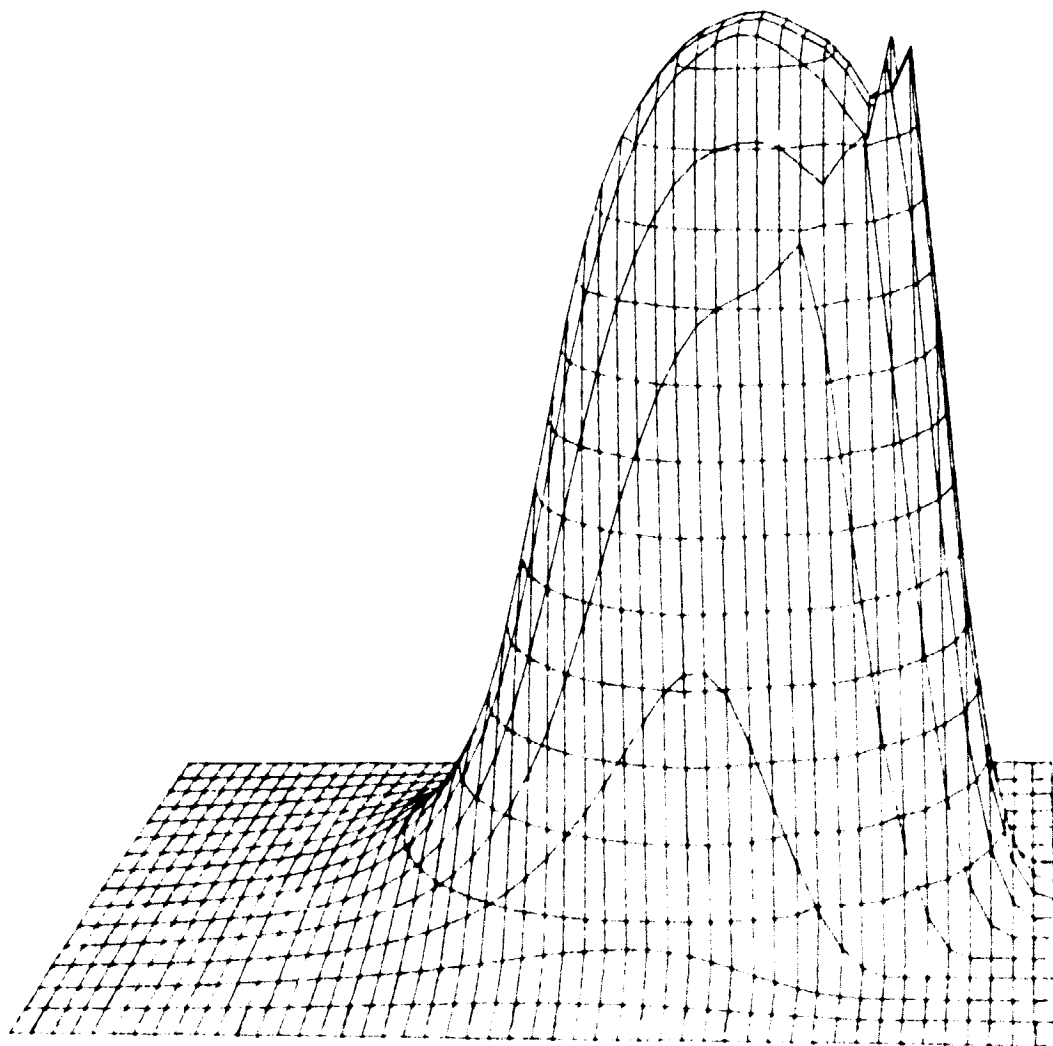
Figure 5.31. - Contour plots of dimensionless pressure and film thickness and three-dimensional representation of pressure for dimensionless load parameter (W) of 0.5528×10^{-6} . The dimensionless parameters k , U , and G are held constant as defined in equation (5.23).

Dimensionless film thickness, $H = h/R_x$	
A	6.5×10^{-6}
B	7.0
C	7.5
D	8.0
E	8.5
F	9.0
G	10.0
H	11.5



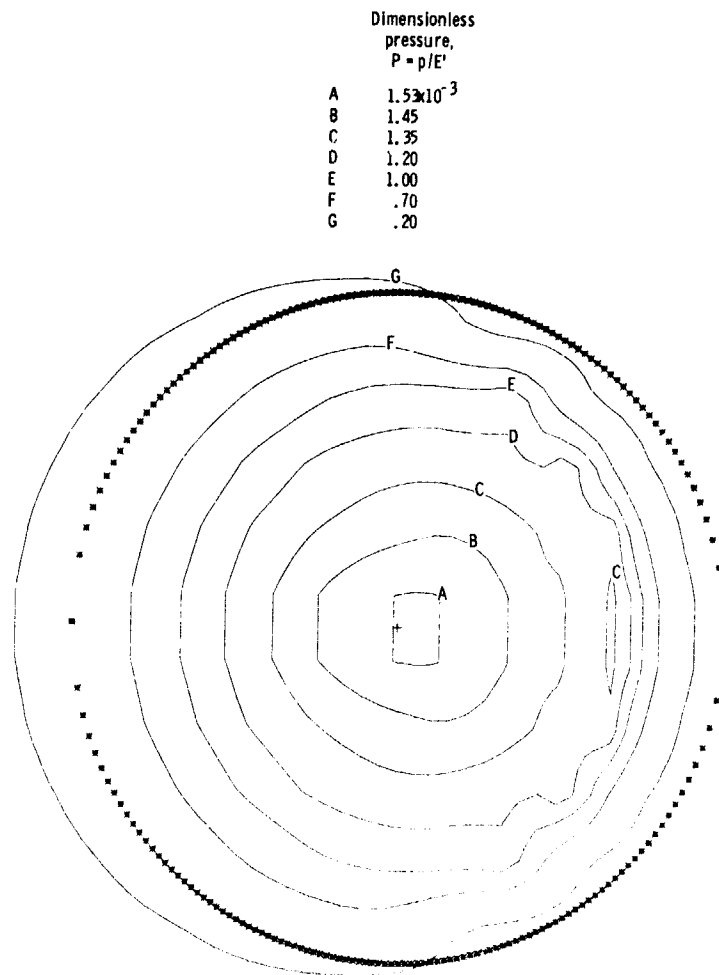
(b) Contour plot of dimensionless film thickness.

Figure 5. 31. - Continued.



(c) Three dimensional representation of pressure.

Figure 5.31. Concluded.

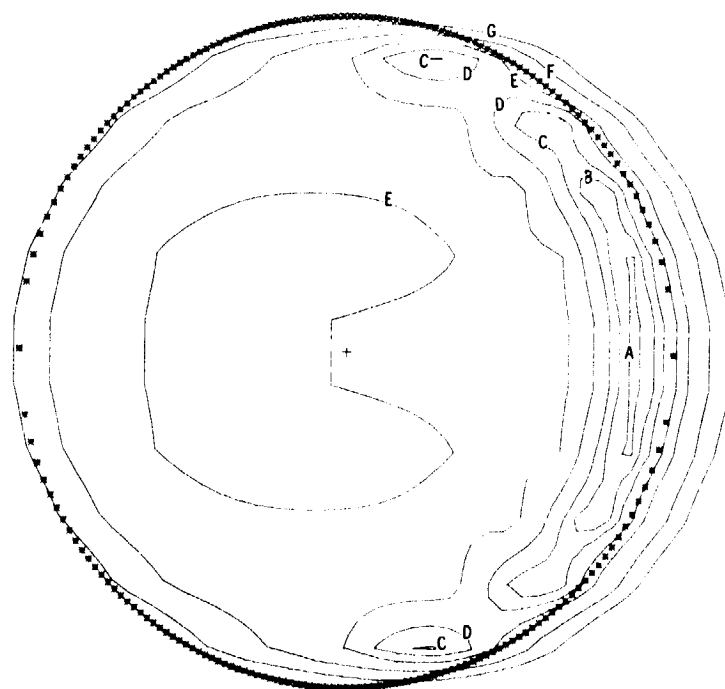


(a) Contour plot of dimensionless pressure.

Figure 5.32. Contour plots of dimensionless pressure and film thickness and three-dimensional representation of pressure for dimensionless load parameter (W) of 0.7371×10^{-6} . The dimensionless parameters k , U , and G are held constant as defined by equation (5.23).

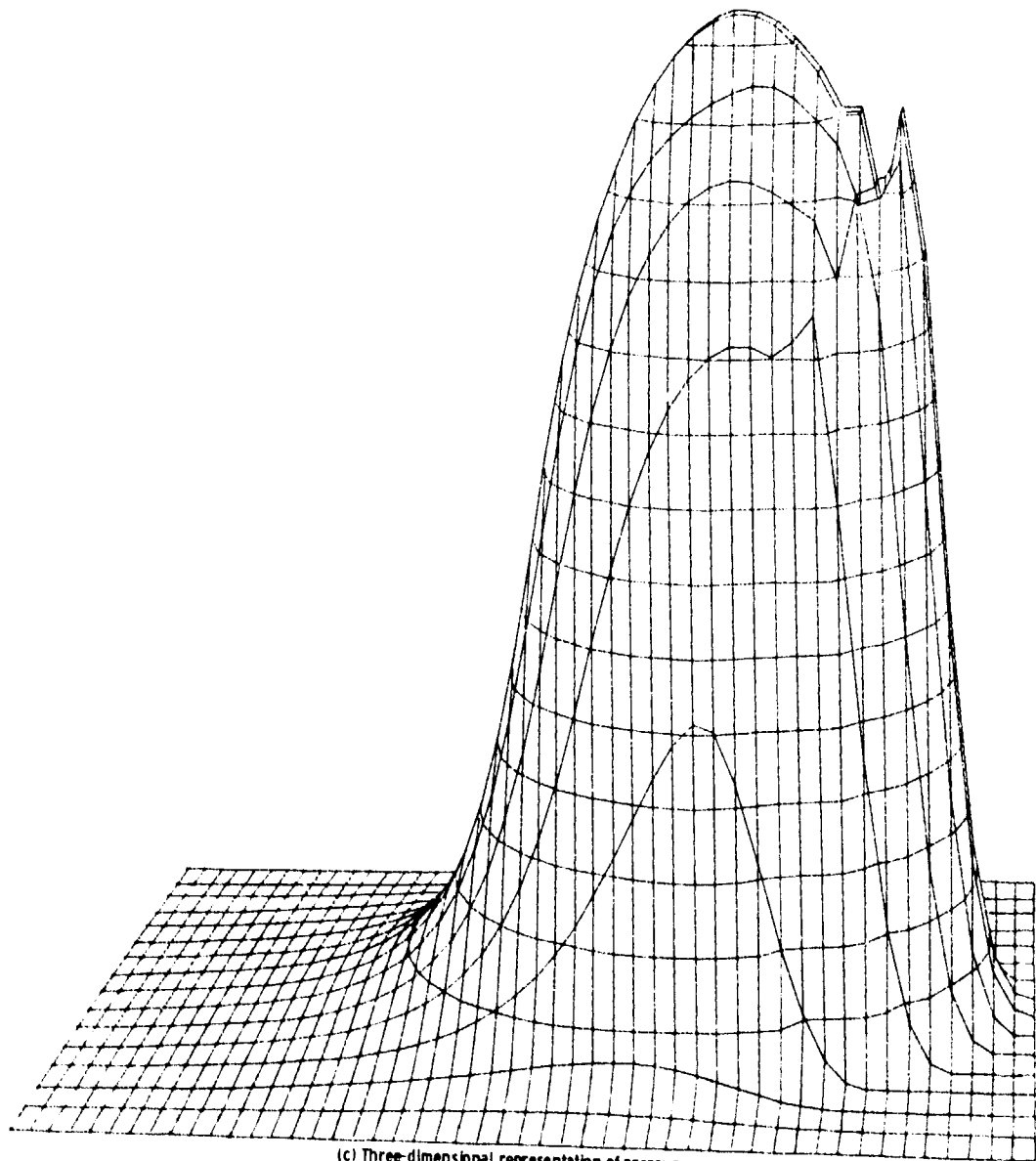
Dimensionless
film thickness,
 $H = h/R_x$

A	6.25×10^{-6}
B	6.40
C	6.60
D	7.00
E	7.50
F	8.70
G	10.00



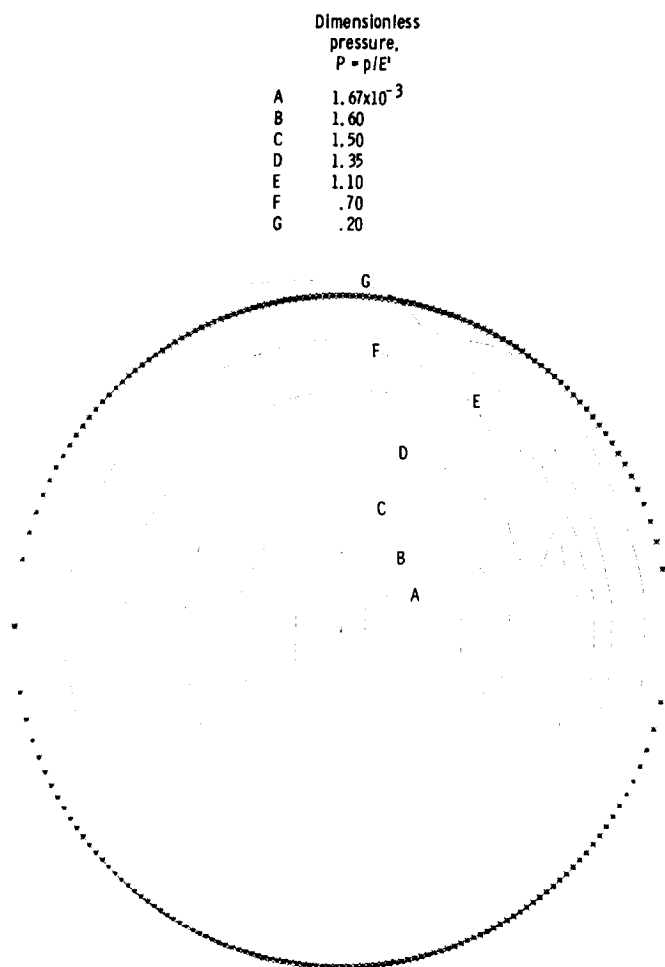
(b) Contour plot of dimensionless film thickness.

Figure 5.32. - Continued.



(c) Three-dimensional representation of pressure.

Figure 5.32. - Concluded.

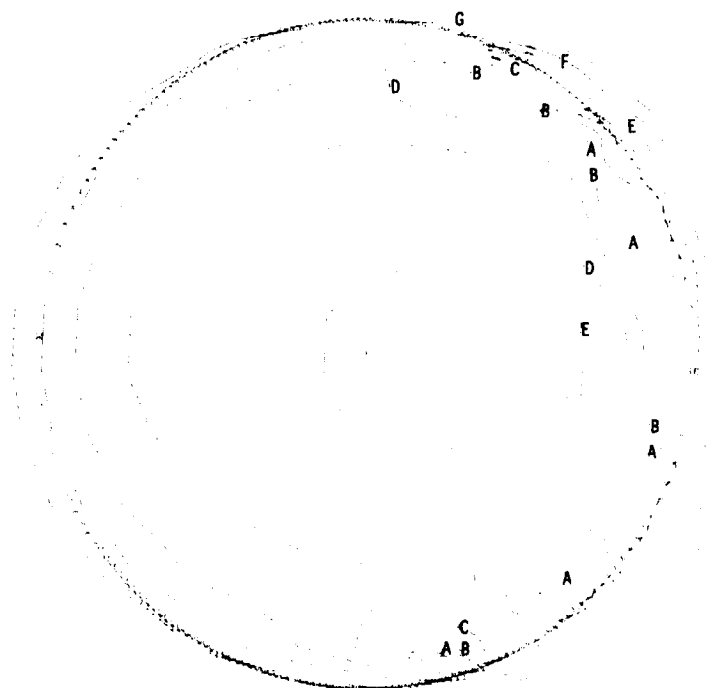


(a) Contour plot of dimensionless pressure.

Figure 5.33. - Contour plots of dimensionless pressure and film thickness and three-dimensional representation of pressure for dimensionless load parameter (W) of 0.9214×10^{-6} . The dimensionless parameters k , U , and G are held constant as defined in equation (5.23).

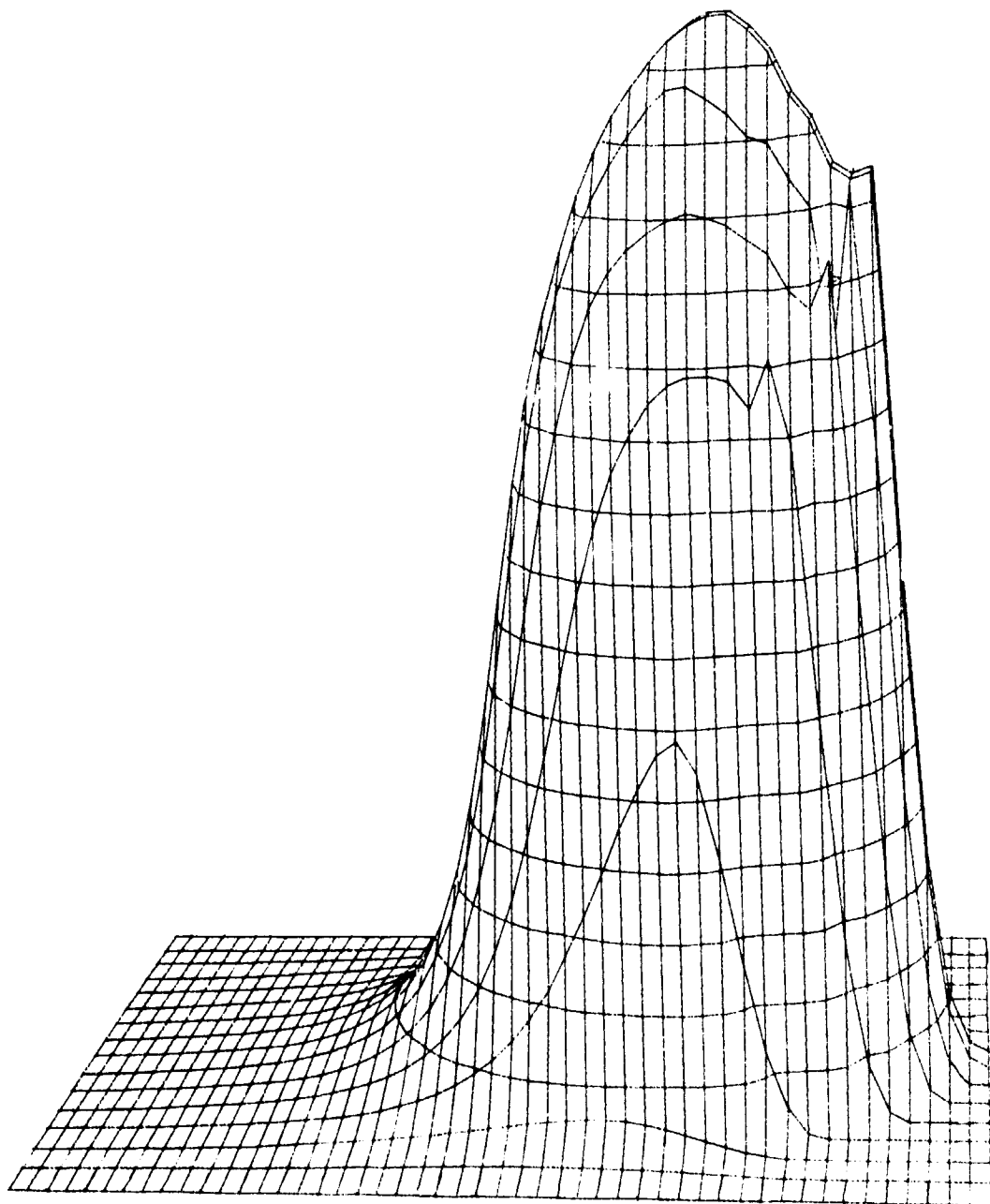
Dimensionless
film thickness,
 $H = h/R_x$

A	6.2×10^{-6}
B	6.5
C	6.9
D	7.4
E	8.2
F	9.4
G	10.0



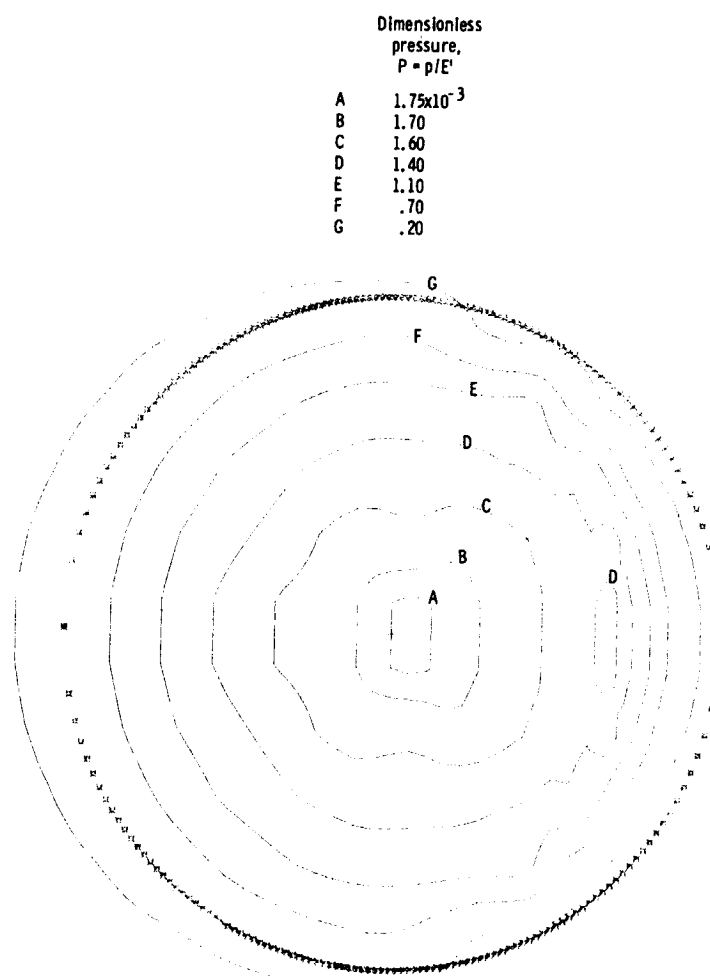
(b) Contour plot of dimensionless film thickness.

Figure 5.33. - Continued.



(c) Three-dimensional representation of pressure.

Figure 5. 33. - Concluded.

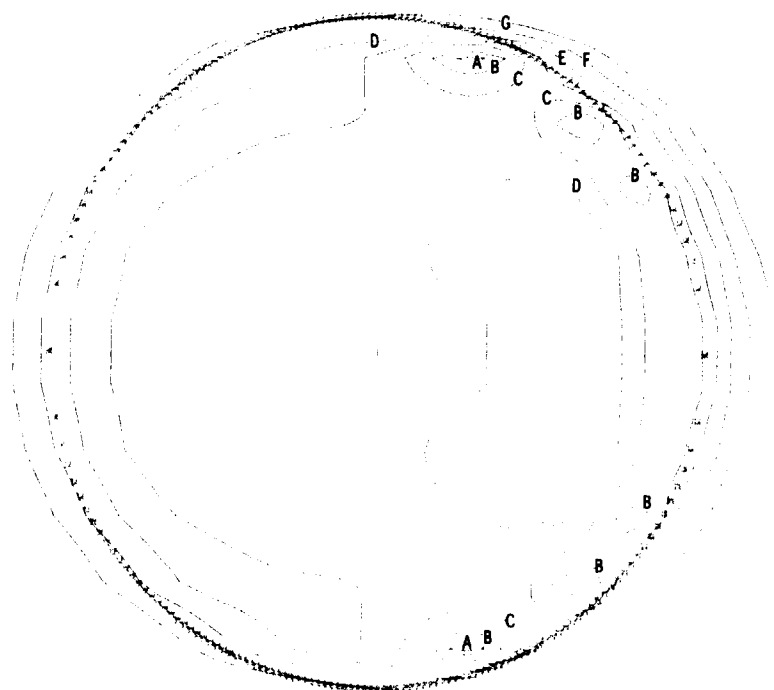


(a) Contour plot of dimensionless pressure.

Figure 5.34. - Contour plots of dimensionless pressure and film thickness and three-dimensional representation of pressure for dimensionless load parameter (W) of 1.106×10^{-6} . The dimensionless parameters k , U , and G are held constant as defined by equation (5.23).

Dimensionless
film thickness,
 $H = h/R_x$

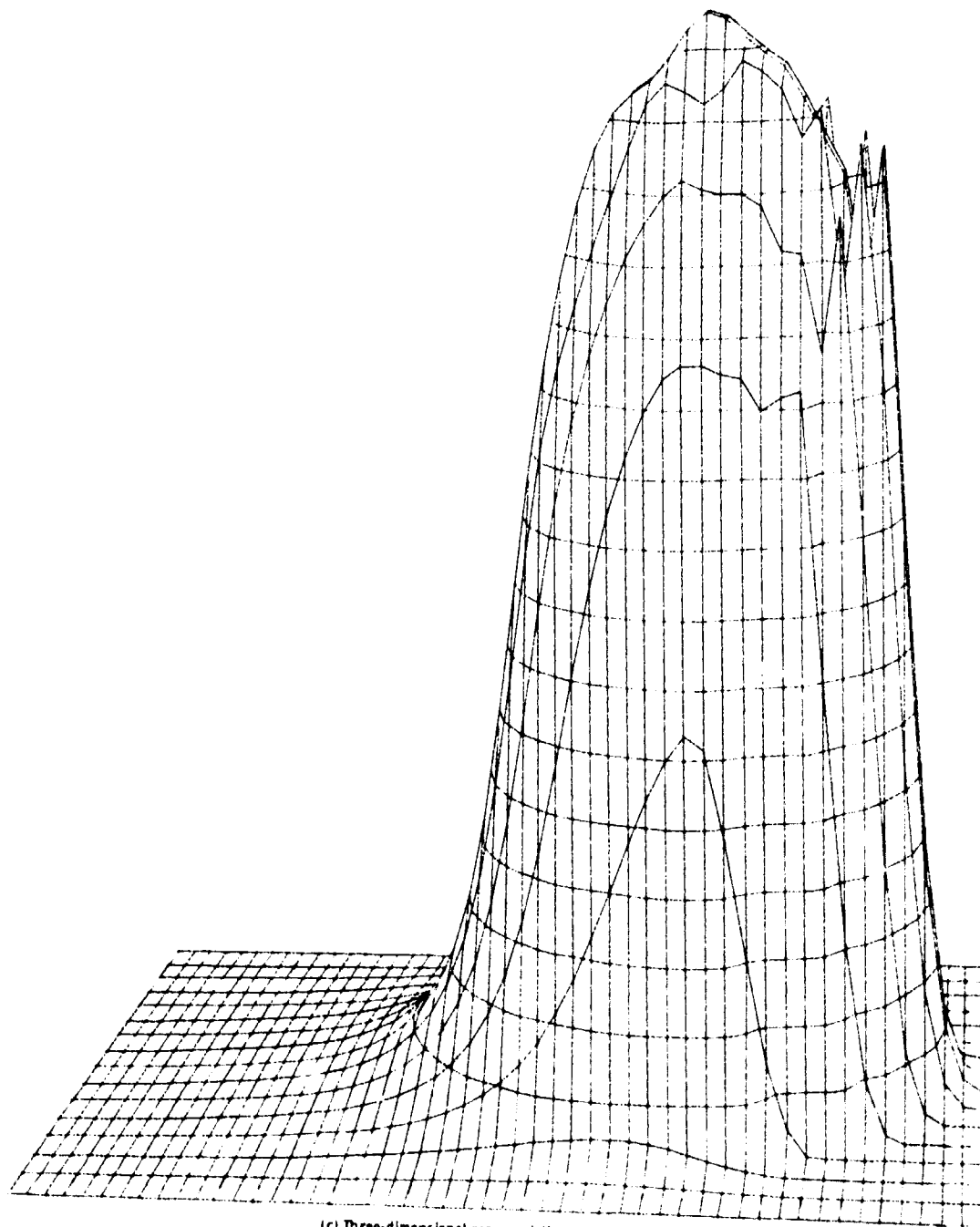
A	6.1×10^{-6}
B	6.4
C	7.0
D	7.7
E	8.7
F	10.0
G	12.0



(b) Contour plot of dimensionless film thickness.

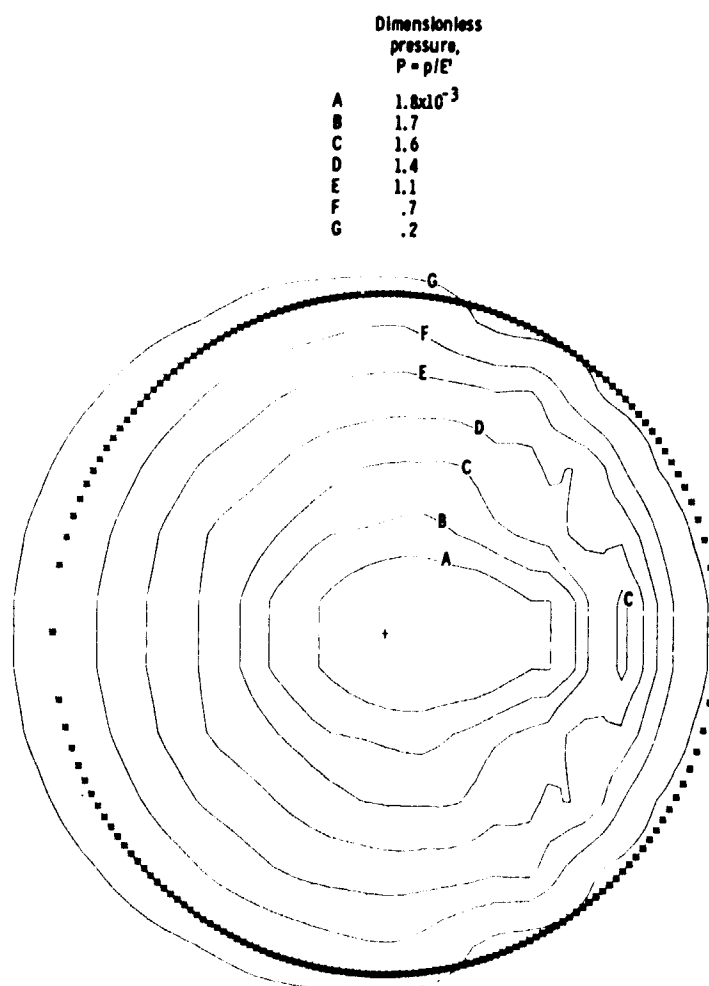
Figure 5.34. - Continued.

REPRODUCIBILITY OF THE
ORIGINAL PAGE IS POOR



(c) Three-dimensional representation of pressure.

Figure 5. 34. - Concluded.

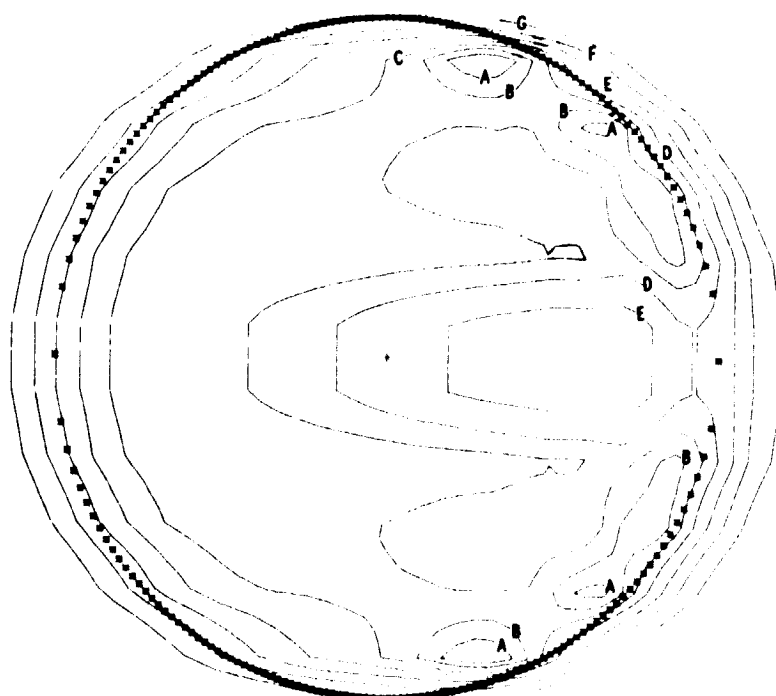


(a) Contour plot of dimensionless pressure.

Figure 5.35. - Contour plots of dimensionless pressure and film thickness and three-dimensional representation of pressure for dimensionless load parameter (W) of 1.29×10^{-6} . The dimensionless parameters k , l , and G are held constant as defined in equation (5.23).

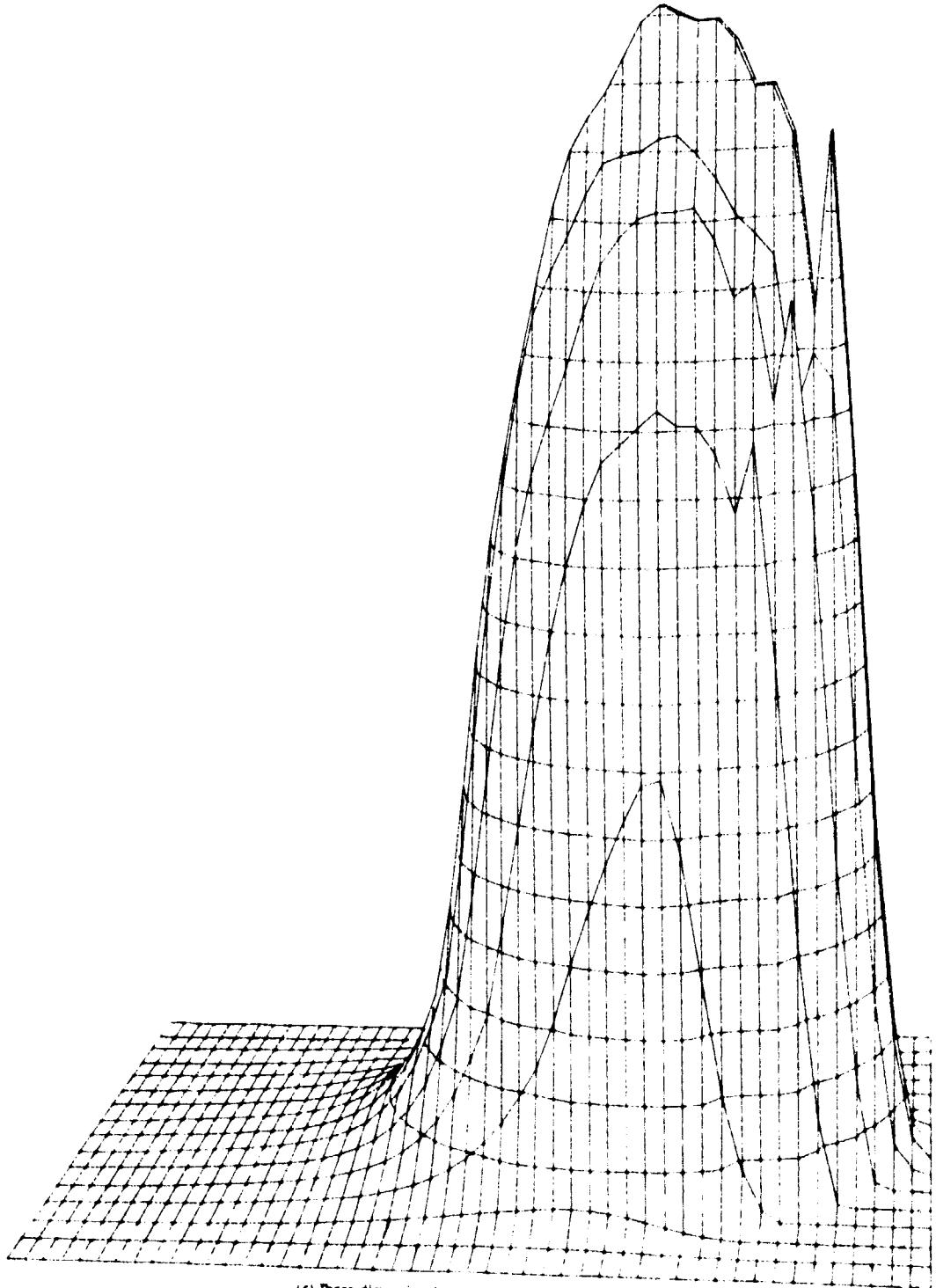
Dimensionless
film thickness,
 $H = h/R_x$

A	6.1×10^{-6}
B	6.5
C	7.0
D	7.7
E	8.7
F	10.0
G	12.0



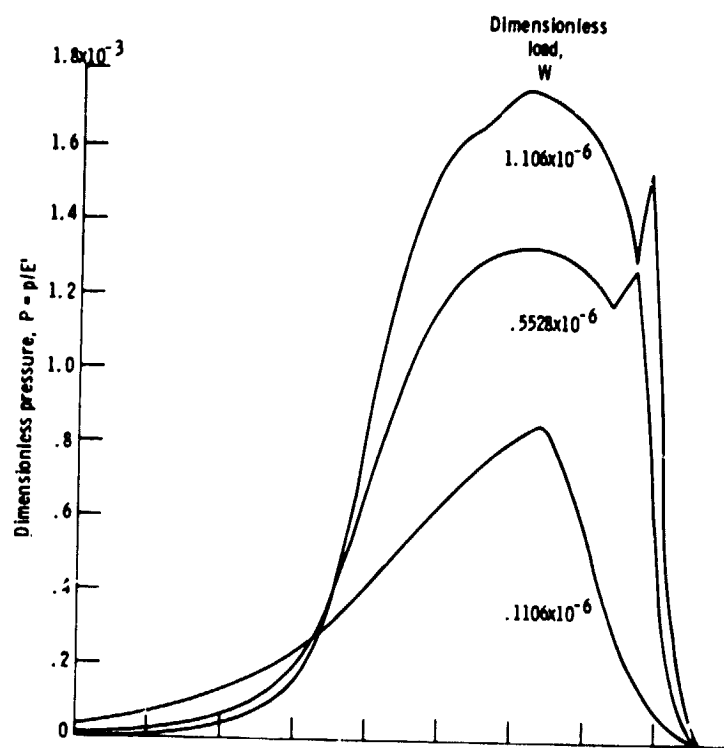
(b) Contour plot of dimensionless film thickness.

Figure 5.35. - Continued.

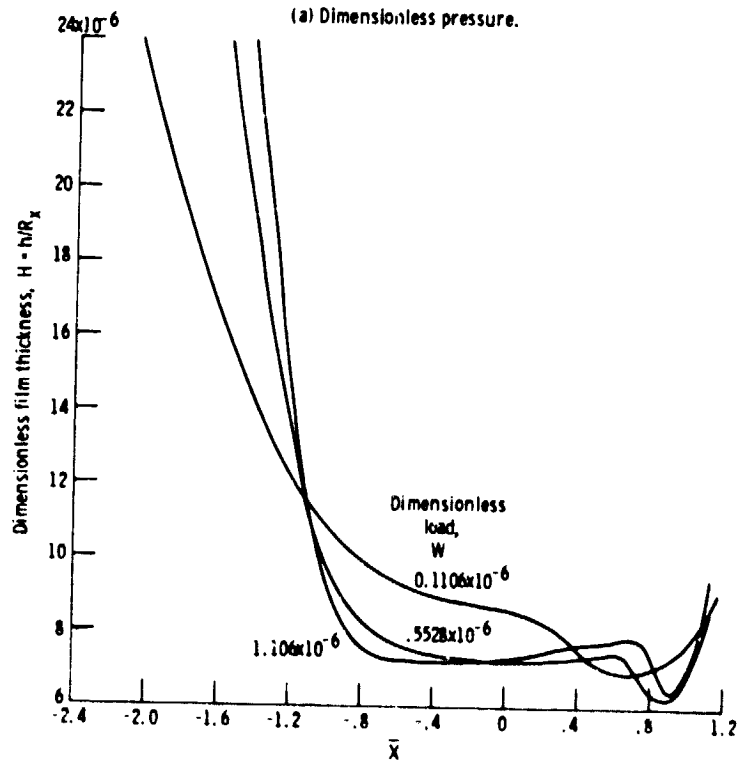


(c) Three dimensional representation of pressure.

Figure 5. 35. - Concluded.



(a) Dimensionless pressure.



(b) Dimensionless film thickness

Figure 5.36. - Variation of dimensionless pressure and film thickness on \bar{x} -axis for three values of dimensionless load parameter. The value of \bar{y} is held fixed near axial center of contact.

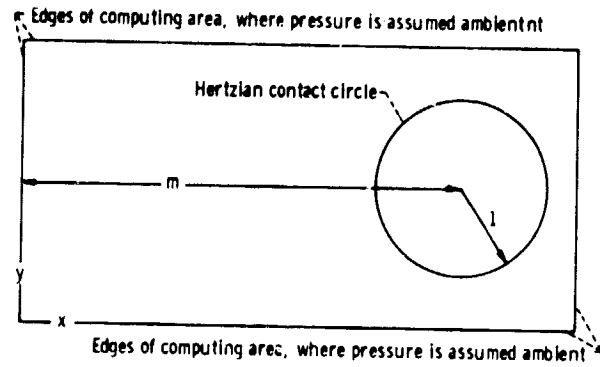


Figure 6.1. - Computing area in and around the Hertzian contact circle.

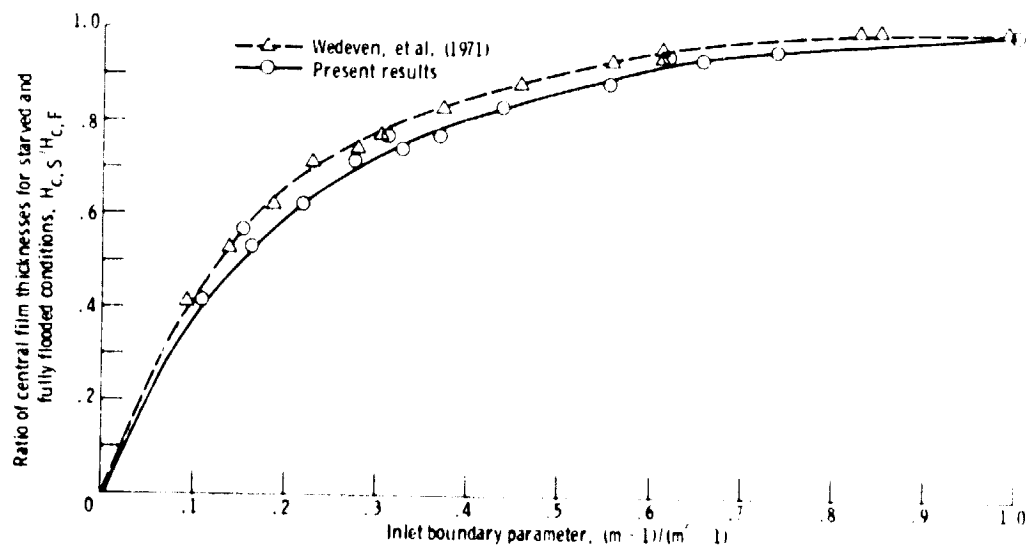


Figure 6.2. - Influence of inlet boundary parameter upon central film thickness ratio.

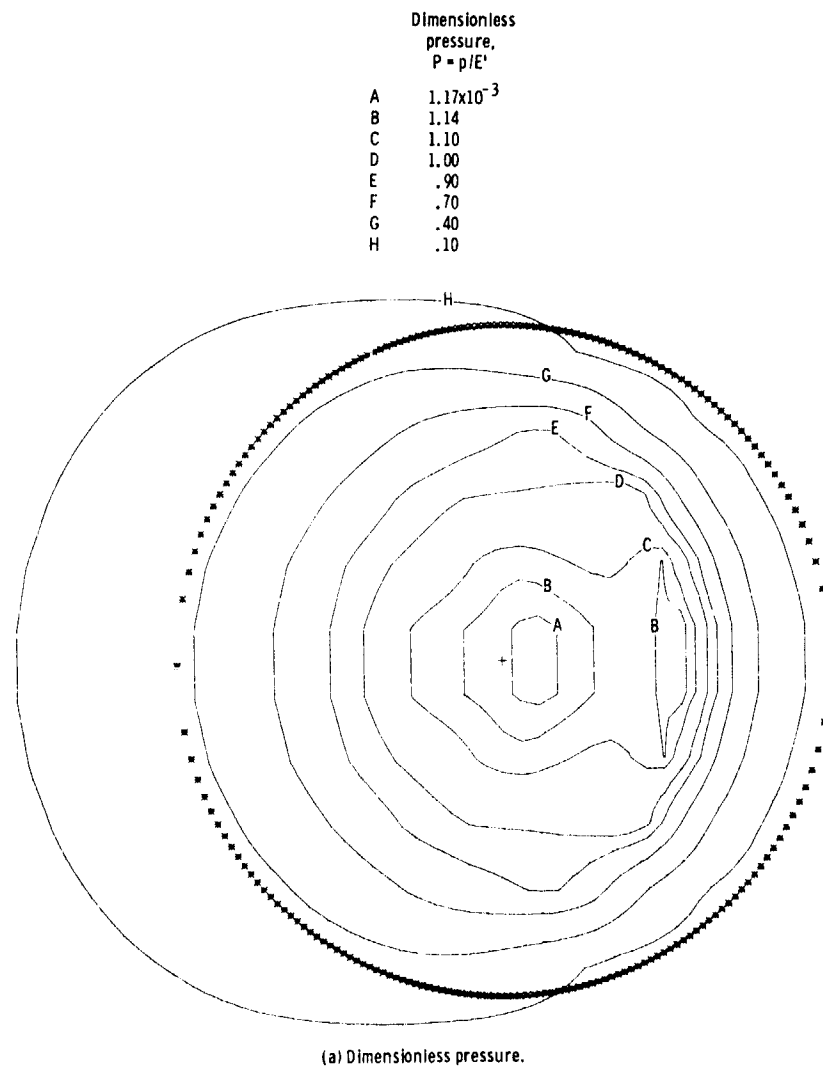
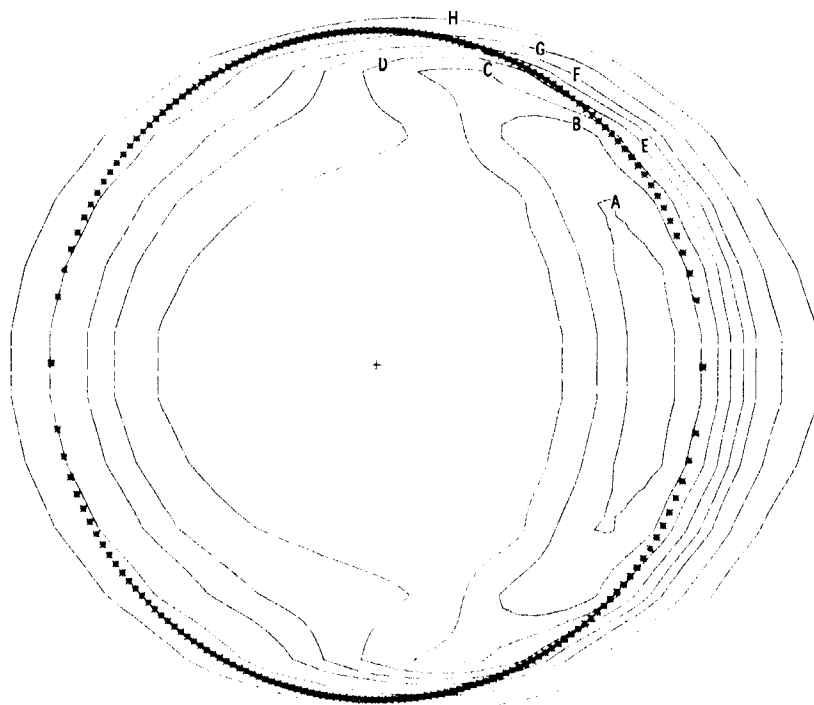


Figure 6.3. - Contour plots of dimensionless pressure and dimensionless film thickness for dimensionless inlet distance m of 4 and group 1 of table 6.2.

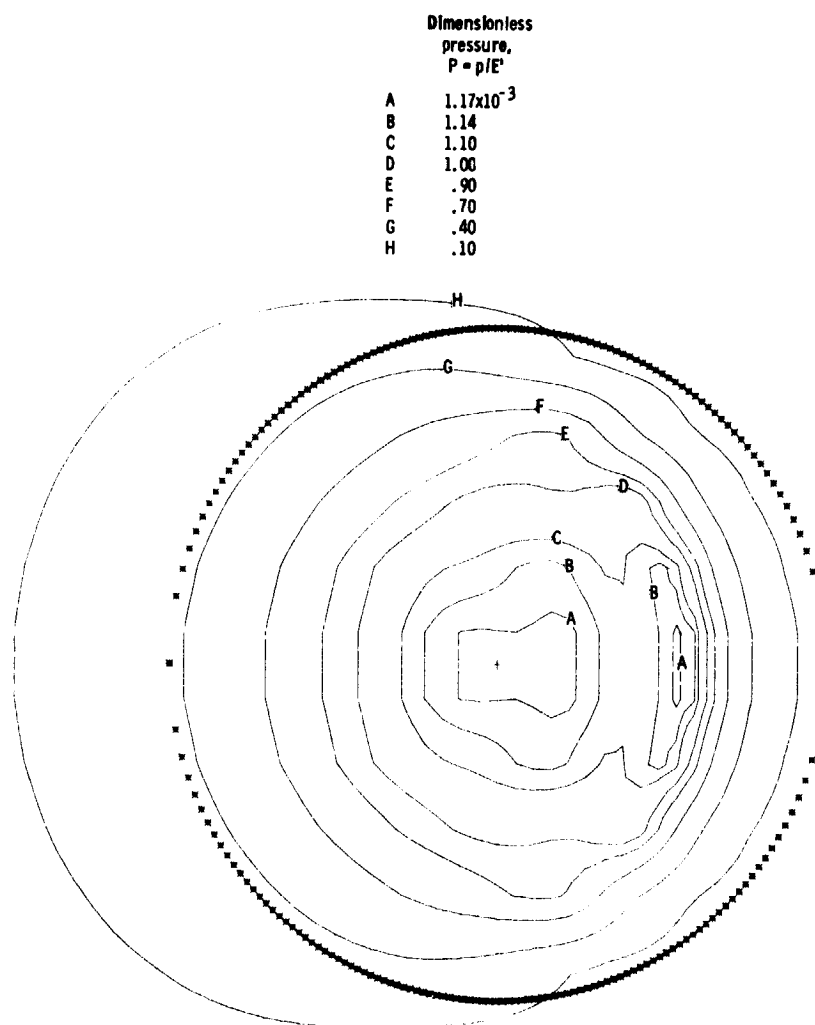
Dimensionless
film thickness,
 $H = h/R_x$

A	6.5×10^{-6}
B	7.0
C	7.5
D	8.0
E	8.5
F	9.0
G	10.0
H	11.5



(b) Dimensionless film thickness.

Figure 6.3. - Concluded.

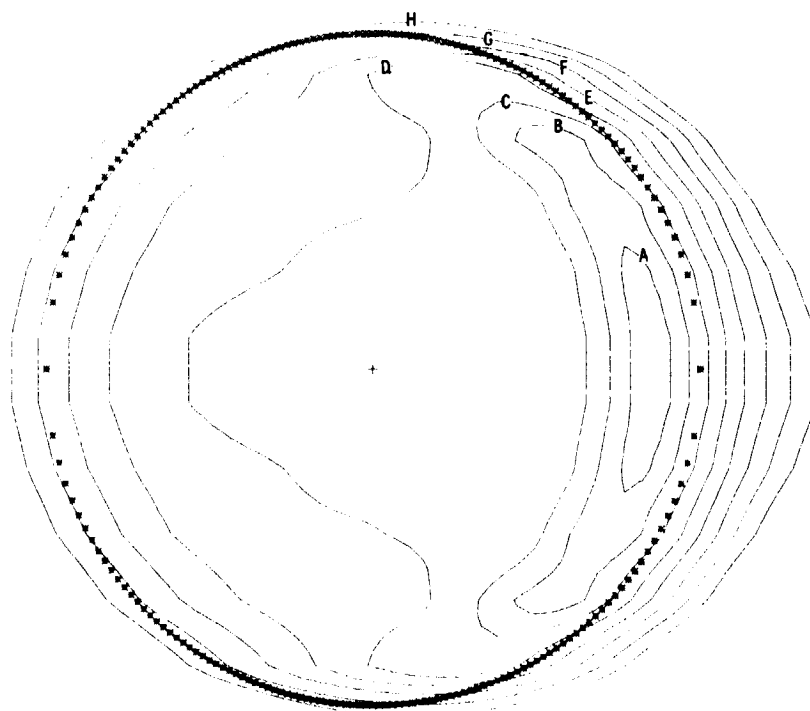


(a) Dimensionless pressure.

Figure 6.4. - Contour plots of dimensionless pressure and dimensionless film thickness for dimensionless inlet distance m of 3 and group 1 of table 6.2.

Dimensionless
film thickness,
 $H = h/R_x$

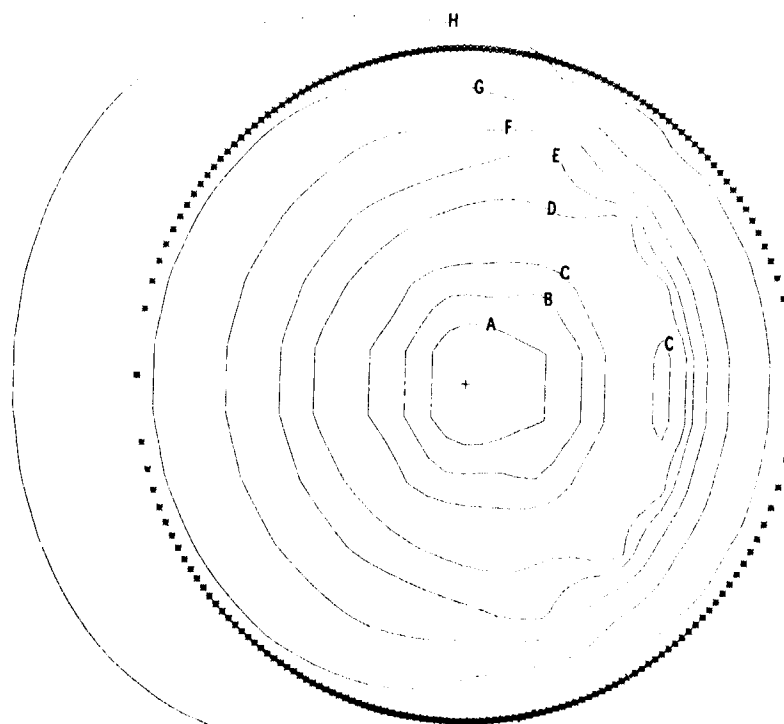
A	6.4×10^{-6}
B	6.7
C	7.2
D	7.8
E	8.5
F	9.3
G	10.2
H	11.2



(b) Dimensionless film thickness.
Figure 6.4. - Concluded.

Dimensionless
pressure,
 $P = p/E'$

A	1.17×10^{-3}
B	1.14
C	1.10
D	1.00
E	.90
F	.70
G	.40
H	.10

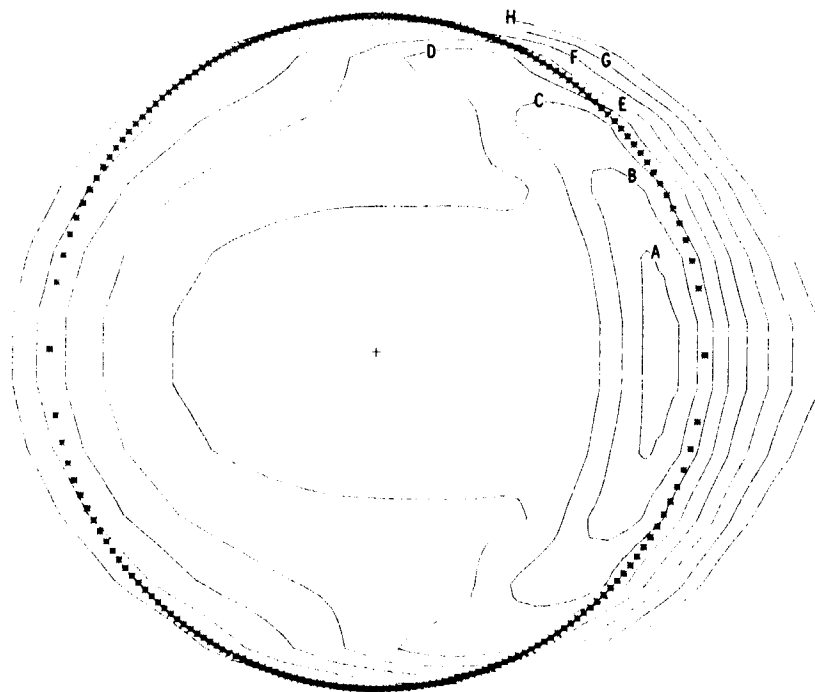


(a) Dimensionless pressure.

Figure 6.5. - Contour plots of dimensionless pressure and dimensionless film thickness for dimensionless inlet distance m of 2 and group 1 of table 6.2.

Dimensionless
film thickness,
 $H = h/R_x$

A	6.1×10^{-6}
B	6.4
C	6.8
D	7.3
E	7.9
F	8.6
G	9.4
H	10.3



(b) Dimensionless film thickness.

Figure 6.5. - Concluded.

REPRODUCIBILITY OF THE
ORIGINAL PAGE IS POOR

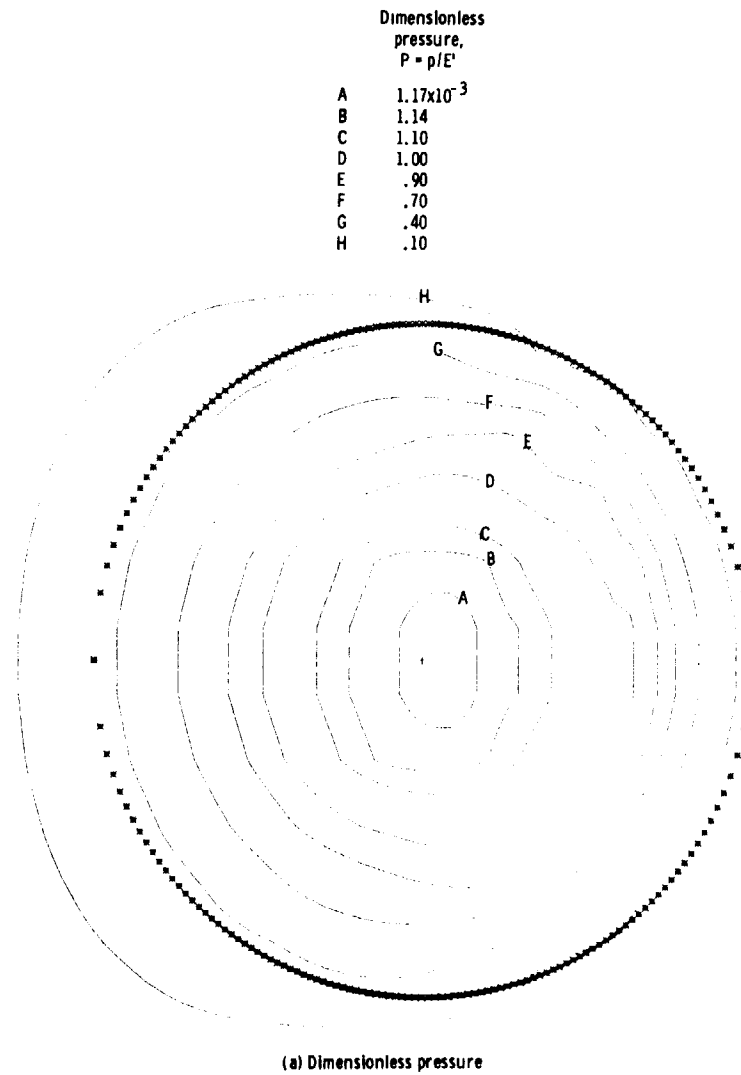
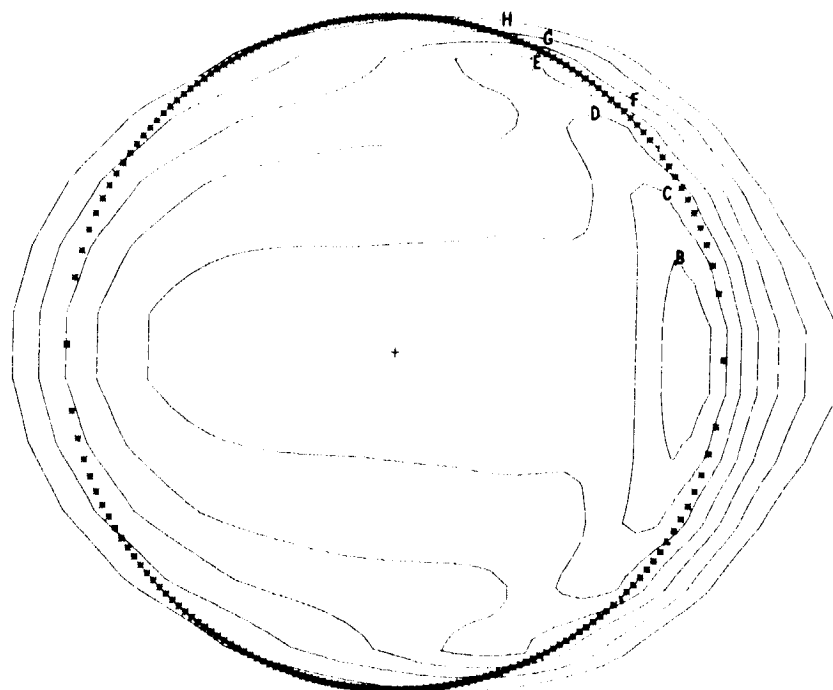


Figure 6.6. - Contour plots of dimensionless pressure and dimensionless film thickness for dimensionless inlet distance m of 1.5 and group 1 of table 6.2.

Dimensionless
film thickness,
 $H = h/R_x$

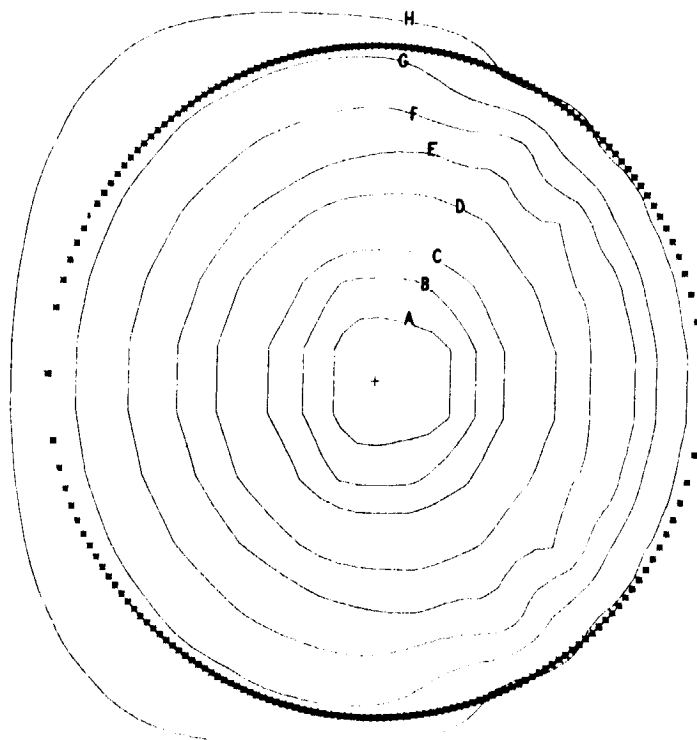
B	5.4×10^{-6}
C	5.7
D	6.1
E	6.6
F	7.2
G	8.0
H	9.0



(b) Dimensionless film thickness.

Figure 6.6. - Concluded.

	Dimensionless pressure, $P = p/E'$
A	1.17×10^{-3}
B	1.14
C	1.10
D	1.00
E	.90
F	.70
G	.40
H	.10

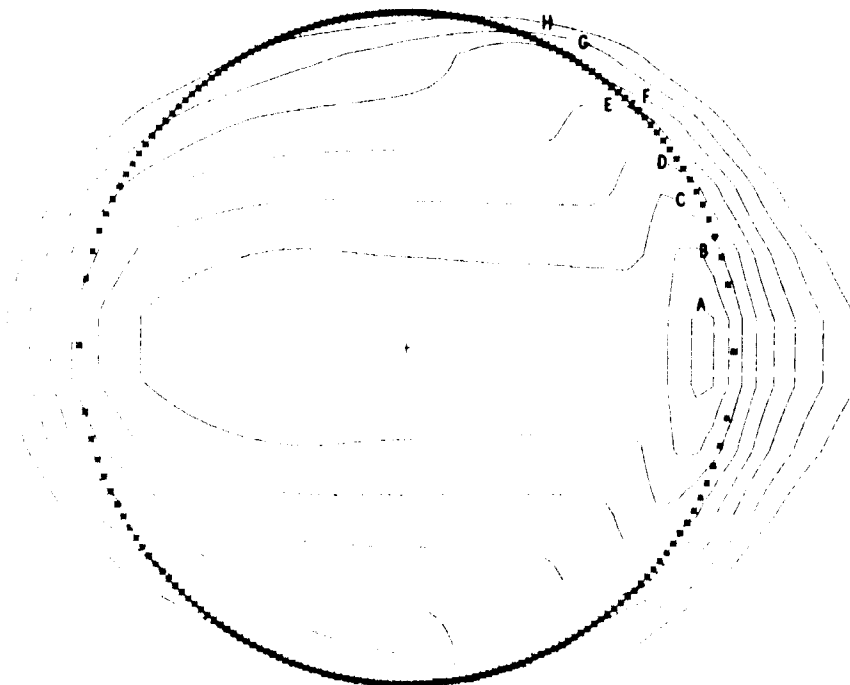


(a) Dimensionless pressure.

Figure 6.7. - Contour plots of dimensionless pressure and dimensionless film thickness for dimensionless inlet distance m of 1.25 and group 1 of table 6.2.

Dimensionless
film thickness,
 $H = h/R_x$

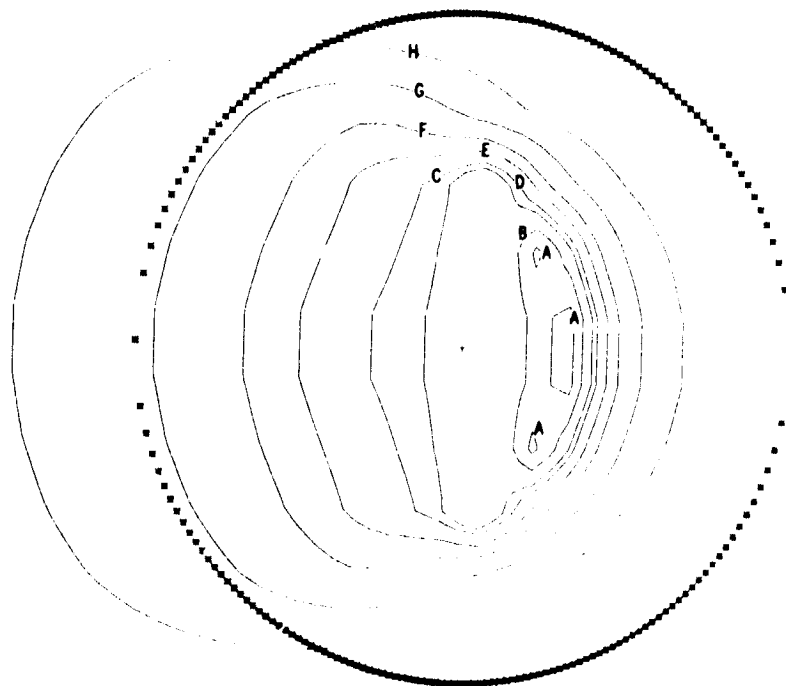
A	4.0×10^{-6}
B	4.2
C	4.5
D	4.9
E	5.4
F	6.0
G	6.8
H	7.8



(b) Dimensionless film thickness.

Figure 6.7. - Concluded.

Dimensionless pressure, $P = p/E'$	
A	1.8×10^{-3}
B	1.6
C	1.4
D	1.3
E	1.1
F	.9
G	.6
H	.3

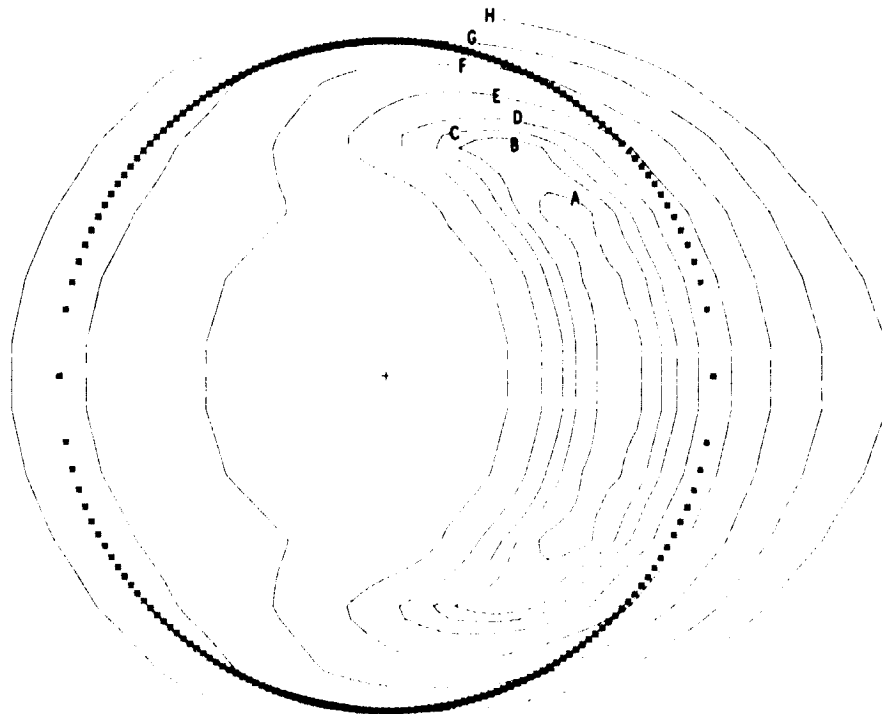


(a) Dimensionless pressure.

Figure 6.8. - Contour plots of dimensionless pressure and dimensionless film thickness for dimensionless inlet distance m of 6 and group 2 of table 6.2.

Dimensionless
film thickness,
 $H = h/R_x$

A	30.0x10 ⁻⁶
B	30.5
C	31.0
D	32.0
E	34.0
F	37.0
G	41.0
H	46.0



(b) Dimensionless film thickness.

Figure 6.8. - Concluded.

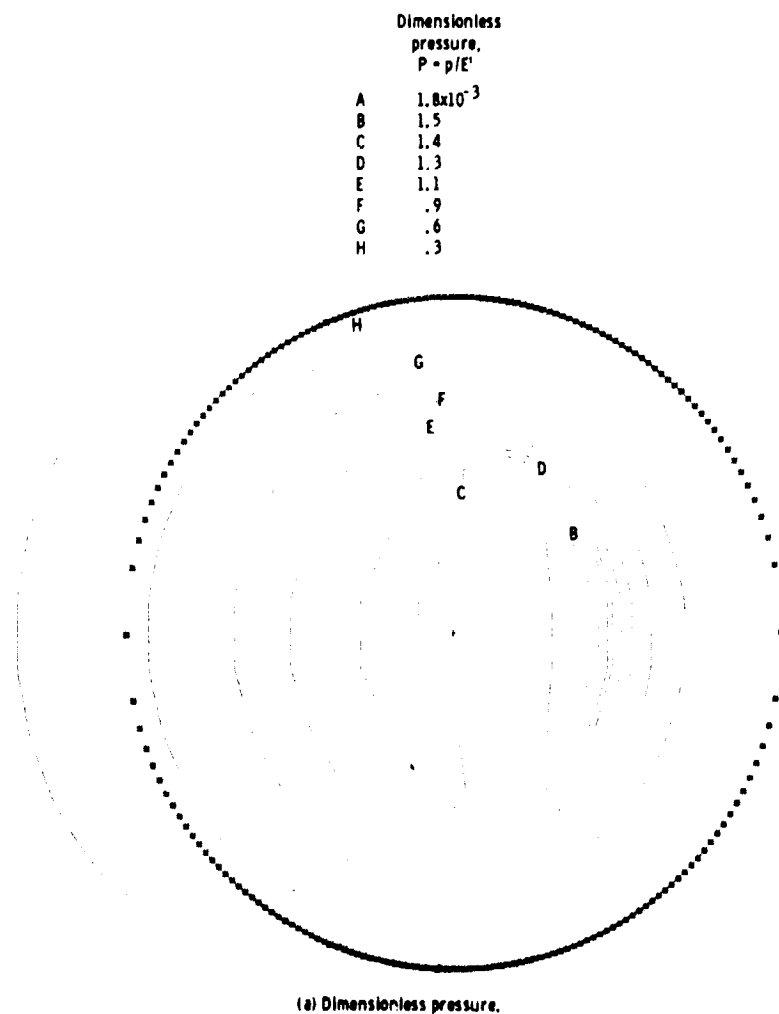
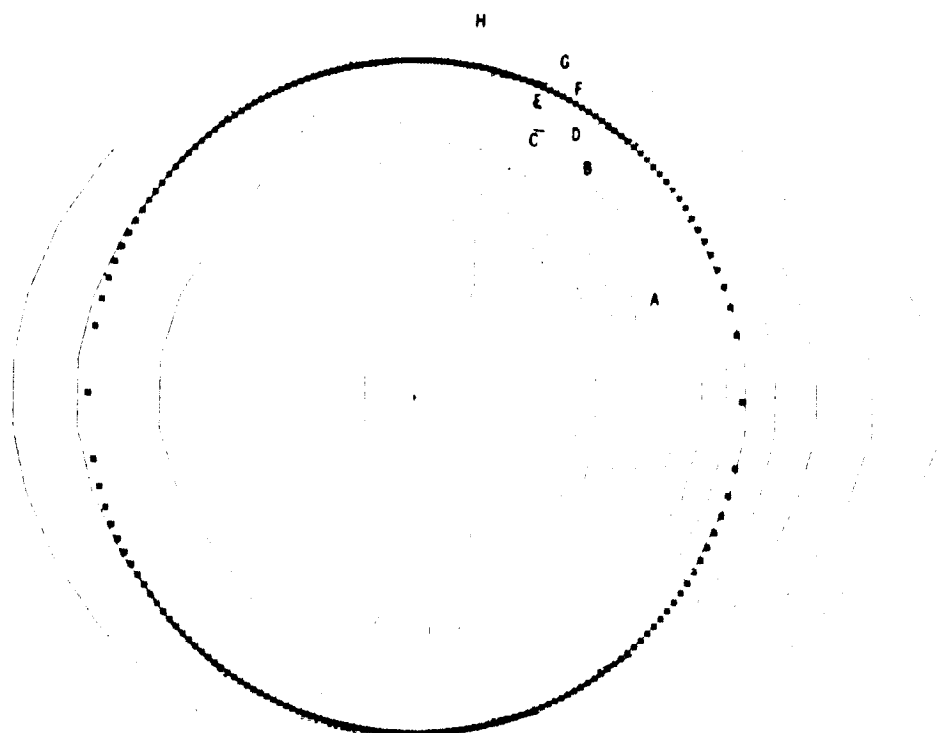


Figure 6.9. - Contour plots of dimensionless pressure and dimensionless film thickness for dimensionless inlet distance m of 4 and group 2 of table 6.2.

Dimensionless
film thickness,
 $H = h/R_x$

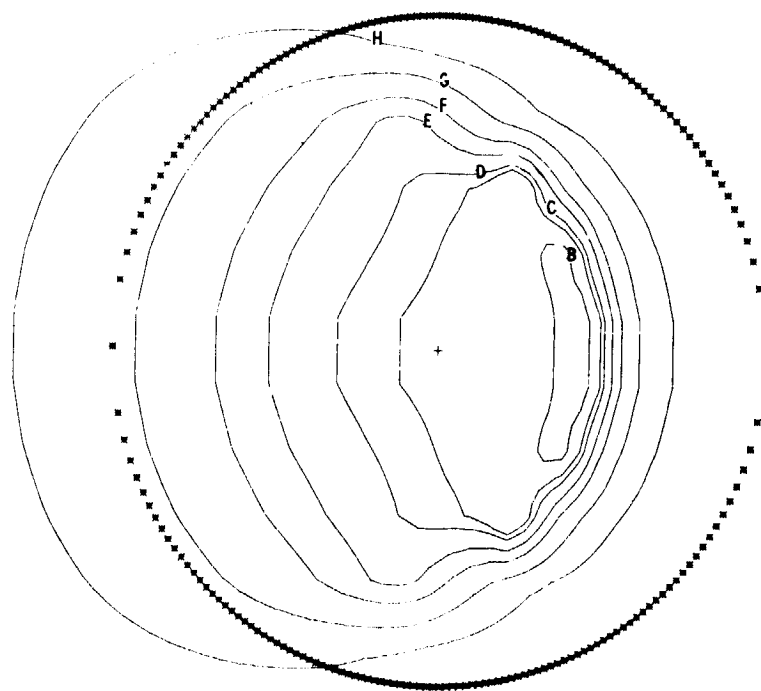
A	29.5×10^{-6}
B	30.0
C	31.0
D	32.0
E	34.0
F	37.0
G	41.0
H	46.0



(b) Dimensionless film thickness.

Figure 6.9. - Concluded.

	Dimensionless pressure, $P = p/E'$
A	1.8×10^{-3}
B	1.6
C	1.4
D	1.3
E	1.1
F	.9
G	.6
H	.3

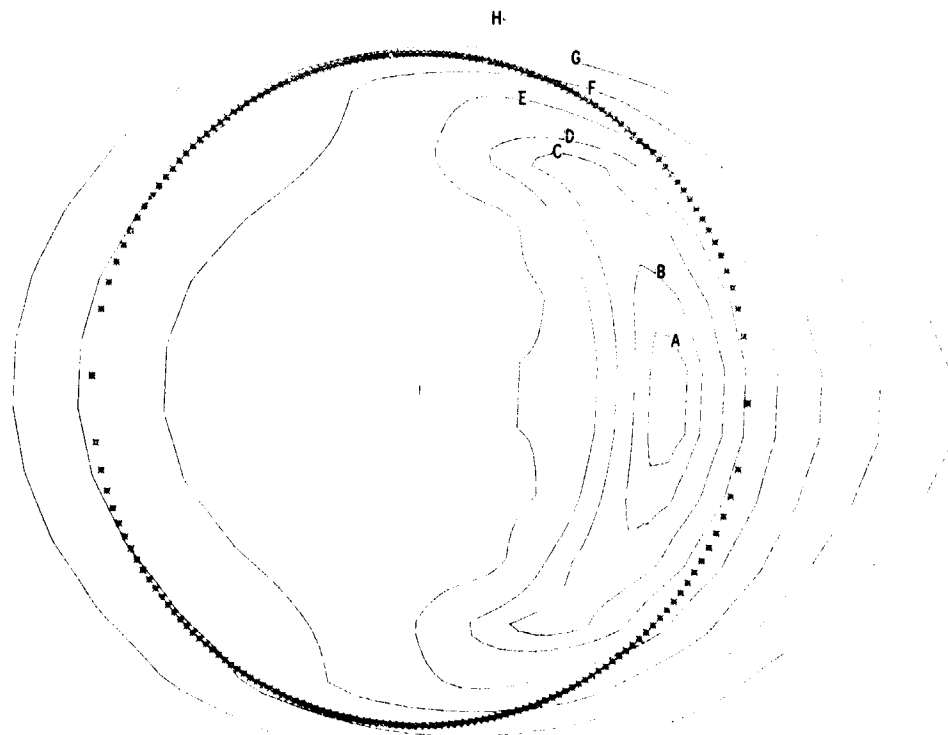


(a) Dimensionless pressure.

Figure 6.10. - Contour plots of dimensionless pressure and dimensionless film thickness for dimensionless inlet distance m of 3 and group 2 of table 6.2.

Dimensionless
film thickness,
 $H = h/R_x$

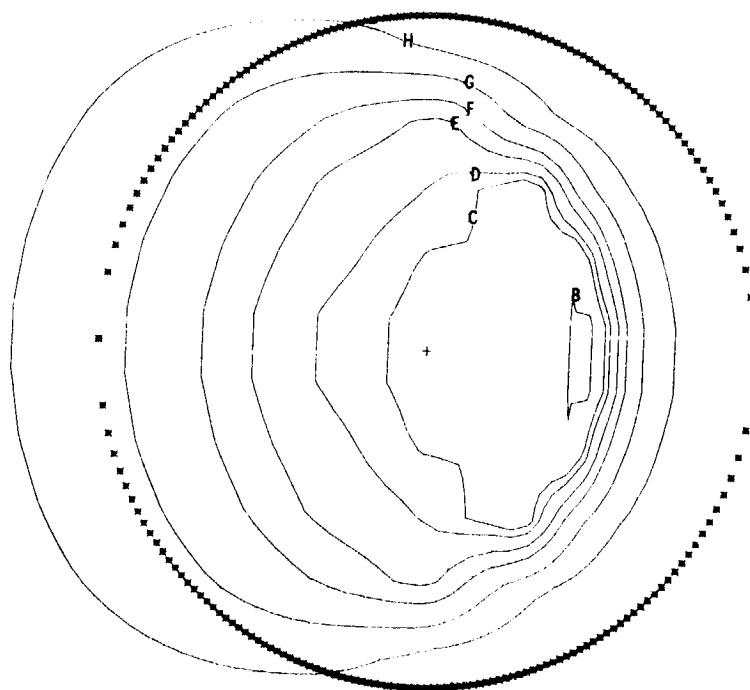
A	28.0x10 ⁻⁶
B	28.3
C	29.0
D	30.0
E	32.0
F	35.0
G	39.0
H	44.0



(b) Dimensionless film thickness.

Figure 6.10. - Concluded.

	Dimensionless pressure, $P = p/E'$
A	1.8×10^{-3}
B	1.6
C	1.4
D	1.3
E	1.1
F	.9
G	.6
H	.3

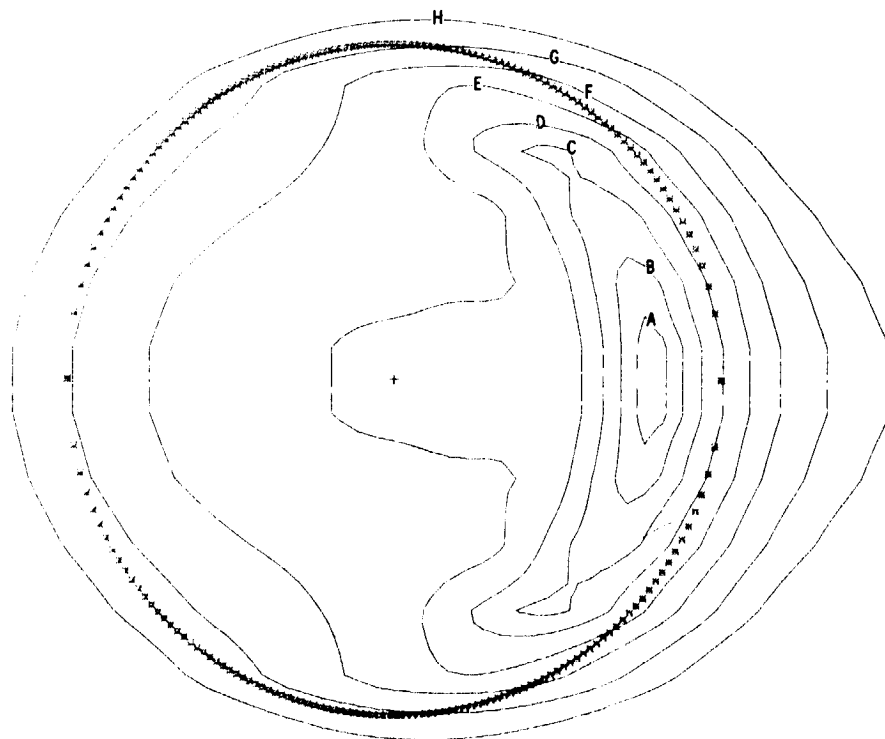


(a) Dimensionless pressure.

Figure 6.11. - Contour plots of dimensionless pressure and dimensionless film thickness for dimensionless inlet distance m of 2.5 and group 2 of table 6.2.

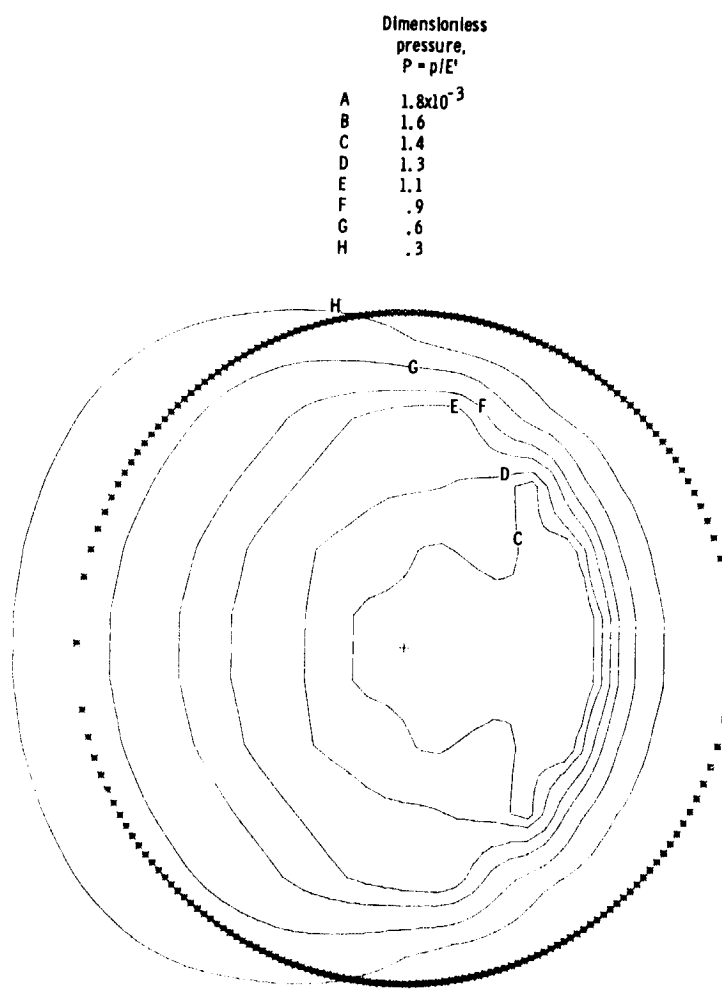
Dimensionless
film thickness,
 $H = h/R_x$

A	26.5×10^{-6}
B	26.8
C	27.4
D	28.4
E	30.0
F	32.0
G	35.0
H	39.0



(b) Dimensionless film thickness.

Figure 6.11. - Concluded.

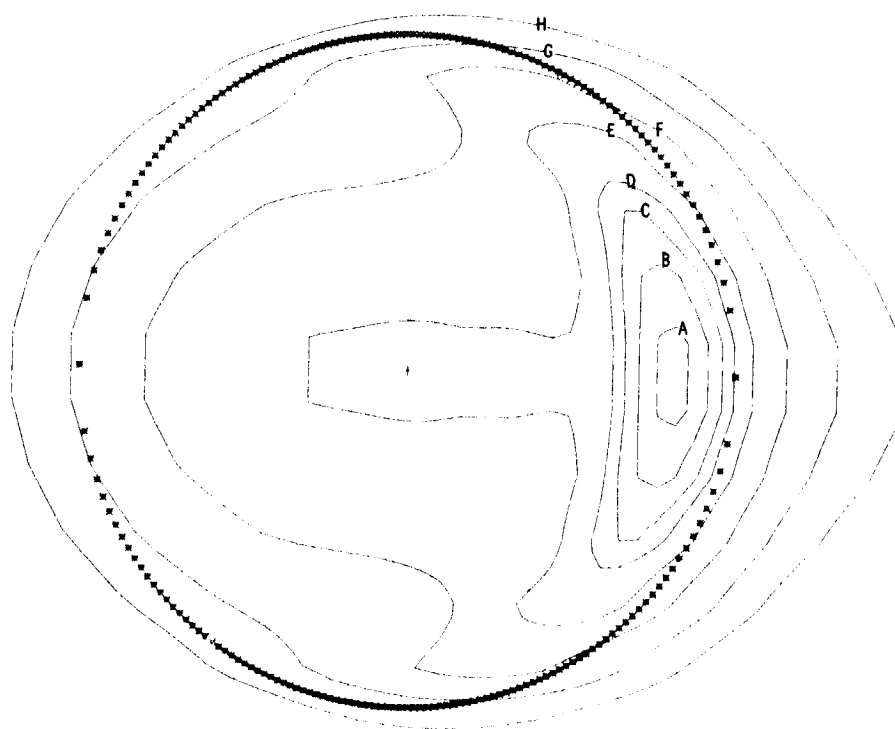


(a) Dimensionless pressure.

Figure 6.12. - Contour plots of dimensionless pressure and dimensionless film thickness for dimensionless inlet distance m of 2 and group 2 of table 6.2.

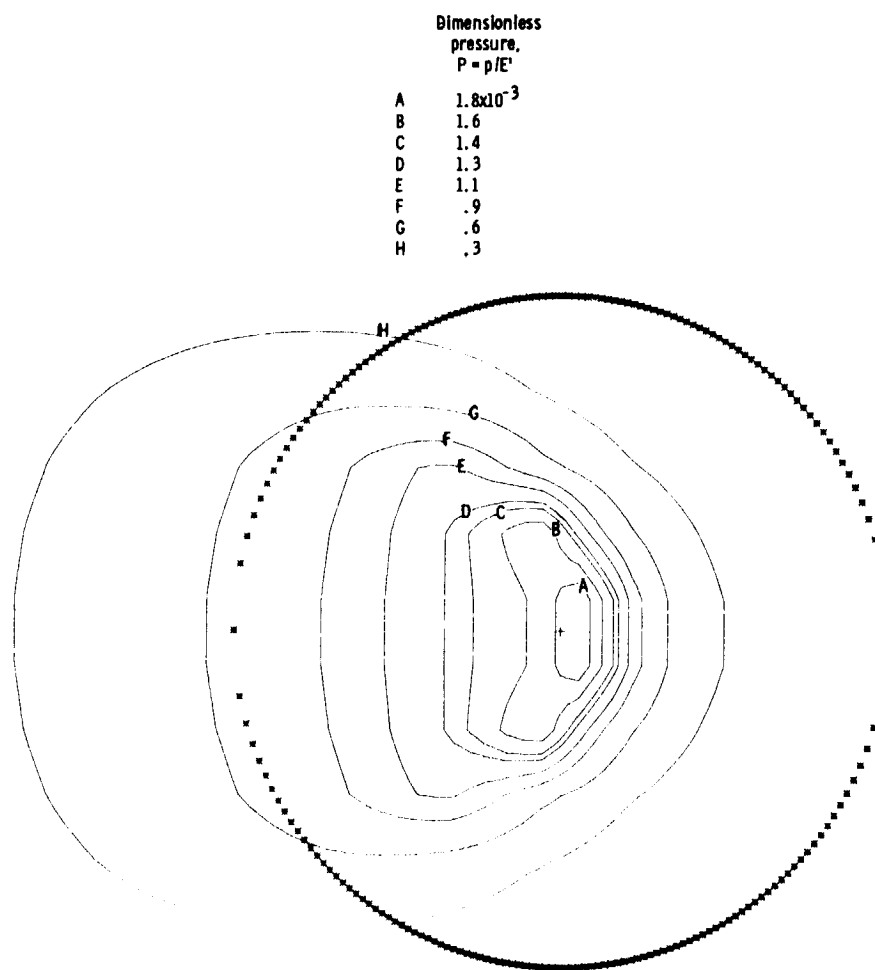
Dimensionless
film thickness,
 $H = h/R_x$

A	23.6×10^{-6}
B	24.0
C	24.5
D	25.0
E	26.0
F	28.0
G	31.0
H	35.0



(b) Dimensionless film thickness.

Figure 6.12. - Concluded.



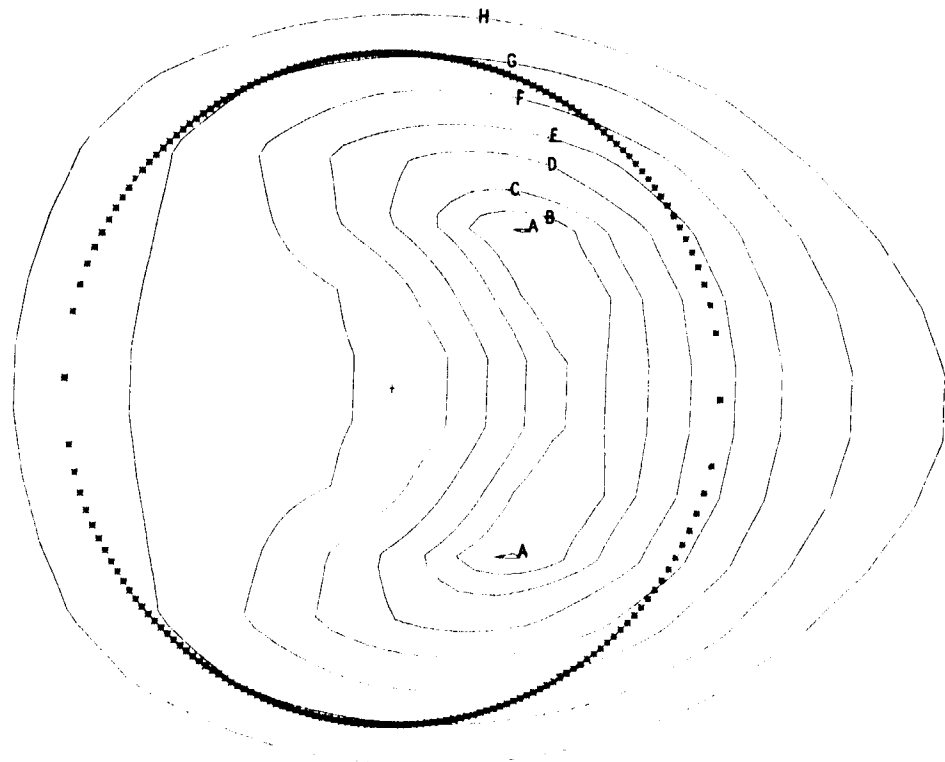
(a) Dimensionless pressure.

Figure 6.13. - Contour plots of dimensionless pressure and dimensionless film thickness for dimensionless inlet distance m of 6 and group 3 of table 6.2.

REPRODUCIBILITY OF THE
ORIGINAL PAGE IS POOR

Dimensionless
film thickness,
 $H = h/R_x$

A	61.4×10^{-6}
B	62.0
C	63.0
D	65.0
E	68.0
F	72.0
G	78.0
H	86.0



(b) Dimensionless film thickness.

Figure 6.13. - Concluded.

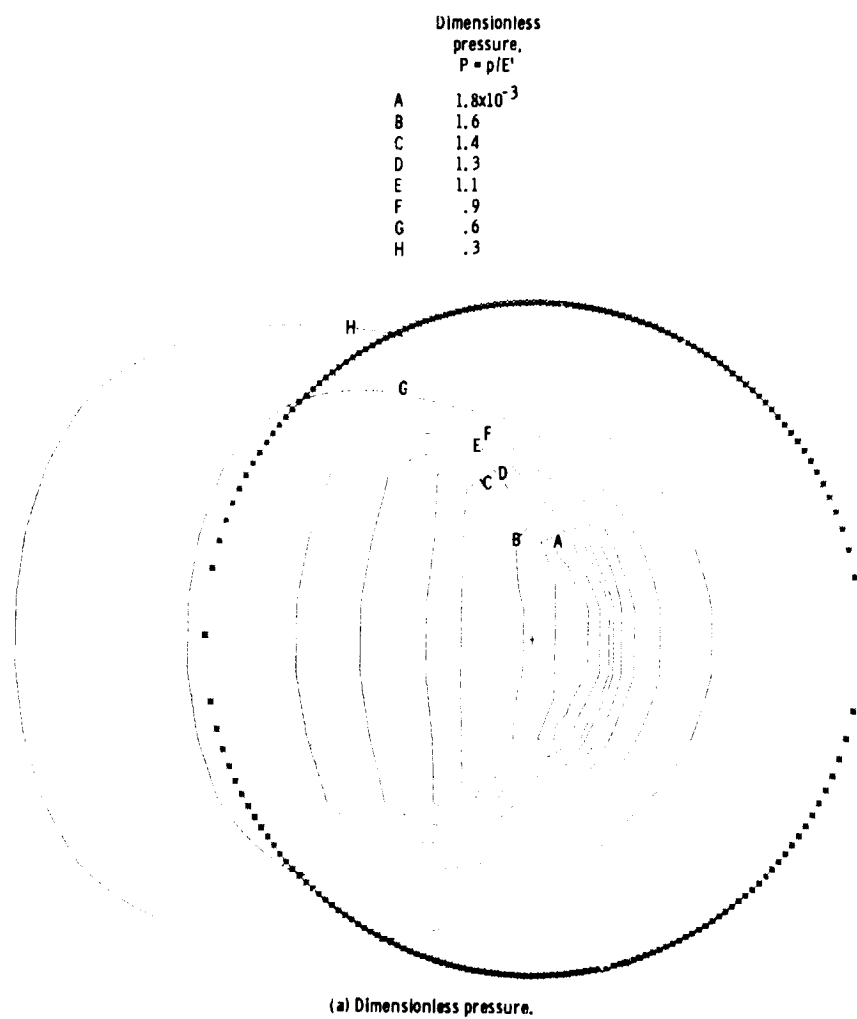
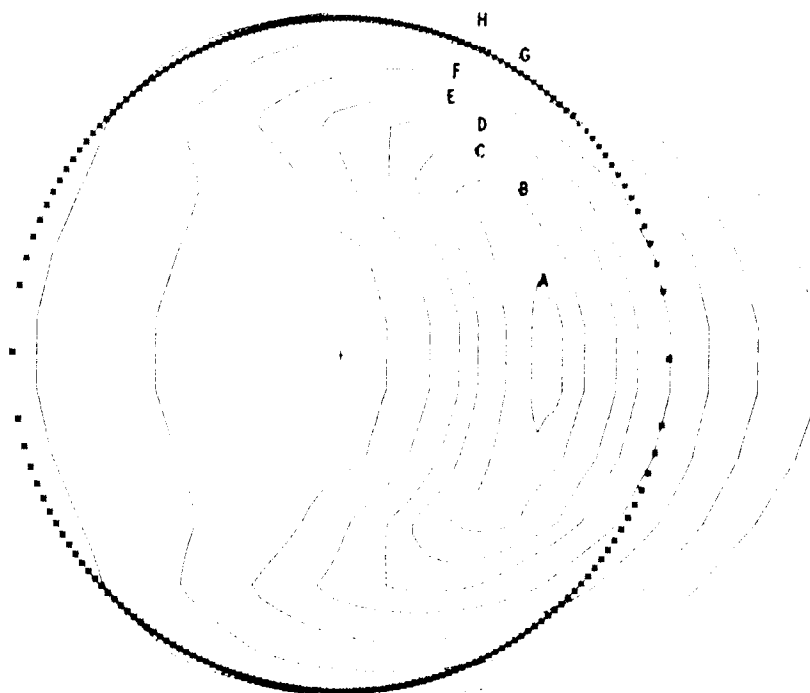


Figure 6.14. - Contour plots of dimensionless pressure and dimensionless film thickness for dimensionless inlet distance m of 4 and group 3 of table 6.2.

Dimensionless
film thickness,
 $H = h/R_s$

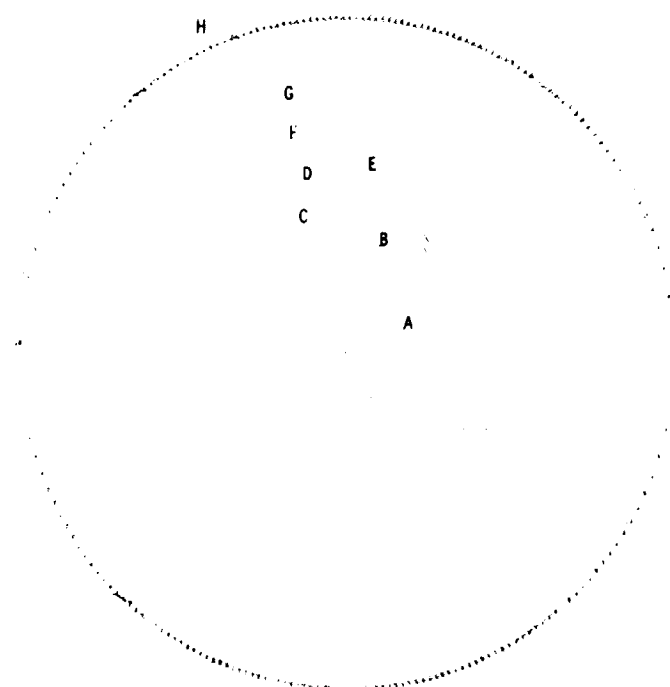
A	57.6×10^{-6}
b	58.0
C	59.0
D	60.0
E	62.0
F	65.0
G	69.0
H	74.0



(b) Dimensionless film thickness.

Figure 6.14. - Concluded.

	Dimensionless pressure, $P = p/E'$
A	1.8×10^{-3}
B	1.6
C	1.4
D	1.3
E	1.1
F	.9
G	.6
H	.3

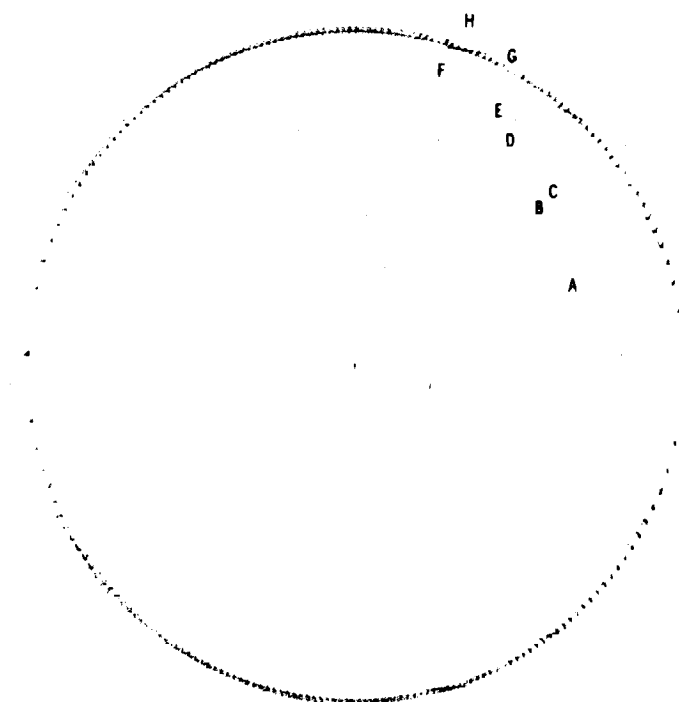


(a) Dimensionless pressure.

Figure 6.15. - Contour plots of dimensionless pressure and dimensionless film thickness for dimensionless inlet distance m of 3 and group 3 of table 6.2.

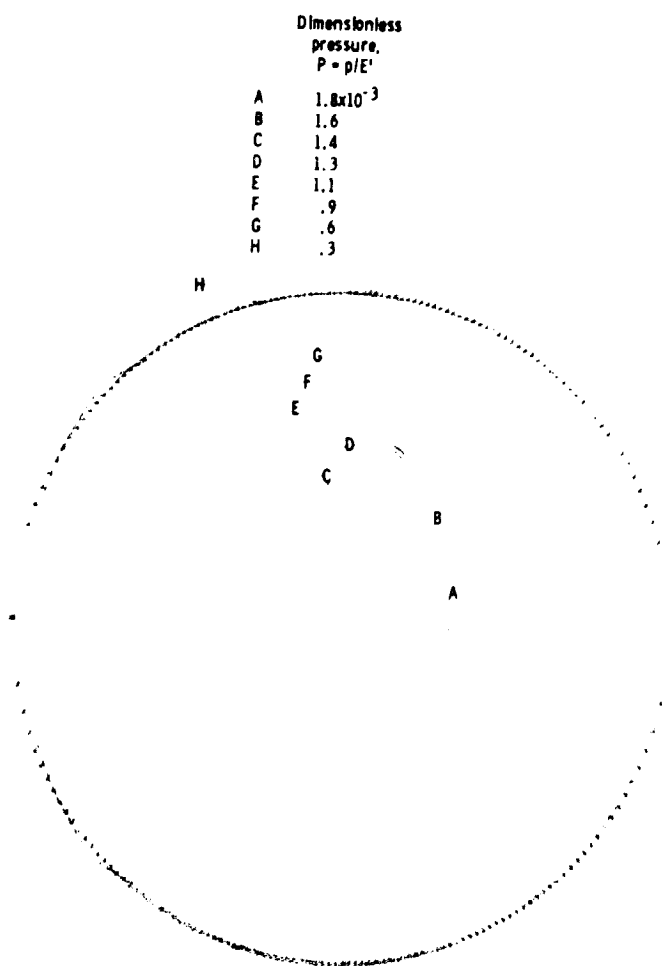
Dimensionless
film thickness,
 $H = h/R_x$

A	52.0x10 ⁻⁶
B	52.5
C	53.0
D	54.0
E	56.0
F	59.0
G	63.0
H	68.0



(b) Dimensionless film thickness.

Figure 6.15. - Concluded.

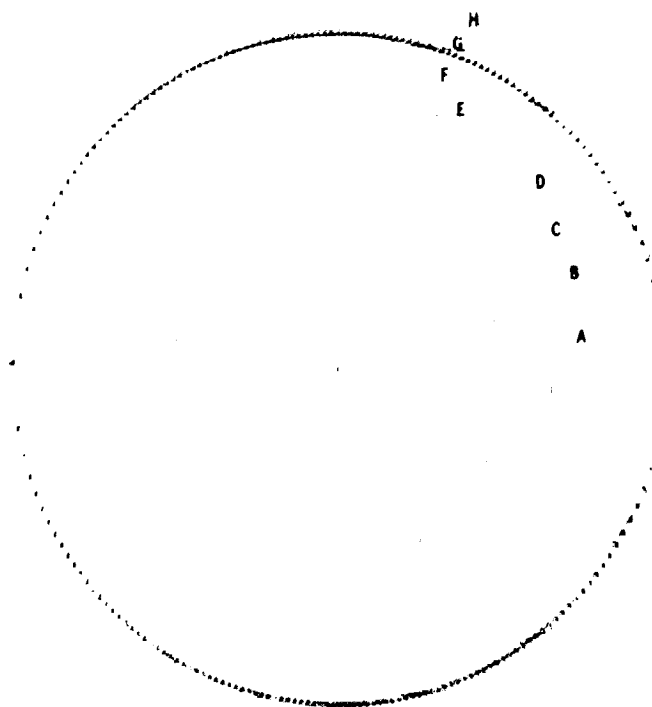


(a) Dimensionless pressure.

Figure 6.16. - Contour plots of dimensionless pressure and dimensionless film thickness for dimensionless inlet distance m of 2.5 and group 3 of table 6.2.

Dimensionless
film thickness,
 $H = h/R_t$

A	47.0x10 ⁻⁶
B	47.5
C	48.0
D	49.0
E	51.0
F	54.0
G	58.0
H	63.0



(b) Dimensionless film thickness.

Figure 6.16. - Concluded.

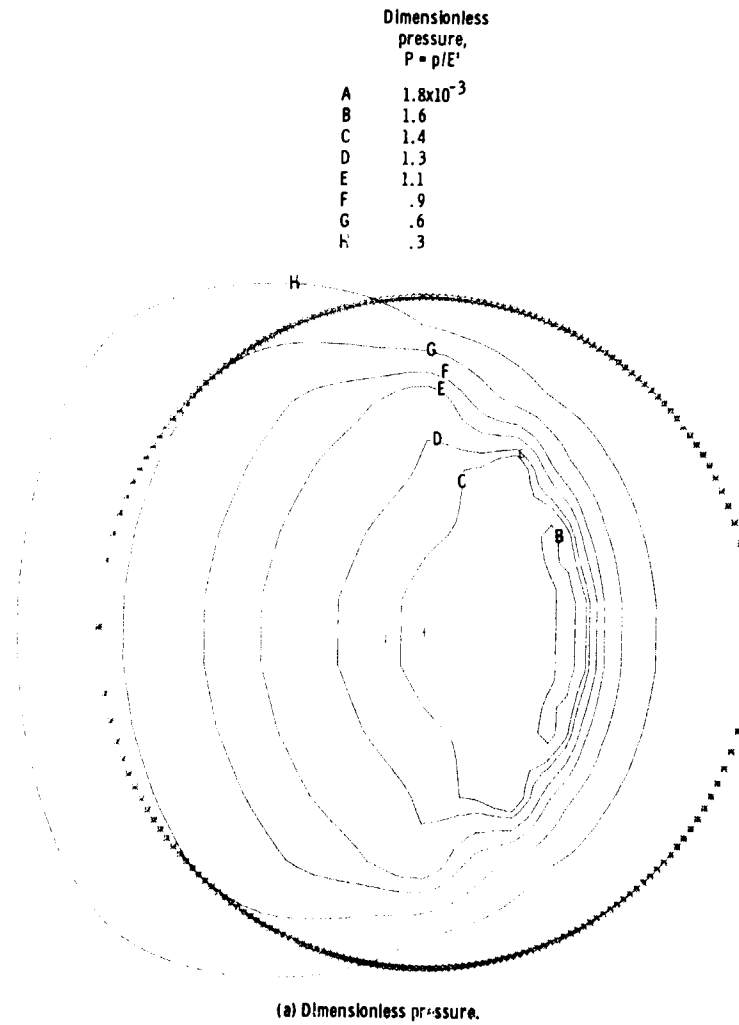
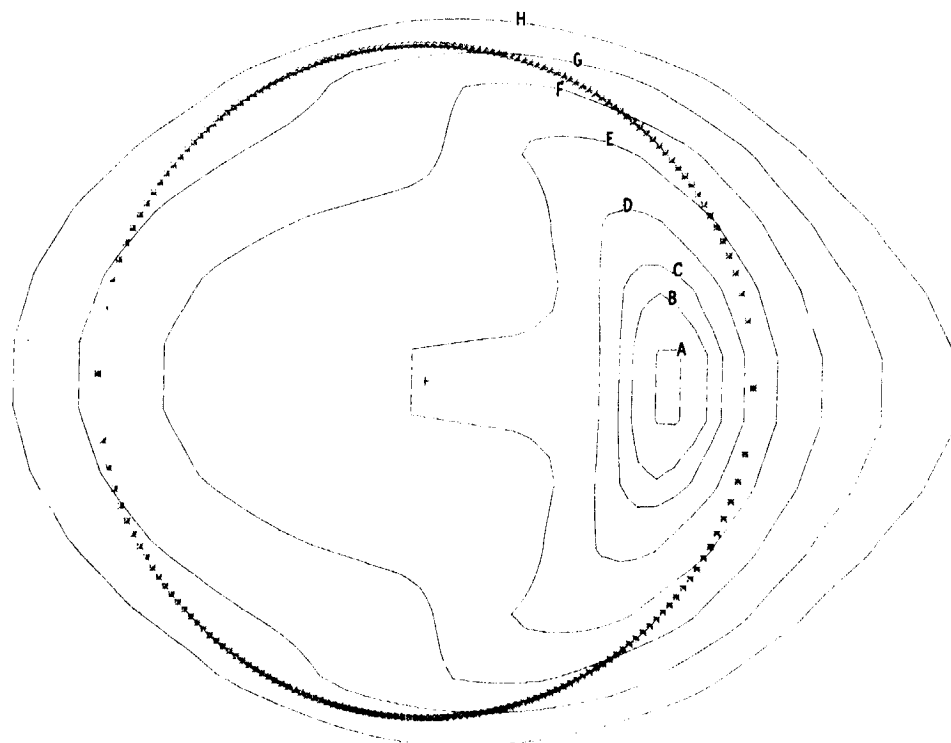


Figure 6.17. - Contour plots of dimensionless pressure and dimensionless film thickness for dimensionless inlet distance m of 2 and group 3 of table 6.2.

Dimensionless
film thickness,
 $H = h/R_x$

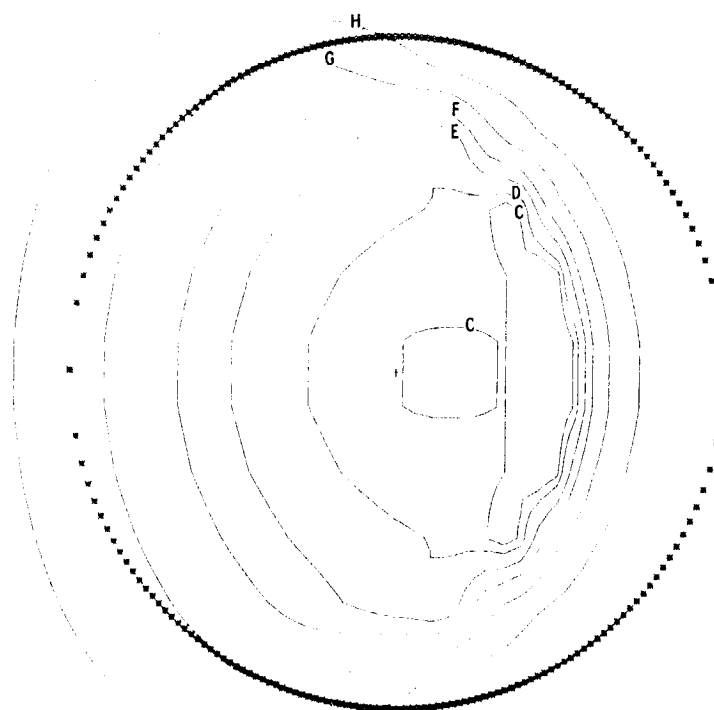
A	40.0×10^{-6}
B	40.5
C	41.0
D	42.0
E	44.0
F	47.0
G	51.0
H	56.0



(b) Dimensionless film thickness.

Figure 6.17. - Concluded.

Dimensionless pressure, $P = p/E'$	
A	1.8×10^{-3}
B	1.6
C	1.4
D	1.3
E	1.1
F	.9
G	.6
H	.3

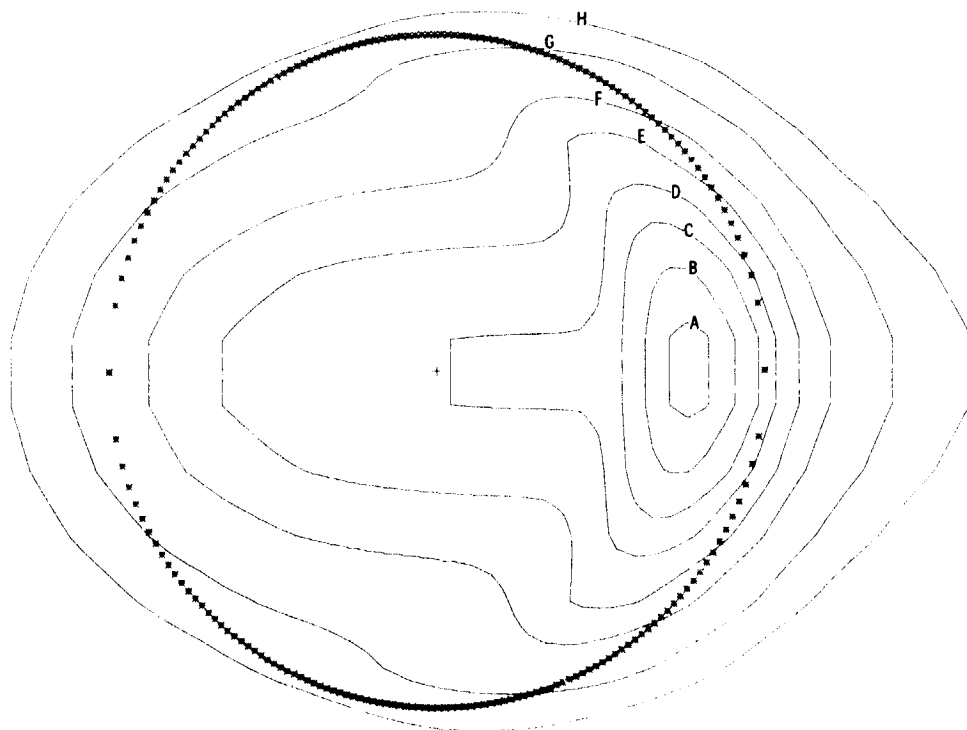


(a) Dimensionless pressure.

Figure 6.18. - Contour plots of dimensionless pressure and dimensionless film thickness for dimensionless inlet distance m of 1.75 and group 3 of table 6.2.

Dimensionless
film thickness,
 $H = h/R_x$

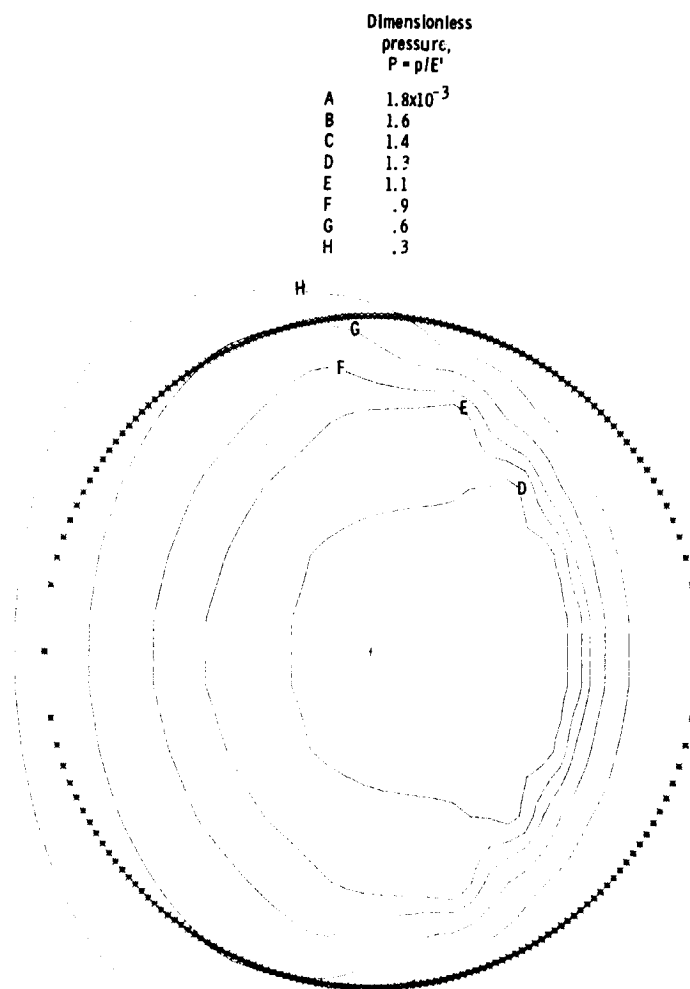
A	34.8×10^{-6}
B	36.5
C	36.5
D	37.5
E	39.0
F	41.0
G	45.0
H	50.0



(b) Dimensionless film thickness.

Figure 6.18. - Concluded.

REPRODUCIBILITY OF THE
ORIGINAL PAGE IS POOR

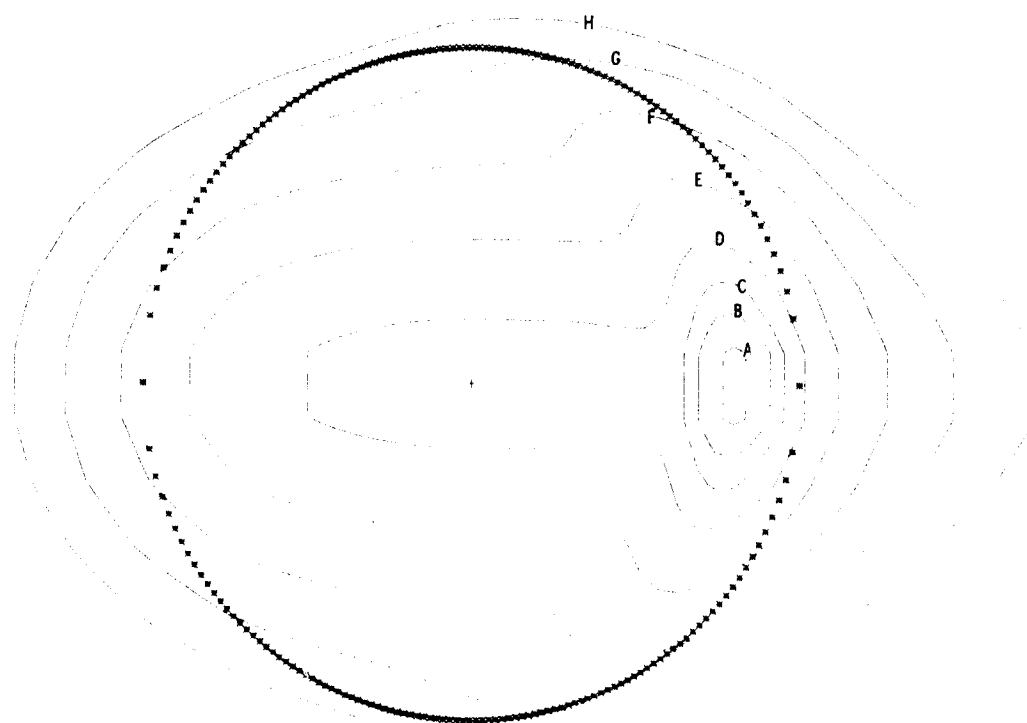


(a) Dimensionless pressure.

Figure 6.19. - Contour plots of dimensionless pressure and dimensionless film thickness for dimensionless inlet distance m of 1.5 and group 3 of table 6.2.

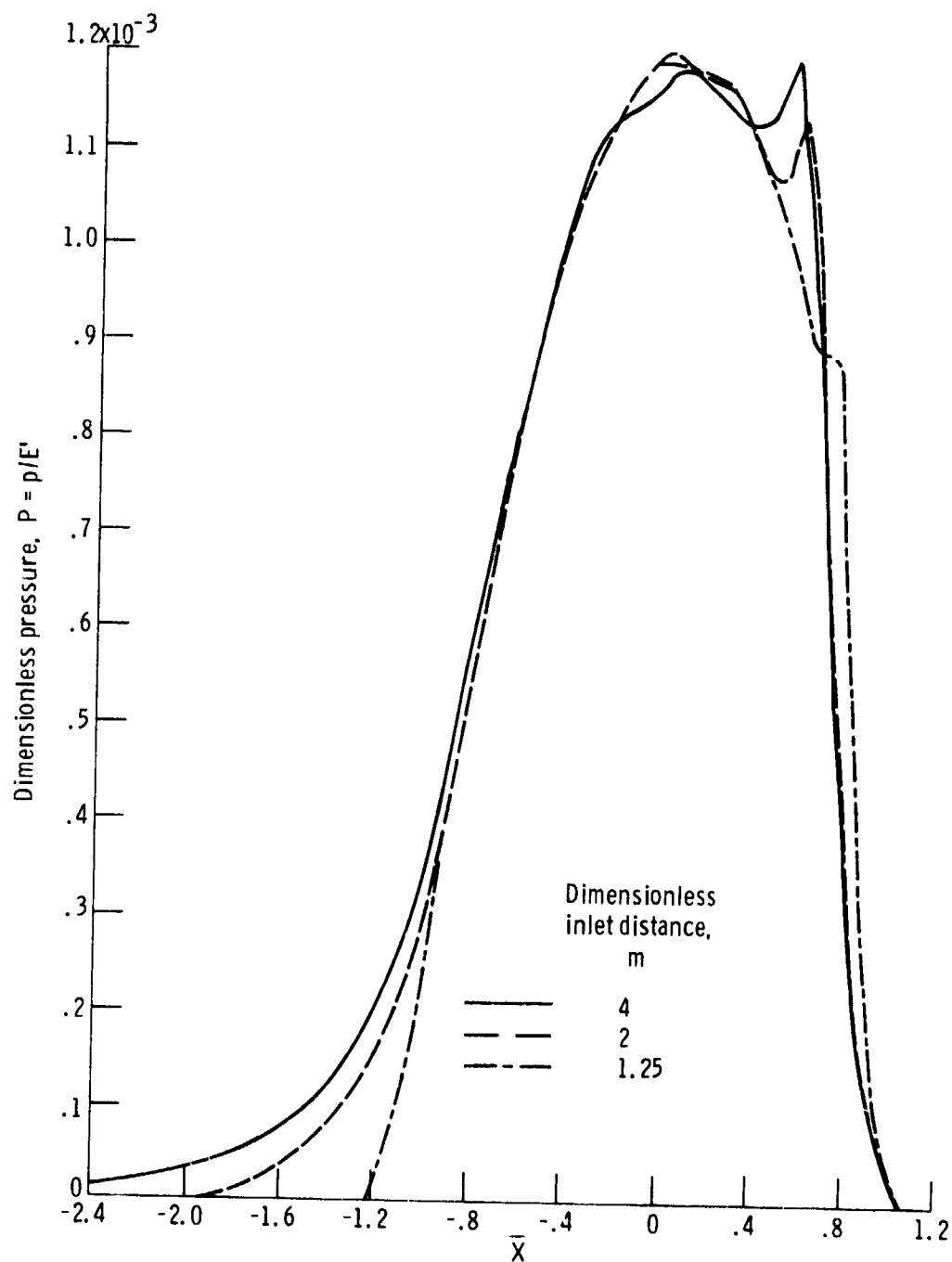
Dimensionless
film thickness,
 $H = h/R_x$

A	28.0×10^{-6}
B	28.5
C	29.0
D	30.0
E	32.0
F	35.0
G	39.0
H	44.0



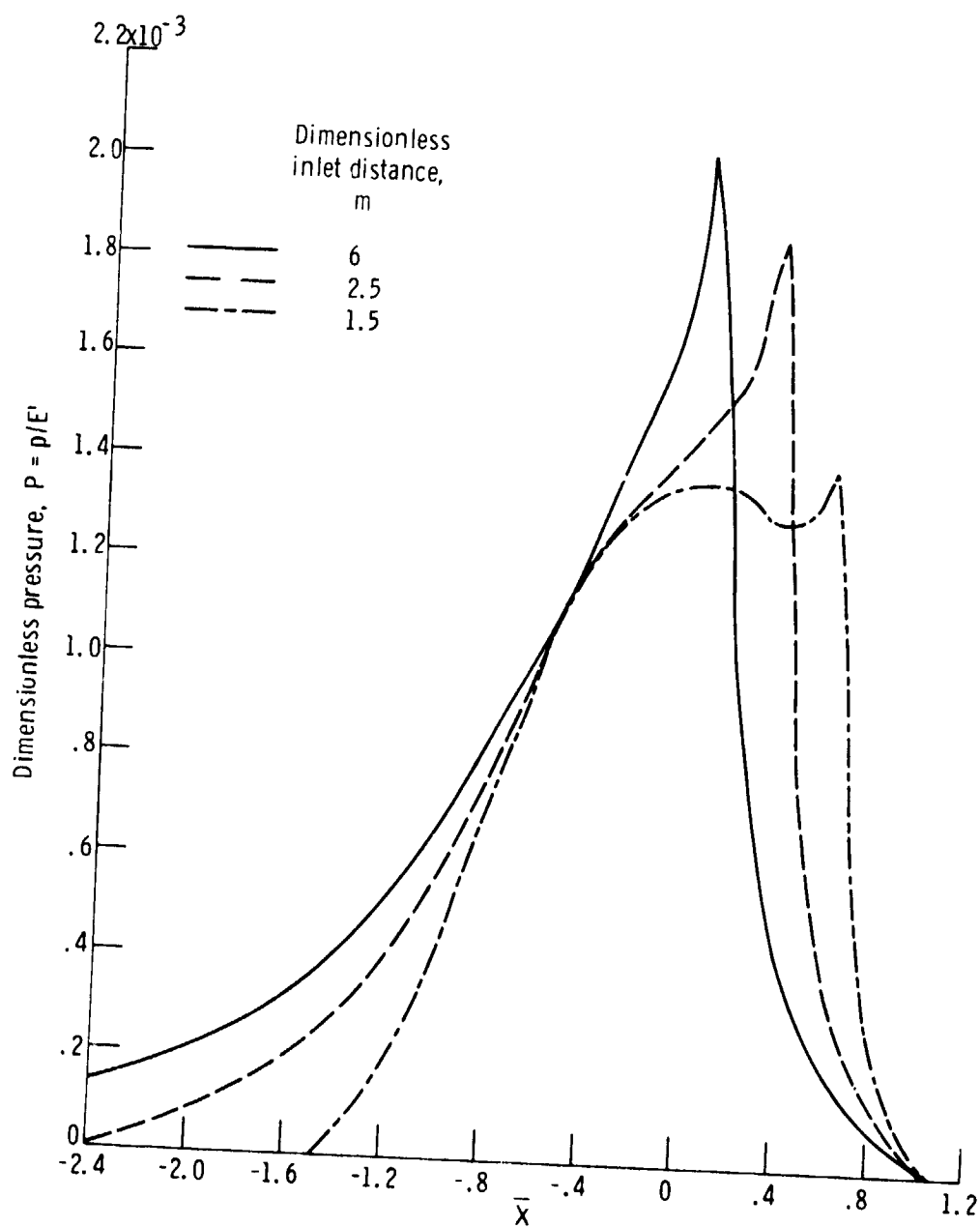
(b) Dimensionless film thickness

Figure 6.19. - Concluded.



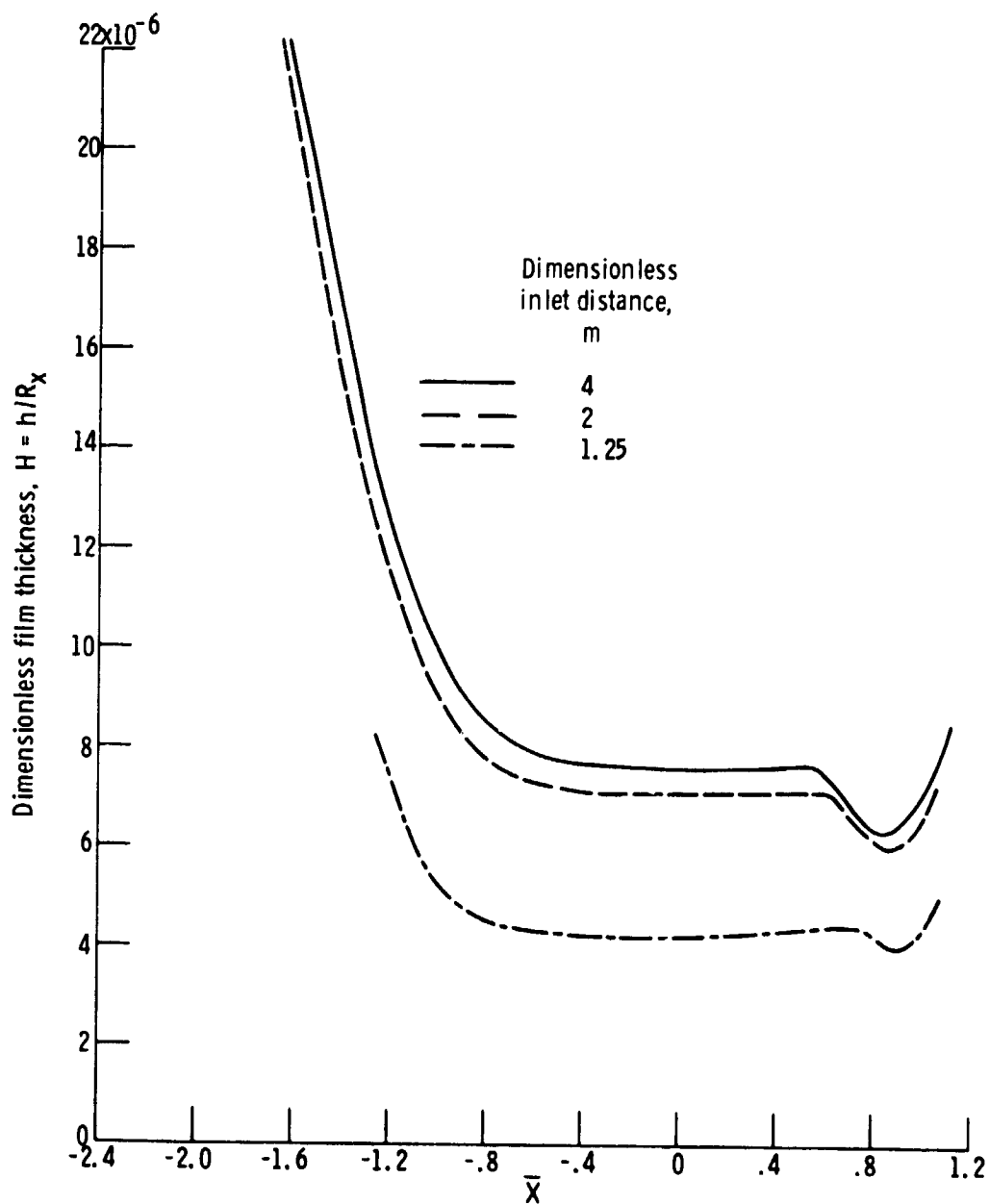
(a) Group 1 of table 6.2.

Figure 6.20. - Effect of dimensionless inlet distance on dimensionless pressure along \bar{X} -axis. The value of \bar{Y} is held fixed near the axis of symmetry of the contact.



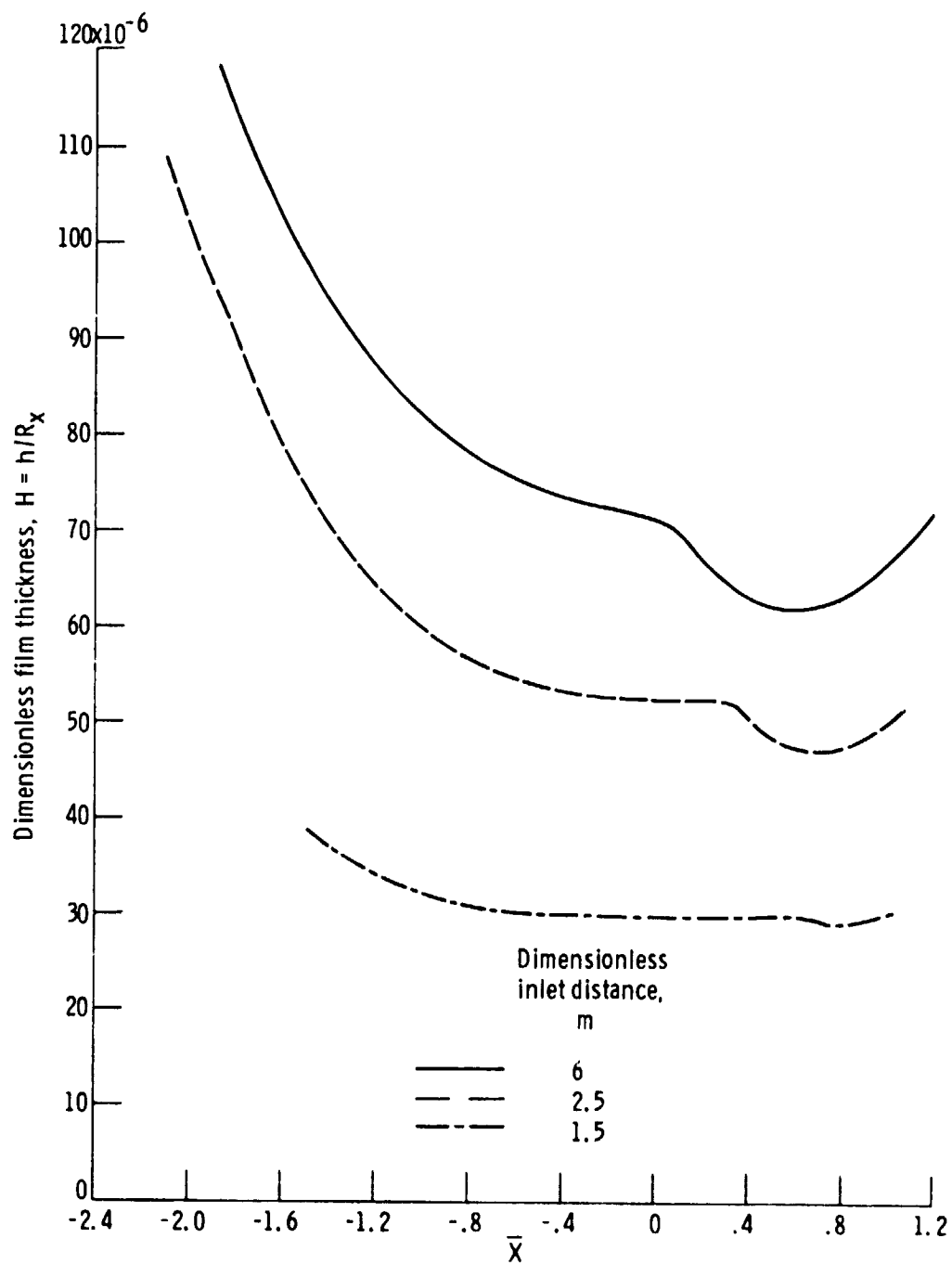
(b) Group 3 of table 6.2.

Figure 6.20. - Concluded.



(a) Group 1 of table 6.2.

Figure 6.21. - Effect of dimensionless inlet distance on dimensionless film thickness along \bar{X} -axis. The value of \bar{Y} is held fixed near the axis of symmetry of the contact.



(b) Group 3 of table 6.2.

Figure 6.21. - Concluded.